Investigation of Transcription Factors Regulating Urothelial Differentiation and Signalling Pathways involved in Urothelial Cancer Cells

Shu Guo

MPhil

University of York

Biology

August 2015

Abstract

Background: Normal human urothelial (NHU) cells can be induced to differentiate by inhibition of the EGFR pathway and activation of PPARγ, which is considered a master transcription factor (TF) for urothelium. Activation of PPARγ results in up-regulation of downstream TFs, amongst which ELF3 was identified as the most up-regulated by microarray. Different phenotypes of NHU cells (proliferating or differentiated) assessed by expression of differentiation markers were found to resemble different types of urothelial cancer (UC) cell lines. The hypothesis is that the differentiation status in UC cell lines reflects cancer evolution pathways, which are selected to be either retained or lost, and define regulatory pathways that UC cells use for growth.

Aim: To understand the role of TFs in regulating urothelial differentiation and pathways regulating proliferation in different UC cell lines.

Results: Knockdown of ELF3 in NHU cells affected the expression of ELF3. Functional study also showed an essential role of ELF3 in maintaining an effective barrier. Evidence suggested that PPARγ was coincidentally knocked down in some cells. Over-expression of ELF3 demonstrated increased ELF3 transcript, but had no effect on phenotype.

A UC cell line (5637) with low expression of differentiation markers resembled non-differentiated NHU cells. When maintained in medium without serum, 5637 cells relied on PPARγ and GSK3β pathways for growth. By contrast, UMUC9 cells, which resembled differentiated NHU cells, could not proliferate when serum or other growth factors were removed.

NHU cells or UC cells maintained in different media (± serum) demonstrated different expressing patterns of PPARγ transcripts and protein isoforms.

Conclusions: ELF3 was important in regulating differentiation in NHU cells and may affect the expression of other TFs, but was not alone sufficient to initiate the differentiation programme. The phenotype and signalling pathways associated with proliferation in 5637 and UMUC9 cells may have implications for different subtypes of Muscle Invasive Bladder Cancer (MIBC).

List of contents

List of tables

List of figures

Acknowledgements

I would like to thank my supervisor, Professor Jenny Southgate, for all the help she provided, without which this thesis would not be in such standard. She has given considerable advice on both the experimental work included in the thesis and the final writing up process.

I would also like to thank Jenny Hinley (soon Dr. Hinley) and Dr. Carl Fishwick for their helpful advice on the work. All the other members from Jack Birch Unit for Molecular Carcinogenesis are also acknowledged for their support technically and generally in life.

The work was supported by the Technology Facility in Department of Biology, to which I would like to give my appreciation.

Finally, I would like to thank my family and my friends for their help and care for me, particularly my parents for their enormous spiritual and financial support.

Author's declaration

The candidate confirms that the work presented in this thesis is her own, and appropriate credit has been given where reference is made to the work of others, or for the collaboration with others.

Chapter 1 Introduction

1.1 The urothelium

Urothelium is the epithelial lining of the urinary tract including the renal pelvis, the ureters, the bladder and the proximal part of the urethra. It consists of three different layers of cells: the basal, intermediate and superficial cells, according to their morphology and localisation relative to the basement membrane (reviewed by Lewis, 2000). The superficial cells in human bladder are larger with occasional binuclear cells compared to the intermediate or basal layer cells. The intermediate layer consists of more than one layer of cells smaller than the superficial cells. Cells in the basal layer are cuboidal and attached to basement membrane (Jost et al., 1989).

Mammalian studies suggested urothelial cells in the healthy adult mouse bladder have an extremely slow turnover, with about one cell cycle per year (Jost, 1986, 1989; Jost and Potten, 1986). During development, the cell cycle time decreases to approximately 30h (Jost, 1989; Jost and Potten, 1986). This relatively quiescent state in adult mice can be interrupted by infection or injury to the urothelium (de Boer et al., 1994; Mysorekar et al., 2002), which stimulated regenerative repair as early as 4 h, as determined from the proliferation rate using BrdU assay. Reinstatement of the quiescent state of mouse urothelium was observed within 24h followed by differentiation of superficial layer cells (de Boer et al., 1994). A recent study in murine urothelium demonstrated that some basal cells showed significantly increased proliferation one day post E.coli inoculation, which reduced significantly two days after infection and returned to non-significant amount compared to control (Colopy et al., 2014).

Human urothelium demonstrated the same features, showing rare Ki67 positive cells in adult tissue (Varley et al., 2005). When wounded *in vitro*, cell cultures also demonstrated ability to recover rapidly (Fleming et al., 2012; Varley et al.,

2005). The features of mitotically quiescence and rapidly repair of urothelium facilitated the tissue to perform its function, which is to stably act as a urinary barrier.

1.2 Differentiation of urothelium and the related features

Early study of rat urothelium described superficial cells as localised at the interface of urothelial tissue and the lumen in contact with urine (Hicks, 1965) and providing a functional barrier to prevent underlying tissue exposure to substances in the urine (Negrete et al., 1996). Superficial cells are highly specialised through differentiation to provide the barrier function. Gene products expressed in urothelium indicating specialisation have been investigated by several studies to understand their roles in urothelial function. The most frequently studied markers are summarised in the following sections.

1.2.1 Uroplakins (UPK)

The highly differentiated superficial cells display multiple plaques of asymmetric unit membrane (AUM) present on the apical cell surface. The plaques consist of thousands of subunits of conserved membrane proteins called uroplakins. Uroplakins (UPK1a, UPK1b, UPK2 and UPK3a/b) are urothelial differentiation-restricted markers that have been demonstrated to have important roles in the urinary barrier (reviewed by Jenkins and Woolf, 2007). Four major UPKs were assembled as heterodimers (UPK1a/UPK2 and UPK1b/UPK3a) at the first stage and then altered their conformation to form 16nm particles essential for the formation of multiple plaques (reviewed by Wu et al., 2009). Transcript expression of UPK1a, UPK2 and UPK3 are urothelium-specific in humans, whereas UPK1b was also detectable in non-urothelial tissues (Olsburgh et al., 2003).

Crucial roles of uroplakin proteins in urinary tract development and urothelial differentiation have been investigated in transgenic mice. UPK2 and UPK3a

knockout mice demonstrated a hyperplastic urothelium with atypical superficial cells (Aboushwareb et al., 2009). The apical cells were much smaller in UPK2 knockout mice and the uroplakin particles were lost in these cells (Kong et al., 2004). Expression of other UPK proteins was reduced in UPK2 KO mice (Kong et al., 2004). Studies of UPK3a deficient mice demonstrated much smaller apical cells with microvilli instead of normal rugged cells (Hu et al., 2002). The knockout of UPK3a led to a compensatory overexpression of UPK1b transcript and abnormal distribution of UPK1b protein (Hu et al., 2000). Features like large plaques and rugged surface of urothelium were lost in UPK3a knock out mice (Hu et al., 2000). Diminished ability to retain methylene blue dye was detected, showing compromised function of urothelium in the UPK3a knock out mice (Hu et al., 2000). Water permeability was significantly higher in UPK3a KO mice than in wild type mice, whereas permeability to urea did not change significantly, suggesting that UPK proteins contribute to maintaining the functional barrier (Hu et al., 2002).

1.2.2 Tight junctions (TJ)

Tight junctions are intercellular junctions localised to the lateral membranes and composed of multiprotein complexes including zonula occludens (ZO) proteins, occluding and claudins. The claudin family consists of 24 distinct members (reviewed by Ichikawa-Tomikawa et al., 2011). The differential expression of claudins by different tissues indicates different roles of individual claudin proteins. For example, in human urothelium, claudin 3 is expressed at the "kissing point" of the terminal superficial junction, whereas claudins 4, 5 or 7 are localised to intercellular borders (Varley et al., 2006). Transgenic mice and shRNA knock down have been used to investigate the physiological roles of specific claudin proteins.

Research on physiological roles of claudin proteins has demonstrated involvement of claudins in salt homeostasis. Knockout of claudin (CLDN) 7 in

mice resulted in chronic dehydration characterised by wrinkled skin and death within 12 days (Tatum et al., 2010). Other study on functions of claudin proteins also suggested their role. Using small interfering RNA targeting claudin 1-4 and 7 in Madin-Darby canine kidney (MDCK) cells showed that knock down of claudin 4 or 7 led to an elevated permeability of Na^+ (Hou et al., 2006).

The essential role of CLDN4 has also been demonstrated by a recent *in vivo* study, showing urothelial hyperplasia and hydronephrosis in CLDN4 knock out mice, which reduced their survival rate to 59% compared to 94% of CLDN4 (+/-) mice. The tight junction structure was not affected, but compensatory enhanced expression of CLDN3 and CLDN8 at renal medullary regions and CLDN7 accumulation at ureters was also observed (Fujita et al., 2012). This finding suggested complementary expression of other claudin proteins, and may indicate the interrelationship of different claudins.

1.2.3 Cytokeratins (CK)

CKs are the intermediate filaments of epithelial cells and constitute a major cytoskeletal component. There are at least 20 isoforms of CKs. The expression and distribution of CK isoforms is epithelial type-specific and related to proliferation and differentiation of the tissue (reviewed by Southgate et al., 1999). In urothelium *in vivo*, CK13 was expressed cytoskeletally in the intermediate and basal layer of urothelium (Varley et al., 2004b). CK20 was only present in the superficial layer and considered a terminal differentiation marker (Harnden et al., 1995; Varley et al., 2004b).

1.3 Models to investigate the urothelium

1.3.1 Normal human urothelial (NHU) cells

To investigate mechanisms of maintaining barrier function and response to injury or infection *in vivo*, NHU cells may be cultured using *in vitro* models. These cells may be isolated from surgical specimens during surgery and

collected with patient consent. Intact sheets of healthy human urothelial tissue were detached from stroma after incubation in EDTA buffer, which enables the urothelial cells to be separated and proliferate as adherent monolayer cultures to form cell lines with a finite lifespan in culture. The cultures demonstrate a basal/intermediate-like proliferative phenotype showing expression of Ki67 as a proliferation marker when maintained in Keratinocyte serum-free medium (KSFM) with growth supplements (Southgate et al., 1994; Southgate et al., 2002). NHU cells have been shown to be able to proliferate *in vitro* and have potential to be used in replacement of defective urothelium as regenerative tissue. A characterisation of normal human urothelial cells suggested that continued subculture may result in culture senescence, which may affect the quality of transplantation, and should be taken into consideration before transplantation (Chamorro et al., 2015).

1.3.2 Differentiation of NHU cells *in vitro*

In order to understand the regulation of development and differentiation of urothelium *in vivo*, two methods were developed to induce a differentiated phenotype from proliferating NHU cells cultured *in vitro*. One method is to add troglitazone (TZ) and PD153035 (PD) to proliferating cells, and induce the expression of terminal differentiation genes (Varley et al., 2006; Varley et al., 2004a; Varley et al., 2004b). However, by addition of TZ/PD, the urothelial cells differentiated but did not form a functional barrier, thus a further biomimetic *in vitro* model was developed involving subculture of NHU cells in medium supplemented with serum (5% ABS) and physiological (2 mM) calcium (ABS/Ca^{2+}) (Cross et al., 2005). ABS/Ca^{2+} induced NHU cells were able to form three morphologically distinguished layers with high transepithelial electrical resistance (TER) (>3000 $\Omega \bullet cm^2$), which represented a functional barrier and simulated the *in vivo* tissue (Cross et al., 2005). These two methods together (TZ/PD and ABS/Ca^{2+}) facilitate the study of urothelial development and differentiation *in vitro*.

In cell culture, NHU cells adapt a non-differentiated basal-like phenotype characterised by a switch to an EGFR autocrine-driven rapidly proliferating CK14+ CK13- phenotype. When induced to differentiate using TZ/PD, NHU cells were switched to a transitional (CK13+, CK14-) differentiated phenotype (Varley et al., 2004b).

The *in vitro* induced differentiated NHU cells can be used to study the effect of altered expression of differentiation-associated proteins on other differentiation-related features. For example, change of claudin protein expression was shown to have affected the expression of other tight junction proteins such as the ZO proteins. Knock down of CLDN3 in NHU cells reduced the protein expression of ZO1α^+, which was more prevalent in differentiated NHU cells than untreated or stratified cells. These CLDN3 knock down cells also demonstrated a significantly impaired ability to form a functional barrier assessed by transepithelial electrical resistance (Smith et al., 2015).

1.3.3 Other models to study urothelium

In order to investigate essential roles of specific genes *in vivo*, transgenic knock out mice have been utilised. Knock out of terminal differentiation-associated genes like UPK2 or UPK3a demonstrated loss of function of bladder urothelium such as non-voiding contractions and increased residual volume of urine (Aboushwareb et al., 2009), whereas knock out of CLDN7 affected the function of urothelium and other tissues and led to death (Tatum et al., 2010). Knock outs of differentiation-associated transcription factors like ELF3 and GRHL3 have been generated to understand their essential roles. ELF3 knock out mice demonstrated dysmorphogenesis of intestinal epithelium and 30% lethality (Ng et al., 2002). Knock out of GRHL3 significantly affected the morphology of murine bladder and resulted in the decreased expression of urothelial differentiation-related downstream genes (Yu et al., 2009).

Furthermore, a UPK2 promoter transgenic mouse demonstrating expression of UPK2 proteins in the suprabasal layer of urothelium was established (Lin et al., 1995). The expression of UPK2 protein in mouse is confined to urothelial tissue, which enabled the transgenic urothelium-specific expression of other genes such as oncogenes or inactivated tumour suppressor genes, resulting in advantage for studies of bladder tumorigenesis (reviewed by Wu et al., 2009).

1.4 Transcription factors that regulate differentiation

To develop from embryo to mature functional tissue, cells are regulated to differentiate. This differentiation process is mediated by transcription factors, demonstrating different roles in controlling distinct stages of development and differentiation.

1.4.1 Regulated differentiation by PPARγ

The thiazolidinediones (TZDs) are regarded as potent insulin sensitizers used for treatment of type II diabetes. To understand the mechanism of reversed insulin resistance by TZDs, nuclear receptor PPARγ was investigated extensively as a nuclear transcription factor stimulated by TZDs. Most studies about PPARγ mainly focused on its role in adipogenesis in the literature. It mainly acts as a central transcription factor in adipocyte differentiation, as knock out of PPARγ in embryonic stem cells by homologous recombination inhibited adipogenesis and abolished the expression of adipocyte-related differentiation markers after induction of differentiation (Rosen et al., 1999). Other studies regarding the characterisation of PPARγ transcript variants and isoforms will be discussed in Chapter 5.

However, the role of PPARγ in normal urothelial differentiation was not greatly investigated until recently. It was shown that in urothelial differentiation, activating PPARγ by TZ (troglitazone, one of the TZD drugs) in proliferating NHU cells significantly induced the expression of differentiation-associated genes, including the UPKs, CLDN3 and CK20. Co-inhibition of the

autocrine EGFR signalling pathway using PD153035 was also required to de-phosphorylate PPARγ for its transcriptional activity (Varley et al., 2006; Varley and Southgate, 2008; Varley et al., 2004a; Varley et al., 2004b). PPARγ antagonists GW9662 or T0070907 reduced the TZ/PD induced transcript or protein expression of differentiation-associated markers (Varley et al., 2006; Varley et al., 2004a), which verified the essential role of PPARγ in regulating urothelial differentiation.

Among the differentiation-associated marker genes, PPREs (peroxisome proliferator response elements) were found within 2kb upstream of the transcriptional start site of CLDN3 and CLDN7 promoters (Varley et al., 2006). However, no PPRE sites were found in 1000bp upstream of CK13 or CK20 promoters (Varley et al., 2004b). Similarly, no PPRE could be observed in many of the UPK genes, and the up-regulation of UPK genes was delayed till 96h (Varley et al., 2004a), suggesting that the induction process by PPARγ ligands was indirect and mediated via intermediary transcription factors.

1.4.2 Other transcription factors related to urothelial differentiation

The role of IRF1 (Interferon regulatory factor 1) and FOXA1 (forkhead box A1) as differentiation-associated intermediate transcription factors in human urothelium was identified by human GeneChip® array (Varley et al., 2009). Binding sites for both IRF1 and FOXA1 were found present in UPK1b, UPK2 and UPK3a. Also, high affinity PPRE site was reported in promoters of IRF1 and FOXA1 (Varley et al., 2009). In TZ/PD induced NHU cells, expression of IRF1 and FOXA1 was massively up-regulated and was inhibited by PPARγ inhibitors. Knock down of IRF1 and FOXA1 using siRNA reduced the protein expression of CLDN3 and CK13, which indicated the essential role of IRF1 and FOXA1 in regulating urothelial differentiation (Varley et al., 2009).

Expression of FOXA1 protein (alternative name: hepatocyte nuclear factor 3α, endodermal marker) was observed on mouse embryonic day 16, postnatal day 1 and adult mice bladder, whereas increased protein expression of UPK (broad-spectrum) was detectable concurrently (Oottamasathien et al., 2007). This result also suggested an essential role of FOXA1 in urothelium development and regulation of differentiation.

Transgenic mice studies demonstrated the role of GRHL3 (grainyhead-like 3) in mouse embryonic development. GRHL3 was highly expressed in superficial cells in mouse urothelium on embryonic days E16.5 and E18.5 (Yu et al., 2009), which were the time of developing the unique urothelial apical plasma membrane (Erman et al., 2006) constituted mainly by uroplakins. The GRHL3 knockout mouse demonstrated smaller and rounded immature superficial cells. Protein expression of uroplakins in these abnormal cells was extremely low. GRHL3 knockout mice developed defective bladders lacking expression of CK18, CK20 and UPK proteins on E18.5 compared to control. These findings suggested the involvement of GRHL3 in urothelial differentiation and development (Yu et al., 2009). UPK2, a terminal differentiation marker, was regulated by GRHL3 directly by binding to its promoter, which also indicating a potential role of GRHL3 as an intermediate transcription factor involved in mouse urothelial development (Yu et al., 2009) .

1.5 Urothelial cancer (UC)

1.5.1 Incidence and causes of bladder cancer

Bladder cancer is the 7th most common cancer in the UK, and the 4th most common cancer in British men (Cancer Research UK). About 60% of bladder cancer cases occurred in more developed countries worldwide, particularly in Europe and North America in 2012 (Ferlay et al., 2015).

Urothelium is the tissue in direct contact with excreted chemicals and waste products in the urine that may cause cancer, and therefore is at risk to develop cancer. It was reviewed that urothelial cancer risk increased in occupations involving exposures to polycyclic aromatic hydrocarbons (Bolt, 2014). Lifetime arsenic exposure, smoking and secondhand smoke also increased the odds ratio of developing bladder cancer (Ferreccio et al., 2013). Exposure to mineral oils, diesel engine exhaust, painting material and aromatic amines was reported to be the main causes for bladder cancer in the UK (Rushton et al., 2012).

1.5.2 Brief classification of bladder cancer

When classifying urothelial cancer according to the extent of differentiation, the morphology can be divided into low grade (well differentiated) and high grade (poorly differentiated) cancers. This is known as the grade of bladder cancer. According to the extent of cancer cell invasion into the detrusor muscle layer of the bladder wall, urothelial cancer is generally divided into non-muscle invasive cancers and muscle invasive bladder cancers (MIBC). In non-muscle invasive cancer, the cancer is confined in the urothelium or lamina propria and did not invade muscle layer. By contrast, MIBC indicate that the cancer cells have invaded into the muscle layer of the bladder wall. This is the staging scale of bladder cancer that indicates the extent of invasion and whether cancer cells have spread. MIBC was reported to have poor prognosis, which is about 50% survival rate 5 years after diagnosis (Cancer Research UK).

In well-differentiated tumours, deletions on chromosome 9 were detected, whereas poorly differentiated muscle invasive cancers were shown to have loss of tumour suppressor genes (p53 and PTEN, for example) and mutation of oncogenes. Carcinoma in situ (CIS) characterised as non-muscle invasive, poorly differentiated cancers was more complicated. Loss of p53 was highly agreed in reports regarding characterization of CIS, but deletion of

chromosome 9 only occurred in some of the cases (reviewed by Goebell and Knowles, 2010).

Recent reports based on large scale transcriptomic studies suggested that muscle invasive bladder cancers can be sub-classified the same as breast cancers, with basal and luminal subtypes (Damrauer et al., 2014). Expression of differentiation-associated genes was detectable in the luminal subtype of MIBC, but not in the basal subtype, which demonstrated expression of basal markers such as CK5/6 (Choi et al., 2014). These recent findings have improved the long standing views about pathways in bladder cancer and broke the boundary between the stage and grade system (reviewed by Knowles and Hurst, 2015).

1.5.3 Urothelial cancer cell lines

In vitro cultured urothelial cancer cell lines have been established and characterised. The stage and grade of UC cell lines and known mutations in cell lines provided background information for following studies. The bladder cancer cell lines used in this study are listed in Chapter 2. Bladder cancer cell lines showing different grade of differentiation can be used to investigate the relationship of differentiation and expression of other differentiation-associated genes to indicate the role of such genes in different cancer cell lines. One example was to knock down the expression of FOXA1 in well differentiated bladder cancer RT4 cell line and over-express it in poorly differentiated T24 cell line (DeGraff et al., 2012). The results suggested the alteration of FOXA1 protein expression increased the cell proliferation in RT4 cells and inhibited both the proliferation and the cell invasion in T24 cells (DeGraff et al., 2012).

It is also suggested that autocrine growth signalling was present in some of the bladder cancer cell lines, as conditioned medium of human bladder cancer cell line 5637 has been used as medium for culture of growth factor-dependent hematopoietic cells. 5637 cells showed secretion of cytokines like granulocyte colony-stimulating factor, granulocyte-macrophage colony-stimulating factor

and interleukin 1β (Quentmeier et al., 1997). An autocrine mechanism has also been found in NHU cells and was regulated by EGFR pathway (Varley et al., 2005). Signalling pathways indicating proliferation of bladder cancer cell lines like EGFR pathway will be explored in Chapter 4.

1.6 Thesis aims

The aims of this thesis were to investigate the role of transcription factors in regulating urothelial differentiation and pathways regulating proliferation in different UC cell lines.

The objectives for the individual chapters were:

- To understand the role of ELF3 as a candidate transcription factor identified by microarray in normal urothelial cell differentiation (Chapter 3).
- To investigate the relationship between the phenotype of UC cells and the signalling pathways they depend on for growth (Chapter 4).
- To explore whether the expression of different PPARγ transcripts was associated with urothelial differentiation or urothelial cancer and investigate the expression and localisation of PPARγ isoforms (Chapter 5).

Chapter 2 Materials and Methods

2.1 General

Experiments were performed in the Jack Birch Unit in Department of Biology at the University of York. The Technology Facility in Department of Biology also provided support and usage of equipment.

Pipette tips (Starlab), Eppendorf tubes (Starlab) and glassware (Scientific Laboratory Supplies; SLS) were either purchased sterile and free of nuclease, or were autoclaved for 20 min at 121 °C. Stock solutions were prepared as described in the buffer recipe and listed in Appendix section 7.4. Tissue culture solutions were prepared in ELGA water from an ELGA water purification system (Veolia Water Technologies) and autoclaved, the other solutions were made with deionised water (dH_2O). All chemicals were obtained from Sigma Aldrich unless otherwise stated. Information of suppliers was listed in Appendix section 7.5.

2.2 Tissue culture

2.2.1 Establishment and maintenance of NHU cells as finite cell lines

Tissue samples were collected from patients undergoing urology-related surgical procedures for non-cancer conditions with appropriate consent and approvals from NHS and local Research Ethics Committees. Each individual sample was allocated with the laboratory sample number (Y number, see Table 2.2.1) showing research-related information. Procedures were followed as described in detail (Southgate et al., 1994; Southgate et al., 2002). After detachment from stroma, urothelial cells were maintained and passaged for a finite life span in Keratinocyte serum-free medium (KSFM; Life Technologies) with supplements, which are recombinant EGF (rEGF; Life Technologies) and

bovine pituitary extract (BPE, Life Technologies) at final concentrations of 5 ng/mL and 50 ng/mL, respectively, and addition of 30 ng/mL cholera toxin (CT). This complete KSFM (KSFMc) was pre-warmed at 37 °C and then utilised to nourish the cells. Cells were cultured either in 25 cm^2, 75 cm^2 flasks or in 6 cm dishes (Primaria™; SLS), and maintained in HERAcell™ 240 incubator (Thermo Scientific) at 37 °C in a humidified atmosphere of 5% CO_2 in air. Cells used in this thesis were provided as growing or cryopreserved cell cultures by Ros Duke (technician, JBU).

Sample ID number	Type of operation	Tissue Type	Age/ sex
Y588	nephrectomy	ureter	?
Y1116	?	ureter	64/F
Y1156	nephrectomy	ureter	72/F
Y1194	nephrectomy	ureter	52/M
Y1233	nephrectomy	ureter	81/F
Y1236	nephrectomy	ureter	57/M
Y1289	nephrectomy	ureter	54/F
Y1436	renal transplant	ureter	73/F
Y1441	renal transplant	ureter	57/M
Y1456	renal transplant	ureter	78/F
Y1529	nephrectomy	ureter	68/F

Table 2.2.1 List of Y numbers and sample information for all NHU cell lines used in this thesis. Question marks indicate unclear information.

NHU cells were cultivated as a monolayer until just confluent. After incubation with 0.1% EDTA for 5-10 min at 37 °C, cells were able to separate from each other. When they visibly dissociated from each other, depending on the size of flasks or dishes, EDTA was replaced with 0.25% (w/v) 0.5-1 mL of trypsin versene (TV) and incubated with cells for 1-2 min until detachment. Cells were then harvested into 5 mL of KSFMc with 1.5mg/mL of trypsin inhibitor (TI). After centrifugation, cells were resuspended in KSFMc before seeding on to fresh flasks or dishes. Cells at passages between 2 to 5 were utilised.

Cells were counted as single cell solution using haemocytometer (VWR) before seeding. Each chamber was filled with 10 μL of cell suspension. Cells were counted in a 5X5 grid and averaged with another chamber. The average number multiplied by 10^4 was the total number of cells in 1 mL of medium.

2.2.2 *In vitro* induction of differentiation in NHU cells

The differentiated phenotype was obtained with two methods (described as TZ/PD (Troglitazone and PD153035) and ABS/Ca^{2+} in section 1.1). When reaching 70-80% confluent, cultures were stimulated with 1 μM TZ and 1 μM PD153035 (Calbiochem) (Varley et al., 2004a). If the treatment is more than 24h, medium with addition of TZ is to be replaced with vehicle control (DMSO) 24h later, whereas medium with PD153035 is to be renewed every 2 or 3 days.

The other method was generated by Cross et al (Cross et al., 2005), which was to treat cultures with serum and physiological concentration of calcium (ABS/Ca^{2+}). Cultures from passage 1-3 were maintained in KSFMc with 5% adult bovine serum (ABS, pretested batch; Harlan Sera-Lab) for 5 days, and then harvested and seeded in flasks, dishes or Snapwell™ membranes, depending on the following experiments. On the next day, 180 μL of 1 M $CaCl_2$ was added into 100 mL of KSFMc to provide 2 mM final calcium concentration.

2.2.3 Maintenance and subculture of established UC cell lines

Urothelial bladder cancer cell lines were cultured in either Dulbecco's Modified Eagle's Medium (DMEM; Life Technologies) or Roswell Park Memorial Institute 1640 medium (RPMI 1640; Life Technologies) supplemented with FBS (Harlan Sera-Lab) and 1% L-glutamine. Table 2.2.2 displays information of UC cell lines and the standard growth medium used for UC cell lines utilised in the study. Cells were sub-cultured when about confluent. When passaging UC cells, no trypsin inhibitor was required as the serum was able to neutralise the effect of trypsin. Cells were seeded in Corning® flasks or dishes and maintained in humidified incubators in 10% CO_2 in air (DMEM) or 5% CO_2 in air (RPMI).

Mycoplasma spp testing was performed. Cells were seeded on 12 well slides at 4-5x10^4 cells /mL for 50 μL each well, immersed with growth medium 2-4 h later and left overnight. Slides were washed with PBS and fixed by Methanol /Acetone (1:1) for 30 s before drying in the air. Slides were incubated with 0.1 μg/mL Hoechst 33258 diluted in PBS-Tween 20 (0.25%, W/V) for 5 min and rinsed with distilled water. After air dry, slides were mounted with antifade, covered using coverslip and sealed using nail polish. Nuclei were visualised as described in section 2.6.6. No extra nuclear DNA staining should be observed otherwise cultures are potentially contaminated with Mycoplasma spp.

Genotyping was performed when cell line first arrived. Table 2.2.2 displays general information of cell lines utilised in the study.

Cell line	Bladder cancer grade	Ref.	Standard medium
5637	Grade II carcinoma	(Fogh et al., 1977)	RPMI (5% FBS)
UMUC9	Grade III carcinoma	(Grossman et al., 1988)	DMEM (10% FBS)
SD48	Carcinoma	N/A	DMEM (10% FBS)
RT4	Grade I carcinoma	(Rigby and Franks, 1970)	DMEM:RPMI (50:50) (5% FBS)
RT112	Grade II carcinoma	(Marshall et al., 1977)	DMEM:RPMI (50:50) (5% FBS)
T24	Grade III carcinoma	(Marshall et al., 1977)	DMEM:RPMI (50:50) (5% FBS)

Table 2.2.2 Urothelial cancer cell lines and their standard growth medium.

2.2.4 Adapting cancer cells to KSFM for growth

Cancer cells were cultivated in medium with serum, which contains many kinds of growth factors. The serum in the medium of the cells grown in was gradually reduced by increasing the percentage of KSFM and decreasing the percentage of standard medium (Table 2.2.2 for information regarding different cell lines). After the medium was changed to 100% KSFM, cells were sub-cultured to check whether they could survive. If the cells were not able to

proliferate in KSFM without serum, the cell line was considered as not adaptable. Information regarding whether cell lines were adaptable is listed in Chapter 4.

2.3 Growth assay (Alamar Blue® assay)

Alamar Blue® (AbD Serotec) is an oxidation-reduction indicator that fluoresces and changes colour when growth medium was metabolised by growing cells. Continued growth produced a reduction environment that results in the alteration of indicator from oxidized (non-fluorescent, blue) form to reduced (fluorescent, red) form. The growth rate of cells then can be calculated from data generated using absorbance-based (or fluorescence-based) instrument. For absorbance-based instrument, absorbance is monitored at 570 nm and 630 nm. No cell control was included by adding Alamar Blue® to empty wells for calculation of reduction rate.

Cells were seeded at $2x10^4$/mL (seeding in 200 μL) on 96 well plates and maintained for 7-9 days. Alamar Blue® was diluted 1/10 on day of assay with growth medium. Medium of cultures was removed and replaced with diluted reagent. Cells were incubated in 200 μL Alamar Blue® solution for 4 h. Absorbance at 570 nm and 630 nm was measured, after which the value was calculated and converted to the reduction rate of Alamar Blue®.

2.4 Transepithelial electrical resistance (TER)

Differentiated cultures were established using the ABS/Ca^{2+} method and seeded onto the upper chamber (growth area 1.12 cm^2) of Snapwell™ membranes (Corning) with 6 replicates of $5x10^5$ cells /well. Voltage and current recording microelectrodes were placed in both the apical and basal chambers and connected to the voltage-current clamp. The voltage and current were recorded and shown as the resistance across the cell sheets by an Electronic Voltage Ohm Meter (EVOM). Medium was renewed with fresh KSFMc containing 5% ABS

and 2 mM calcium after the first reading and on alternative days. Once the measurements stabilised, a single scratch about 250 μm wide was generated in the culture using a 20 μL pipette tip. TER readings were recorded regularly until the value returned to and stabilised around its initial number.

2.5 Analysis of gene expression

2.5.1 RNA isolation and DNA digestion

Cultures were washed with phosphate buffered saline (PBS) before addition of Trizol®. After 5 min of incubation on a rocking platform, cultures with Trizol® solution were scraped and transferred to a sterile centrifuge tube pre-treated with 0.1% diethylpyrocarbonate (DEPC) water (diluted in ELGA water) overnight. RNA lysates could be stored at -80 °C and remain stable. On day of extraction, RNA lysates were thawed completely and left at ambient temperature for 5 min. 0.2 mL chloroform was added to the solution per mL of Trizol®. Following 15 sec of vortex and a further 2-3 min incubation, RNA was extracted and remained solubilised in the upper aqueous phase. After 15 min of 12000 g centrifugation at 4 °C, the aqueous phase was aspirated to a fresh tube. 0.5 mL of isopropanol (Fisher Scientific) per mL of Trizol® was utilised to precipitate the RNA before centrifugation for 20 min at 12000 g at 4 °C and washed with 70% ethanol. After a 5 min 7500 g centrifugation, 70% ethanol wash was repeated to improve the quality of RNA isolated. The final pellet generated by centrifugation for 5 min at 7500 g was solubilised in 30 μL of DEPC treated water. RNA was stored at -80 °C.

DNA-easy AMBION kit (Ambion) was utilised to remove any residual DNA. 1 μL of DNase I (2 U/μL) was added to 30 μL of obtained RNA with DNAse 1 buffer at a 1/10 dilution. After 30 min incubation at 37 °C, the enzyme was inactivated and precipitated. Solution containing RNA was transferred to a fresh tube. 40 U of RNAseOUT (Life Technologies) was added to the solution to prevent any degradation of RNA.

The quality of RNA was inspected by NanoDrop™ spectrophotometry. The ratio of absorbance at 260 nm and 280 nm would indicate whether the sample had any protein or phenol contamination, whereas 260/230 ratio indicates the possibility of salt contamination. High quality RNA shows a ratio of 260/280 between 1.9 to 2.1 and a 260/230 ratio between 1.5 to 2.0.

2.5.2 Synthesis of complementary DNA (cDNA)

Random hexamers (50 ng) were added to equal amount of RNA samples and diluted with DEPC water to obtain same volume. The mixture was incubated at 65 °C for 10 min to anneal the primers before 0.1 M DTT and 10 mM dNTP were added. Equal amounts of RNA from each sample were converted to cDNA by addition of 50 U SuperScript II (Life Technologies) per 20 μL and incubated at 25 °C for 10 min and 42 °C for 50 min. Samples without addition of SuperScript II were included as RT negative control to confirm no DNA contamination was present. Inactivation of reverse transcription was achieved by heating the mixture for 15 min at 70 °C.

2.5.3 Reverse Transcription Polymerase Chain Reaction (RTPCR)

RTPCR was performed using GoTaq™ polymerase (Promega) in T100 thermal cycler (BioRad). A typical 20 μL reaction contains 4 μL of GoTaq buffer, 0.4 μL of dNTP (10mM), 2 μL of $MgCl_2$, 2 μL of each forward and reverse primer (10μM) and 0.1 μL of GoTaq polymerase. For positive control, human genome DNA was added to the reaction, whereas only nuclease-free water was added to the no-template negative control.

PCR cycle was initialised at 95 °C for 2 min for denaturation, followed by generally 25 to 30 cycles of amplification depending on the abundance of the templates. The amplification cycle was 30 sec denaturation at 95 °C, 30 sec annealing at 45-65 °C depending on the optimal temperature of primers and extension at 72 °C. The time for extension depends on the length of product, for

about 1 min every 1 kb DNA amplified. A final extension period was added after the amplification cycles for 7 min followed by incubation at 4 °C.

2.5.4 Gel electrophoresis

1%-2% (w/v) electrophoresis grade agarose was solubilised in 1x Tris Borate EDTA (TBE) microwave boiled buffer and cooled to around 50 °C before addition of 1/10000 SYBR® safe stain (Life Technologies). Gels were poured and allowed to set. PCR products and Hyperladder IV ladder (Bioline) were electrophoresed on the gel covered by 1x TBE for required amount of time to separate the bands. DNA products were visualised under UV light. Gel images were captured using a Gene Genius Gel Imaging System (Syngene) with GeneSnap™ software.

2.5.5 RT quantitative PCR (RTQPCR)

Complementary DNA samples were diluted 1 in 5 with nuclease-free water to a final volume of 100 μL. 5 μL of cDNA was mixed with 300 nM sense and antisense primers and Fast SYBR® Green (Life Technologies) QPCR master mix. PCR reactions were completed on 96 well plates on StepOnePlus™ QPCR System (Applied Biosystems) using the comparative quantification method (Schmittgen and Livak, 2008). GAPDH was utilised as an internal control. Negative controls using RT negative samples as template were included.

2.5.6 Primer design and list of primers

Transcript information of specific genes was obtained from the Ensembl Genome Browser (http://www.ensembl.org/index.html). Primers for RT-PCR were designed using Primer Blast (http://www.ncbi.nlm.nih.gov/tools/primer-blast/). Primers for RTQPCR were either available in the lab or were designed using Primer Express® Software (Applied Biosystems) and purchased (Eurofins). The best ten sets of primers were checked for specificity using Primer Blast.

Primers were designed to target all known transcript variants unless otherwise stated.

To demonstrate the efficiency of the primer sets, newly designed primers for RTQPCR were tested using gradient diluted (1:10, 1:100 and 1:1000) positive control cDNA samples. The standard curves of primers showing a slope of -3.333 and R^2 of 0.999 within ±10% deviation were consider as acceptable for further study. Figures demonstrating standard curves of newly designed acceptable primers are displayed in Appendix 7.2. Primer sets used in the thesis are listed in Table 2.5.1.

Gene		Sequence
ELF3 q	Fwd	TCAACGAGGGCCTCATGAA
ELF3 q	Rev	TCGGAGCGCAGGAACTTG
GRHL3 q	Fwd	TGGAATATGAGACGGACCTCACT
GRHL3 q	Rev	CAGACACGTTCTCTGTCAGGAATT
IRF1 q	Fwd	CTGTCGCCATGTGCTGTCA
IRF1 q	Rev	TGTCCGGCACAACTTCCA
FOXA1 q	Fwd	CAAGAGTTGCTTGACCGAAAGTT
FOXA1 q	Rev	TGTTCCCAGGGCCATCTGT
CLDN7 q	Fwd	GCAGTGGCAGATGAGCTCCTAT
CLDN7 q	Rev	CATCCACAGCCCCTTGTACA
GAPDH q	Fwd	CAAGGTCATCCATGACAACTTTG
GAPDH q	Rev	GGGCCATCCACAGTCTTCTG
UPK3A q	Fwd	CGGAGGCATGATCGTCATC
UPK3A q	Rev	CAGCAAAACCCACAAGTAGAAAGA
GATA3 q	Fwd	CTTCCCCAAGAACAGCTCGTT
GATA3 q	Rev	GGCTCAGGGAGGACATGTGT
KLF5 q	Fwd	TTCTTCCACAACAGGCCACTT
KLF5 q	Rev	TCTGCTTGTCTATCTGGACTTCCA
PPARG2 q	Fwd	TCCTTCACTGATACACTGTCTGC
PPARG2 q	Rev	CAAAGGAGTGGGAGTGGTCT
UPK2 q	Fwd	CAGTGCCTCACCTTCCAACA
UPK2 q	Rev	TGGTAAAATGGGAGGAAAGTCAA
KRT20 q	Fwd	CAAAAAGGAGCATCAGGAGGAA
KRT20 q	Rev	CAACCTCCACATTGACAGTGTTG
GAPDH	Fwd	ACCCAGAAGACTGTGGATGG
GAPDH	Rev	TTCTAGACGGCAGGTCAGGT
ELF3	Fwd	GTTCATCCGGGACATCCTC
ELF3	Rev	GCTCAGCTTCTCGTAGGTC

Table 2.5.1 List of primers. Primers utilised for RTQPCR are marked with a q. Forward and reverse primers were noted as Fwd and Rev, respectively. Sequence of the primers was displayed from 5′ to 3′.

2.6 Analysis of protein expression

2.6.1 Protein lysis and quantification

Cultures were washed with cold PBS and scrape-harvested with Sodium dodecyl sulphate (SDS) lysis buffer containing 2 mg/mL DTT and 0.2% Protease Inhibitor Cocktail Set 3 (Calbiochem). Lysates were collected into chilled microfuge tubes on ice and sonicated with Branson Sonifier probe set to 25 W, 40% amplitude for 2x 10 sec bursts with 10 sec rest between bursts. Cell lysates were left on ice for 30 min and centrifuged for 30 min at 18000 g at 4 °C. Solutions were transferred to a fresh chilled tube and stored at -80 °C. Samples used for Polyacrylamide gel electrophoresis (PAGE) were whole cell lysates unless otherwise noted.

Protein lysates were diluted 1/12.5 in water. Samples were added to 96 well plates as duplicates and mixed with 200 μL of Coomassie protein assay reagent (Pierce). Absorbance of samples was measured using a MRX II 96-well plate spectrophotometer (Dynex). Bovine serum albumin (BSA, Pierce) standard curve was generated every time with standard proteins diluted to different concentrations (0-1000 μg/mL). The concentration of protein samples was calculated according to the standard curve generated by standard proteins. Equal amounts of proteins from each sample were mixed with 4X Lithium Dodecyl Sulphate (LDS, Life Technologies) sample buffer and 10X reducing agent (Life Technologies).

2.6.2 Cytoskeletal extraction (CSK extraction)

This method was used to separate soluble proteins from DNA-bound proteins by using different concentrations of salt with 0.1% Triton X-100 or DNA digestion enzyme. The experiment included in this thesis used a 0.5 M NaCl solution. The buffer recipe was originally obtained from (Ainscough et al., 2007) and is listed in Appendix 7.4.

Three dishes of cells were required for each time point /treatment. One dish was used for whole cell extraction, and two dishes for salt extraction followed by DNA digestion (DNase I or buffer as digestion control).

Buffer used was chilled on ice before harvesting cells. For 6 cm dishes, 3 mL of ice-cold 0.1 M NaCl solution without TX-100 was used to wash the cells. 1 mL 0.1 M NaCl buffer without TX-100 was supplemented with 1 mM PMSF, 0.1 mM ATP, 1 mM DTT and 0.2% Protease Inhibitor Cocktail Set 3 (Calbiochem) to each dish, after which the cells were scrape-harvested. Cell suspension was centrifuged at 10,000 g for 1 min. Supernatant was discarded.

For salt and DNA enzyme extraction samples, the pellet was flipped gently and resuspended using 100 μL of 0.5 M NaCl with 0.1% TX-100 and other supplements added from previous step. The suspension was incubated for 5 min on ice, mixed by pipetting gently and centrifuged at 4 °C for 1 min at 10,000 g. The supernatant was retained as the soluble protein sample. The pellet was washed in 1X DNase I buffer without breaking apart. After centrifuging briefly as previous steps, the pellet was resuspended in either 50 μL 1X DNase I buffer without enzyme or 50 μL 1X DNase I buffer with 1:30 DNase I (Qiagen). The cell suspension was incubated at 37 °C for 30 min.

For whole cell extract, pellet was resuspended in 50 μL 0.1M NaCl solution without TX-100. Microfuge tubes were left on ice until processing of next step.

After DNA enzyme digestion, 50 μL of 1 M NaCl with 0.2% TX-100 was added to the suspension and mixed by pipetting gently 3 times to adjust the concentration of NaCl and TX-100 to 0.5 M and 0.1%, respectively. The suspension was incubated on ice for 5 min and centrifuged at 10,000 rpm for 2 min. Supernatant from digested and non-digested samples was retained and kept on ice. Pellets were washed with 0.1M NaCl (no TX-100) without being disturbed and collected by centrifuging at 10,000 rpm for 2 min. Supernatant

was removed and discarded. Pellets were resuspended in 100 μL of 0.1 M NaCl without TX-100.

To supernatants and pellets, 4X LDS and 10X reducing agent were added to achieve 1X final concentration. All pellets were sonicated 3X 10 s on ice and centrifuged for 10 min at 14,000 g as the procedure for preparation of protein lysates. For western blot, 5-10 μL of extracts was loaded per well. As LDS was used for protein lysis, Coomassie protein assay was not available for protein quantification.

2.6.3 Immunoblotting

Protein samples were heated at 70 °C for 10 min and loaded on 4-12% Bis-Tris NuPage polyacrylamide gels (Life Technologies) with 5 μL of All-Blue pre-stained ladder (BioRad). Electrophoresis was performed after addition of 200 μL antioxidant (Life Technologies) to the inner chamber in 1X MOPS buffer (Life Technologies) for about 1h at 200 V.

Gels were removed and cut to appropriate size before equilibrating in transfer buffer. PVDF-FL (Polyvinyldifluoride-fluorescence) 0.45 μm membranes (Millipore) were cut and dipped to wet in methanol. After rinsing with distilled water, membrane was then equilibrated in transfer buffer with filter paper (Whatman® grade 1) and fibre blotting pads (Life Sciences, E-PAGE™ Blotting Pads). Proteins were electro-transferred to PVDF membrane at 30 V for 3 h.

The membrane was washed with Tris buffered saline (TBS), checked with Ponceau red for transfer efficiency and then blocked with Odyssey blocking buffer (Li-CoR) 1:1 diluted by TBS for 1h and probed with primary antibody (Table 2.6.1) diluted in Odyssey blocking buffer/ TBST (1:1) overnight at 4 °C. Secondary antibody (Goat anti-mouse IgG Alexa 680 or Goat anti-Rabbit IRDye 800) was diluted 1/10000 in Odyssey blocking buffer/ TBST (1:1) and incubated with the membrane for 1h in the dark. Membrane was washed four times with

0.1% Tween 20 in TBS (TBST) before and after incubation with secondary antibody.

Detection of labelled proteins was performed by scanning the membrane on a Li-CoR® Odyssey infrared imaging system. Scans were analysed using Odyssey v1.1 software (Li-CoR). Band intensity was analysed using Odyssey software by drawing boxes around the bands and subtracting the background using the median intensity of pixels. Densitometry of β-actin bands was calculated for normalisation of loading difference.

Membranes were stripped using western blot recycling kit (Source Bioscience) for 30 min to remove bound antibodies before analysis of other antibodies. To ensure no binding of remnant antibodies, membrane was incubated in secondary antibody and scanned before applying of other primary antibodies.

2.6.4 Immunohistochemistry (IHC)

After TER measurements (section 2.4), differentiated cell sheets on Snapwell™ membranes were harvested by 2% (w/v) dispase (Roche) treatment at 37 °C for 30 min to release intact cell sheets. Intact cell sheets were put into histology cassettes, fixed in 10% formalin overnight and transferred to 70% ethanol solution until further processing.

Samples were dehydrated by incubation in 70% ethanol, absolute ethanol, isopropanol and xylene (Fisher Scientific) sequentially. Samples were transferred to molten paraffin wax (Thermo Scientific) at 60 °C for incubations. Following 4X 15 minutes incubation in molten wax, cell sheets were removed from the cassette into metal moulds and embedded in molten wax. Cell sheets in the metal moulds were left on a cold table (RA Lamb) to allow the wax to cool. Wax blocks were cut to 5 μm sections using a Leica RM 2135 microtome. Cut sections were floated into a water bath at 37 °C and collected onto Superfrost Plus™ microscope glass slides (VWR). Once air-dried, sections were

stored temporarily at ambient temperature or melted on a hot block (RA Lamb) at 50 °C for one hour.

Sections were de-waxed and rehydrated by submerging the slides in xylene, absolute alcohol, 70% alcohol and then water. Antigen retrieval was performed to restore the immunoreactivity of antigens masked by tissue processing (Shi et al., 1997). Methods of antigen retrieval used depended on the primary antibody (Table 2.6.1). The best retrieval method was identified by comparing sections restored with different methods. For trypsinisation, sections were incubated in 0.1% (w/v) trypsin in 0.1% (w/v) calcium chloride solution at 37 °C for 10 min. For microwave heating, sections were placed in a Pyrex™ dish filled with 350 mL10 mM citric acid buffer and microwaved for 13 minutes at 900 W. After heating, sections in the dish were cooled on ice and washed with tap water.

Slides were placed in multi-well Shandon Sequenza units using cover plates (Thermo Scientific). Appropriate sealing between slides and cover plates was checked by filling wells with TBS. Avidin and biotin (blocking kit, Vector Laboratories) were added separately to block any endogenous non-specific binding site by incubation the slides for 10 min, with TBS wash in between. 10% normal serum (Dako) of the host of secondary antibody was added to slides to block non-specific antibody binding. Sections were incubated with diluted primary antibody (Table 2.6.1) at 4 °C overnight. For each different secondary antibody, one well was incubated with TBS as negative control.

Biotinylated secondary antibody (rabbit anti-mouse IgG at 1/200, goat anti-rabbit IgG at 1/600 or rabbit anti-goat IgG at 1/600) was applied for 30 min before further 30 min incubation with (Strept) avidin-biotin complex (Dako). Signal amplification reagent was applied if using a CSA (catalysed signal amplification) kit (Dako) to amplify the reactions undetectable using Strept avidin-biotin method. After incubation with Diaminobenzidine (DAB) solution (SigmaFast™ DAB tablets dissolved in 5 mL distilled H_2O), sections were

counterstained with haematoxylin and dehydrated through 70% alcohol, absolute alcohol and 2X xylene. Dehydrated sections were mounted in DPX and covered by glass coverslips (SLS). Sections were visualised on an Olympus BX60 microscope under bright-field illumination with x60 oil immersion objectives. Images were captured and analysed using Image-Pro™Plus software (Media Cybernetics).

2.6.5 TissueGnostics analysis

For sections showing difference between control and test samples, slides were scanned using AxioScan.Z1 slide scanner (Zeiss). The images were captured by the scanner and further analysed with HistoQuest software (TissueGnostics).

Haematoxylin and DAB staining were used as markers of nuclear labelling. After defining the size of nuclei, the staining background and setting of the threshold, the nuclei were picked up by the software. Manual corrections were applied if the nuclei were not selected correctly.

Cut-off value was set based on the DAB staining of positive/negative cell population. Individual cells were linked with corresponding data points and can be visualized by backward gating. Diagram showing the intensity of DAB and the area of nucleus was analysed to determine the cut off. The number of positive DAB staining cells distributed in the upper quadrant was divided by total cell number, which was indicated by area of haematoxylin. The ratio of positive cell number to total cell number was calculated and considered as percentage of positive cell population to further indicate whether the expression of nuclear protein was different between control and treatment.

2.6.6 Immunofluorescence (IF) labelling

Cells were seeded on 12 well slides in chambers of Heraeus boxes (Greiner) and treated for appropriate time as required according to individual experiment. To maintain antigenicity, two fixation methods were used. For methanol/acetone

fixation, slides were washed with methanol/acetone (50:50) for 30 sec and air-dried. For formalin fixation, slides were incubated with 10% formalin for 10 min and permeabilised in 0.1% Triton X100 for 30 min, then washed in PBS.

Primary antibodies (Table 2.6.1) were diluted in TBS with 0.1% (w/v) bovine serum albumin (BSA) and 0.1% NaN_3. Wells on slides were separated using liquid repellent grease pen to confine antibodies in individual wells. Negative wells were filled with TBS only to check for background binding of secondary antibody.

Primary antibodies (Table 2.6.1) were incubated overnight at 4 °C, and then slides were washed with PBS on an orbital shaker. For methanol/acetone fixed slides, another 30 sec methanol/acetone wash was applied before air dry. Secondary antibodies (Alexa Fluor 594 goat anti-mouse IgG (A-11005, Molecular Probes) at 1:700 dilution and Alexa Fluor 488 goat anti-rabbit IgG (A11008, Molecular Probes) at 1:400 dilution) were added on slides after removal of excess PBS or air dry (methanol/acetone fixed slides) and incubated at ambient temperature in the dark for 1 h. Slides were washed in PBS as before, and incubated for 5 min with 0.1 μg /mL Hoechst 33258 in PBS for nuclear staining. Slides were washed in PBS and in distilled water. After air-drying, slides were covered in antifade solution (Appendix 7.4 for recipe), mounted with glass coverslips and sealed with nail polish at the edge. Slides were visualised on an Olympus BX60 microscope under epifluorescent illumination with x60 oil immersion objectives unless otherwise noted. Images were captured using respective channels depending on the secondary antibodies, and analysed with Image-Pro™Plus software (Media Cybernetics). Same exposure time was used for individual antibodies to make sure the amount of fluorescence was related to the amount of protein expressed.

2.6.7 List of antibodies

Antigen	Cat. No	Supplier	Host	Application
Claudin 7	34-9100	Zymed	R	WB 1/1000 IHC 1/100 MW
CK13 (1C7)	MAB1864	Abnova	M	WB 1/1000 IF 1/500 IHC 1/500 MW+Tr
CK14 (LL001)	N/A	Gift	M	IF 1/5
CK14 (LL002)	MCA890	Serotec	M	WB 1/1000
CK20.3	03-61032	Cymbus	M	IF 1:100
CK7	NCL-CK7-OVTL	Novocastra	M	IF 1:40
PPARγ (E8)	sc-7273	Santa Cruz	M	WB 1/500 IHC 1:4000 MW+Tr CSA
PPARγ2	ab45036	Abcam		WB 1/500
PPARγ2 (A-1)	sc-166731	Santa Cruz		IF 1/100
ELF3	ab97310	Abcam	R	IHC CSA 1/750 MW
ELF3	ab133621	Abcam	R*	WB 1/10000 IF 1/1000
HNF-3α (C20)	sc-6553	Santa Cruz	G	IHC 1/150 MW
Claudin 4	32-9400	Zymed	M	WB 1/1000
p-SMAD3 (S423&S425)	ab52903	Abcam	R	WB 1/2000
Active β-catenin(8E7)	05-665	Millipore	M	IF 1/100
Phospho-Akt(Ser 473)	9277	Cell Signaling	R	IF 1:200
p-ERK	9101	Cell Signaling	R	WB 1/1000
Total ERK	610123	Becton-Dickinson	M	WB 1/2000
PPARγ		GSK	M	IF 1/400
E-cadherin (HECD-1)	ab1416	Abcam	M	IF 1/1000
Vimentin (V9)	V6630	Sigma Aldrich	M	IF 1/800
ZO-1	339100	Invitrogen	M	WB 1/500
ZO-3	3704	Cell signaling	R*	WB 1/1000
β-actin	A5441	Sigma Aldrich	M	WB 1/250000

Table 2.6.1 Antibodies utilised in the study. M, mouse; R, rabbit; G, goat. Rabbit monoclonal antibodies were noted with *. Antigen retrieval methods for antibodies used by IHC were noted as MW for microwave heating and Tr for trypsinisation. CSA indicates the CSA kit used for signal amplification. For detailed information, see section 2.6.4. Detailed information regarding two ELF3 antibodies is included in Appendix 7.1.4.

2.7 Establishment of ELF3 modified NHU cell lines

2.7.1 ELF3 over expressing NHU cell lines

ELF3 was amplified from cDNA of NHU cells and enzyme digested using EcoRI and HpaI. The fragment was ligated with digested pGEM-T vector. After transformation into E.coli, positive colonies were selected. Plasmid DNA was extracted and double digested using the same enzymes (EcoRI and HpaI). Gel electrophoresis was performed to detect whether the inserted fragment was the correct size before confirming with DNA sequence.

The ELF3 inserted plasmids were sequenced to confirm the cloning sequence and then double digested with EcoRI and HpaI from pGEM-T vector and ligated into pLXSP vector. The backbone of pLXSP contains a puromycin resistance cassette, which enabled the post-transduction selection. This vector has parts of the retroviral gene integrated, except for the structural genes expressed in the packing PT67 cell line.

PT67 packaging cell line (Clontech) was used for the production of infectious virus, as the essential retroviral genes gag, pol and env were integrated. PT67 cultures at 60% confluency were transfected with 3 μg of plasmid DNA using the Effectene™ Transfection Reagent Kit (Qiagen). At 48h post transfection, cells were sub-cultured into medium with 4 μg/mL puromycin to select transfected cells. A mock transfected flask was included to indicate whether the antibiotic selection succeeded.

PT67 cells were cultured to 100% confluence in DMEM with 10% FBS. On the day before transduction, PT67 cells were washed in Dulbecco`s Phosphate Buffered Saline (DPBS, Life Technologies) followed by medium replacing with DMEM: RPMI (1:1) with 5% FBS to reduce the concentration of serum and calcium. The conditioned medium containing virus was aspirated, filtered

through 0.45 μm Tuffryn filter to remove any cellular debris. With addition of 8 μg /mL polybrene to enhance the transduction efficiency, filtered medium was added to actively proliferating NHU cultures. The medium of transduced NHU cultures was changed to KSFMc 6 h post transduction. NHU cells were selected with 1 μg/mL puromycin after being passaged 48 h post transduction.

Genome of control and ELF3 transduced cells was extracted and analysed by gel electrophoresis to check whether the ELF3 gene was successfully integrated to the genome of NHU cells.

2.7.2 ELF3 knock down NHU cell lines

ELF3 ShRNA was cloned into pSiren-RetroQ plasmid, transfected into PT67 cell line and integrated into NHU cell line by Jenny Hinley before the work started.

Sequence for ELF3 ShRNA is listed below:

- ELF3-ShRNA-01 GCTACCAAGTGGAGAAGAACA
- ELF3- ShRNA-02 GCTCTTCTGATGAGCTCAGTT
- ELF3- ShRNA-03 GCTCAGTTGGATCATTGAGCT

2.8 Statistics

Statistical analysis was performed using InStat3 software (GraphPad). Mean and standard deviation (SD) were used to describe statistics. Error bars on figures represent SD obtained from technical or experimental replicates stated individually.

Data was input to the software before selection of calculating the ANOVA using appropriate method. For data showing relationship between groups, a Bonferroni multiple comparisons post-test was performed; for data indicating the difference between two types, an unpaired t-test was performed. It was considered as statistically significant if the p value was less than 0.05.

Chapter 3 Role of ELF3 in Urothelial Differentiation

3.1 Introduction

3.1.1 ELF3 and its expression in humans

ELF3 (E74-like factor 3) is localised to human chromosome 1q32.2, which is an epithelial cancer-related region associated with breast, lung and prostate cancers (Tymms et al., 1997). The human ELF3 gene contains 9 exons and spans 5.8kb of genomic DNA (Oettgen et al., 1999). ELF3 belongs to the ETS (E26 transformation specific) family, which is a group of proteins sharing a similar ETS domain (35% amino acid identity for the most two divergent proteins) and binds to the conserved core motif (C/A)GGA(A/T) as transcription factors to transactivate target genes (reviewed by Wasylyk et al., 1993).

ELF3 is expressed by epithelial tissues, and particularly the lung in human fetal tissues and small intestine in adult tissue, illustrating a specialised expression associated with tissues showing a high content of epithelial cells (Oettgen et al., 1997). It is not expressed in hematopoietic organs like spleen and thymus or peripheral blood lymphocytes, which distinguishes ELF3 from other ETS family proteins (Oettgen et al., 1997; Tymms et al., 1997).

The tissue specificity of ELF3 also limits its transcriptional activity. Andreoli et al. showed that transcriptional activity of terminal epidermal differentiation markers like TGM3 (transglutaminase 3) and profilaggrin genes were up-regulated by ELF3 only in epithelial primary cells or cell lines. The transactivation by ELF3 was more prominent in normal human epidermal keratinocyte (NHEK) cultures with high calcium (Andreoli et al., 1997). These findings suggest that ELF3 is massively involved in regulating differentiation in epithelial cells.

3.1.2 Structure of ELF3

3.1.2.1 Cis-regulatory elements on ELF3 genes

The 5'-flanking region of ELF3 genes has been implicated as an upstream regulatory region with binding motifs of other transcription factors. A CCAAT box, an ESE (ERT promoter specific element) and a NF-κB site were found both in human and murine ELF3 sequence (Hou et al., 2004; Oettgen et al., 1999; Park et al., 2001). The ESE site at -186 to -183 in human ELF3 acted as an enhancer element and was essential for promoter activity of ELF3 in a human gastric cancer cell line expressing ELF3 (Park et al., 2001). A 94bp DNA sequence 2kb upstream of the transcription start site was sufficient to elevate the promoter activity of murine ELF3 in F9 differentiated EC (embryonal carcinoma) cells, although the sequence showed no consensus with any known eukaryotic transcription factors (Hou et al., 2004). So far no reports confirmed any site for known transcription factors within this 94bp sequence. The findings suggest that ELF3 has essential elements in its promoter or enhancer region, which facilitates the regulation by other transcription factors.

3.1.2.2 Trans-activation by ELF3 and functions of different ELF3 domains

To analyse the function of particular regions in full length murine ELF3 protein (371 amino acids, 89% identity and 93% similarity to human ELF3 cDNA (Tymms et al., 1997)), reporter assay was utilised on TGFβRII (type II transforming growth factor receptor) with point mutated ELF3 proteins in differentiated mouse F9 EC cells (Kopp et al., 2007), as it was shown that transactivation of TGFβRII, which contains two ETS sites, was regulated by ELF3 in differentiated mouse F9 EC cells (Kopp et al., 2004). Several domains common to other ETS family members or other factors are shown with different colours in Fig 3.1.1.

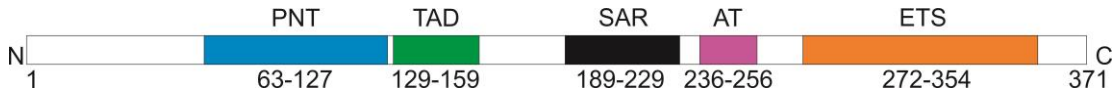

Fig 3.1.1 Domains of murine ELF3 cDNA. Diagram adapted from (Kopp et al., 2007). N and C indicate two terminals. Numbers indicate the amino acids counted from N terminal. PNT, pointed domain. TAD, transactivation domain. SAR, serine- and aspartic acid-rich domain. AT, A/T hook domain. ETS, E26 transformation specific domain.

Site-directed mutations on three different helixes in the ETS domain (orange part in Fig 3.1.1, 272th-354th amino acid, 100% identical to human ELF3 cDNA (Tymms et al., 1997)) led to a complete loss of TGFβRII promoter activity, whereas mutations in between the helix did not affect the ability of transactivation of TGFβRII by ELF3 (Kopp et al., 2007). The regions flanking the ETS domain in ELF3 cDNA at both the N-terminal and the C-terminal played an essential role for ELF3 binding to the ETS motifs, as the deletion of part or all of either side disrupted the transactivation (Kopp et al., 2007).

In addition to an ETS domain, ELF3 has a unique A/T hook domain (pink part in Fig 3.1.1). Role of A/T hook domain (236th-256th amino acid) in transcriptional activation is promoter specific, as deletion of A/T hook domain in ELF3 did not affect the transactivation of TGFβRII, but reduced the promoter activity of collagenase-1(contains only one ETS site) and mutated TGFβRII promoter containing only one ETS site (Kopp et al., 2007). This A/T hook domain is common to a series of nuclear factors, particularly HMG (high mobility group) proteins (Oettgen et al., 1997), which are the second most abundant chromatin proteins after histones. One important feature of the HMG proteins is that they play important roles in regulating transcription and differentiation. A subgroup of HMG protein called HMGA proteins are expressed mostly during embryonic development (Bianchi and Agresti, 2005). The structural homology of ELF3 and HMG proteins may suggest a potential role of ELF3 in embryonic development.

A serine- and aspartic acid-rich (SAR) domain (black part in Fig 3.1.1, 189th - 229th amino acid) was significantly essential for ELF3 to regulate the activity of TGFβRII promoter. (Kopp et al., 2007).

Removal of the TAD (transactivation domain, green part in Fig 3.1.1, 129th-159th amino acid) increased the ability of ELF3 binding to TGFβRII promoter. Specifically, point mutations of leucine 142 or tryptophan 137 to proline within the TAD domain led to the increased binding ability (Kopp et al., 2007).

Mutation of PNT domain (pointed domain, blue part in Fig 3.1.1, 63th -127th amino acid), which was verified as a protein- protein interaction dependent domain in other ETS family proteins (Foulds et al., 2004; Seidel and Graves, 2002), did not affect the transcriptional activity of ELF3 on TGFβRII promoter, indicating a direct regulation of TGFβRII by ELF3 (Kopp et al., 2007). Table 3.1.1 summarised the essentiality of domains on mELF3 proteins.

Domains	PNT	TAD	SAR	AT	ETS
Influence	Not affected	Binding ↑	Transcriptional ↓	Transcriptional ↓*	Transcriptional ↓

Table 3.1.1 Influence of mELF3 domains. Either the binding activity or transcriptional activity was assessed when certain domain was mutated or deleted. Increased activity was shown by ↑; decreased activity was shown by↓. * suggested a promoter specific influence.

3.1.3 Requirement of ETS motif when regulating target genes by ELF3

To be trans-activated by ELF3, ETS motifs in promoters or enhancers of genes were essential. Band shift assay demonstrated that ELF3 could bind to ETS motif of TGM3 (transglutaminase 3) but not mutated motifs, which indicated that the ETS binding site was critical for binding of ELF3 (Andreoli et al., 1997).

Some other reports also demonstrated the regulation on epithelial-related genes by ELF3. In human keratinocytes cultured *in vitro*, transcript expression of ELF3 accumulated dramatically at 12h after induced differentiation by treating keratinocytes with calcium and serum. Simultaneously, increased ELF3 up-regulated transcript expression of SPRR2A, which is a terminal differentiation marker in keratinocytes with ETS motif on its promoter. At 24h, ELF3 increased the transcript expression of CK8, which is primarily expressed in epithelial cells

and contains ETS sites on its enhancer. The transcriptional regulation on SPRR2A and CK8 by ELF3 was conducted by directly binding to the ETS binding sites, as mutants of ETS domain in SPRR2A or CK8 reduced dramatically the transcriptional activity induced by ELF3 (Oettgen et al., 1997).

Similarly, ELF3 was able to bind to the ETS motif at -150bp of CLDN7 promoter and directly regulate the transcriptional activity of CLDN7 in human synovial sarcoma tumor tissue and cell lines with epithelial structure. Mutations on the ETS motif in CLDN7 abolished the transactivation. Transcript expression of CLDN7 was simultaneously decreased along with knock down of ELF3 in a 120h time course. De novo transcript expression of CLDN7 was induced by exogenous ELF3 at 48h, but there was no CLDN7 protein accumulation, which suggested that the ETS motif was essential for regulating of target genes like CLDN7 by ELF3, but the regulation was not sufficient. Other factors may also be involved in determining the expression of CLDN7 (Kohno et al., 2006).

Taken together, these findings suggest that ELF3 was associated with regulating epithelial-related genes, and was able to bind to ETS motif in promoters or enhancers of target genes when mediating transactivation directly, in which case, any mutation would abolish the ability of regulating by ELF3.

3.1.4 Regulating differentiation from embryonic development to tissue regeneration

As a transcription factor, roles of ELF3 regulating its target genes has been reported in various tissues or cells, a majority of which were induced to differentiate, suggesting a central role of ELF3 in regulating differentiation.

This importance in regulating differentiation by ELF3 was found in embryonic development. It is reported that in early development of mouse gastrointestinal tube, ELF3 was not essential. On embryonic day E17.5, however, the ELF3-

deficient embryos showed a delay in the formation of villi, the villi are fewer and abnormally shaped as well. Dysfunction of ELF3 led to abnormal phenotype of enterocytes compared to the wild type ones in mice embryo cells. The sialomucin (nonsulfated acidic mucin glycoproteins) secreted by goblet cells also reduced significantly in both duodenum and ileum, suggesting the requirement of ELF3 in morphogenesis and maturation of cells in mouse small intestine.

In vivo experiment demonstrated that expression of TGFβRII was reduced in ELF3 deficient mice, which verified the *in vitro* study showing TGFβRII as a potential target of ELF3 and the expression of TGFβRII was directly regulated by ELF3 (Ng et al., 2002). Exogenous expression of the TGFβRII transgene in small intestinal epithelium of ELF3-null mice restored the morphogenesis of small intestine and enabled the differentiation and polarization of enterocytes. With restored TGFβRII in ELF3 deficient mice, goblet cells were able to synthesise acidic mucins as normal enterocytes, which supported the important role of ELF3 as a regulator of TGFβRII expression in intestinal development (Flentjar et al., 2007).

Another report regarding a role of ELF3 in embryonic development demonstrated the expression of ELF3 in cornea epithelium on embryonic day E16.5 by in situ hybridization in mouse. Localisation and expression of ELF3 demonstrated a similar pattern compared to CK12, which is a cornea differentiation marker, suggesting that ELF3 was involved in corneal epithelial cell differentiation. Forced expression of ELF3 antisense RNA led to a significant ($P<0.05$) reduction of differentiated human corneal epithelial (HCE) cells (Yoshida et al., 2000), indicating a crucial role in regulating differentiation in cornea epithelium.

ELF3 was also shown as an important factor involved in regulating regeneration of damaged tissue. The renewal of Clara cells (also known as

bronchiolar exocrine cells) was delayed in ELF3 knockout mice compared with normal mice. Following Clara cell damage, cell proliferation and mitosis was postponed in the bronchiolar airway epithelium of ELF3 deficient mice. TGFβRII protein was up-regulated significantly in the repair process in ELF3 positive mice, but maintained a low level in ELF3 deficient mice, implicating participation of ELF3 during airway injury repair (Oliver et al., 2011).

In *E. coli* infected mouse bladder urothelium, expression of ELF3 increased rapidly at 1.5h only after inoculation of FimH+ strain but not FimH- strain. An ELF3 target gene, iNOS, was significantly accumulated at transcript level and acted as the host defense response to FimH+ UPEC infection (Mysorekar et al., 2002).

3.1.5 Requiring other factors to regulate target genes by ELF3

When regulating expression of target genes, other factors were found to be recruited to enhance the effect of ELF3. In human skin, ELF3 was shown to cooperate with Oct 11, up-regulating the transcription of SPRR2A in a synergistic dose-dependent manner (Cabral et al., 2003).

In intestinal epithelium, Crif (CR6-interacting Factor) 1 was reported to regulate the development and differentiation of the cells. Crif1 interacted with ETS domain (Not PNT domain which is associated with protein-protein binding) and increased the DNA binding activity of ELF3, which further regulated the promoter activity of TGFβRII. Knock out of Crif1 led to similar morphology and function of intestinal cells compared to ELF3 knock out mice, implicating possibly a central role of ELF3 but requiring co-activator in mediating intestinal differentiation (Kwon et al., 2009).

In human esophageal squamous epithelium, ELF3 was able to enhance the transcriptional activity of SPRR2A. However, promoter activity of CK4, representing early differentiation of the esophageal squamous epithelium, was

repressed by ELF3. Deletion of various regions in the CK4 promoter did not reverse the suppression of transcription activity, indicating that ELF3-regulated repression may not be caused directly by binding to the promoter region. A PNT domain (pointed domain) deletion of ELF3 in the N-terminal amino acids was able to reverse the suppression of the CK4 promoter activity, whereas deletion of ETS domain only partially rescued the suppression (Brembeck et al., 2000). This finding indicated a dual role of ELF3 in regulating the early differentiation and the involvement of other proteins in mediating downstream target in esophageal squamous epithelium, as PNT domain has been implicated in protein-protein interaction in other ETS family proteins (Foulds et al., 2004; Seidel and Graves, 2002).

3.1.6 Signalling pathways mediated ELF3 regulation

Apart from recruitment of co-factors, the regulation of target genes by ELF3 was reported to be mediated by signalling pathways. Otero et al. recently found that in human primary osteoarthritis (OA) articular chondrocytes, ELF3 regulated MMP13 (Matrix metalloproteinase 13) expression, which was indirectly affected by MAPK pathway activity (Otero et al., 2012). MMP13 is a key factor associated with cartilage remodelling and degradation. In human primary OA chondrocytes, IL-1β treatment increased the expression of ELF3 and endogenous ELF3 binding to MMP13 promoter, which was further transactivated by enhanced expression of ELF3. The transactivation of the MMP13 promoter was also enhanced by overexpression of MEK1/ERK1 in chondrocytes. Such enhancement of MMP13 promoter regulation by ELF3 after IL-1β treatment was reduced significantly by inhibition of MEK/ERK signalling pathway. Also, MKP1 (MAPK phosphatase 1), acted as a repressor of MAPK mediated pro-inflammatory in airway smooth muscle cells (Manetsch et al., 2012), reduced ELF3-induced MMP13 activation (Otero et al., 2012). These findings indicate the regulation by ELF3 in inflammation was via a MAPK-mediated pathway.

3.1.7 Involvement of ELF3 in cancer development

Several reports have shown the involvement of ELF3 during cancer development, but the role of ELF3 is not consistent. In human prostate cancer, ELF3 repressed androgen receptor (AR) mediated transcriptional activity by interacting with AR directly, and further impaired the ability for AR to be recruited to target genes with specific ARE binding sites. Knock down of ELF3 reversed the suppression and increased migration of LNCaP (androgen-sensitive human prostate adenocarcinoma) cells. Tumour growth was inhibited by ELF3 expression in mouse xenograft model, suggesting an anti-cancer role of ELF3 in prostate cancer (Shatnawi et al., 2014).

In human breast cancer cell line Hs578T over-expression of ELF3 dramatically increased endogenous expression of TGFβRII and reduced the growth of Hs578T cells by 50% in presence of exogenous TGFβ1. Time of forming tumours was delayed in nude mouse inoculated with ELF3 over-expressing Hs578T cells compared to control Hs578T cells. The size of xenograft tumour decreased to 30% (Chang et al., 2000). But whether this cancer cell growth and tumour formation inhibition was related to the regulation of TGFβRII by ELF3 or the expression of ELF3 directly was not further investigated.

Another report suggested that endogenous ELF3 was restricted to the cytoplasm in human breast cancer T-47D cell line and normal breast tissue, but its protein was nuclear in transiently-transfected MCF-12A cells. This nuclear localization induced apoptosis in MCF-12A and MCF-10A cells. Deletion of the ELF3 TAD domain impaired its apoptotic function (Prescott et al., 2004).

However, other reports indicate a carcinogenesis role of ELF3. In breast cancer, frequent copy number amplification at 1q21 and 1q32 indicated three ETS genes, one of which is ELF3. 1q21 and 1q32 were the two chromosome bands showing the most frequent genomic copy number gains among 141 breast carcinomas by

chromosomal CGH (comparative genomic hybridisation) (Mesquita et al., 2013).

Also, in cervical carcinomas, 13% of somatic mutation was observed in 24 samples of adenocarcinoma. Frame shift insertional events were found in AT/hook domain and ETS domain, suggesting ELF3 might be involved in development of epithelial cancers (Ojesina et al., 2014). In bladder cancer, ELF3 was reported to have 8% mutation, which was statistically significant and mostly occurred in papillary tumours (Cancer Genome Atlas Research, 2014).

These contrary reports indicate different roles of ELF3 implicated for cancer. Further investigation is still required to verify the link between expression alteration of ELF3 and development of cancer.

3.1.8 Summary

Studies of ELF3 in various tissues, primary cells and cell lines demonstrated a major role of ELF3 in regulating epithelial differentiation. ELF3 was also involved in other cellular activities by interacting with other transcription factors or directly binding to the promoter of its potential targets, with ETS binding site especially. Detailed mechanism is not completely investigated, thus requires further research, which would provide implication towards tissue development, cell differentiation, host defence and cancer therapy.

3.2 Experimental approach

3.2.1 Aims and hypothesis

The aims for this chapter were to characterise the expression pattern of ELF3 in normal human urothelial tissues and cells and investigate whether it is a differentiation-related transcription factor in urothelium, which would affect the function of urothelial cells when the expression of ELF3 was modified in NHU cells.

The hypothesis is that as a transcription factor regulating differentiation, ELF3 would alter the phenotype of proliferating NHU cells to a differentiated phenotype when it was over expressed *in vitro* in NHU cells.

3.2.2 Differentiation-associated markers

To indicate the phenotype of urothelial tissues or NHU cells cultured *in vitro*, differentiation-associated genes/proteins were investigated either by RT-QPCR for transcript expression or by other approaches (Western blotting (WB), immunohistochemistry (IHC), and immunofluorescence (IF)) for protein expression. Table 3.2.1 displays applications for each individual marker assessed.

Name	Transcript	Protein (WB)	Protein (IHC)	Protein (IF)	Function
CK13		√	√	√	Urothelial differentiation
CK14		√			Squamous
CK20	√			√	Terminal urothelial differentiation
CLDN4		√			Late urothelial differentiation
CLDN7	√	√	√		Target of ELF3
UPK2	√				Terminal urothelial differentiation
UPK3A	√				Terminal urothelial differentiation
ZO1		√			Urothelial differentiation
ZO3		√			Terminal urothelial differentiation

Table 3.2.1 Applications performed for examining of differentiation-associated markers. Functions showed the general role of these genes/proteins in urothelium. Checks (√) indicate the assessed application for individual markers.

3.2.3 Expression profile of ELF3 in human urothelium

To demonstrate the expression profile of ELF3 in situ, immunohistochemistry was performed using formalin-fixed paraffin wax embedded sections of urothelial tissue.

To study which factors affected the expression of ELF3, NHU cell cultures were treated for a time course (6h, 24h and 96h) with DMSO (vehicle control), TZ, PD153035 or TZPD. Transcript expression of differentiation-associated genes and transcription factors (ELF3 and FOXA1) was examined by RT-QPCR. PPARG2 was assessed as one of the PPARγ transcript variants (chapter 5 for detailed information).

Expression of ELF3 protein was assessed by immunofluorescence on vehicle control (DMSO) or TZPD treated NHU cells. Protein expression of CK13 and CK20 was used as positive control to demonstrate that TZPD-treated NHU cells had undergone transitional differentiation.

3.2.4 Genetic modification of ELF3 expression in NHU cells

In order to understand whether ELF3 is important in regulating differentiation, the expression of ELF3 in NHU cells was modified by manipulating the genome of NHU cells using retroviral integration.

Retroviral transduction was performed either with shRNA pSiren-retroQ system to knock down the expression of ELF3 or with ELF3 cDNA ligated into pLXSP vector to increase its expression. To knock down ELF3 expression, scrambled shRNA that did not target specific genes was integrated in parallel to ELF3 shRNA as an experimental control. For ELF3 over expression, full length of ELF3 coding sequence inserted into pLXSP vector and transfected into PT67 packaging cells was performed in parallel to empty pLXSP vector as control. After selection with puromycin, conditioned medium containing retroviral particles from cultured PT67 cells was aspirated and added to proliferating NHU cells. NHU cells were selected with puromycin until the mock transduced cells died.

Assessment of changes in ELF3 expression was performed by RT-PCR before further experiments performed. Growth assays were performed to study the effect of ELF3 modification on cell proliferation in retroviral integrated NHU cells using the Alamar Blue assay.

3.2.5 Effect of ELF3 knock down on NHU cells

Transcript expression of ELF3 was examined to indicate whether the modified expression was successful. RT-PCR was performed to show the alteration of ELF3 transcript expression. RT-QPCR was utilised to quantify the altered expression of ELF3 transcript. For assessment of ELF3 knock down, scrambled shRNA control and ELF3 shRNA knock down NHU cells were treated with TZPD to differentiate for a time course (12h, 24h, 48h and 72h). 72 hours treatment was selected for RT-QPCR, as the transcript expression in the control was the most abundant in the time course. Transcript expression of other

transcription factors (ELF3, GRHL3, IRF1, FOXA1 and KLF5) and differentiation-associated genes was examined.

To indicate the impact of ELF3 expression on urothelial differentiation, the ability to form a functional barrier was assessed using cell sheets constructed from ELF3 knock down and scrambled control cell sheets. NHU cells were induced to differentiate and form cell sheets using the ABS/Ca^{2+} method and assessed to demonstrate the formation of a functional barrier. TER measurements indicating the barrier of stratified cell sheets were taken every day for control and ELF3 knock down NHU cells. Scratch wound healing assay was performed after the values of TER stabilised to show the recovery time of damaged cell sheets. During the healing process, images of cultures were captured at different time points to illustrate the relative closure of the scratch wound.

Stratified cell sheets (scrambled shRNA control and ELF3 knock down) were harvested intact using dispase and then fixed and embedded in paraffin wax to investigate the effect on expression of differentiation-associated proteins by IHC when ELF3 was down regulated. Expression of transcription factors PPARγ and FOXA1 along with ELF3 was examined to show the effect of ELF3 knock down. CK13 and CLDN7 were included to demonstrate the polarisation of cell sheets and show the effect of ELF3 knock down on differentiation-associated proteins.

Differentiation-associated proteins were assessed by western blotting to demonstrate the effect of ELF3 knock down. Scrambled shRNA control and ELF3 shRNA knock down cells were pre-treated with 5% ABS and seeded on 60mm dishes; medium was replaced with 5% ABS and 2mM calcium the next day. Cultures were harvested after 2 days, 4 days and 6 days of incubation. Expression of ELF3 was examined by immunoblotting to indicate the knock down effect on protein expression. PPARγ protein was also assessed to verify

the effect of ELF3 knock down observed by IHC. Downstream proteins CLDN4 and CLDN7 were examined to indicate the effect of ELF3 knock down. Phosphorylated SMAD3 was assessed to suggest whether the delay of wound closure was associated with TGFβ pathway (Fleming et al., 2012).

3.2.6 Effect of ELF3 over-expression on NHU cells

To determine whether ELF3 was over-expressed, transcript expression of ELF3 was assessed in both empty vector control and ELF3 over-expressed NHU cells. In order to explore the effect of TZPD on ELF3 over-expressed cells, control and ELF3 over-expressed cells were induced to differentiate by TZPD for 6h to indicate whether the effect of TZPD was magnified by ELF3 over-expression. Transcript expression of PPARG2, IRF1, GRHL3 and FOXA1 genes was examined.

To further testify the role of ELF3 in urothelial differentiation and the hypothesis, western blotting was performed to indicate whether over-expression of ELF3 would alter the phenotype of proliferating NHU cells. Lysates from proliferating NHU cells integrated with ELF3 were utilised to first verify the integration of ELF3 into NHU cells and to illustrate the phenotype of proliferating NHU cells integrated with either empty vector or ELF3 full length cDNA.

The importance of ELF3 was also assessed by examining differentiation-associated proteins in ABS and/or calcium induced NHU cells. Empty vector control and ELF3 over expressed NHU cells were seeded in 35mm dishes, and treated with ABS alone, calcium alone or combined ABS/calcium for a time course. Protein expression of both transcription factors and differentiation-associated markers was analysed. Expression of ZO proteins (ZO1 and ZO3) was assessed to indicate the differentiated barrier phenotype. ZO1α^+ and ZO1α^- are two isoforms of ZO1 proteins. Increased expression of ZO1α^+ should suggest a more differentiated barrier phenotype (Smith et al., 2015).

3.3 Results

3.3.1 Expression and localisation of ELF3 *in situ*

In urothelial tissue, ELF3 was expressed in the nuclei of all layers of urothelial cells in the ureter. Occasionally absent expression of ELF3 was observed in dispersed urothelial cells (Fig 3.3.1, noted by arrows). CLDN7 showed intercellular junction expression in basal, intermediate and superficial layers (Fig 3.3.1). Expression of CK13 was confined to the cytoplasm in basal and intermediate layers and was absent from superficial cell layer (Fig 3.3.1).

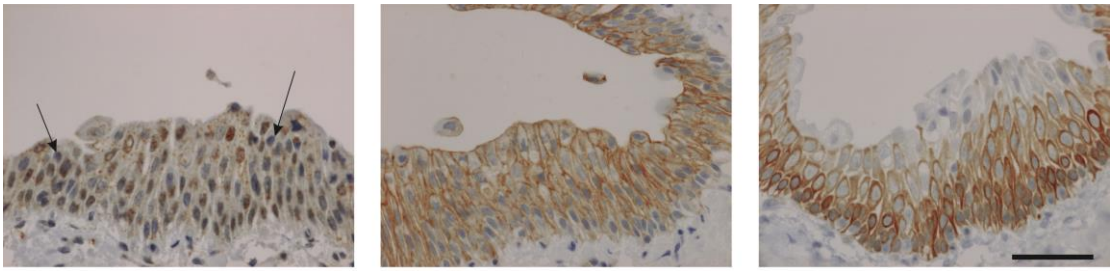

Fig 3.3.1 Expression of differentiation-associated proteins in urothelial tissue (Ureter, Y1233). Immunohistochemistry labelling was performed following IHC protocol with primary antibodies specific to ELF3, CLDN7 and CK13, respectively. Arrows indicate absent expression of ELF3 in some nuclei. Scale bar equals 50μm.

3.3.2 Expression and localisation of ELF3 in NHU cells *in vitro*

3.3.2.1Transcript expression

NHU cells were treated with DMSO, TZ, PD153035 and TZPD for a time course. Transcript expression of ELF3 was significantly synergistically up-regulated by TZPD combined treatment and increased over time, suggesting that ELF3 was induced following *in vitro* differentiation of NHU cells by activation of PPARγ. The accumulation was dramatic at 96h by TZPD treatment. PD153035 alone increased the expression of ELF3, which was not significant though. In vehicle control (DMSO) treated cells, low but still noticeable expression of ELF3 was observed after 96h growth in culture. Transcript expression of FOXA1 was up-regulated significantly by activation of PPARγ after 6h of treatment. It increased dramatically at 24h but decreased slightly afterwards. The increase

was significant in all time points by TZ only and TZPD, which may suggest its direct regulation by PPARγ. The transcript expression of PPARG2 was up-regulated at 6h by TZPD and decreased at late time point (Fig 3.3.2).

Elevation of UPK2 and CK20 transcript expression indicated that differentiation of NHU cells was achieved by TZPD at 96h. CLDN7 showed similar transcript expression pattern as ELF3 (Fig 3.3.2).

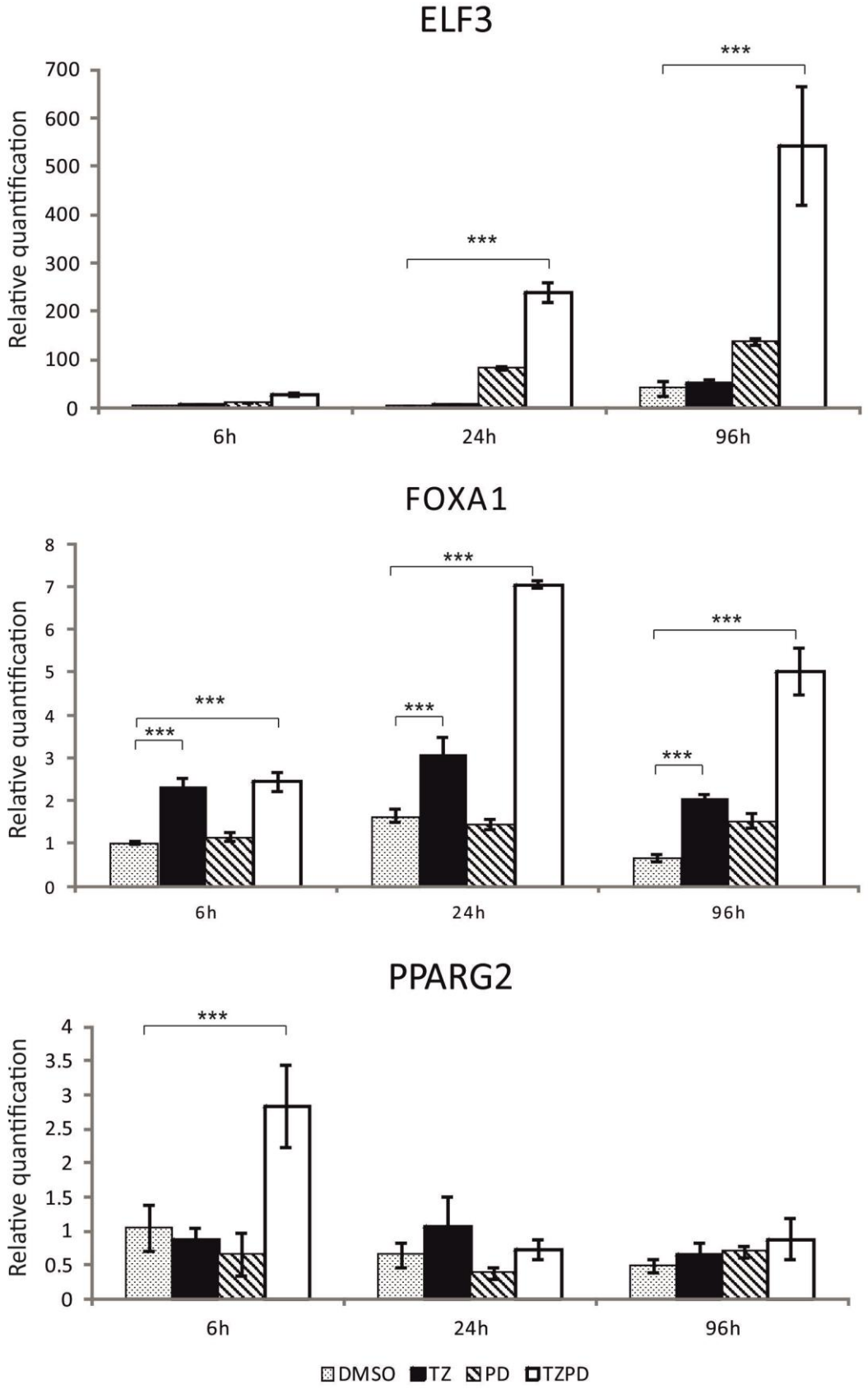
ELF3
Relative quantification
700
600
500
400
300
200
100
0
***
***
6h
24h
96h
FOXA1
Relative quantification
8
7
6
5
4
3
2
1
0
***
***
***
***
***
6h
24h
96h
PPARG2
Relative quantification
4
3.5
3
2.5
2
1.5
1
0.5
0
***
6h
24h
96h
DMSO
TZ
PD
TZPD

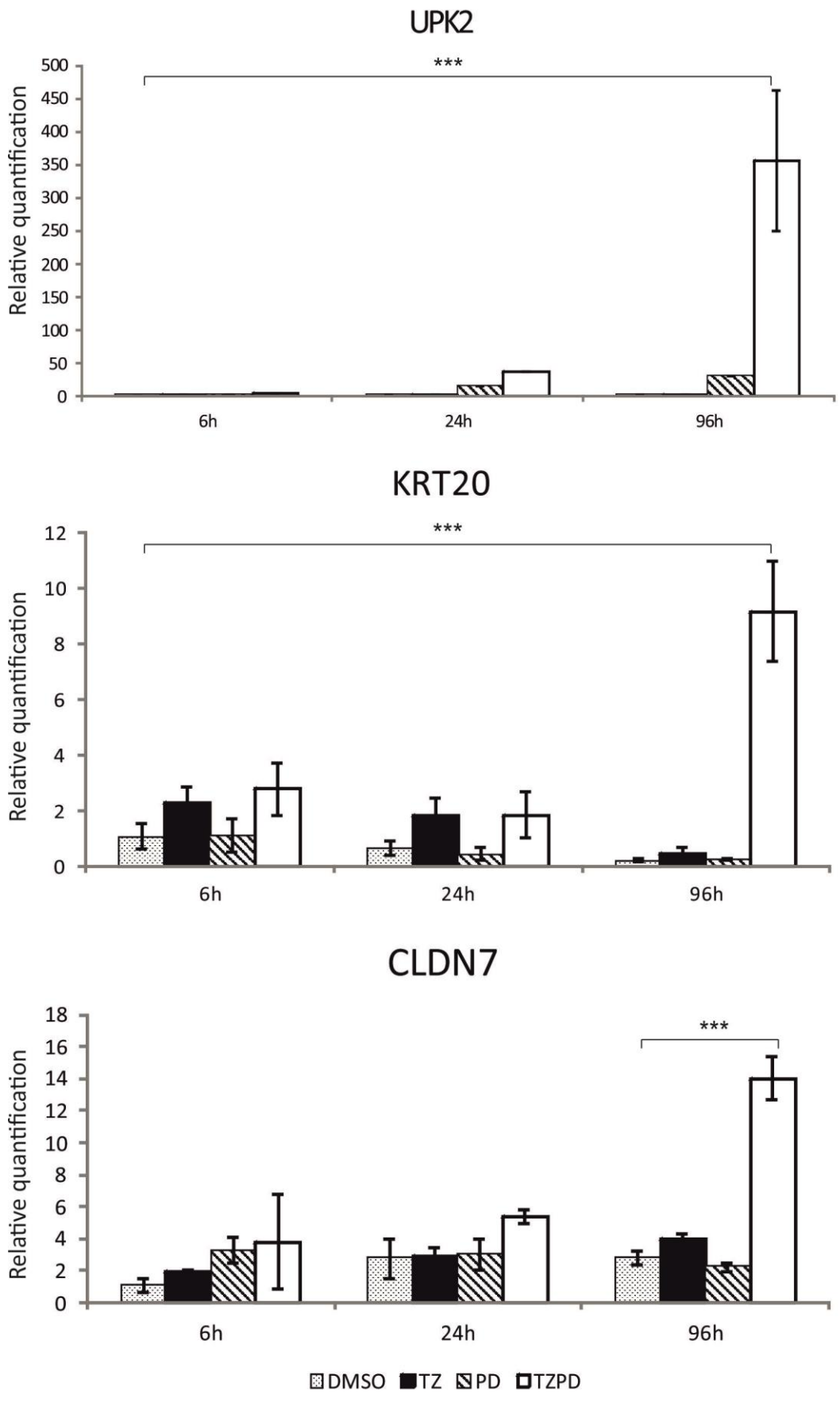
UPK2
***
Relative quantification
500
450
400
350
300
250
200
150
100
50
0
6h
24h
96h
KRT20
***
Relative quantification
12
10
8
6
4
2
0
6h
24h
96h
CLDN7
***
Relative quantification
18
16
14
12
10
8
6
4
2
0
6h
24h
96h
DMSO
TZ
PD
TZPD

Fig 3.3.2 Transcript expression of transcription factors and differentiation-associated genes in NHU cells (Y1194) pharmacologically induced to differentiate. Cells were treated with vehicle control (DMSO, 0.1%), TZ (1μM), PD153035 (1μM) or TZPD (1μM) for 6h, 24h and 96h. RT-QPCR was performed as described in the method. Transcript expression of ELF3, FOXA1, PPARG2, UPK2, CK20 and CLDN7 was normalized to expression of GAPDH in each sample. Fold changes were obtained by comparing to 6h DMSO treated control. Error bars indicate the standard deviation of three technical replicates. Statistical analysis was calculated by one-way ANOVA with Bonferroni multiple comparisons post-test (*** P<0.001).

3.3.2.2Protein expression by immunofluorescence

Immunofluorescence showed that ELF3 was diffuse and the expression was low but unequivocal in proliferating cells, whereas in differentiated NHU cells ELF3 was mainly localised in the nuclei (Fig 3.3.3). However, several cells showed low expression even in differentiated NHU cells, which was consistent with localisation of ELF3 in urothelial tissues (Fig 3.3.3, indicated by arrowhead).

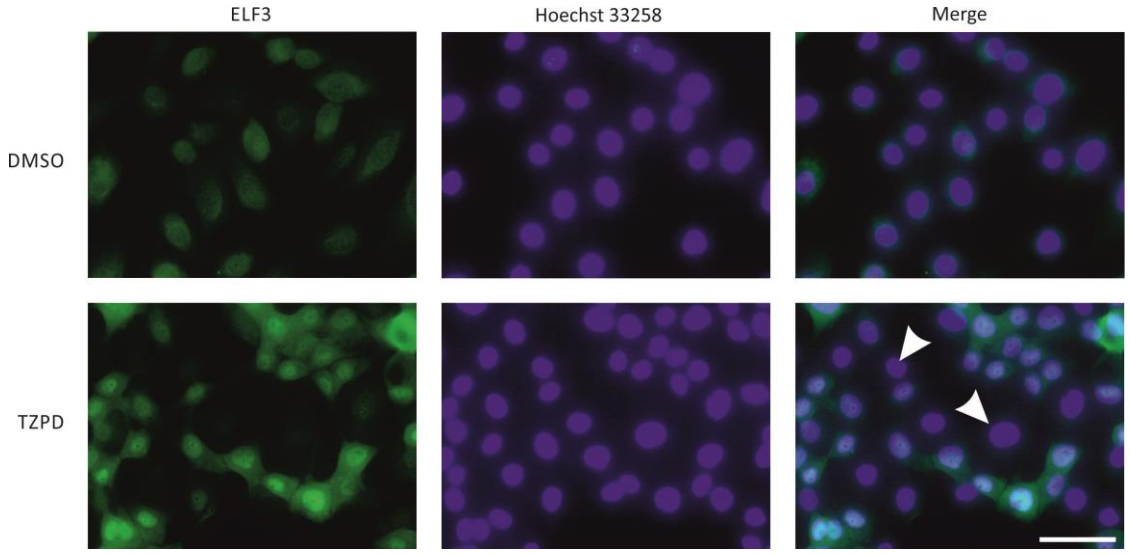

Fig 3.3.3 Expression and localisation of ELF3 in proliferating and differentiated NHU cells (Y1436). Cells were treated with either DMSO (0.1%) or TZPD (1μM) for 4 days. Slides were fixed using 50:50 Methanol/Acetone fixation and incubated with ELF3 primary antibody following immunofluorescence protocol. Hoechst 33258 was used to stain the nuclei. Pictures were taken with constant exposure time for comparison. Colour information was extracted from each channel and merged to a new image (Merge). Scale bar represents 50μm. Note, low expression of ELF3 pointed by arrowheads in some differentiated cells.

A differentiated phenotype was demonstrated by expression of CK13 and CK20 in TZPD differentiated NHU cells. CK13 was localised to the cytoplasm of differentiated cells, indicating a transitional differentiated phenotype of NHU cells (Fig 3.3.4). CK20 was only present in some cells indicating a terminal

differentiated phenotype. The expression of CK20 was less than that of CK13, as it is a late differentiation marker.

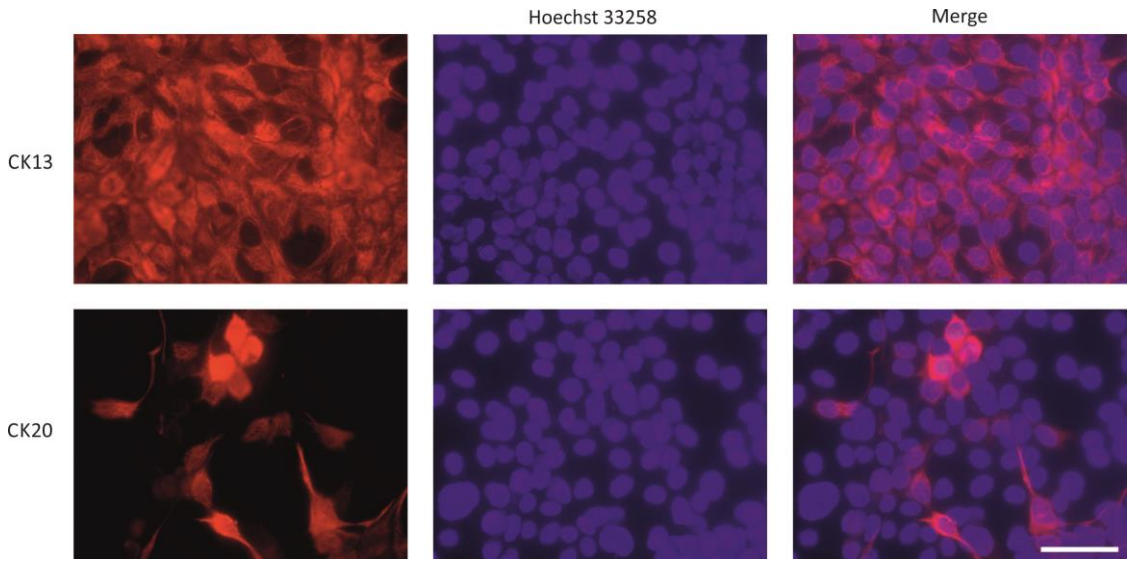

Fig 3.3.4 CK13 and CK20 proteins in NHU cells (Y1116). Primary antibodies for CK13 and CK20 were applied on cells treated with TZPD for 72h and fixed using Me/Ac method. Hoechst 33258 was used to stain the nuclei. Colour information was extracted from each channel and merged to a new image (Merge). Scale bar represents 50μm.

3.3.3 Effect of ELF3 knock down on NHU cells *in vitro*

3.3.3.1 Verification of ELF3 knock down

ELF3 knock down NHU cells were generated using shRNA retroviral integration. Transcript expression of ELF3 was up-regulated following TZPD induced differentiation and accumulated mostly at 72h. Knock down of ELF3 by retroviral integration in NHU cells reduced the transcript expression of ELF3. The most efficient knock down effect was obtained after 72h TZPD treatment, to about 60% of its original transcript amount. It appeared that there was no knock down effect at 12h, which might be due to the low amount of transcript expression of ELF3 (Fig 3.3.5).

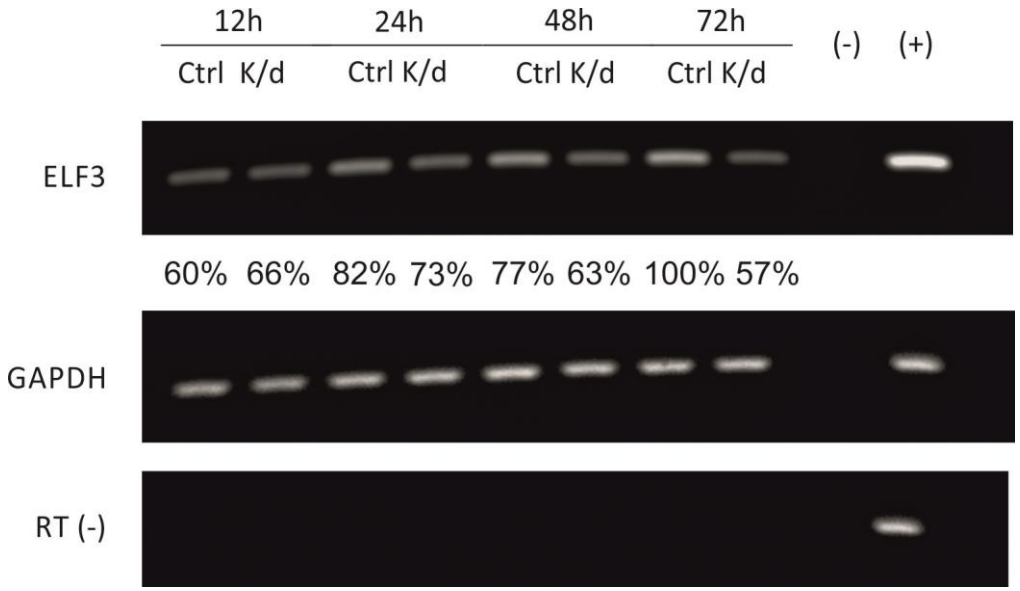

Fig 3.3.5 Transcript expression of ELF3 in scrambled shRNA control (Ctrl) and ELF3 knock down (K/d) NHU cells (Y1117). Cultures were harvested after incubation with TZPD (1μM) for 12h, 24h, 48h and 72h. The transcript expression was shown as percentage compared to the expression of ELF3 after 72h TZPD treatment after normalisation to the amount of GAPDH in each sample. Densitometry of each band was measured using Image J software. No reverse transcription enzyme was added in RT (-) samples. GAPDH showed the equal amount of cDNA and was included as internal control. Water or genomic DNA was utilised as template in (-) and (+) samples, respectively.

Control and knock down cells were induced to differentiate by TZPD for 72h, at which point the knock down of ELF3 was most effective. RT-QPCR result showed that after induction of a differentiated phenotype, knock down of ELF3 was significant at transcript level to around 40% of control sample. Transcript expression of GRHL3, IRF1 and FOXA1 was reduced significantly by ELF3 knock down to about 50%. Knock down of KLF5 transcript expression was about 40% and less significant. As a potential target of ELF3, transcript expression of CLDN7 was significantly knocked down to 30% of control sample (Fig 3.3.6A).

The amount of UPK3A transcript was similar in control and ELF3 knock down cells and relatively low compared to GAPDH. The effect of ELF3 knock down was not significant on UPK3A. Transcript expression of KLF5 was the most abundant among candidate genes in TZPD differentiated NHU cells (Fig

3.3.6B), suggesting its essential role in regulating differentiation, but may not be an ELF3 downstream transcription factor.

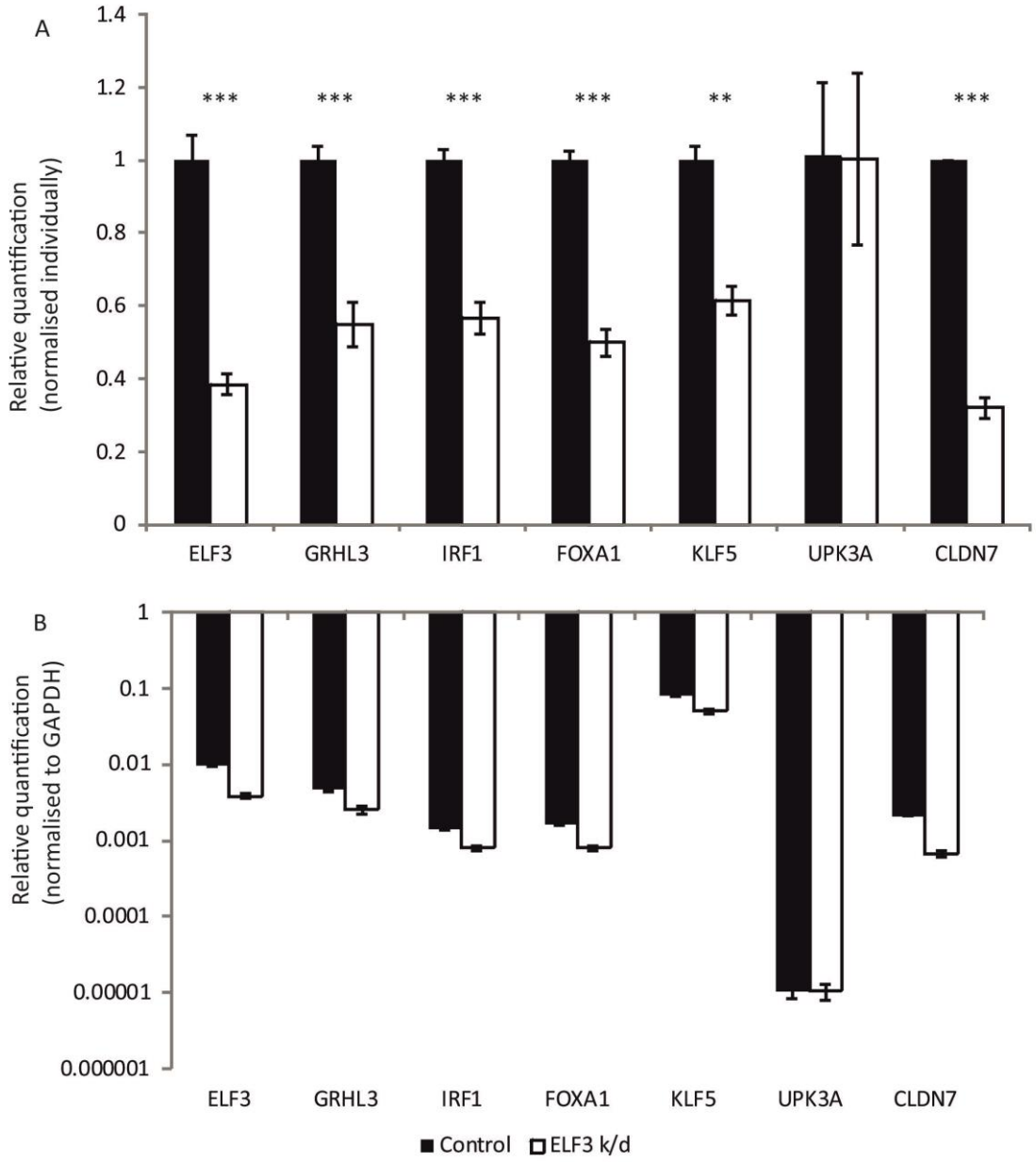

Fig 3.3.6 Transcript expression of candidate genes (Y1117). (A) Scrambled shRNA control (Control) and ELF3 knock down (ELF3 k/d) cells were incubated with TZPD (1μM) for 72h. RT-QPCR was performed following the protocol. Transcripts of GAPDH in both control and knock down samples were used as internal control for comparison of expression of other genes. Transcript expression of ELF3, GRHL3, IRF1, FOXA1, KLF5, UPK3A and CLDN7 was calculated and displayed as fold change of knock down to control. Statistical analysis was calculated by one-way ANOVA with Bonferroni multiple comparisons post-test (**P<0.01, *** P<0.001). (B) Relative transcript expression of each sample was compared to the relative amount of GAPDH in each sample to indicate the relative amount of individual transcripts. Error bars indicate the standard deviation of three technical replicates.

3.3.3.2 Proliferation

To assess whether knock down of ELF3 affected the proliferation of NHU cells, a growth assay was performed.

Knock down of ELF3 reduced the growth rate compared to control cells. The growth reduction was significant from day 3 until the plateau on day 10. Knock down of ELF3 not only slowed down cell proliferation but also prevented cells reaching maximal density compared to control cells, as the reduction of Alamar Blue in ELF3 knock down cells was less than that in control cells through the time course (Fig 3.3.7).

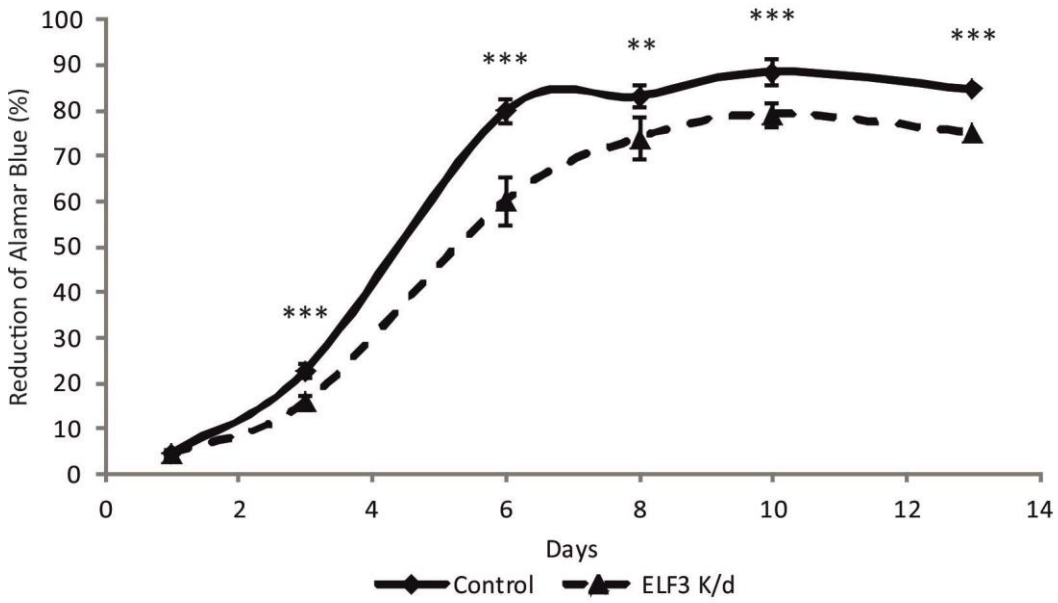

Fig 3.3.7 Effect of ELF3 knock down on proliferation of non-differentiated NHU cells (Y1117). Scrambled shRNA control (Control) and ELF3 knock down (ELF3 K/d) cells were seeded on day 0 and incubated for different days indicated in the graph. Reduction of Alamar Blue demonstrated proliferating rate of NHU cells shown as the reduction percentage. Error bars indicate the standard deviation of six experimental replicates. Statistical analysis was calculated by ANOVA with unpaired t-test at each time point (**P<0.01, *** P<0.001).

3.3.3.3 Barrier function

Inhibition of ELF3 expression reduced the ability for differentiated NHU cells to form an effective barrier (less than 2000 $\Omega \cdot cm^2$ compared to 3500 $\Omega \cdot cm^2$ in control differentiated cells), which was statistically extremely significant on day 4, day 7 and the following days (Fig 3.3.8A).

After wounding, TER values of both control and ELF3 knock down cell lines dropped down to around 200 Ω·cm^2 and increased afterwards gradually. Wound healing process was slowed down in ELF3 knock down cells significantly. Knock down of ELF3 did not affect the ultimate recovery from wounding, as TER value of ELF3 knock down cells returned to its original amount (Fig 3.3.8B), suggesting that ELF3 was crucial in developing an effective barrier, but may not be the pivotal factor determining the formation of the barrier.

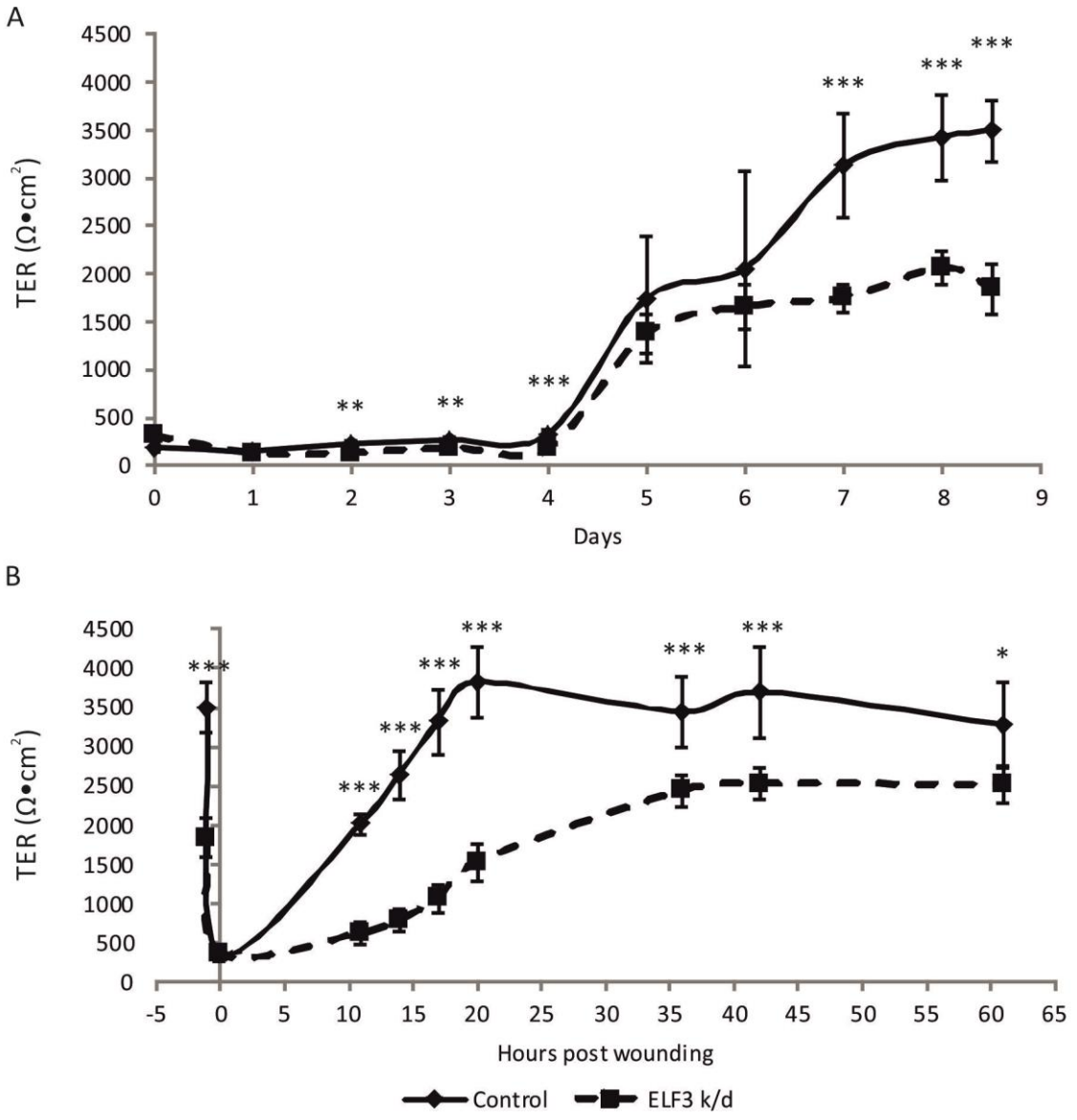

Fig 3.3.8 Effect of ELF3 knock down on formation of functional barrier in NHU cells (Y1117). Scrambled shRNA control (Control) and ELF3 knock down (ELF3 k/d) cells were induced to differentiate following the ABS/Ca^{2+} method. (A) TER measurements were taken every day for 8 days. (B) Cultures were wounded on day 8. TER values were measured before and after

wounding for 61h. Error bar indicates standard deviation of six experimental replicates. Statistical analysis was calculated by ANOVA with unpaired t-test at each time point (*P<0.05, **P<0.01, *** P<0.001).

Images in Fig 3.3.9 showed that ELF3 knock down delayed the wound healing process. The wound was closed at between 17 to 20 hours in control cells, whereas knock down of ELF3 slowed down the healing to more than 20 hours. The wound in both control and ELF3 k/d cell sheets were able to heal within 36 hours (Fig 3.3.9). These images suggested that the less effective barrier after wounding was due to slow migration, which may suggest a direct or indirect role of ELF3 in regulating cell migration.

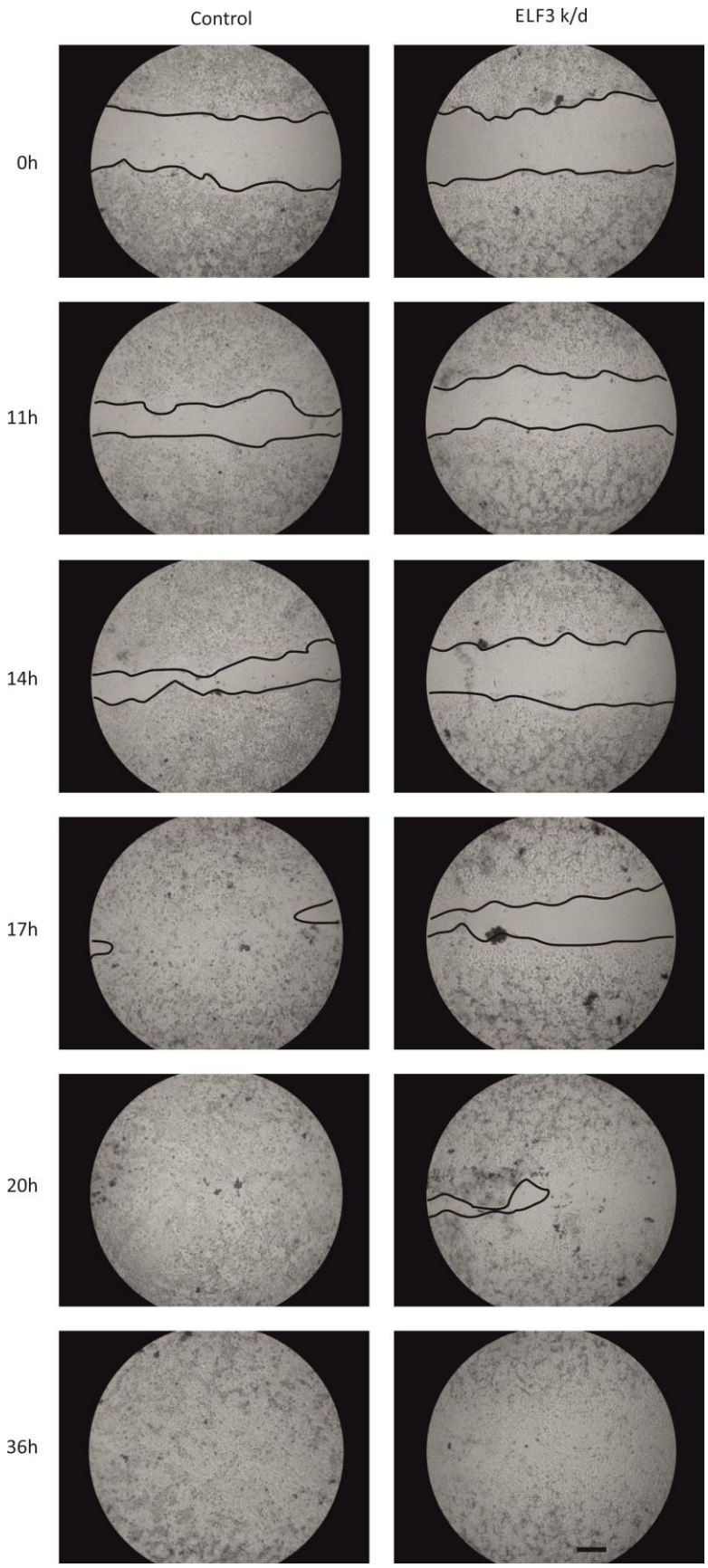

Fig 3.3.9 Effect of ELF3 knock down on wound healing in NHU cells (Y1117). Scrambled shRNA control (Control) and ELF3 knock down (ELF3 k/d) cells were treated as described in Fig. 3.3.8. Images were taken after cultures wounded on day 8 at different time points. Scale bar represents 200μm.

3.3.3.4 Differentiation-associated proteins by immunohistochemistry

Barrier study indicated that ELF3 was essential in urothelial differentiation. To further confirm the ELF3 knock down effect and determine the effect on expression of downstream proteins, ELF3 and other proteins were examined by immunohistochemistry with control and ELF3 knock down cell sheets. As seen previously (Fig 3.3.1), ELF3 showed occasional absence in positive ureter control (Fig 3.3.10 positive control). However, no prominent change of ELF3 expression was observed, as both control and ELF3 knock down cell sheets showed absent nuclear expression in some of the cells (examples were pointed out with arrows, Fig 3.3.10). The relatively stable ELF3 protein expression in control and ELF3 knock down cell sheets might be caused by the non-specific binding of the antibody, which requires further experiments to confirm.

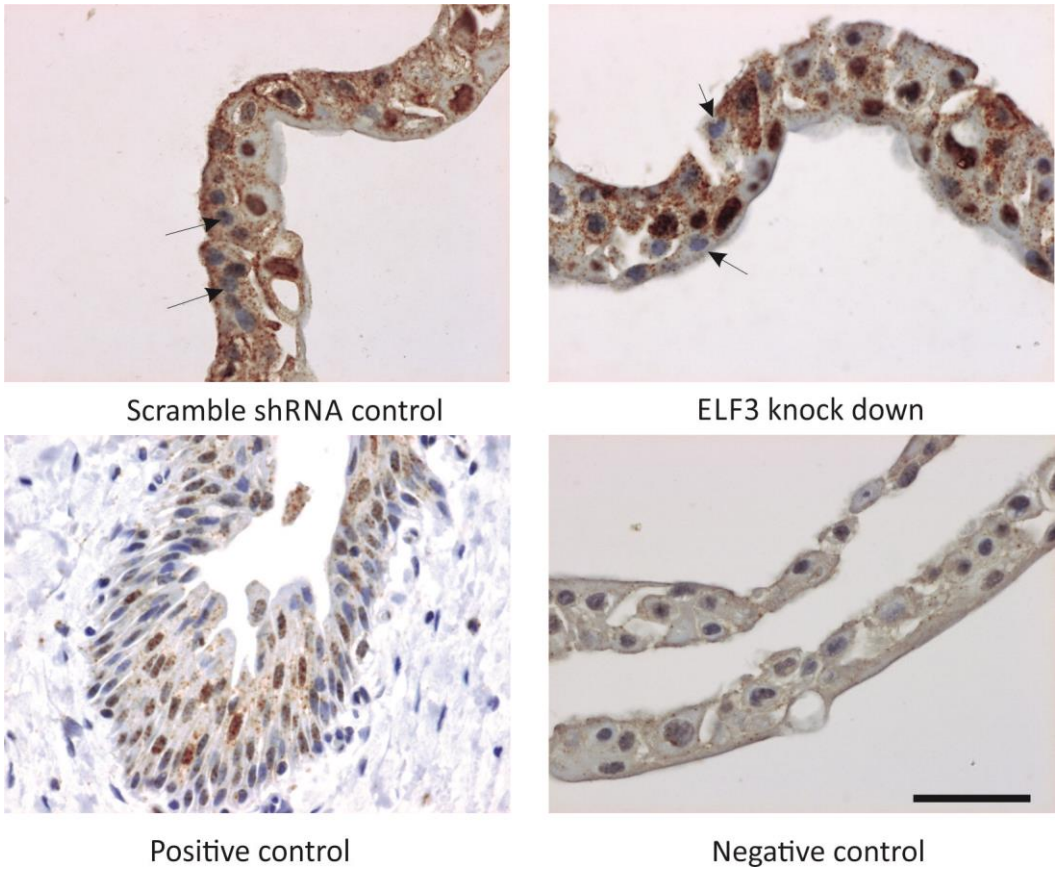

Fig 3.3.10 Effect of ELF3 knock down in cell sheets (Y1117). Scrambled shRNA control and ELF3 knock down cell sheets were treated as described in method for immunohistochemistry using CSA kit and incubated with ELF3 primary antibody. Positive control, ureter section (Y1233). Negative control was shown to inform the background. Scale bar represents 50μm.

Differentiation-associated proteins were assessed to indicate the polarisation of cell sheets and to show the effect of ELF3 on their expression

In both shRNA control and ELF3 knock down cell sheets, CK13 demonstrated cytoplasmic localisation, which was the same as in ureter section (positive control). Any difference between control and ELF3 knock down was not obvious (Fig 3.3.11).

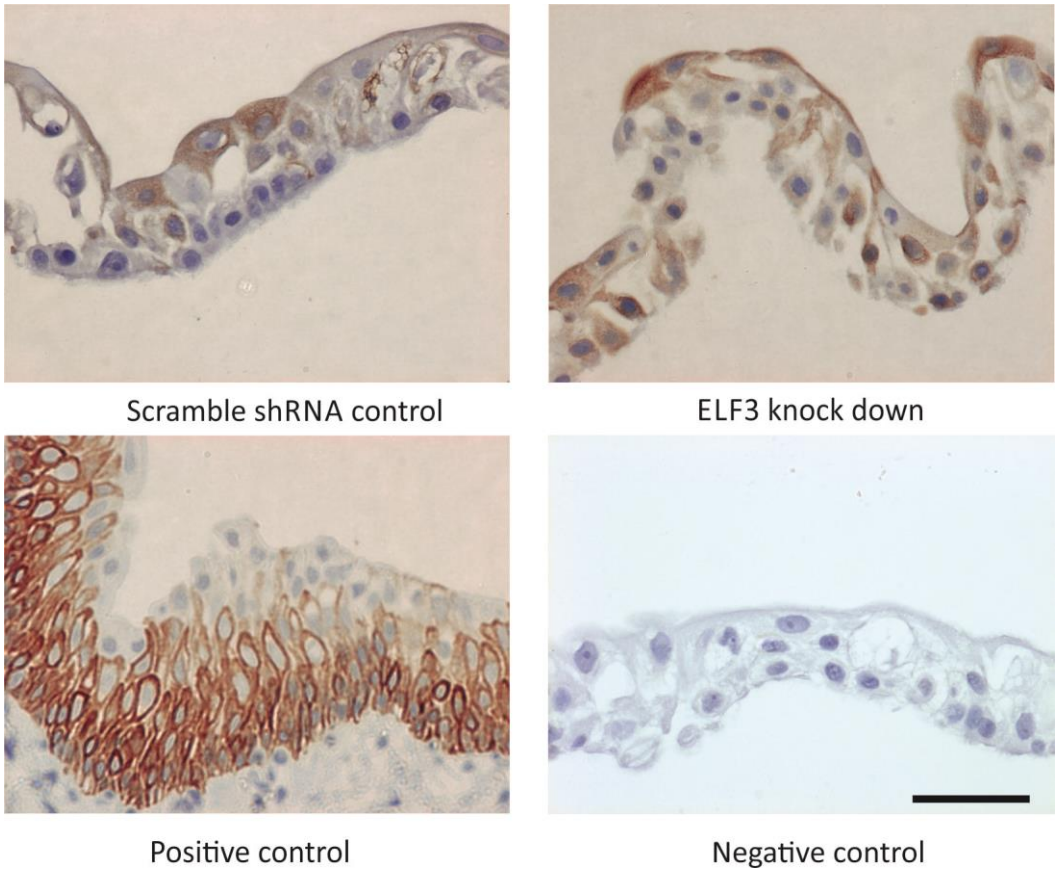

Fig 3.3.11 Effect of ELF3 knock down on localisation and expression of CK13. Scrambled shRNA control, ELF3 knock down cell sheets (Y1117) and ureter section (positive control, Y1233) samples were incubated with CK13 primary antibody. Secondary only negative control was also included. Scale bar represents 50μm.

Localisation of CLDN7 was confined to intercellular junctions in ureter section (positive control), shRNA control and ELF3 knock down cell sheets, suggested that there was no apparent knock down of CLDN7 protein expression (Fig 3.3.12).

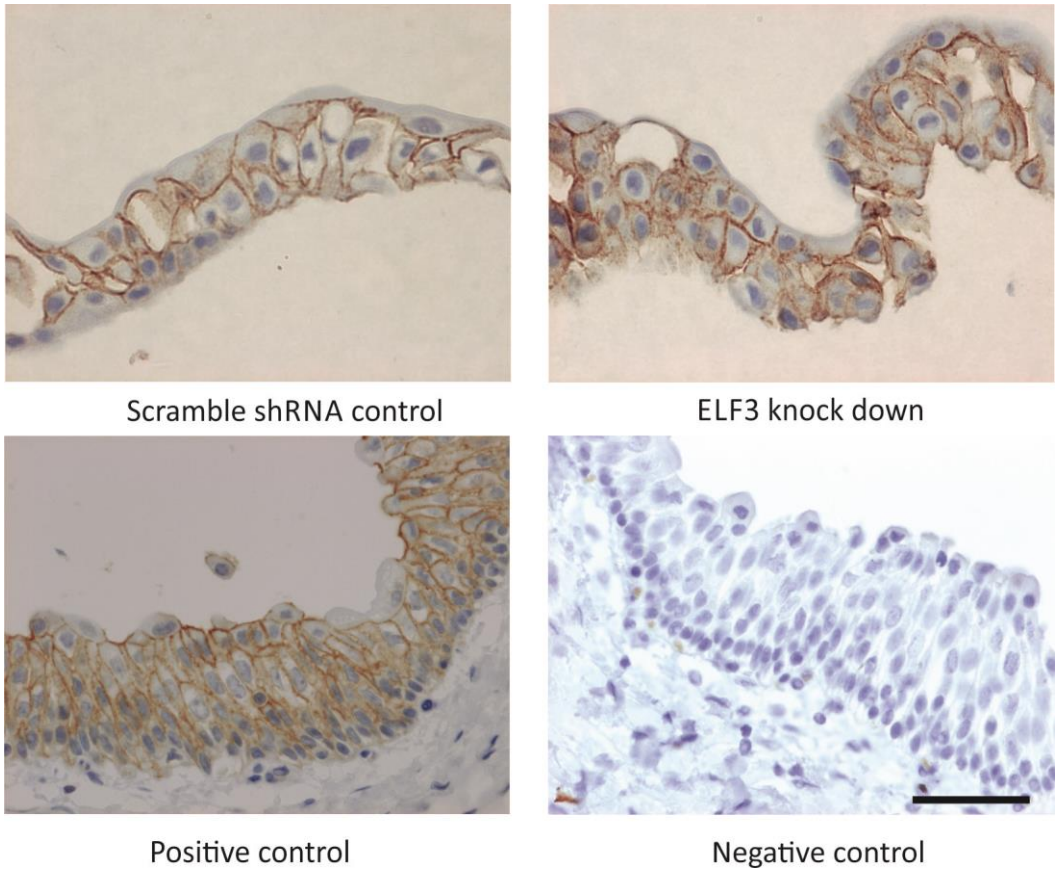

Fig 3.3.12 Effect of ELF3 knock down on localisation and expression of CLDN7. Scrambled shRNA control, ELF3 knock down cell sheets (Y1117) and ureter section (positive control, Y1233) samples were incubated with CLDN7 primary antibody. Secondary only negative control was examined. Scale bar represents 50μm.

As a transcription factor, FOXA1 was localised to the nuclei in normal tissue mostly in basal and intermediate layers (positive control). Both shRNA control and ELF3 knock down cell sheets showed nuclear expression with occasional absence (Fig 3.3.13, noted by arrows).

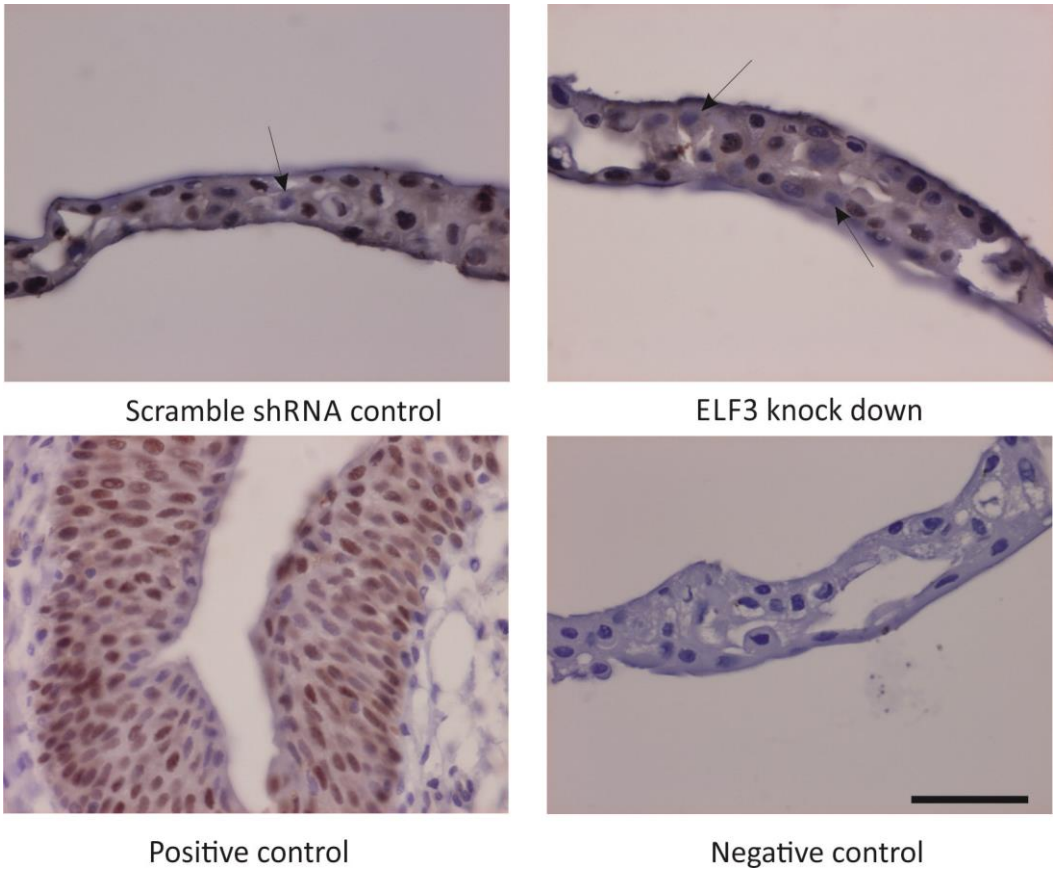

Fig 3.3.13 Effect of ELF3 knock down on localisation and expression of FOXA1. Scrambled shRNA control, ELF3 knock down cell sheets (Y1117) and ureter section (positive control, Y1441) samples were incubated with FOXA1 primary antibody. Secondary only negative control was included to show the background. Scale bar represents 50μm.

PPARγ demonstrated consistent nuclear expression in shRNA control cell sheets and ureter section (positive control). In ELF3 knock down cell sheets, nuclear expression of PPARγ was absent in some cells (Fig 3.3.14, pointed out by arrows), suggesting a possible feedback of ELF3 knock down to PPARγ.

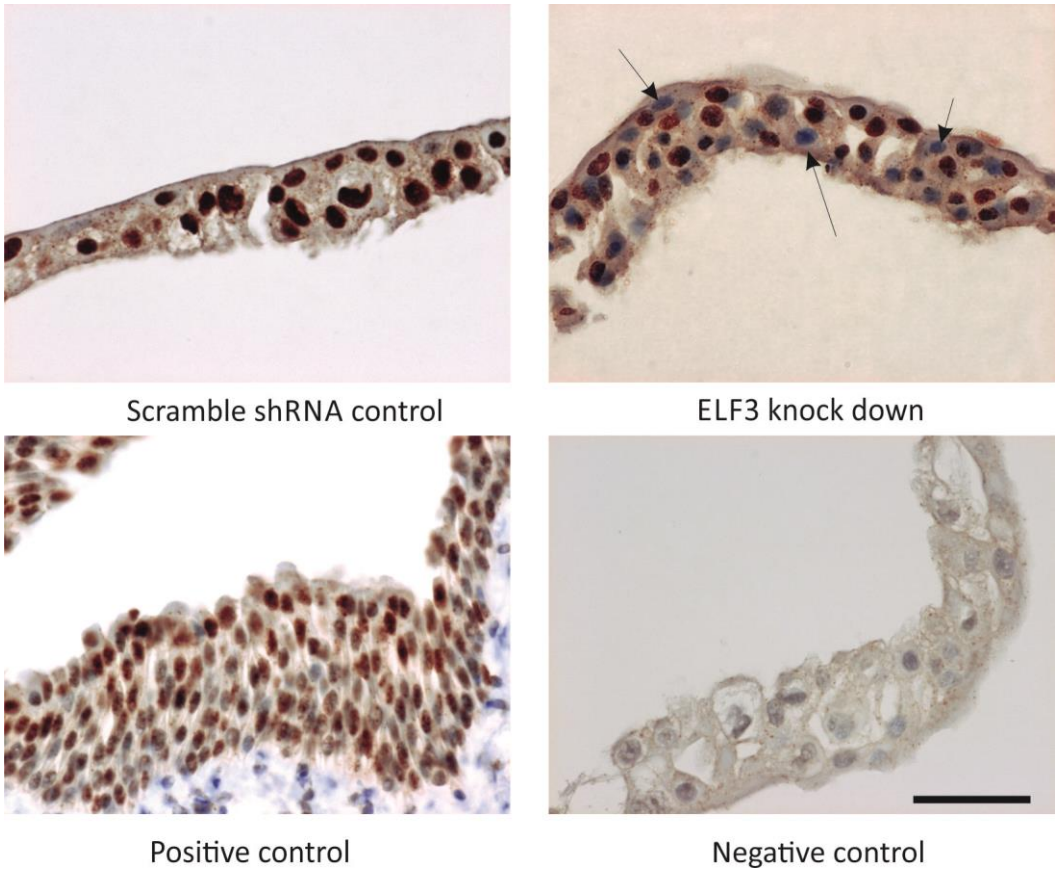

Fig 3.3.14 Effect of ELF3 knock down on localisation and expression of PPARγ. Scrambled shRNA control and ELF3 knock down cell sheets were treated as described in method for immunohistochemistry using CSA kit and incubated with PPARγ primary antibody. Positive control, ureter section (Y1233). Negative control is shown to inform the background. Scale bar represents 50μm.

To quantify the effect on PPARγ expression by ELF3 knock down, cell sheets were scanned using the AxioScan.Z1 slide scanner and analysed using HistoQuest software. The analysis process of one ELF3 knock down cell sheet slide stained with PPARγ was captured as screenshots and shown as workflow in Appendix 7.3. Analysed in the same way, control samples showed 94% and 97% positive PPARγ nuclear staining, whereas ELF3 knock down samples demonstrated 57% and 52% positive cells (Fig 7.3.9, Appendix 7.3), suggesting 40%-50% cells in ELF3 knock down cell sheets were absent of PPARγ nuclear expression.

3.3.3.5 Differentiation-associated proteins by immunoblotting

Protein expression of ELF3 was assessed by immunoblotting to verify the knock down of ELF3 in ABS/Ca^{2+} differentiated NHU cells. Expression of full length ELF3 protein (41kDa) was reduced in retroviral-transduced ELF3 knock down NHU cells (Fig 3.3.15, labelled as ELF3-1). Lower band (25kDa) was observed, which was speculated to be a 3′ incomplete coding sequence (Ensembl, ENST00000446188, see 6.1 for discussion) (Fig 3.3.15, labelled as ELF3-2). Expression of both ELF3 isoforms was knocked down and the effect was more obvious in samples harvested on day 6.

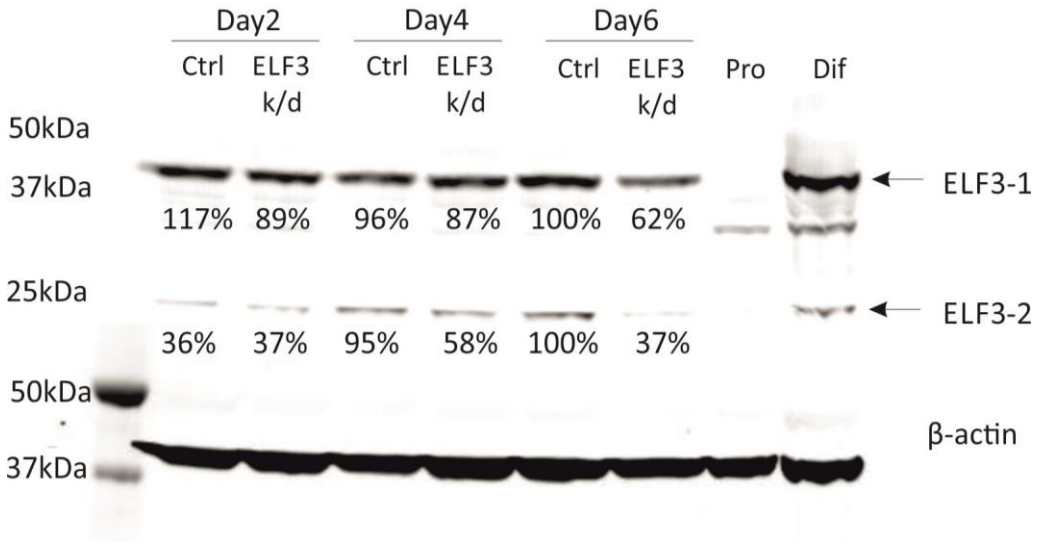

Fig 3.3.15 Effect of ELF3 knock down at protein level in NHU cells (Y1117). Scrambled shRNA control (Ctrl) and ELF3 knock down (ELF3 k/d) cells were harvested and seeded on 6 cm dishes

after 5 days of 5%ABS treatment. Medium was changed with final concentration of 2mM Ca^{2+} and 5% ABS on the next day and alternative days. Protein lysates were harvested on day 2, day 4 and day 6, respectively. Proliferating (Pro) and TZ/PD differentiated (Dif) NHU cells (Y1456) were included as control. Arrows indicate the two ELF3 bands (ELF3-1 and ELF3-2). β-actin was included as loading control.

Knock down of PPARγ by ELF3 knock down was assessed by immunoblotting. Two main PPARγ isoforms were knocked down slightly (Fig 3.3.16). Knock down effect on the lower band (B) was more obvious, as it had more protein expression than PPARγ upper band (A). On day 6, knock down effect of PPARγ band B was obvious (Fig 3.3.16).

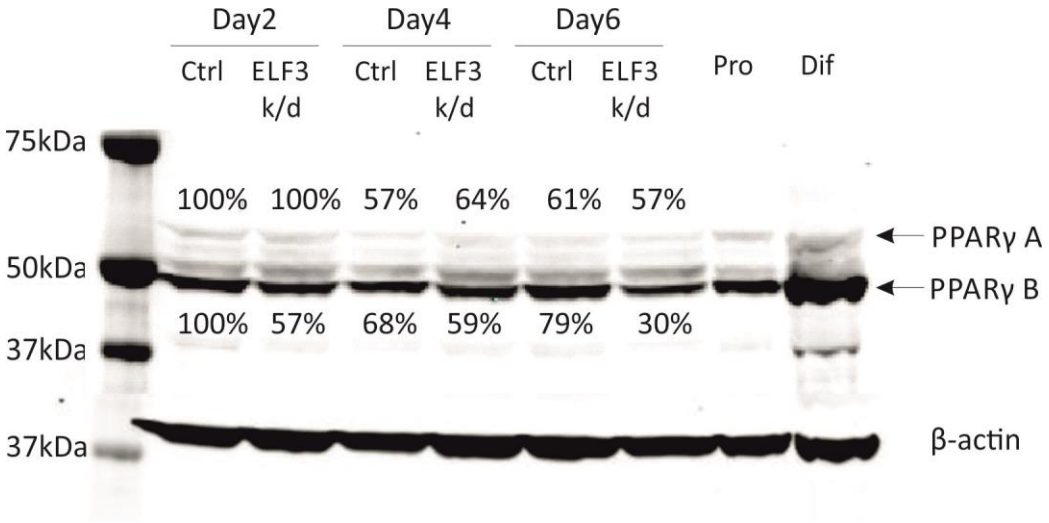

Fig 3.3.16 Effect of ELF3 knock down on PPARγ protein expression (Y1117). Scrambled shRNA control (Ctrl) and ELF3 knock down (ELF3 k/d) cells were treated as described in Fig 3.3.15. Proliferating (Pro) and TZ/PD differentiated (Dif) NHU cells (Y1456) were included as control. Arrows indicate the two PPARγ bands (PPARγ A and PPARγ B). β-actin was included as loading control.

Downstream differentiation-associated tight junction proteins CLDN4 and CLDN7 were selected to verify the effect on differentiation-associated proteins by Western blotting. The blots did not show obvious protein expression changes (Fig 3.3.17).

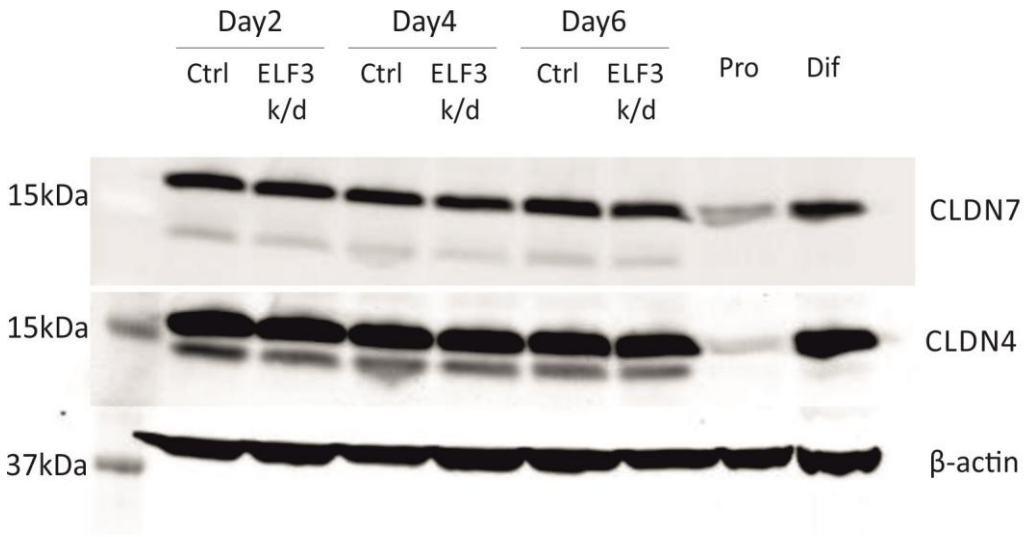

Fig 3.3.17 Effect of ELF3 knock down on expression of tight junction proteins (Y1117). Scrambled shRNA control (Ctrl) and ELF3 knock down (ELF3 k/d) cells were treated as described in Fig 3.3.15. Proliferating (Pro) and TZ/PD differentiated (Dif) NHU cells (Y1156) were included as control. CLDN7 and CLDN4 were selected as candidates of barrier-associated proteins. β-actin was included as loading control.

Whether the TGFβ pathway was associated with the delay of wound healing in ELF3 knock down samples was assessed by p-SMAD3. The activated p-SMAD3 in ELF3 knock down cells was reduced by ELF3 knock down to 57%, although the activation was not dramatic compared to the activation of p-SMAD3 in control (last three lanes, Y1545), which demonstrated the involvement of TGFβ pathway in differentiated NHU cells and TGFβ1 treated differentiated cells. This result suggested that knock down of ELF3 might have affected the TGFβ pathway (Fig. 3.3.18).

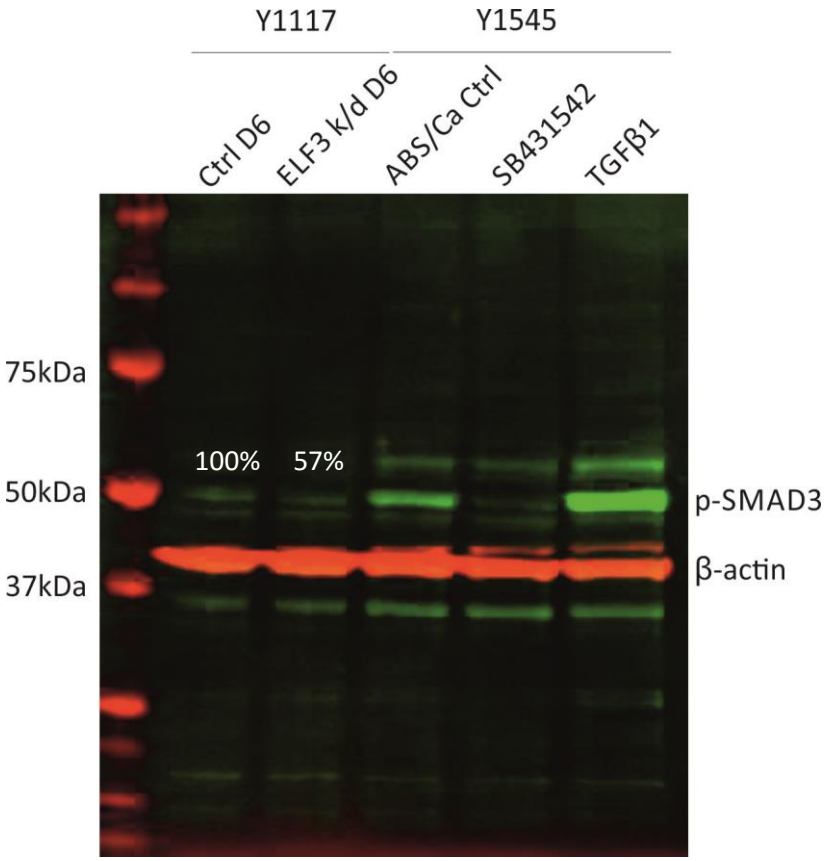

Fig 3.3.18 Effect of ELF3 knock down on TGFβ pathway (Y1117). Scrambled shRNA control (Ctrl) and ELF3 knock down (ELF3 k/d) cells were seeded in 6cm dishes, after which the cells were treated with 5% ABS for 5 days and 5% ABS and 2mM Ca^{2+} for 6 days. NHU cells (Y1545, lysates taken by Jennifer Hinley) were included as controls, which were induced to differentiate using the ABS/Ca^{2+} method. Sample labelled as ABS/Ca ctrl was used as non-treated control. Differentiated cells from the same line (Y1545) were also treated with SB431542 or TGFβ1, as negative or positive controls, respectively. Picture was taken with combination of two colour channels to indicate the relative expression of p-SMAD3 (green channel) compared to β-actin (red channel). Percentage of activated p-SMAD3 expression after normalisation with β-actin is shown for control and ELF3 knock down samples.

3.3.4 Effect of ELF3 over-expression on NHU cells *in vitro*

3.3.4.1 Establishment of ELF3 over-expressed NHU cell line

To further understand role of ELF3 in urothelial differentiation, ELF3 was over-expressed in NHU cells by cloning into an expression vector and integrated into genome of urothelial cells using retroviral transduction. The insertion was cut off using EcoRI and HpaI, demonstrating a band at the size of ELF3 full length cDNA by electrophoresis (Fig 3.3.19 Lane 2-5).

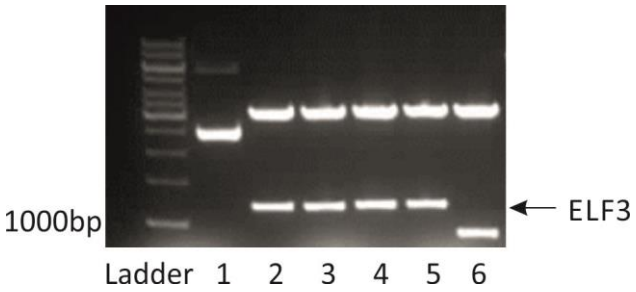

Fig 3.3.19 Double digestion of pGEM-T vectors. Lane 1 demonstrated a non-digested plasmid as control. Bands on lane 2-6 showed the double digestion of five colonies. Bands at 1116bp were cut off by double digestion, indicating the correct insertion of ELF3 (lane 2-5).

To investigate whether the over-expression of ELF3 in NHU cells was successful, genomic DNA of transduced NHU cells was isolated and amplified using primers binding to the vectors. ELF3 integrated sample demonstrated a band at the same size compared to the ELF3 band amplified from ELF3-pGEM-T plasmid (Fig 3.3.20, lane 2, noted by arrow).

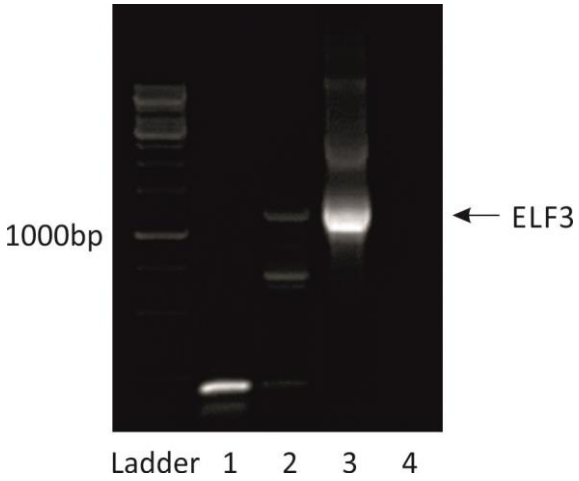

Fig 3.3.20 Amplification of ELF3 from genomic DNA of transduced NHU cells (Y1365). Templates in lane 1 and 2 were genomic DNA from transduced NHU cells, empty vector and ELF3-inserted vector, respectively. ELF3-inserted plasmid was used as positive control and is shown in lane 3. Lane 4 was negative control using water as template.

3.3.4.2 Proliferation

In order to understand whether over-expression of ELF3 affected the proliferation of NHU cells, growth assay was performed in ELF3 over-expressing and control cells. Growth rate of empty vector control and ELF3 over-expressed NHU cells showed similar trend initially. Control cells were still able to proliferate until 12 days after seeding, whereas ELF3 over-expressed cells demonstrated growth arrest 8 days afterwards, which was statistically significant, suggesting that over-expression of ELF3 had some effect on population doubling rate of cells, which may imply an alteration of proliferative phenotype. Empty vector and ELF3 integrated cells showed reduction of Alamar blue for less than 50% or 30%, respectively (Fig 3.3.21). A lower density of ELF3 over-expressed cells when arrested for growth was observed.

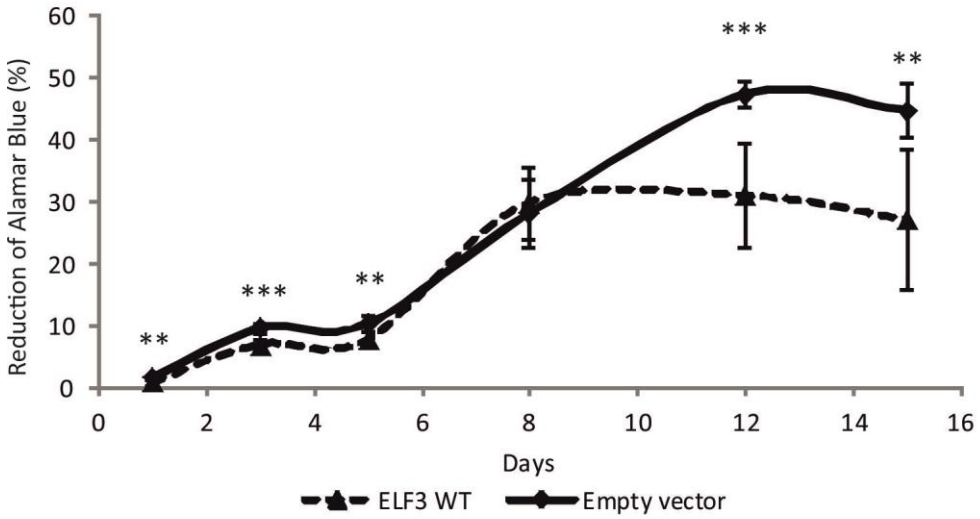

Fig 3.3.21 Over-expression of ELF3 on proliferation. Empty vector or ELF3 wild type (ELF3 WT) integrated cells (Y1314) were seeded on day 0 and incubated for different days indicated in the graph. Reduction of Alamar Blue demonstrated proliferating rate of NHU cells shown as the reduction percentage. Error bars indicate the standard deviation of six experimental replicates. Statistical analysis was calculated by ANOVA with unpaired t-test at each time point (**P<0.01, *** P<0.001).

3.3.4.3 Phenotype of NHU cells

To investigate whether growth arrest was the result of a differentiated phenotype that might be due to the over-expression of ELF3, western blotting was performed using vector and ELF3 over-expressed NHU cells.

Full length of ELF3 cDNA was integrated into NHU cells, which is about 41kDa indicated by arrow. Lower band (25kDa) was observed in all NHU cell lysates. In ELF3 integrated cells, protein level of ELF3 was increased compared to vector only integrated cells, but the expression was less than differentiated NHU cells (Fig 3.3.22).

Expression of CK13 and CK14 suggested the over-expression of ELF3 did not alter the phenotype of proliferating NHU cells (Fig 3.3.22), which was CK13 (-) and CK14 (+). By contrast, differentiated control cells demonstrated a phenotype showing CK13 (+) and CK14 (-).

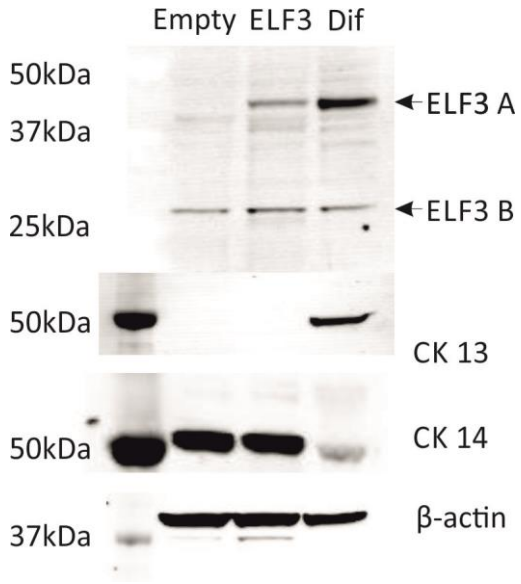

Fig 3.3.22 Over-expression of ELF3 and the effect on phenotype of NHU cell (Y1365). Empty vector (Empty) and ELF3 full length cDNA (ELF3) integrated NHU cells were harvested at 90% confluence. Untransduced differentiated NHU lysate (Dif, Y1156) was included as positive control for differentiation. Primary antibodies for ELF3, CK13 and CK14 were applied to the blot separately. β-actin was included as loading control.

3.3.4.4 Differentiation-associated transcripts

Since over-expression of ELF3 did not affect the CK13 (-) and CK14 (+) phenotype, control and ELF3 integrated cells were utilised to examine whether ELF3 over-expressed cells demonstrated more abundance of differentiation-associated genes and proteins when induced to differentiate.

To investigate the transcript expression of ELF3 and whether TZPD stimulated cells affected ELF3 transcript expression. ELF3 over-expressed cells were induced to differentiate by TZPD treatment for 6h, at which time point the expression of ELF3 was little in non-transduced control cells (Fig 3.3.2).

Transcript expression of ELF3 was dramatically up-regulated in ELF3 integrated NHU cells. TZPD increased the transcript expression slightly in vector only integrated cells shown as a faint band. No obvious expression change can be observed between vehicle control (DMSO) and TZPD treated samples in ELF3 integrated cells, suggesting treatment of TZPD for 6h might be not sufficient to induce any visible change (Fig 3.3.23).

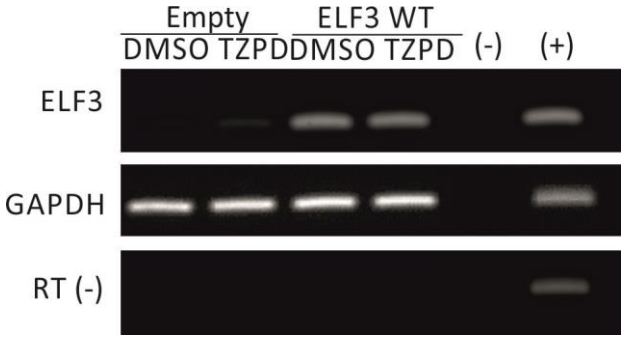

Fig 3.3.23 Effect of TZPD induced differentiation on ELF3 integrated cells (Y1314). Empty vector (Empty) and full length ELF3 (ELF3 WT) induced cells were treated with either vehicle control (DMSO, 0.1%) or TZPD (both at 1μM) for 6h. No reverse transcription enzyme was added in RT (-) samples. GAPDH showed the equal amount of cDNA and was included as internal control. Water and genomic DNA was utilised as template in (-) and (+) samples, respectively.

ELF3 over-expressed cells were utilised to further investigate the effect of ELF3 on PPARγ transcripts. Primer set (2F & 4R, see chapter 5 for detailed information) targeting both PPARγ isoforms was utilised. Transcript expression of PPARγ by RT-PCR did not show expression alteration by 6h of TZPD treatment or ELF3 over-expression (Fig 3.3.24).

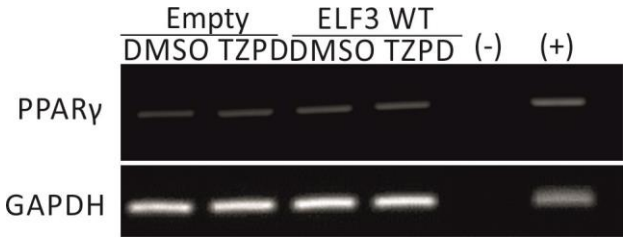

Fig 3.3.24 Transcript expression of PPARγ in ELF3 over expressed cells (Y1314). Empty vector (Empty) and full length of ELF3 (ELF3 WT) samples were treated with either vehicle control (DMSO, 0.1%) or TZPD (both at 1μM) for 6h. GAPDH showed the equal amount of cDNA and was included as internal control. Water and genomic DNA was utilised as template in (-) and (+) samples, respectively.

By RT-QPCR, the over expression of ELF3 was confirmed. Dramatic increase of ELF3 transcript expression was significant, to about 100 times of its original amount in both empty and ELF3 integrated cells. Expression of ELF3 in vector integrated cells was induced by 6h TZPD treatment, but the induction was not significant. The expression of ELF3 in ELF3 over-expressed cells was down-regulated by 6h TZPD treatment significantly (Fig 3.3.25). To confirm this finding, the experiment needs to be repeated with biological replicates.

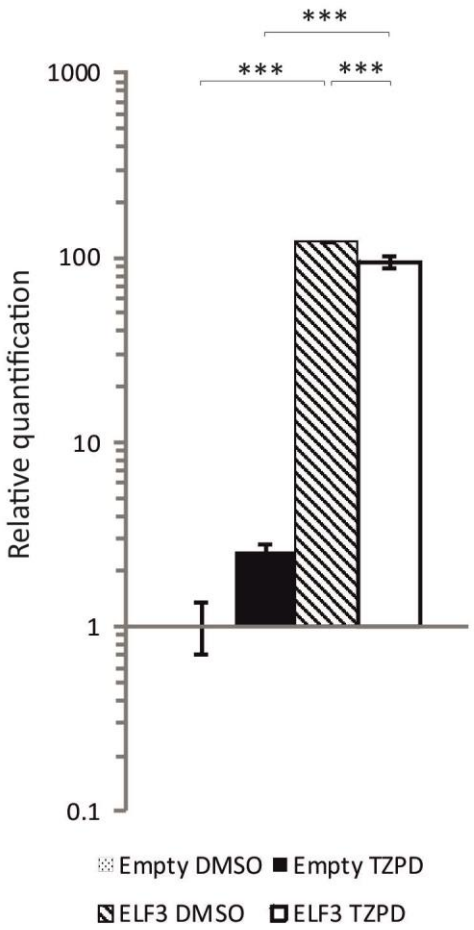

Fig 3.3.25 Effect of TZPD induced differentiation on ELF3 transcripts in ELF3 transduced cells (Y1314). Empty vector (Empty) and full length of ELF3 samples were treated with either vehicle control (DMSO, 0.1%) or TZPD (both at 1μM) for 6h. Transcript expression of ELF3 was normalised to GAPDH and compared to empty vector transduced DMOSO treated cells. Error bars indicate the standard deviation of three technical replicates. Statistical analysis was calculated by one-way ANOVA with Bonferroni multiple comparisons post-test (*** P<0.001).

By RT-QPCR (primer set 1F 2R, see chapter 5 for detailed information), PPARγ2, which is one of the PPARγ isoforms showed no statistically significant change. Transcript expression of IRF1 and FOXA1 was up-regulated by 6h of TZPD treatment in both control and ELF3 over-expressed cells, but was not statistically significant. Increase of GRHL3 transcript expression by 6h of TZPD treatment was significant, suggesting that GRHL3 might be an intermediate transcription factor expressed at early stage during differentiation. However, the effect on expression alteration of transcription factors by ELF3 over-expression was not significant (empty samples vs. ELF3 samples, Fig 3.3.26).

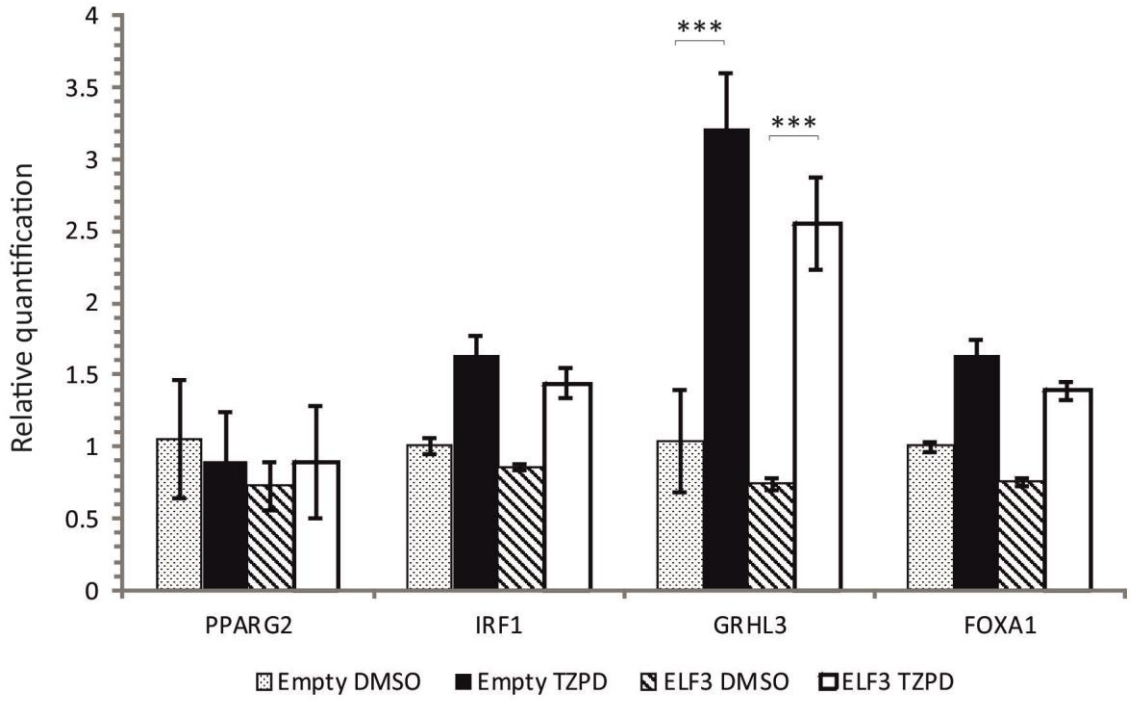

Fig 3.3.26 Transcript expression of transcription factors in ELF3 over-expressed cells (Y1314). Empty vector (Empty) and full length of ELF3 samples were treated with either vehicle control (DMSO, 0.1%) or TZPD (both at 1μM) for 6h. Transcript expression of all tested genes was normalised with expression of GAPDH. Transcript expression in treated and/or transduced cells was compared to that of vehicle treated empty vector transduced cells, and demonstrated as fold change. Error bars indicate the standard deviation of three technical replicates. Statistical analysis was calculated by one-way ANOVA with Bonferroni multiple comparisons post-test (*** P<0.001). All other comparisons not noted were considered as not significant.

3.3.4.5 Differentiation-associated proteins

Over-expression of ELF3 was confirmed at the transcript level, but did not induce the proliferating NHU cells to differentiate. Whether it would enhance expression of differentiation-associated proteins in differentiated NHU cells was further investigated. Serum and calcium were applied to cultures separately or simultaneously to identify whether ELF3 over-expressed cells would be affected by different treatments. Expression of ELF3 and PPARγ was assessed (Fig 3.3.27) together with differentiation-associated proteins (Fig 3.3.28).

Full length ELF3 was detected at about 41kDa (labelled as ELF3-1, Fig 3.3.27). The effect of over expression on ELF3 proteins was detectable but not as dramatic as transcripts. Treatment with both ABS and calcium did not affect ELF3-1 obviously. However, ELF3-2 protein, which was a truncated ELF3 isoform, appeared to be up-regulated by ABS or calcium only treatment (Fig 3.3.27, noted by a rectangular).

Two PPARγ antibodies were applied to demonstrate the effect of ELF3 over expression on PPARγ. PPARγ2 antibody demonstrated two main bands showing no obvious pattern. The lower band was the same one as raised by PPARγ E8 antibody. Another band was also observed at 80kDa, and suggested to be a sumoylated form of PPARγ (Fig 3.3.27). PPARγ E8 antibody was designed to bind to all PPARγ isoforms. The main band shown on the blot at about 50kDa appeared that the amount of protein was reduced by ELF3 over-expression (Fig 3.3.27).

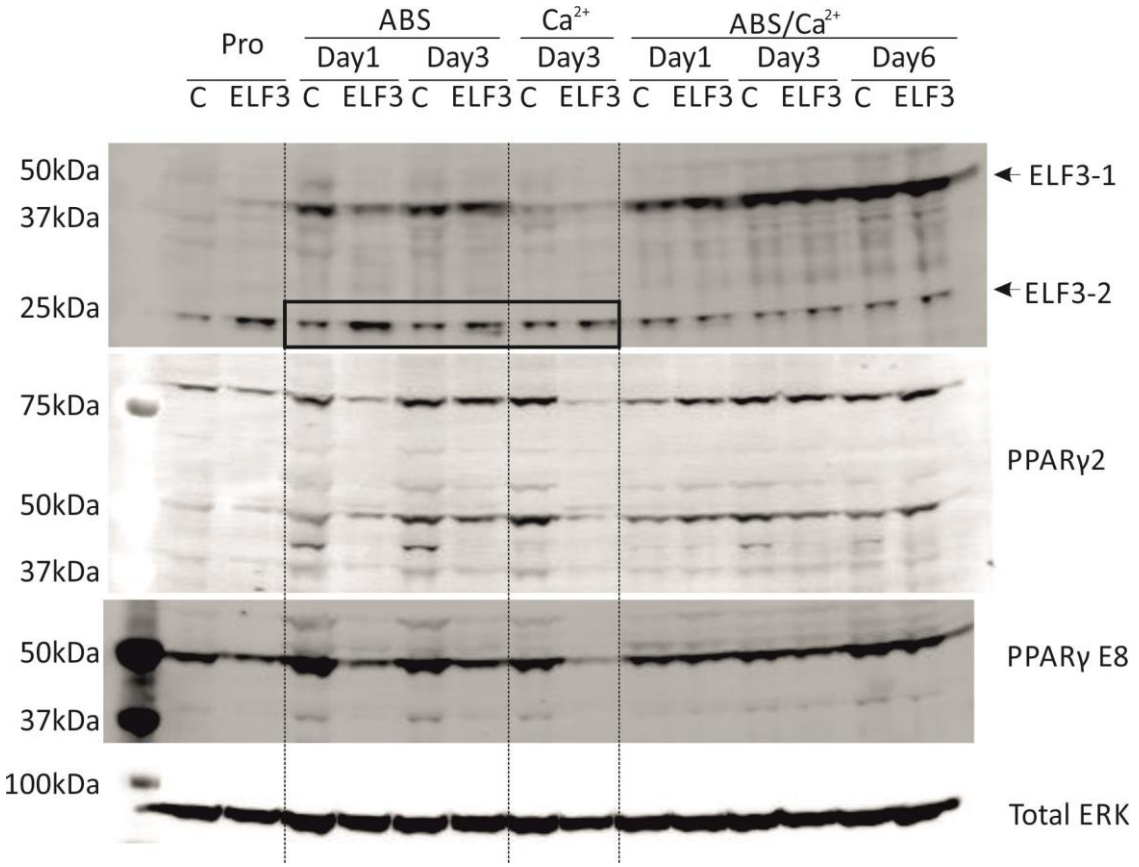

Fig 3.3.27 Effect of ELF3 over-expression on ELF3 and PPARγ (Y1314). Empty vector control (C) and full length ELF3 integrated cells (ELF3) were harvested and seeded on 35 mm dishes. Upon reaching 90% confluence, cells were either harvested as proliferating samples (Pro) or treated with 5% ABS alone, 2mM calcium alone or ABS/Ca^{2+} for 1 day, 3 days or 6 days. Medium was changed on alternative days. Protein lysates were harvested after the treatment. PPARγ2 antibody binds to N terminal of PPARγ2, whereas PPARγ E8 antibody binds to the PPARγ protein C terminal, which is shared among majority of PPARγ isoforms. Total ERK was applied on the blot as loading control. Note, the expression of ELF3-2 protein was increased slightly by over-expression of ELF3.

Whether over-expression of ELF3 affected the differentiated phenotype was assessed by examining transitional and terminal differentiation-associated proteins (Fig 3.3.28). Protein expression of CK13 was increased slightly by over-expression of ELF3 in calcium or ABS/calcium treated cells (Fig 3.3.28, noted with a rectangular). CK14 proteins decreased in ELF3 over expressed cells, with dramatic effect in ABS or calcium only treatment cultures especially (Fig 3.3.28, noted with a rectangular). However, expression of tight junction proteins showed no obvious pattern. ZO1 and ZO3 were expressed mostly in ABS/calcium treated cells without apparent difference by ELF3 over-expression (Fig 3.3.28).

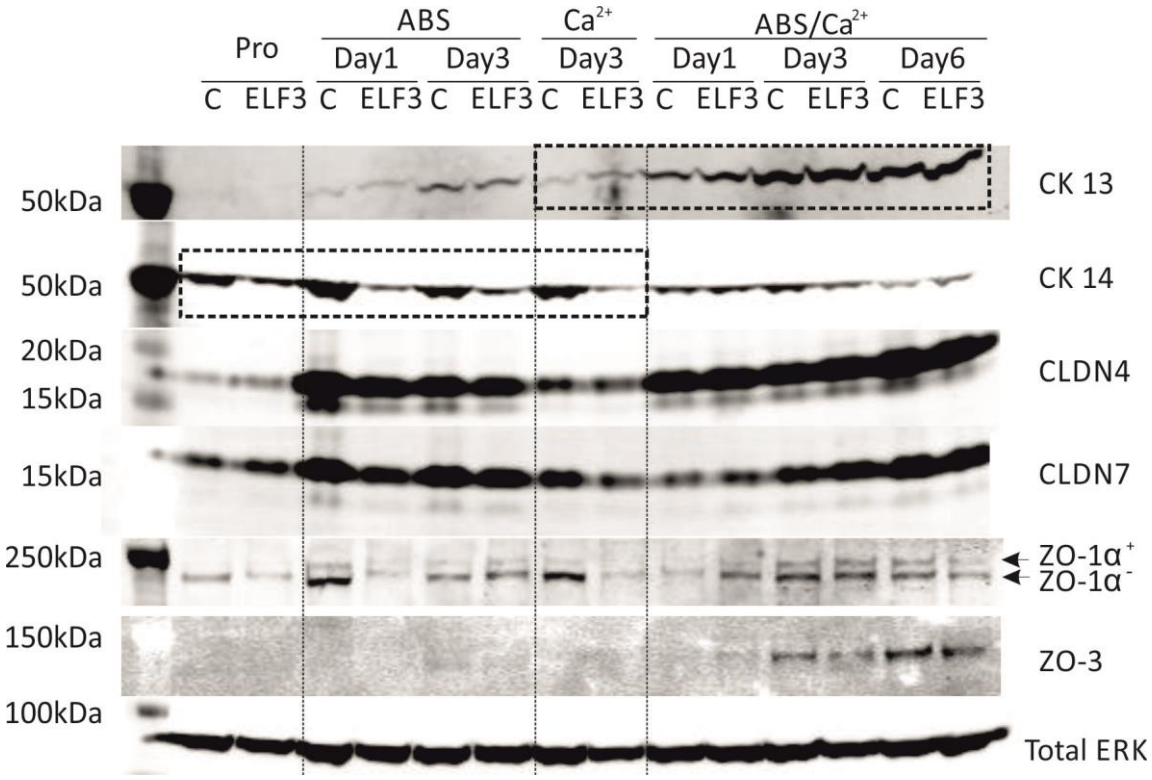

Fig 3.3.28 Effect of ELF3 over-expression on differentiation-associated proteins (Y1314). Empty vector control (C) and full length ELF3 integrated cells (ELF3) were treated as described in Fig 3.3.27. Total ERK was applied on the blot as loading control. Note, expression of CK13 and CK14 was altered by ELF3 over-expression (indicated by a rectangular).

3.3.5 Summary of results

ELF3 was localised to the nuclei in urothelial tissue samples. *In vitro* expression of ELF3 was up-regulated by TZPD induced differentiation, which also resulted in translocation of ELF3 to nuclei.

Knock down of ELF3 reduced transcript expression of other transcription factors such as IRF1, FOXA1 and GRHL3. An ELF3 downstream gene CLDN7 was down-regulated by ELF3 knock down.

However, knock down of ELF3 did not obviously affect protein expression of tight junction proteins or transitional differentiation marker CK13.

A feedback of ELF3 knock down to PPARγ protein expression may be present, as absent nuclear expression of PPARγ was observed in two different cell sheet samples (generated from the same ELF3 knock down cell line).

The formation of a functional barrier in ABS/calcium differentiated NHU cells was delayed by ELF3 knock down significantly, suggesting an essential role of ELF3 in maintaining differentiated phenotype of NHU cells.

The original hypothesis that over-expression of ELF3 would induce the differentiated phenotype in NHU cells was disproved by the observation of stable expression of CK14, as well as no visible expression of CK13 in ELF3 over-expressed proliferating cells.

Transcript expression of ELF3 was massively up-regulated by ELF3 over-expression, which was independent of induction of differentiation.

Protein expression of ELF3 was not dramatically affected after induction of differentiation. The expression of CK13 and CK14 was slightly altered by ELF3 over-expression after calcium treatment. But no convincing change regarding terminal differentiation-associated markers by ELF3 over-expression was observed (ZO1 or ZO3).

3.4 Future work

The knock down of PPARγ was observed when the expression of ELF3 was knocked down. To investigate whether there is a feedback to PPARγ by ELF3 knock down and confirm the previous results, immunohistochemistry experiments regarding the expression of PPARγ in other ELF3 knock down NHU cell lines are worth doing.

The functional role of ELF3 was demonstrated by TER study, but little effect in terms of differentiation-associated proteins expression was observed. Further studies about proteins associated with formation of functional barrier may suggest link between ELF3 and other target proteins or mechanisms of regulating differentiation in NHU cells.

As the protein expression of ELF3 was not significantly up-regulated by over-expression, whether it was degraded after translation or not being translated may indicate the mechanism of regulating the expression of ELF3 in NHU cells, or the initiation of differentiation programme.

For ELF3 over-expressed NHU cells, the functional study by measuring TER in differentiated cells may provide further information about the role of ELF3.

Assessment of PPARγ expression in ELF3 over-expressed NHU cell sheets may be important to investigate the relationship between ELF3 and PPARγ. Protein expression of other transcription factors related to urothelial differentiation in ELF3 over-expressed cells may provide further information.

Chapter 4 Signalling Pathways involved in UC

4.1 Introduction

4.1.1 Classification and general characterisation of pathways in UC

There are two main pathways associated with development of bladder cancer, the Ta pathway associated mainly with FGFR3 mutation and the CIS pathway associated with TP53 mutation. Ta tumours contribute to 50% of bladder cancer, but although they often recur, they rarely progress to T2-T4 via T1. By contrast, CIS tumours have 50% incidence to progress via T1 to T2-T4 tumour, which indicates the tumour has invaded to the smooth muscle layer of the bladder (Billerey et al., 2001; Biton et al., 2014). Recent studies have distinguished three different types of muscle invasive bladder cancers (MIBC): luminal cancers (with PPARγ activation and FGFR3 activating mutation), basal cancers with P63 activation, and P53-like cancers (Choi et al., 2014).

The main difference between basal and luminal MIBC was that the luminal cancers had differentiation-associated genes expressed at both transcript and protein level (CK20, PPARγ, FOXA1, for example). Transcription factors like PPARγ and FOXA1 were up-regulated in luminal MIBCs and down-regulated in basal MIBCs (Choi et al., 2014). In all three subtypes of MIBC, activated transcription factors were found to induce both the up-regulation and down-regulation of different genes. For example, in the PPARγ pathway, transcripts of PPARγ, CK18 and CK20 were up-regulated, whereas vimentin (an intermediate filament protein expressed in mesenchymal cells) was down-regulated in luminal MIBC (Choi et al., 2014).

4.1.2 Genome-wide alteration of genes in urothelial cancer

Analysis utilising various types of UC samples suggested that somatic mutation and copy number alteration were involved in urothelial cancer with high incidence. P53/Rb pathways had 93% alteration. 49% of samples had TP53 gene inactivating mutations (Cancer Genome Atlas Research, 2014). P63 showed a significant reduction at protein level in high grade invasive cancers. Transcript expression of P63 also demonstrated a dramatic decrease in high grade bladder cancer cell lines (e.g. T24) compared to low grade bladder cancer lines (RT4, for example) (Urist et al., 2002). RTK (Receptor tyrosine kinases)/PI3K pathway had 72% mutation, among which included FGFR3, EGFR family members and PIK3CA(Cancer Genome Atlas Research, 2014).

Histone modification was another highly altered system (89%) (Cancer Genome Atlas Research, 2014). Frequent chromatin remodelling event has been reported in urothelial cancer (59% of 97 samples), and was regarded as hallmark of bladder cancer (Gui et al., 2011). The role of EGFR family members and the PI3K pathway and the influence of pathway alteration will be introduced in more detail in the following sections.

4.1.3 Role of the EGFR pathway in normal urothelial cells and the alteration in cancer

The EGFR pathway is important in regulating cell proliferation and thus plays crucial roles in cultures of normal urothelial cells *in vitro* (Varley et al., 2005). By binding of its specific ligands, EGFRs are activated and form homodimer (or heterodimer with other ERBB family members) to stimulate cascades of downstream pathways. In proliferative NHU cells, EGFR pathway autocrine activated by amphiregulin was the dominant pathway. Inhibition of EGFR tyrosine kinase (TK) by PD153035 significantly inhibited the wound repair and migration of NHU cells *in vitro* (Varley et al., 2005). Inhibition of EGFR pathway by EGFR TK inhibitor, or a downstream MAPK/ERK inhibitor decreased the

proliferation. Inhibition of MAPK/ERK by U0126 led to activation of AKT pathway (MacLaine et al., 2008). Regeneration of *in vitro* cultured urothelial cells were shown to be inhibited by EGFR inhibitor AG1478 and anti-EGFR antibody (LA22) at 50% and 30% respectively, and stimulated by amphiregulin, EGF and TGFα added exogenously (Daher et al., 2003).

In bladder cancer, expression of EGFR increased significantly compared to normal tissue. A dramatic increase of EGFR transcript was observed in higher stages of bladder cancer biopsies among 45 tumour samples compared to 5 normal samples (Chang et al., 2013). Also, in cancer treatment, anti-EGFR therapy in basal-like MIBC was demonstrated as therapeutic target in both human bladder cancer cell lines and chemically induced bladder cancer mouse model (Rebouissou et al., 2014). However, over-expression of EGFR in transgenic mice showing up-regulation of EGFR and hyperplasia of urothelium did not induce tumour formation on its own (Cheng et al., 2002).

ERBB2, also known as HER2 or EGFR2, was another EGFR family member expressed more in confluent and differentiated NHU cells compared to freshly isolated cells or proliferating cells (Varley et al., 2005). ERBB2 was reported to play essential role in urothelial wound repair process. Only the antisense oligonucleotides of c-erbb2 (blocked the production of endogenous ERBB2 protein) delayed the regeneration of damaged primary urothelial cultures by up to 50%, whereas the sense or the mutated antisense oligonucleotides showed no effect. The inhibition of wound repair was not affected through the proliferative ability, as all three oligonucleotides (sense, antisense and mutated antisense to c-erbB2) showed similar influence on proliferation of urothelial cultures by BrdU assay, suggesting a role of ERBB2 in migration of normal urothelium (Bindels et al., 2002).

ERBB2 showed the highest mutation frequency in bladder cancer among all tested tumour types (Cancer Genome Atlas Research, 2014). Translocation of

ERBB2 was found in four tumours with different fusion partners. One case showed that exon 4 to 29 of ERBB2 was fused to promoter plus exon1 of DIP2B (disco-interacting protein 2 homolog B), which contains a binding site for the transcriptional regulator DNA methyltransferase 1 associated protein 1. The fused product was amplified, which resulted in over-expression of ERBB2 (Cancer Genome Atlas Research, 2014). Breast cancer cells depleted of ERBB2 on the cell surface lost the ability of EGF family induced migration, whereas over-expression of ERBB1 (EGFR) partly compensated the EGF induced migratory ability in ERBB2 devoid cancer cells (Spencer et al., 2000), suggesting a crucial role of ERBB2 in mediating EGF induced migration of carcinoma cells.

4.1.4 PI3K /AKT pathways and the alteration in UC

The PI3K (Phosphoinositide 3-kinase)/AKT (also known as protein kinase B, PKB) pathway is downstream of the EGFR pathway and involved in cell proliferation, differentiation, survival and motility. In cultures with low calcium (0.09 mM), NHU cells mainly utilised the MAPK (mitogen-activated protein kinases)/ERK (extracellular signal-regulated kinases) pathway downstream of EGFR pathway for growth, whereas in high calcium condition (physiological concentration, 2 mM), NHU cells depended on the PI3K pathway to proliferate, as AKT pathway was activated whereas inhibition of PI3K using LY294002 reduced the proliferation of calcium induced growth acceleration significantly (Georgopoulos et al., 2010). During wound healing process in NHU cells, the AKT pathway also contributed to the regulation of cell migration, which was prevented by inhibition of the AKT pathway using LY294002 (Varley et al., 2005).

The increased calcium concentration in NHU cultures led to plasma membrane expression of E-cadherin, which is a calcium dependent homotype cell-cell adhesion glycoprotein (Georgopoulos et al., 2010). To form intercellular bonds, E-cadherin dimerised between cells and integrated in cytoplasm with either β-

catenin or γ-catenin, which integrated to α-catenin linking to actin cytoskeleton. This interaction of E-cadherin with β-catenin was essential in normal tissue and cancer cell lines with a well differentiated phenotype. In fibroblast-like cell lines, loss of E-cadherin and expression of truncated β-catenin were often seen and resulted in increased cell mobility (reviewed by Wijnhoven et al., 2000). In controlling cell migration, the β-catenin pathway is also associated with cadherin pathway and GSK3β (Glycogen synthase kinase-3β) /Wnt pathways (reviewed by Nelson and Nusse, 2004), and will be introduced in the next section.

Activation of PI3K/AKT pathway may also be associated with urothelial cancer. In T24 bladder cancer cells, the PI3K inhibitor LY294002 reduced the proliferation of T24 cells via PI3K/AKT pathway significantly, as expression of phosphorylated AKT decreased (Fan et al., 2014), which suggested an important role of AKT pathway in cancer proliferation. PIK3CA demonstrated 15% somatic mutation and 5% copy number alteration, both of the two alteration resulted in activation of PI3K pathway. Within the altered cases (17%), all the mutations were recurrent point mutations (Cancer Genome Atlas Research, 2014). The crosstalk of PI3K/AKT pathway with other pathways and the activating mutations found in urothelial cancer may play important roles and thus worth to be further investigated.

4.1.5 GSK3β/Wnt/β-catenin pathway and insight for tumorigenesis by crosstalk with other pathways

GSK-3β is a serine/threonine protein kinase. In absence of a Wnt signal, GSK-3β combines with other proteins to form a destruction complex, which targets and ubiquitinates β-catenin for degradation. With Wnt signal present, β-catenin is released and translocated to the nucleus to activate expression of genes downstream, which is known as canonical Wnt signalling pathway. SB415286 is a GSK3β inhibitor, which also disrupts the destruction complex and stimulates

canonical Wnt signalling pathway, resulting in release of β-catenin from the destruction complex (MacAulay et al., 2003). Inactivation of GSK3β also activated a β-catenin-LEF/TCF sensitive reporter vector in HEK293 cells, suggesting direct regulation of β-catenin by GSK3β pathway (Coghlan et al., 2000). But a new model suggested that activation of the Wnt pathway only blocked the ubiquitination of β-catenin without releasing it from the destruction complex (reviewed by Clevers and Nusse, 2012).

Another Wnt related pathway, Wnt/Ca^{2+} pathway, was considered as one of the two noncanonical Wnt pathways that does not stimulate β-catenin. Recent result showed that, however, the canonical and noncanonical pathways were not independent of each other (Thrasivoulou et al., 2013). They demonstrated that in prostate cancer PC3 cell line and bladder cancer cell line 253J, Wnt5A increased the intracellular calcium concentration and further caused the translocation of β-catenin to nucleus. Such β-catenin translocation was inhibited significantly by incubation cells with thapsigargin, an inhibitor to Wnt induced intracellular calcium release (Thrasivoulou et al., 2013). But in normal urothelial cultures, when the extracellular calcium concentration was escalated, β-catenin translocated to the intercellular membranes and bound to E-cadherin, of which the interaction was enhanced by the calcium concentration increase (Georgopoulos et al., 2010). E-cadherin mutated NHU cells in physiological calcium concentration demonstrated an abolished E-cadherin expression and nuclear localisation of β-catenin (Georgopoulos et al., 2010). In PC3 cell line, when expression of E-cadherin was increased by stimulation of luteolin, a common dietary flavonoid, invasion was inhibited by the induction of E-cadherin, but can be reversed by siRNA against E-cadherin (Zhou et al., 2009), suggesting an anti-invasion role of E-cadherin. Taken together, the expression of E-cadherin in normal cells might be related to the calcium-induced translocation of β-catenin and involved in Wnt signalling pathway related gene regulation.

Research on GSK3β/β-catenin pathway also suggests its interaction with other carcinogenesis related pathways in normal cells and cancer cell lines/ tissues. An interaction between MAPK and GSK3β/β-catenin pathways was demonstrated in proliferative NHU cells (Georgopoulos et al., 2014). Active β-catenin was up-regulated 48h post seeding along with increase of phosphorylated ERK. This enhanced β-catenin expression was inhibited by either EGFR inhibitor (PD153035) or ERK pathway inhibitor (U0126). Knock down of β-catenin reduced the proliferation of NHU cells together with attenuated phosphorylated ERK signal expression (Georgopoulos et al., 2014).

In prostate cancer cell line, inactivation of GSK3β increased the protein expression of β-catenin and further induced EGFR proteins. This correlated link was further confirmed by shRNA silence of β-catenin transcript and protein showing down regulation of EGFR, and inhibition of EGFR demonstrating reduction of active β-catenin expression (Guturi et al., 2012). Human urothelial carcinoma samples also have demonstrated expression of both β-catenin and p-ERK, which did not express in normal tissue (Ahmad et al., 2011). To further confirm the correlation, transgenic mice were generated with mutated Ras and/or activated β-catenin. Within 12 months, neither mutated Ras or activated β-catenin alone induced tumour formation, but urothelial carcinoma was rapidly formed in mice with both mutated Ras and activated β-catenin, which suggested an important relationship between co-expression of Ras/β-catenin and formation of urothelial carcinoma (Ahmad et al., 2011). The mechanism of this interaction was not yet clear but may indicate a dual target for tumour therapy.

Crosstalk between Wnt/GSK3β and PI3K/AKT was shown in cancer cell lines. GSK3β is a downstream effector of the PI3K/AKT pathway. It can be phosphorylated by EGF-induced activation of AKT pathway in human prostate cancer cell lines DU145 and PC3. This process can be reversed by inhibition of

AKT (Gan et al., 2010). In metastatic T24-L (lung metastasis) cell line, inhibition of PI3K/AKT by LY294002 reduced the phosphorylated AKT and downstream phosphorylated GSK3β in a dose-dependent manner, resulted in activation of GSK3β and followed by suppression of β-catenin transcription activity, which led to reduced invasive ability (Wu et al., 2012).

In colon cancer cells, over expression of β-catenin induced the expression of PPARγ protein, which can also be achieved by inhibition of GSK3β pathway using LiCl. The promoter activity of PPARγ was enhanced dramatically, which may suggest a cross talk between Wnt/β-catenin and nuclear receptor PPARγ in cancer formation, as expression of PPARγ in colon cancer was aberrantly abundant (Jansson et al., 2005).

These findings regarding the role of canonical and noncanonical Wnt/GSK3β pathways and the interaction with other signalling pathways provide evidence of involvement of Wnt/GSK3β pathway in carcinogenesis.

4.1.6 PPARγ pathway and its importance in controlling cell proliferation and differentiation

PPARγ pathway is considerably involved in urothelial differentiation, for example, activating PPARγ pharmacologically in EGFR inhibited NHU cells can induce a differentiated phenotype (Varley et al., 2004a). Phosphorylation of PPARγ by MAPK suppressed the transcriptional activity of PPARγ (Camp and Tafuri, 1997). Another report suggested the PPARγ agonist troglitazone was able to induce phosphorylation of ERK pathway in EGFR exogenous expressed porcine aorta endothelial (PAE) cells, and such process was PPARγ independent as PPARγ antagonist GW9662 did not abolish the phosphorylated MAPK, though it reduced the PPRE promoter activity stimulated by troglitazone (Li et al., 2009).

In cancer cells, a few studies have shown different roles of PPARγ. In bladder cancer cell line 5637, knock down of PPARγ significantly reduced the migration of cells. When treated with rosiglitazone (PPARγ agonist), cell migration and invasion was increased in 5637 cells (Yang et al., 2013). By contrast, other studies showed growth inhibition on cancer cells by activation of PPARγ pathway. Combined treatment of EGFR inhibitor gefitinib and PPARγ agonist DIM-C sensitised EGFR inhibitor gefitinib resistant bladder cancer cell lines (UMUC3, UMUC13 and KU7) (Mansure et al., 2013). *In vivo* experiment also showed that combined treatment of EGFR inhibition and PPARγ activation reduced the tumour weight significantly compared to control (Mansure et al., 2013). In colon cancer, one therapy method suggested that troglitazone, as one of the PPARγ modulators, was used to demonstrate compromised cell growth compared to vehicle control treated cells in several colon cell lines. This decreased proliferation was caused by induction of differentiation assessed using CEA (carcinoembryonic antigen, a marker of differentiation in colon cancer cell lines). It was also shown that this effect was not observed by using ligands having no PPARγ binding abilities, suggesting a specific PPARγ induced growth inhibition. Significantly reduced tumour volume in nude mice was detected in troglitazone fed mice compared to vehicle controls after implanting human colon carcinoma CX-1 tumour cells and allowing the tumour to grow to 70 mm^3 (Sarraf et al., 1998). These findings indicate that activation of PPARγ signalling pathway may play different roles in cancer development or metastasis in different circumstances.

However, the effect of PPARγ ligands on apoptosis of cancer cells should be considered with caution, as it may be caused by off target concentration of PPARγ ligands, which was demonstrated by PPARγ independent mechanism such as activation of store-operated calcium channel (SOC) (Chopra et al., 2009).

Other differentiation-associated transcription factors like FOXA1 were shown to play roles in preventing cancer cell proliferation. It was suggested that poorly differentiated cancers were associated with loss of transcription factors, as loss of FOXA1 expression at transcript and protein level was associated with high grade of bladder cancer. FOXA1 negative tumours were more proliferative (DeGraff et al., 2012). Over expression of FOXA1 in bladder cancer cell line T24 cells increased the expression of E-cadherin and reduced the proliferating rate. By contrast, knock down of FOXA1 promoted the growth of bladder cancer cell line RT4 cells (DeGraff et al., 2012).

Biton et al. showed that most superficial tumour samples (papillary luminal tumours, for example) displayed a differentiated phenotype, as the majority of superficial tumour samples were distributed at the differentiated side in the heatmap, which showed the distribution of various genes in different types of tumours. Differentiation-associated markers (CK20, UPK1A, GRHL3, PPARγ, etc.) that generally expressed in normal tissue were also distributed at the differentiated side (Biton et al., 2014).

Other reports also suggested high protein expression of PPARγ and DNA copy number gain were related to high grade bladder cancer (Conconi et al., 2012; Yang et al., 2013). The region in genome 3 encompassing PPARγ gene showed 29% (in 51 of the 178 tumours) of copy number gains, whereas only 4% (in 7 of the 178 tumours) of copy number loss was detected. This event of copy number gain was not correlated with differentiation, as CK20 showed no consistent expression pattern (Biton et al., 2014). The somatic copy number alteration was confirmed by another study showing that 17% of UC samples had PPARγ amplified mutation, the amplification of which increased to at least 3 copies, to more than 5 copies in some cases (Cancer Genome Atlas Research, 2014). The exact link between PPARγ expression and urothelial cancer is yet to be understood and requires further investigation.

4.1.7 Summary

Regarding differentiation, different types of bladder cancer have demonstrated different phenotype, with which they may have distinct signalling pathways associated. Understanding role of signalling pathways in regulating normal urothelium and alteration of such pathways in carcinogenesis may facilitate the study of normal urothelial function and tumourigenesis.

4.2 Experimental approach

4.2.1 Aims and hypothesis

The aims of this chapter were to investigate the pathways utilised by established *in vitro* UC cell lines and to understand the relationship between the phenotype of UC cells and the signalling pathways they depend on for growth.

The hypothesis for this chapter was that the UC cells demonstrating a differentiated phenotype depend on tissue regenerating pathways for growth, for which it is predicted that they retain expression of transcription factors involved in regulating urothelial differentiation.

4.2.2 Characterisation of urothelial cancer cell lines

UC cell lines were cultured in medium with serum. To eliminate the effect of serum, 5637, T24 and UMUC9 cells were selected as candidates to adapt to KSFM.

To understand whether the phenotype of these cells changed when cultured in different media and characterise the phenotype of all the cultured cell lines, UPK2, CLDN7 and CK20 were selected as differentiation-associated genes. Transcripts of these genes were analysed by RT-QPCR. Transcripts of PPARγ2, ELF3 and FOXA1 were also examined to suggest any possible links between expression of transcription factors and phenotype of UC cell lines. PPARγ2 is one of the PPARγ isoforms regulating differentiation in adipogenesis (See detailed information in chapter 5).

To confirm the phenotype of cell lines and examine whether there was difference of PPARγ protein expression among cell lines, western blots were performed. Protein lysates were harvested from cell lines cultured in different media. PPARγ protein was analysed using PPARγ (E8) antibody. CK13, CK14, CLDN4 and CLDN7 were analysed to indicate the phenotype.

Immunofluorescence was performed to characterise the UC cell lines. CK13, CK14 and CK20 were examined to confirm whether the cells were transitional differentiated, squamous proliferating or differentiated, respectively. PPARγ and ELF3 were examined to indicate the expression of transcription factors in different UC cell lines. Markers of pathways that resulted in cell proliferation in NHU cells, like phosphorylated ERK, phosphorylated AKT and active β-catenin (Georgopoulos et al., 2014; Georgopoulos et al., 2010) were further examined.

4.2.3 Growth assay to determine essential signalling pathways

Alamar Blue assay was performed to determine whether addition of exogenous factors would be able to affect the proliferation of UC cells. Table 4.2.1 displays the factors used for the assay.

Name	Final Conc.	Function/Effect
DMSO	0.1% (V/V)	Vehicle control
FBS	2% (V/V)	Positive control
TZ	1 μM	Activator of PPARγ (Varley et al., 2004a)
TGFβ	2 ng/mL	Promote migration in differentiated NHU cells (Fleming et al., 2012)
EGF	5 ng/mL	Growth factor that promotes proliferation of NHU cells (Varley et al., 2005)
SB415286	10 μM	GSK3β inhibitor, which further activates β-catenin pathway
PD153035	1 μM	Inhibitor of EGFR pathway
U0126	5 μM	Inhibitor of MEK/ERK
LY294002	5 μM	Inhibitor of PI3K/AKT pathway
BPE	50 μg/mL	Enable the proliferation of NHU cells (Southgate et al., 1994)
CT	30 ng/mL	Increase initial plating efficiency of NHU cells (Southgate et al., 1994)
T0070907	1 μM	Inhibitor of PPARγ pathway (Varley et al., 2006)
SB431542	3 μM	Inhibitor of TGFβ pathway

Table 4.2.1 Tested factors on proliferation of UC cells.

To identify key factors or combination of factors promoting proliferation, cells were seeded on plates before application of treatments. Growth factors known as activators for NHU cells were added to cultures demonstrating low

proliferation. By contrast, factors known as inhibitors for proliferation of NHU cells were added to cultures showing proliferative phenotype.

4.2.4 Immunofluorescence to identify specific pathways promoting proliferation

Immunofluorescence was performed with added inhibitors or activators affecting the cell proliferation. Associated pathways were analysed. CK13, CK14 and CK20 were examined to define the phenotype of cells when growth was modified. Transcription factors like PPARγ or ELF3 were assessed to check whether the added factors had altered the localisation and expression of transcription factors.

The fluorescence intensity of nuclei was calculated using Image-Pro Plus software to suggest the amount of proteins expressed in the nucleus. Intensity of nuclei in images were measured and averaged. Bar charts for individual proteins were generated with fluorescence intensity of images captured for each treatment.

4.3 Results

4.3.1 Adaption of UC cell lines

In order to identify the key factors maintaining the cell growth and to compare to NHU cells that grown in serum-free medium (KSFM), cancer cells were adapted to grow in KSFM (Table 4.3.1). 5637 cells were able to grow in KSFM or KSFMc, whereas T24 cells were only able to proliferate in KSFM without supplements. After a week of incubation in KSFM, UMUC9 cells were still not able to grow in KSFM. To improve the growth of UMUC9 in KSFM, other factors were added to cultures and the detailed results are listed in 4.3.4.

Cell line	Standard medium	KSFMc	KSFM	KSFM+Ca^{2+}
5637	RPMI (5% FBS)	Y	Y	No data
T24	DMEM:RPMI 50%:50% (5% FBS)	N	Y	No data
UMUC9	DMEM (10% FBS)	*	N	N

Table 4.3.1 Cell lines adapted to serum-free medium. Y indicates cell growth; N indicates no growth in at least one week. *, see 4.3.4 for more information of UMUC9 in complete KSFM (KSFMc). 5637 cells and T24 cells were able to be adapted to KSFM, so no more supplements was added (No data).

4.3.2 Characterisation of UC cell lines

4.3.2.1 Transcripts of Transcription factors and differentiation-associated genes by RT-QPCR

To characterise the phenotype of urothelial cancer cell lines cultured *in vitro*, RT-QPCR was performed using primers of differentiation-associated genes. Transcript expression of UPK2 was variable between UC cell lines, suggesting that phenotype of cancer cell lines in terms of the degree of differentiation were different from each other. In NHU cells shown as control, the transcripts of UPK2 were only present in differentiated cells. UMUC9 was the most differentiated cell line demonstrating a similar amount of UPK2 expression as differentiated NHU cells. RT4, SD48 and RT112 cells had less UPK2 transcripts expressed. 5637 and T24 cells had little UPK2 expression, which resembled the

UPK2 transcripts in proliferative NHU cells and demonstrated non-differentiated phenotypes (Fig. 4.3.1).

Expression of CLDN7 was minimal in RT4 cells and T24 cells. Among the cancer cell lines, UMUC9 showed the most abundant CLDN7 transcript (Fig. 4.3.1).

CK20 demonstrated strikingly high transcript expression in UMUC9 and SD48 cells (Fig. 4.3.1). A log scale bar chart is included in Appendix (Fig 7.1.1) to show the more detailed information of CK20 transcripts in differentiated NHU cells and other UC cell lines.

The difference of differentiation-associated genes expressed by 5637 and T24 cells in different media was not dramatic. These two cell lines demonstrated a non-differentiated phenotype, which was independent of the presence of serum.

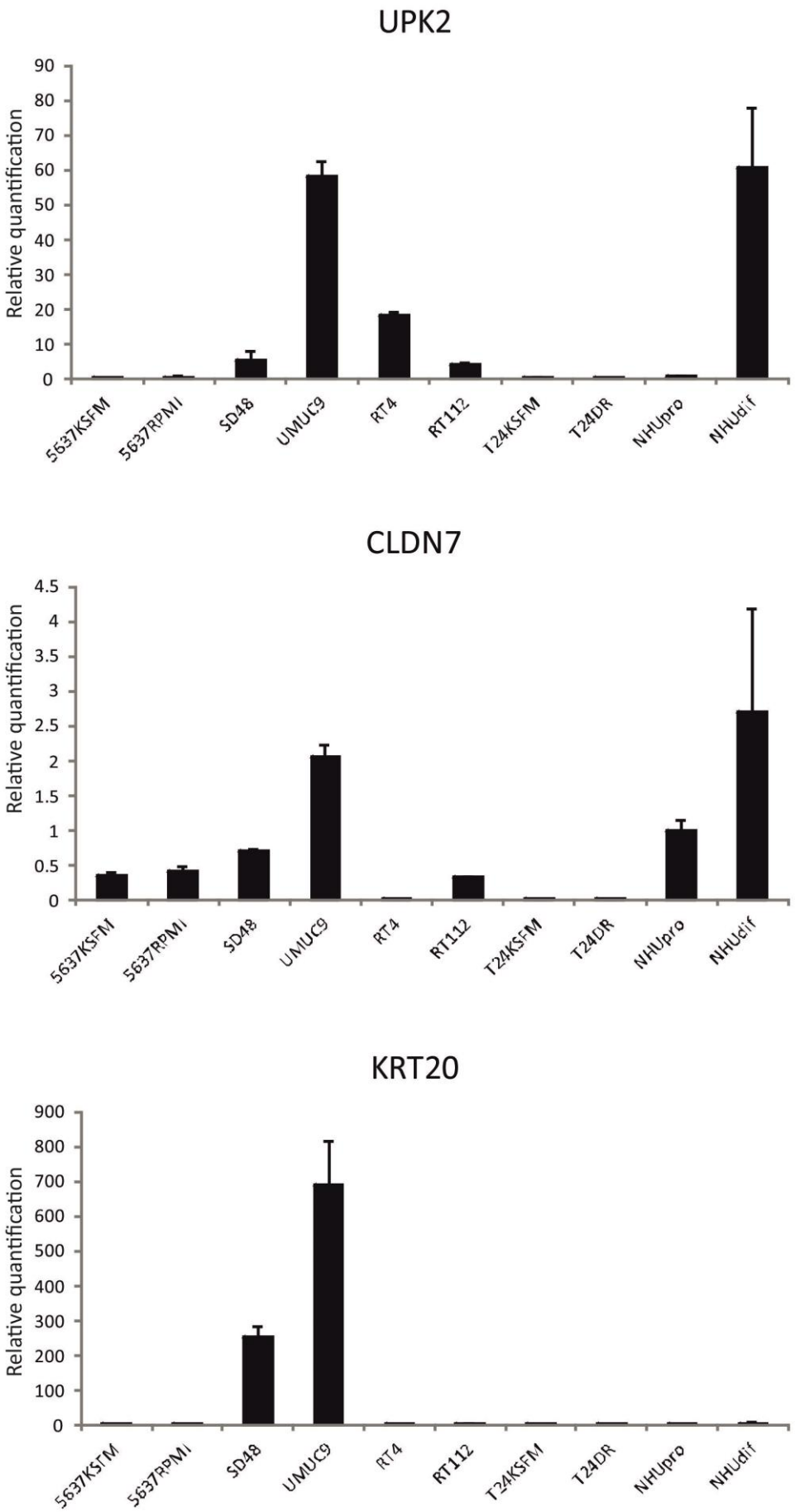
UPK2
Relative quantification
90
80
70
60
50
40
30
20
10
0
5637KSFM
5637RPMI
SD48
UMUC9
RT4
RT112
T24KSFM
T24DR
NHUpro
NHUdif
CLDN7
Relative quantification
4.5
4
3.5
3
2.5
2
1.5
1
0.5
0
5637KSFM
5637RPMI
SD48
UMUC9
RT4
RT112
T24KSFM
T24DR
NHUpro
NHUdif
KRT20
Relative quantification
900
800
700
600
500
400
300
200
100
0
5637KSFM
5637RPMI
SD48
UMUC9
RT4
RT112
T24KSFM
T24DR
NHUpro
NHUdif

Fig 4.3.1 Transcript expression of differentiation-associated genes. RNA samples were obtained from cancer cells cultured in medium with serum or adapted to KSFM (5637 cells and T24 cells). 5637RPMI indicates RNA sample of 5637 cells cultured in RPMI with serum; T24DR indicates RNA sample of T24 cells cultured in DMEM& RPMI with serum. Proliferating (NHU pro) and 7 days TZ/PD differentiated (NHU dif) NHU cells (Y1289) were included as control. RT-QPCR was performed. Gene expression of UPK2, CLDN7 and KRT20 was normalized to GAPDH. Fold change of each sample was obtained by comparing to the proliferating NHU cell sample. Error bars indicate standard deviation of three technical replicates. Note the high expression of UPK2, CLDN7 and KRT20 in the UMUC9 cell line.

With a differentiated phenotype, UMUC9 cells also showed the most abundant expression of ELF3 and PPARG2 of all tested cell lines. Transcript of PPARG2 was massively expressed in UMUC9, whereas ELF3 was expressed most abundantly in differentiated NHU cells. Another cell line (SD48) also showing a differentiated phenotype had the most abundant transcript of FOXA1 expressed (Fig 4.3.2).

Though there was almost no diversity regarding expression of downstream differentiation-associated genes between 5637 or T24 cells grown in different media, the expression of transcription factors was more abundant in medium supplemented with serum. This finding may suggest that the expression of transcription factors can be up-regulated by factors in the serum, but for cells showing non-differentiated phenotype, the difference of transcription factors expression did not affect either the phenotype or the proliferation of cells necessarily, as both 5637 cells and T24 cells were able to proliferate regardless the absence of serum in the medium (Fig 4.3.2).

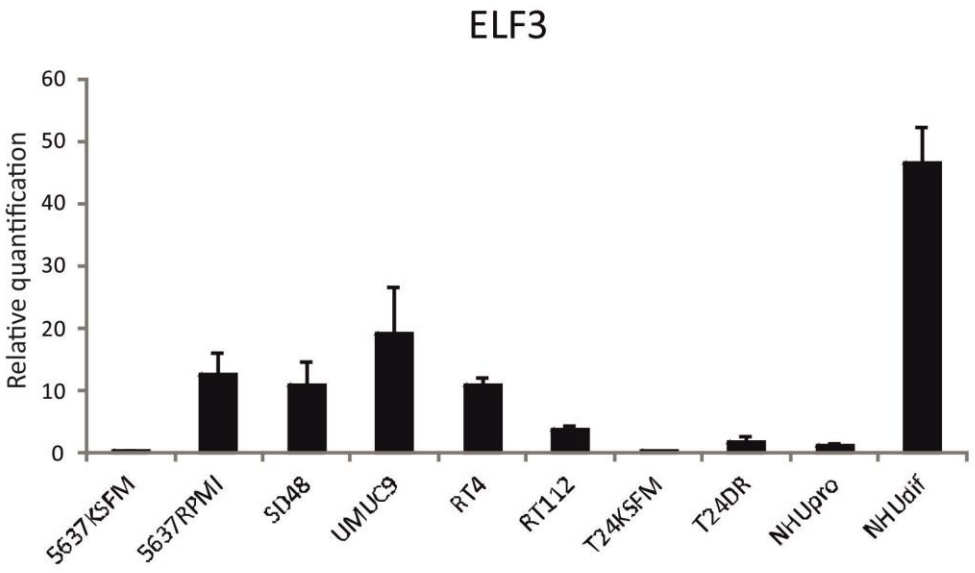
ELF3
Relative quantification
60
50
40
30
20
10
0
5637KSFM
5637RPMI
SD48
UMUC9
RT4
RT112
T24KSFM
T24DR
NHUpro
NHUdif

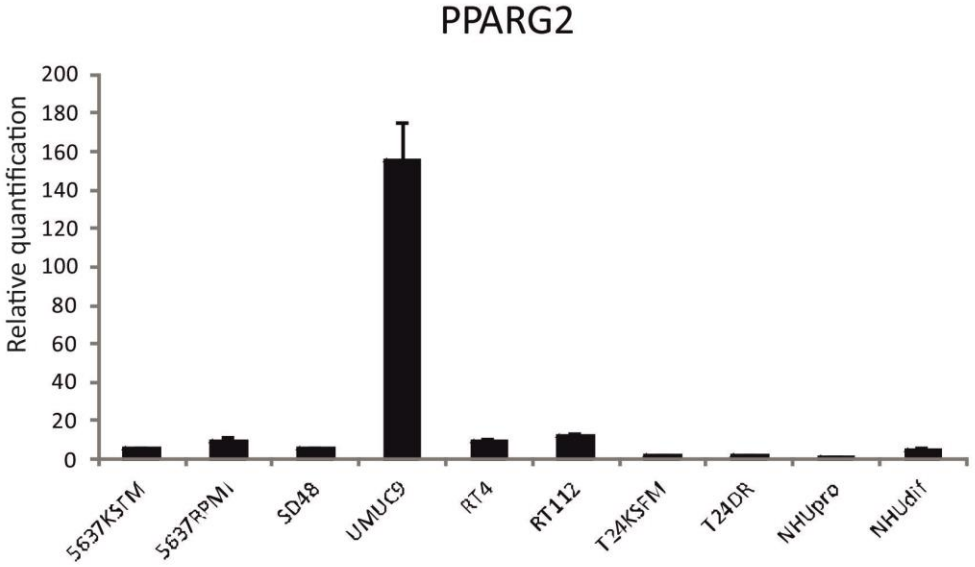
PPARG2
Relative quantification
200
180
160
140
120
100
80
60
40
20
0
5637KSFM
5637RPMI
SD48
UMUC9
RT4
RT112
T24KSFM
T24DR
NHUpro
NHUdif

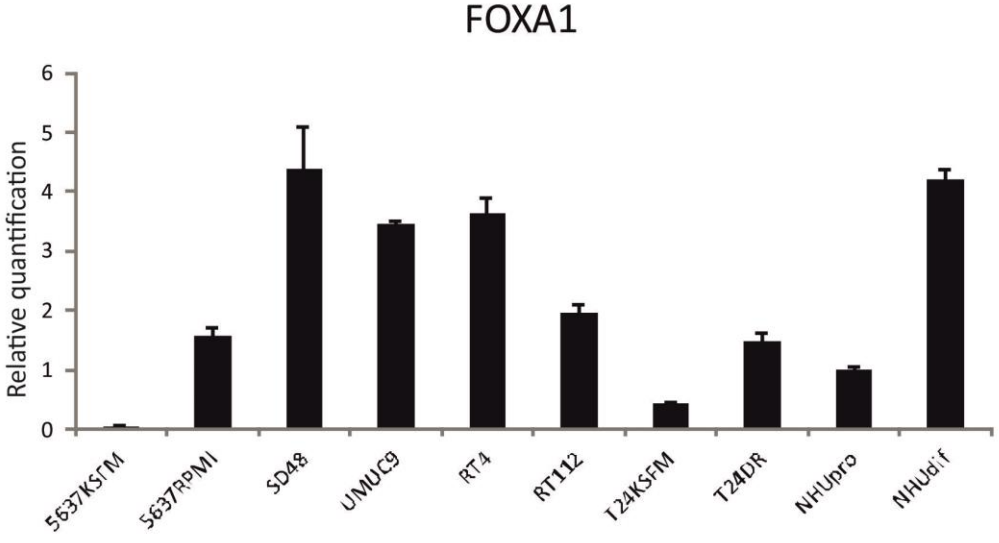
FOXA1
Relative quantification
6
5
4
3
2
1
0
5637KSFM
5637RPMI
SD48
UMUC9
RT4
RT112
T24KSFM
T24DR
NHUpro
NHUdif

Fig 4.3.2 Transcript expression of transcription factors. RNA samples were obtained as described in Fig 4.3.1. Proliferating (NHU pro) and 7 days TZ/PD differentiated (NHU dif) NHU cells (Y1289) were included as control. 5637RPMI indicates RNA sample of 5637 cells cultured in RPMI with serum; T24DR indicates RNA sample of T24 cells cultured in DMEM& RPMI with serum. RT-QPCR was performed as described in the methods. Gene expression of PPARG2, ELF3 and FOXA1 was normalized to GAPDH. Fold change of each sample was obtained by comparing to the proliferating NHU sample. Error bars indicate standard deviation of three technical replicates. Note the high expression of PPARG2 in the UMUC9 cell line.

4.3.2.2 Protein expression of PPARγ and other differentiation markers

To further confirm the characterisation of UC cell lines, protein expression of PPARγ and differentiation-associated markers was examined by western blotting.

On the blot, multiple protein bands appeared after incubation of PPARγ E8 antibody. A band at about 40 kDa (Band D) was expressed in almost all samples, with the most expression in NHU cells. The 50/52 kDa bands (Band C / B) were present in all tested cell lines. The least amount of 50/52 kDa bands was observed in the T24 cell line. A switch of 50/52 kDa bands in 5637 cells cultured in different media was observed, suggesting a possible induction of different PPARγ isoform by factors in the serum .The 58 kDa band (Band A) was present in NHU cells and 5637 cells, but it was not always detectable (see chapter 3 for other PPARγ blots). UMUC9 cells displaying most abundant PPARG2 transcript expression did not demonstrate any visible difference compared to the other cell lines. Bands with higher and lower molecular weight were also present on the blots (Fig 4.3.3). Expressing pattern of UC cells compared with lysates from other tissues/species is shown in Appendix (Fig 7.1.2).

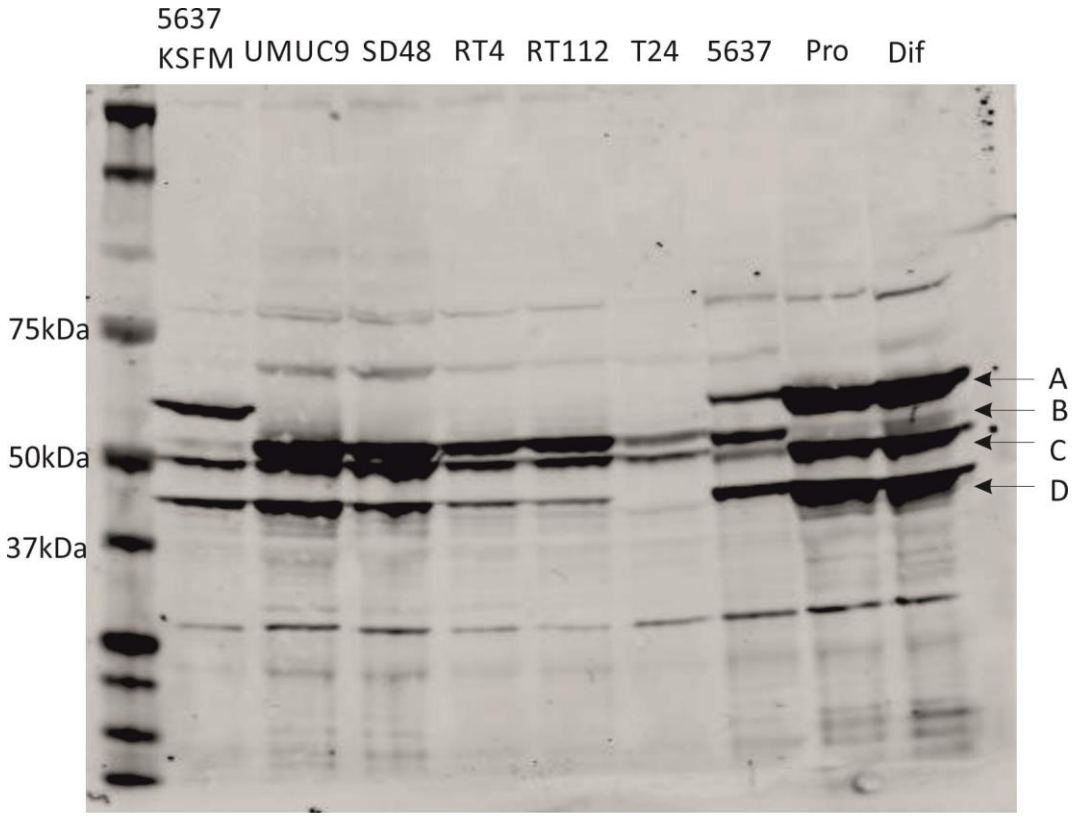

Fig 4.3.3 PPARγ E8 blot of different urothelial cancer cell lines. Lysates were obtained from cancer cells cultured in medium with serum or adapted to KSFM (5637 cell line, labelled as 5637 KSFM). Proliferating (Pro) and 6 days ABS/ Ca^{2+} differentiated (Dif) NHU cells (Y588, lysates were taken by Ros Duke) were included as control. PPARγ E8 antibody was applied and detected following the western blotting protocol. Four main PPARγ bands appeared on blots were pointed by arrows and labelled as A, B, C and D.

To obtain more information about the phenotype of the cell lines, expression of CK proteins and tight junction proteins was examined. Proliferating NHU cultures showed CK14 expression, whereas only differentiated NHU cells expressed CK13 proteins. RT112 cells demonstrated the expression of both CK13 and CK14. 5637 cells cultured in KSFM showed CK14 expression, whereas cells in RPMI with serum were CK14 negative, suggesting the adapting of 5637 cells into serum-free medium might have affected their phenotype, which was also associated with a distinct PPARγ expression pattern (Fig 4.3.4).

The protein expression of CLDN7 was similar to the CLDN7 transcripts (negative in RT4 and T24 cells, see Fig 4.3.1). CLDN4 protein was expressed in all cell lines except T24, suggesting that T24 was poorly differentiated with

nearly no expression of differentiation-associated markers. A small band slightly lower than the main band of CLDN4 was detectable in UMUC9, SD48 and differentiated NHU cells, all showing a differentiated phenotype (Fig 4.3.4).

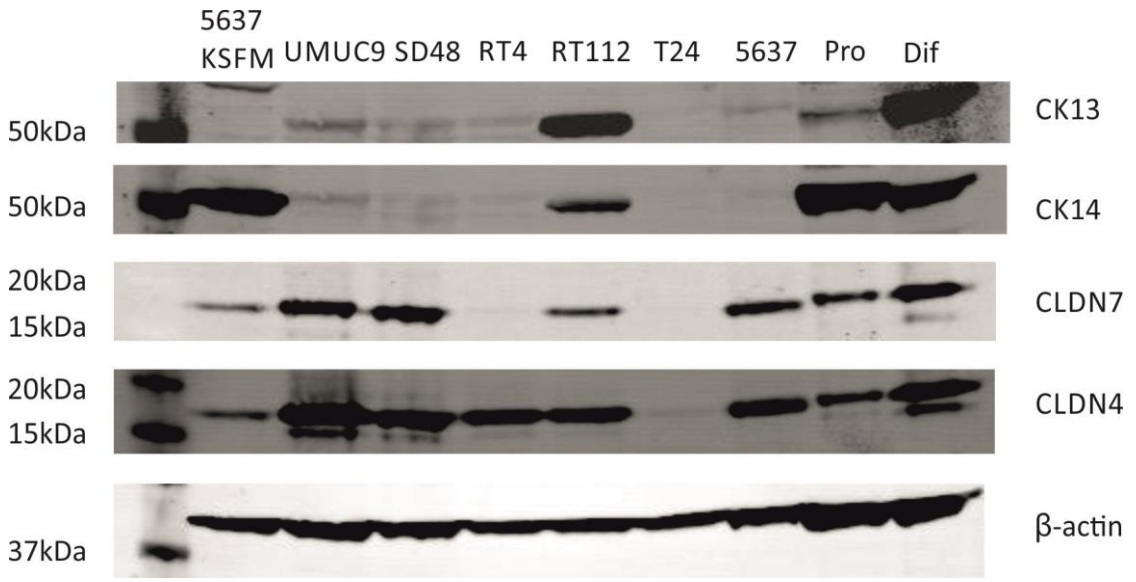

Fig 4.3.4 Expression of differentiation-associated proteins. Lysates were obtained as described in Fig 4.3.3. Proliferating and 6 days ABS/ Ca2+ differentiated NHU cells (Y588, lysates were taken by Ros Duke) were included as control. CK13, CK14, CLDN4 and CLDN7 antibodies were applied and detected following the western blotting protocol. β-actin was utilised as loading control.

From the RT-QPCR and western blotting results, UMUC9 cell line was selected as the most differentiated urothelial cancer cell line among the tested cell lines and utilised to understand the importance of maintaining a differentiated phenotype. 5637 cell line was chosen as another candidate for further investigation, as it was less differentiated and showed different phenotypes in different media (with or without serum) by western blotting.

4.3.3 Characterisation of UMUC9 cells by immunofluorescence

UMUC9 cells demonstrated a differentiated phenotype with dramatic amount of PPARG2 transcript expression. Whether there is a relationship between such phenotype and PPARG2 transcript expression requires further investigation of the signalling pathways involved. Characterisation of UMUC9 cells by immunofluorescence was performed.

UMUC9 cells demonstrated negative CK14 expression along with positive cytoplasmic phosphorylated ERK. The expression of CK14 was present in proliferating NHU cells, which also showed the phosphorylated ERK expression in the nuclei (Fig 4.3.5).

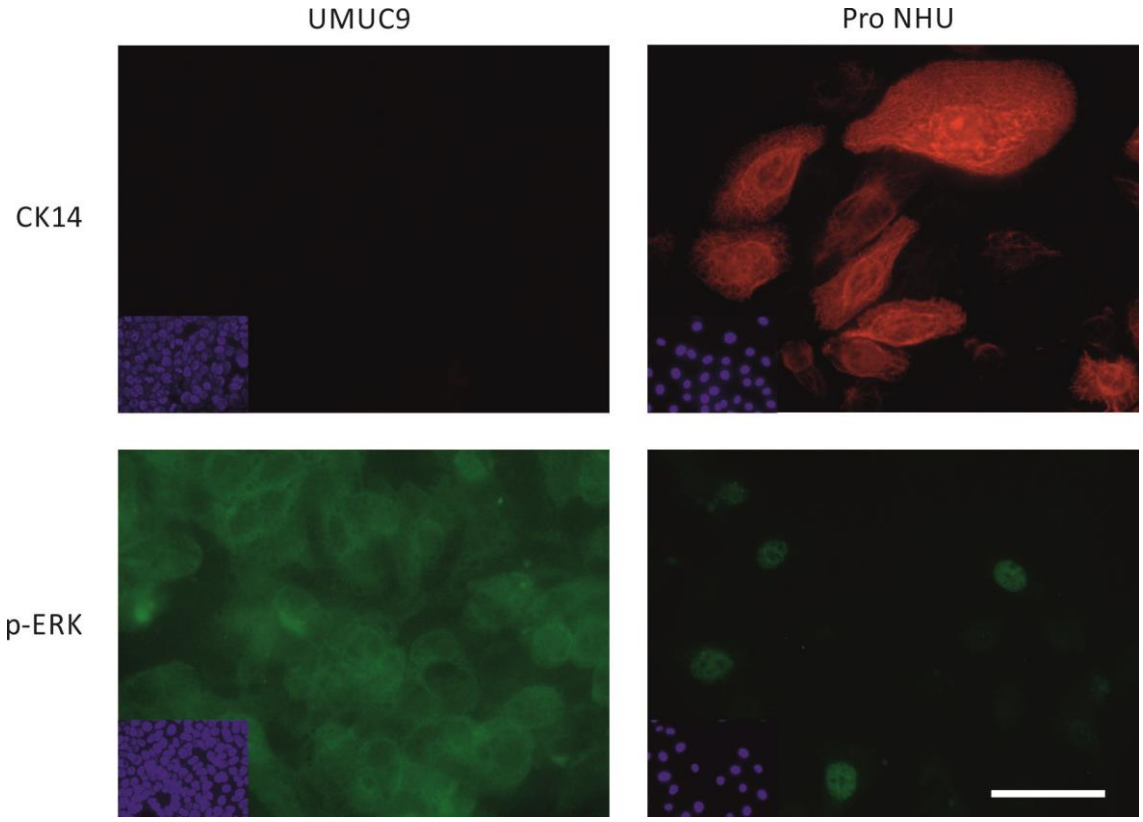

Fig 4.3.5 Expression of CK14 and p-ERK in UMUC9 cells. UMUC9 cells were cultured in DMEM (10% FBS) and seeded on slides. Proliferating NHU cells (Y1156) showed expression of both CK14 and p-ERK. Slides were fixed using 50:50 of Methanol:Acetone fixation (Me:Ac) for 30s and incubated with primary antibodies of CK14 and p-ERK. Scale bar represents 50μm.

Differentiation-associated cytokeratin proteins were examined as well. UMUC9 cells cultured in DMEM with serum did not show any CK13 expression. By contrast, CK20 demonstrated ubiquitous expression in UMUC9 cells. In differentiated NHU cells as positive control, CK13 and CK20 were both present, but the expression of CK20 was sporadic and only detectable in some cells (Fig 4.3.6).

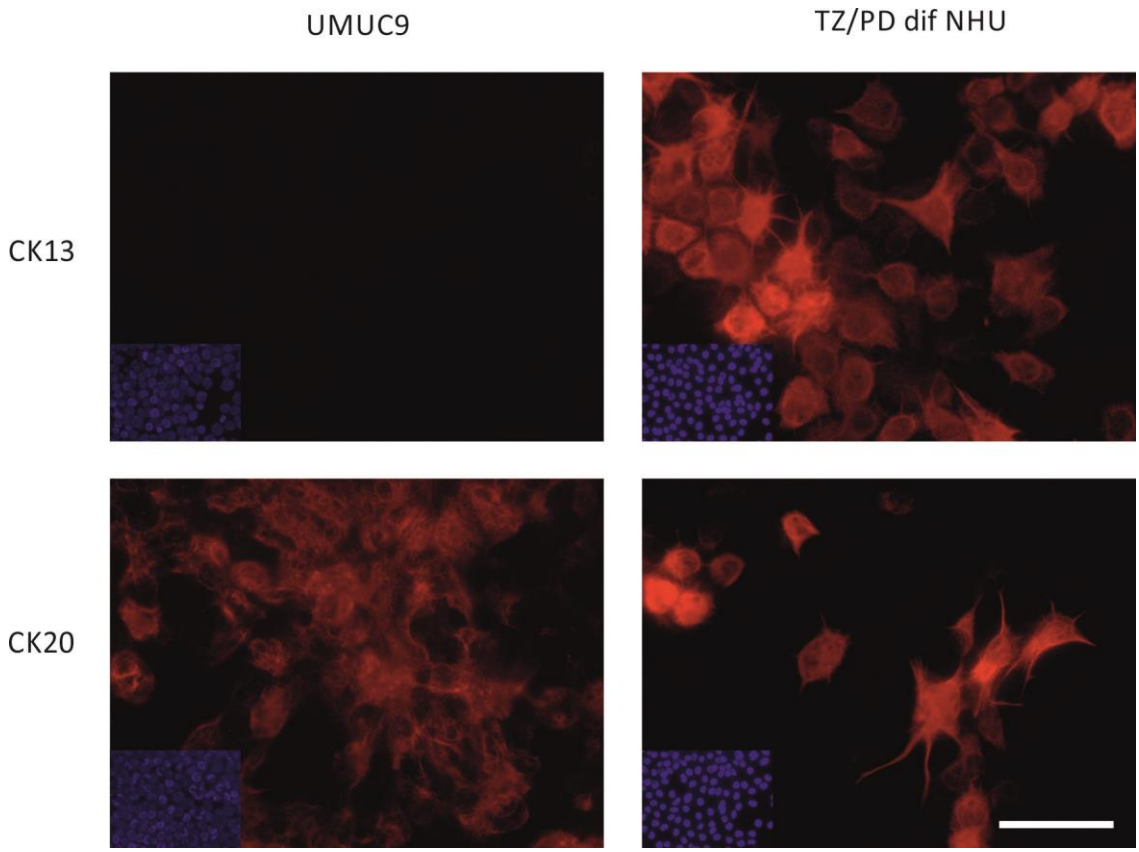

Fig 4.3.6 Expression of CK13 and CK20 in UMUC9 cells. UMUC9 cells were seeded in DMEM with 10% FBS and fixed using Me:Ac fixation method. NHU cells (Y1156) were induced to differentiate with TZ/PD for 72h as a differentiated control (TZ/PD dif NHU). Primary antibodies of CK13 and CK20 were applied on the slides. Scale bar represents 50μm.

UMUC9 cells showed a differentiated phenotype without CK13 expression. To explore the difference between differentiated NHU cells and UMUC9 cells, expression of transcription factors was further analysed. PPARγ and ELF3 demonstrated nuclear expression in UMUC9 cells, which resembled the expression of PPARγ and ELF3 in NHU cells. PPARγ2 that showed considerable transcript expression in UMUC9 cells was analysed to verify the

expression and indicate the localisation. It suggested that the expression of PPARγ2 was considerable and localised to nuclei of cells specifically (Fig 4.3.7).

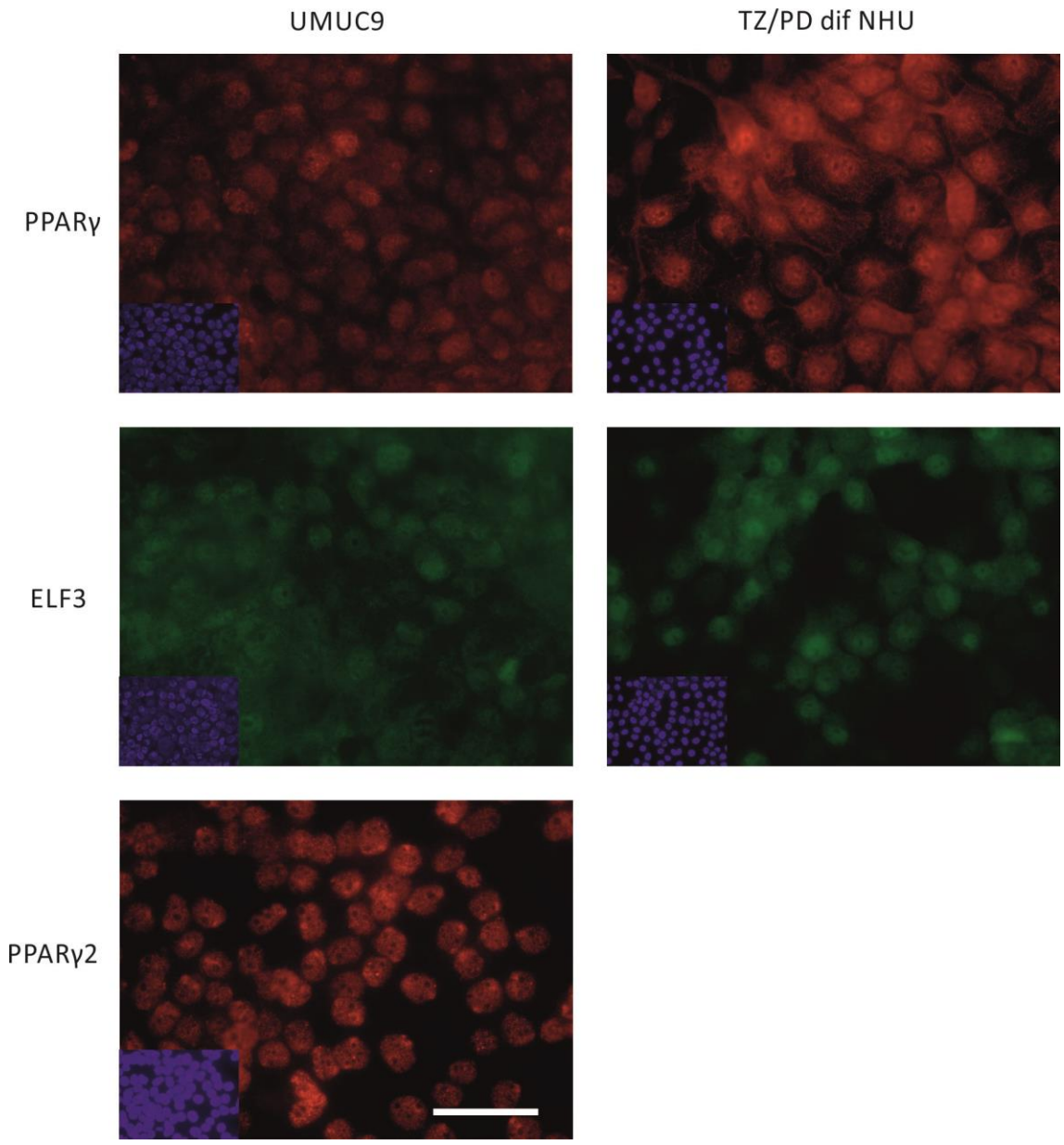

Fig 4.3.7 Expression of PPARγ and ELF3 in UMUC9 cells. UMUC9 cells were seeded in DMEM with 10% FBS and fixed using Me:Ac fixation. Differentiated NHU cells (Y1156) were induced to differentiate for 72h and shown as differentiation control (TZ/PD dif NHU). Primary antibodies of PPARγ and ELF3 were applied to UMUC9 and NHU cells. PPARγ2 was applied to UMUC9 cells. Scale bar represents 50μm.

To understand the pathways UMUC9 cells dependent on for growth, the pathways driving proliferation in NHU cells were examined. In DMEM with serum, UMUC9 cells showed membrane expression of E-cadherin, active β-catenin and phosphorylated AKT. When treated with calcium at physiological

concentration (2mM), NHU cells showed membrane E-cadherin and nuclear active β-catenin expression (Fig 4.3.8).

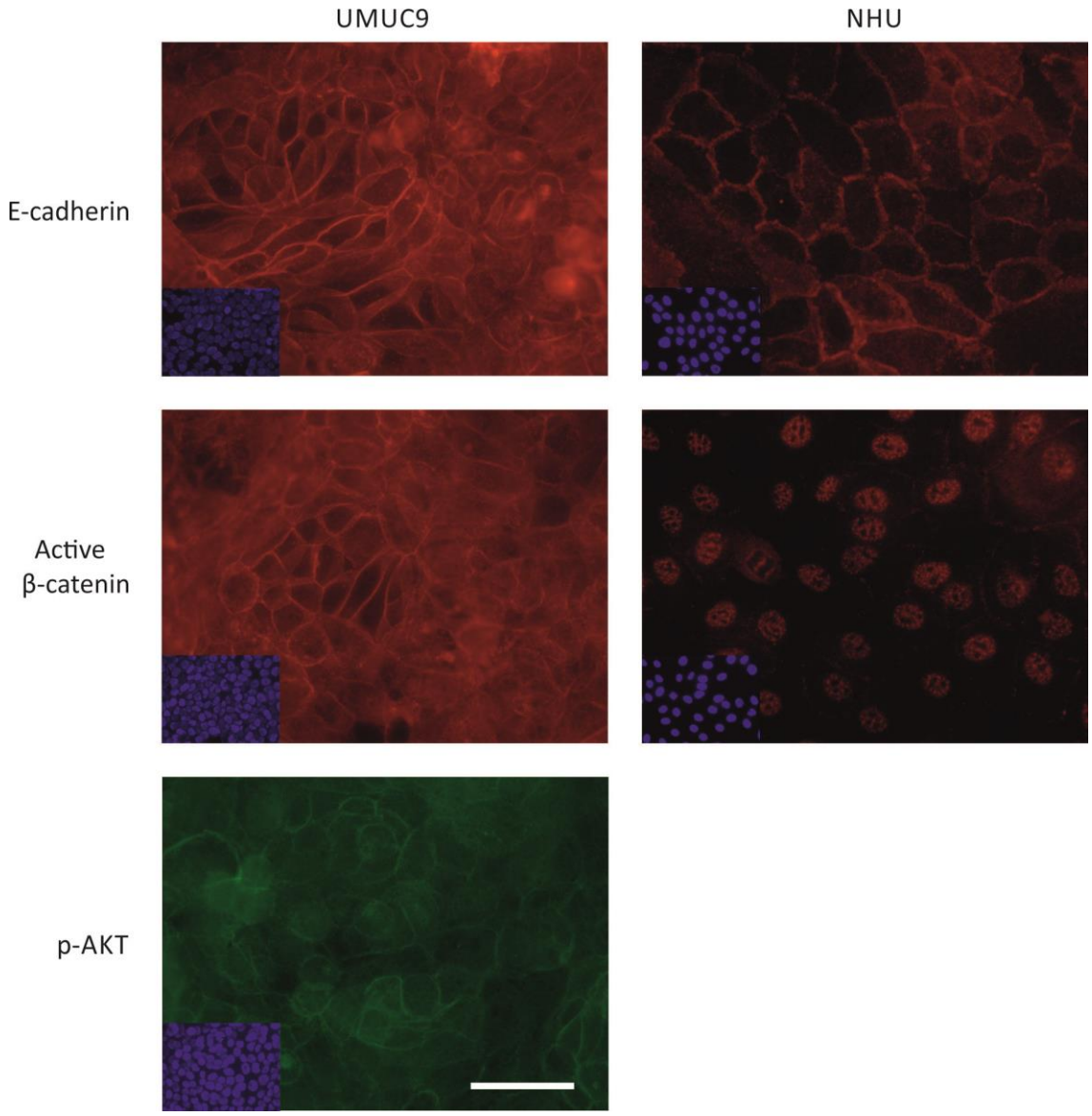

Fig 4.3.8 Expression of proteins associated with proliferation in UMUC9. UMUC9 cells were seeded in DMEM with 10% FBS. Slides were either fixed with Me/Ac for examining of E-cadherin or fixed with 10% formalin and permeabilised with 0.5% Triton X-100 for 30 min for detecting of active β-catenin and p-AKT. NHU cells (Y1156) were treated with 2mM calcium for 72h as positive control and fixed with Me/Ac. Primary antibodies against E-cadherin, active β-catenin and phosphorylated AKT were applied. Scale bar represents 50μm.

UMUC9 cells cultured in DMEM with serum demonstrated a differentiated phenotype with features similar to NHU cells cultured in physiological calcium concentration. In order to understand the pathways driving proliferation in UMUC9 cells, and minimise the effect of serum on growth. UMUC9 cells were

adapted to 80% KSFM and 20% DMEM with serum (2% FBS as final conc.), as cells were unable to adapt to proliferate in 100% KSFM.

4.3.4 Effect on proliferation of UMUC9 cells in KSFM by various factors

UMUC9 cells were cultivated in 80% KSFM and 20% DMEM with 2% FBS as final concentration. To further investigate the pathways involved in proliferation of UMUC9 cells, inhibitors were added to cultures (See Table 4.2.1). Growth assay showing the reduction of Alamar Blue on day 6 suggested that MEK/ERK pathway and Wnt/β-catenin pathway were associated with proliferation of UMUC9 cells significantly. But the decrease of cell growth was not dramatic, suggesting the role of these pathways was not critical or the remnant of serum was still able to promote proliferation (Fig 4.3.9).

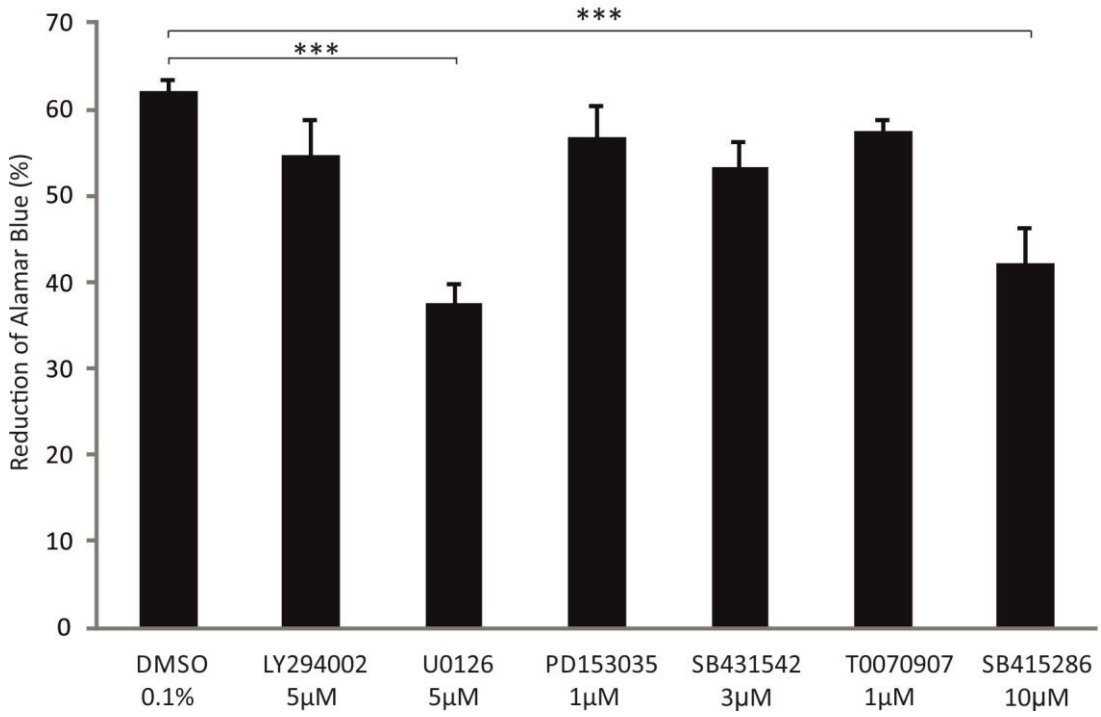

Fig 4.3.9 Growth inhibition on UMUC9 cells. UMUC9 cells were seeded at $2X10^4$ /mL cultured in 80% KSFM and 20% DMEM (2% FBS). Various inhibitors were added to cultures. Growth assay was performed as described in the methods on the 6th day. Error bars indicate standard deviation of five experimental replicates. Statistical analysis was calculated by one-way ANOVA with Bonferroni multiple comparisons post-test (*** P<0.001).

Because the remnant of serum might affect the proliferation of UMUC9 cells, a further experiment was performed with UMUC9 cells seeded in 100% KSFM. Treatments of different media were added to cultures to indicate whether any additional factor was able to promote the growth of UMUC9 cells.

In 100% KSFM, UMUC9 cells were unable to proliferate for almost two weeks. Physical calcium concentration did not promote proliferation. Cells cultured in medium with serum showed continuous proliferation, regardless of the concentration of serum (KSFM+10% FBS or 80% KSFM containing 2% FBS). KSFMc or KSFM supplemented with EGF promoted the cell growth after days of treatment but with a lower growth rate than cultures in media with serum. The cells with different treatments were cultured in 5% CO_2, which might have affected the cell proliferation in DMEM (10% FBS, should be incubated in 10% CO_2) (Fig 4.3.10).

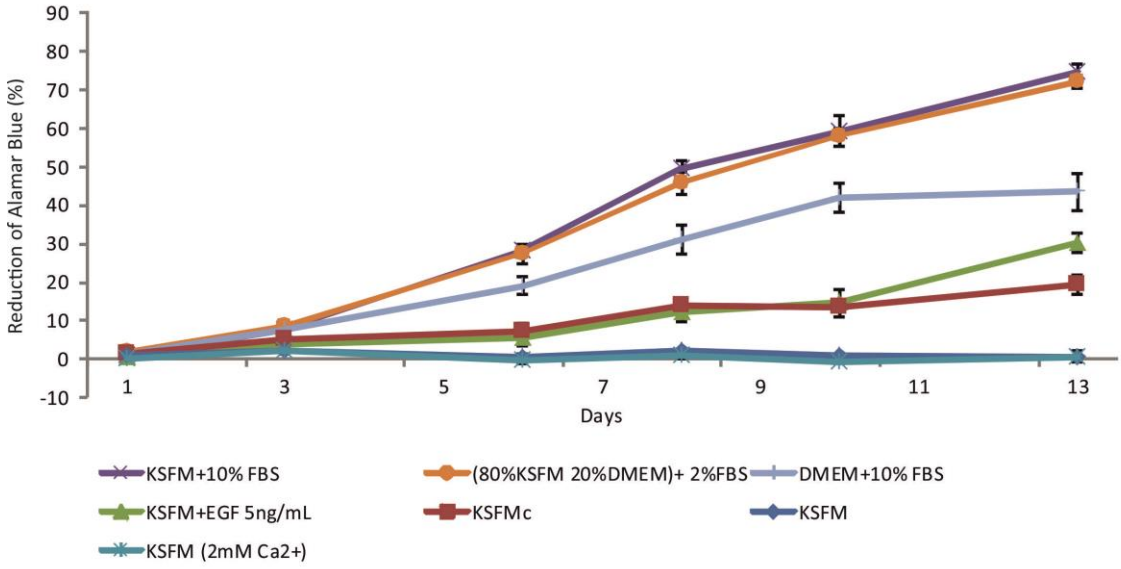

Fig 4.3.10 Growth assay of UMUC9 cells. Cells were seeded at $2X10^4$ /mL in 100% KSFM on 96 well plate and treated the next day with various media. For cells grown in 80% KSFM, the rest of the medium was DMEM (10% FBS). Growth assay was performed as indicated with separate plates as described in the methods. Error bars indicate standard deviation of six experimental replicates.

To display the difference of population doubling rate of UMUC9 cell in various media, the reduction of Alamar Blue on the 8th day was extracted and shown in a bar chart. Statistical analysis suggested that all the other media except for KSFM with calcium added significantly improved the growth rate, though it was not as tremendous as positive controls.

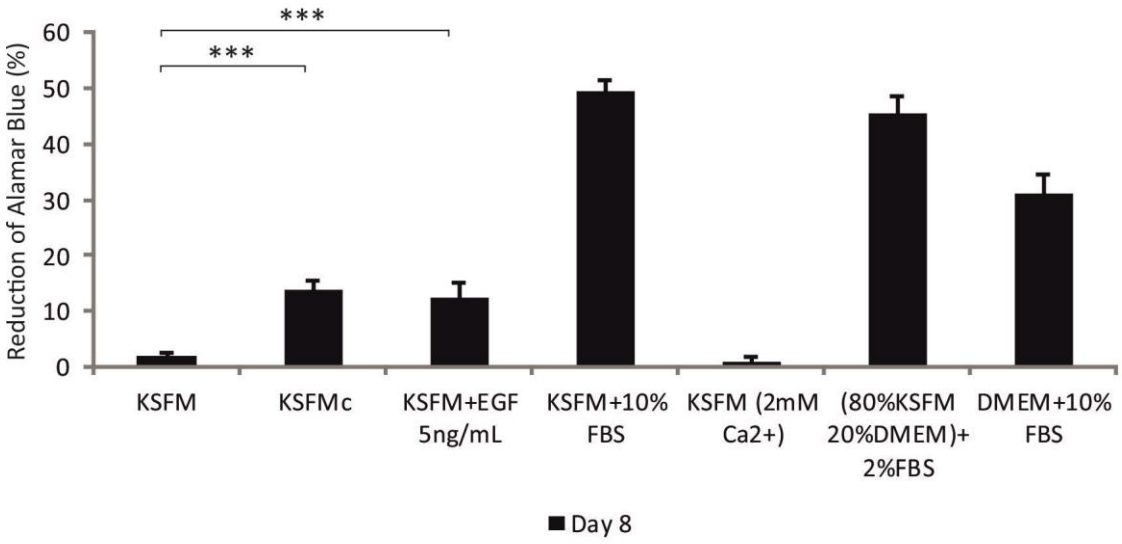

Fig 4.3.11 Effect of different media on growth of UMUC9 on day 8. Bar chart was generated using the 8th day data. Error bars indicate standard deviation of six experimental replicates. Statistical analysis was calculated by one-way ANOVA with Bonferroni multiple comparisons post-test (*** P<0.001). Reduction rates of cells grown in media with serum supplied were shown as positive controls.

To further investigate the factor promoting growth, UMUC9 cells were treated with various growth factors listed in Table 4.2.1. Treatments are grouped and listed in Table 4.3.2.

DMSO **(-)**	U0126	LY294002	PD153035
TZ	**TZ** U0126	**TZ** LY294002	**TZ** PD153035
TGFβ	**TGFβ** U0126	**TGFβ** LY294002	**TGFβ** PD153035
SB415286	**SB415286** U0126	**SB415286** LY294002	**SB415286** PD153035
EGF	BPE	CT	**EGF** BPE CT (KSFMc)
TGFβ EGF	**TGFβ TZ**	**TGFβ SB415286**	2% FBS **(+)**

Table 4.3.2 Growth factors added in cultures. Treatments are listed in the table. DMSO was used as vehicle control. 2% FBS was added to cultures to demonstrate the standard proliferative phenotype. Groups are shown either with different font colour or gray highlight in columns. Concentration of individual factor was listed in Table 4.2.1 along with their function on NHU cells.

Cell images of treatments that promote cell proliferation were displayed. EGF promoted proliferation of UMUC9 cells without apparently changed the shape of cells. The combination of EGF and TGFβ increased the proliferation as well, but the morphology of cells was altered from cuboidal shape (see positive control cells cultured in 2% FBS) to elongated fibroblast-like shape, which resembled the EMT process. KSFMc increased growth to a similar extent as EGF induced proliferation (Fig 4.3.12).

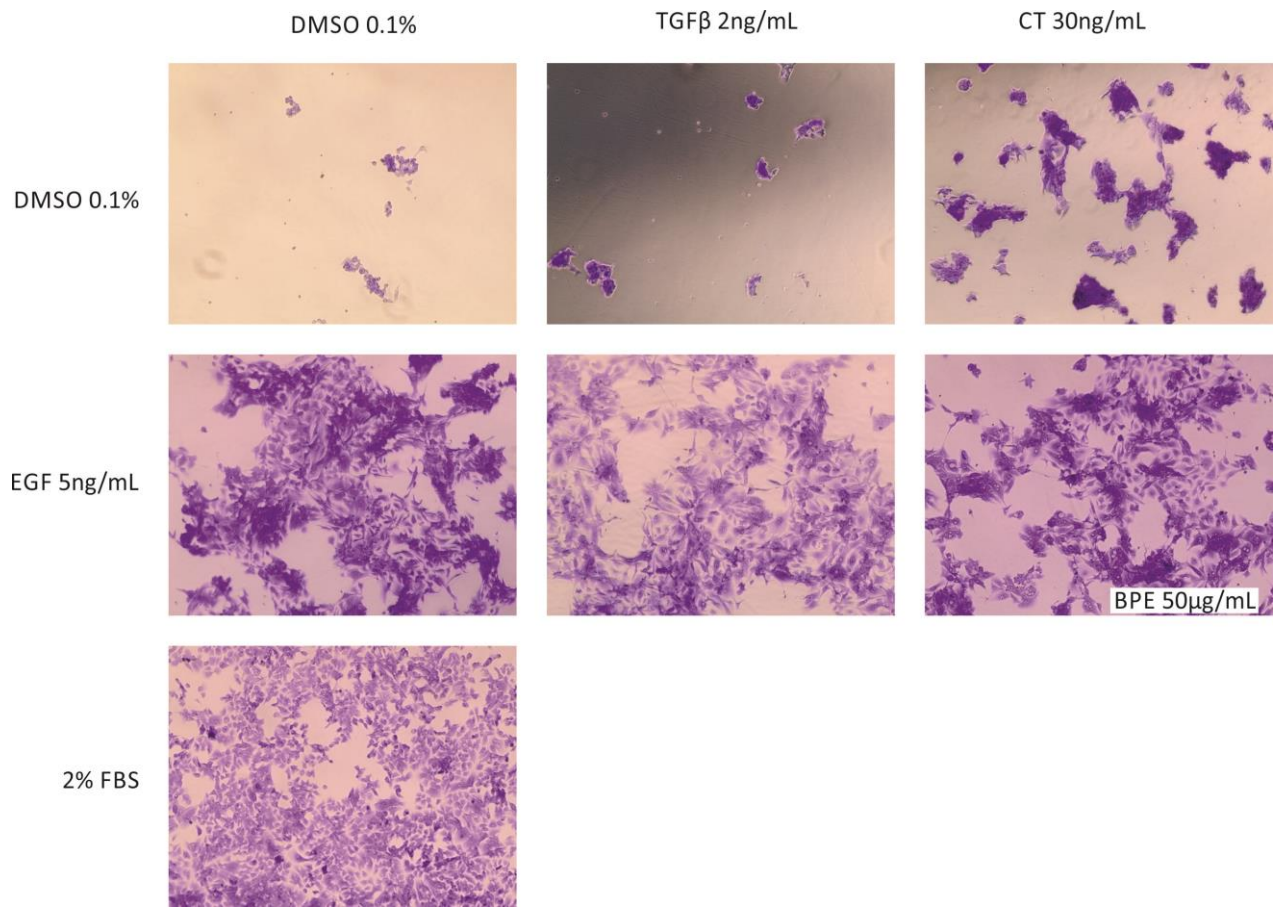

Fig 4.3.12 Combination of factors required to promote growth in UMUC9 cells. Cells were seeded at 2.5X10^4 /cm^2 in KSFM on 24 well plates and treated the next day. Media were replaced every other day for one week. Cultures were fixed with 50:50 of Methanol:Acetone for 30s, leaving only attached cells which were then stained with 0.1% w/v Crystal Violet (made up with 20% ethanol) for 5min. Phase contrast micrographs were taken after wash with distilled water. 0.1% DMSO was utilised as negative control demonstrating minimal proliferation. 2% FBS was included as positive control. Images with Crystal Violet staining shown fixed cells were displayed. Cell images of non-effective treatments that led to cell floating were not included. Treatments were combination of headings listed for individual row/column. For example, the last image on the second row indicates the UMUC9 cells treated with EGF, BPE and CT. Scale bar equals 200µm.

Growth assay with EGF and TGFβ was performed to test the growth promoting effects on UMUC9 cells cultured in KSFM. TGFβ treatment alone did not affect cell growth dramatically. Treatment with combined EGF and TGFβ showed similar proliferating trend to EGF alone, suggested that EGF was the main factor regulating growth. But the reduction rate of Alamar blue was less across the treatment compared to 2% FBS treated one, indicating other untested factors in the serum were critical for cell growth as well (Fig 4.3.13).

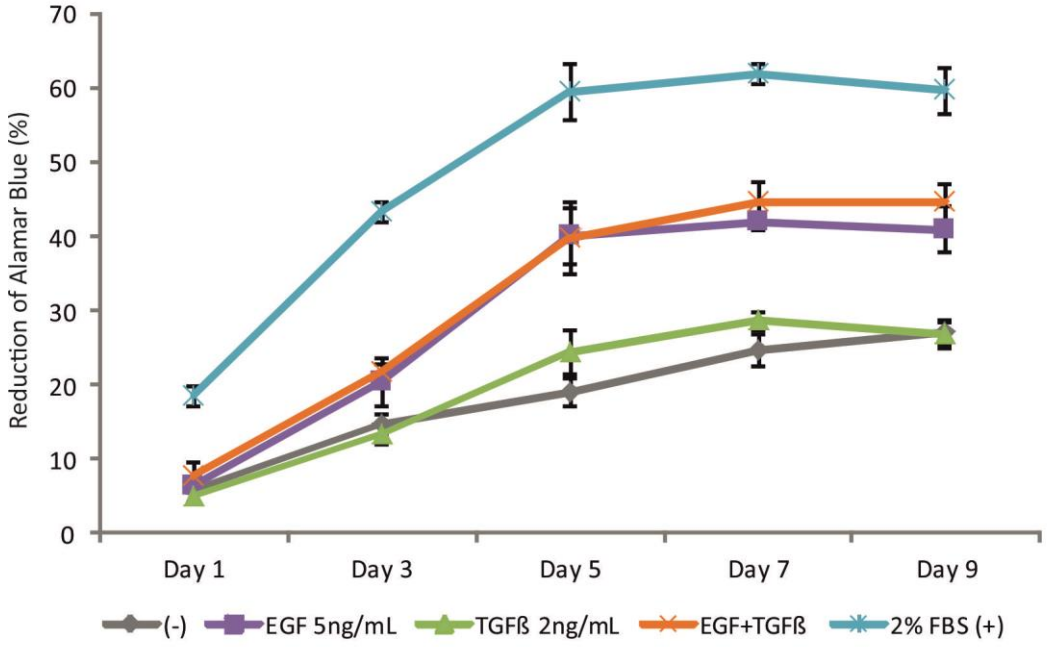

Fig 4.3.13 Growth assay to test the effect of EGF and TGFβ in UMUC9. Cells were seeded at $5X10^4$ /mL in KSFM and treated on the next day. Error bars indicate standard deviation of six experimental replicates.

To understand the significance of growth promotion by EGF and TGFβ, reduction rate of Alamar Blue on the 5th day was displayed as bar chart in Fig 4.3.14, which confirmed EGF as main growth promoting factor for UMUC9 cells growing in KSFM.

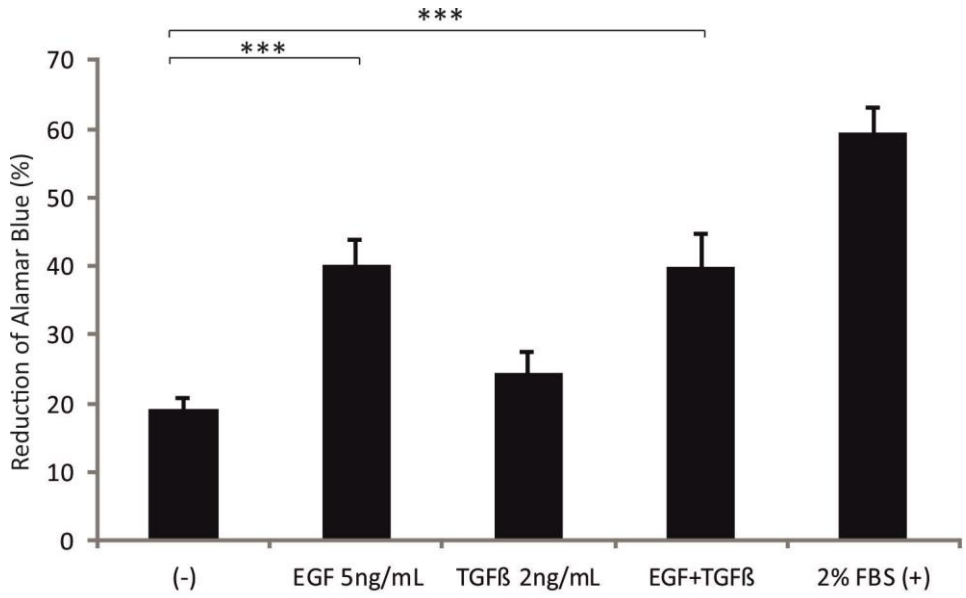

Fig 4.3.14 Effect of EGF and TGFβ on UMUC9 cell growth. Bar chart was generated with the 5th day data from Fig 4.3.13. Reduction rate of cells in 2% FBS was shown as positive control. Error bars indicate standard deviation of six experimental replicates. Statistical analysis was calculated by one-way ANOVA with Bonferroni multiple comparisons post-test (*** P<0.001).

In conclusion, EGF promoted the proliferation of UMUC9 cells, but the proliferation was not comparable to cells cultured in serum. Combined with TGFβ, EGF altered the morphology of UMUC9 cells to fibroblast-like cells.

4.3.5 EGF-induced phenotype alteration of UMUC9 cells

Immunofluorescence was performed to understand whether the phenotype had altered after EGF and TGFβ combined treatment. As UMUC9 cells were not proliferating in KSFM, negative control was not included.

Transcription factors like ELF3 and PPARγ were expressed mostly in the nuclei in UMUC9 cells as shown in Fig 4.3.7. When treated with EGF and/or TGFβ in KSFM, however, UMUC9 cells showed diffuse cytoplasmic and peri-nuclear ELF3 and PPARγ expression. Localisation of PPARγ switched to the nucleus with diffuse cytoplasmic expression by 7 days EGF treatment. TGFβ treatment alone appeared to enhance the total amount of PPARγ expression. The expression of ELF3 and PPARγ in KSFM with 2% FBS was less abundant compared to the expression of cells cultured in DMEM (10% FBS), which might

be due to the decrease of calcium and serum concentration in KSFM with 2% FBS (Fig 4.3.15).

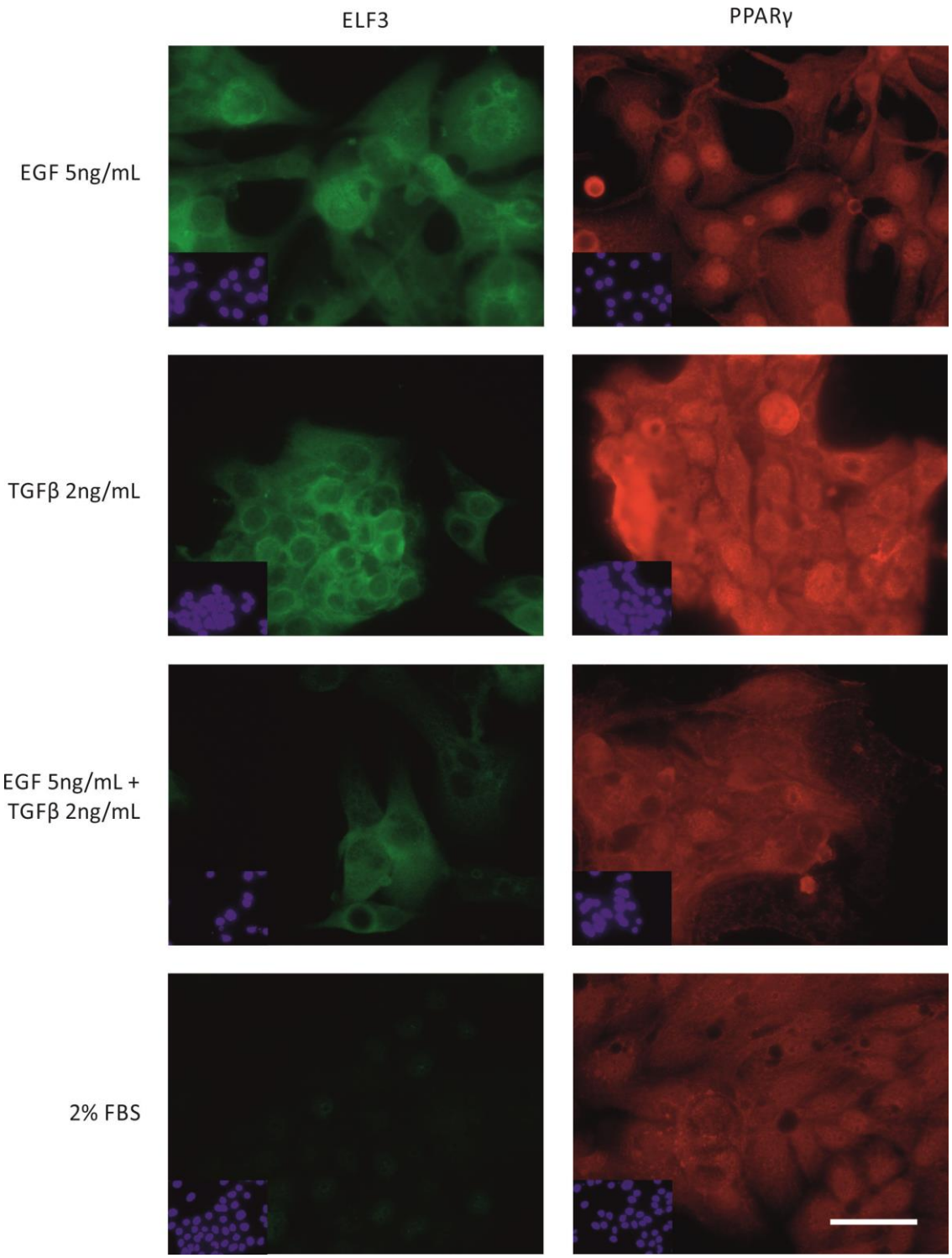

Fig. 4.3.15 Expression of ELF3 and PPARγ in UMUC9 cells. UMUC9 cells were seeded at 1X10^5 /mL on 12 well slides in KSFM with various treatments. Slides were fixed using methanol/acetone after 7 days of treatment. Primary antibodies against PPARγ and ELF3 were

applied. Pictures were taken with constant exposure time for individual antibodies for comparison. Scale bar represents 50μm.

To confirm the expression alteration of PPARγ by TGFβ alone treatment, images showing a wider region were captured, in which PPARγ demonstrated nuclear localisation by EGF treatment. The fluorescence intensity was enhanced by TGFβ treatment, suggesting a possible up-regulation of PPARγ by TGFβ (Fig 4.3.16).

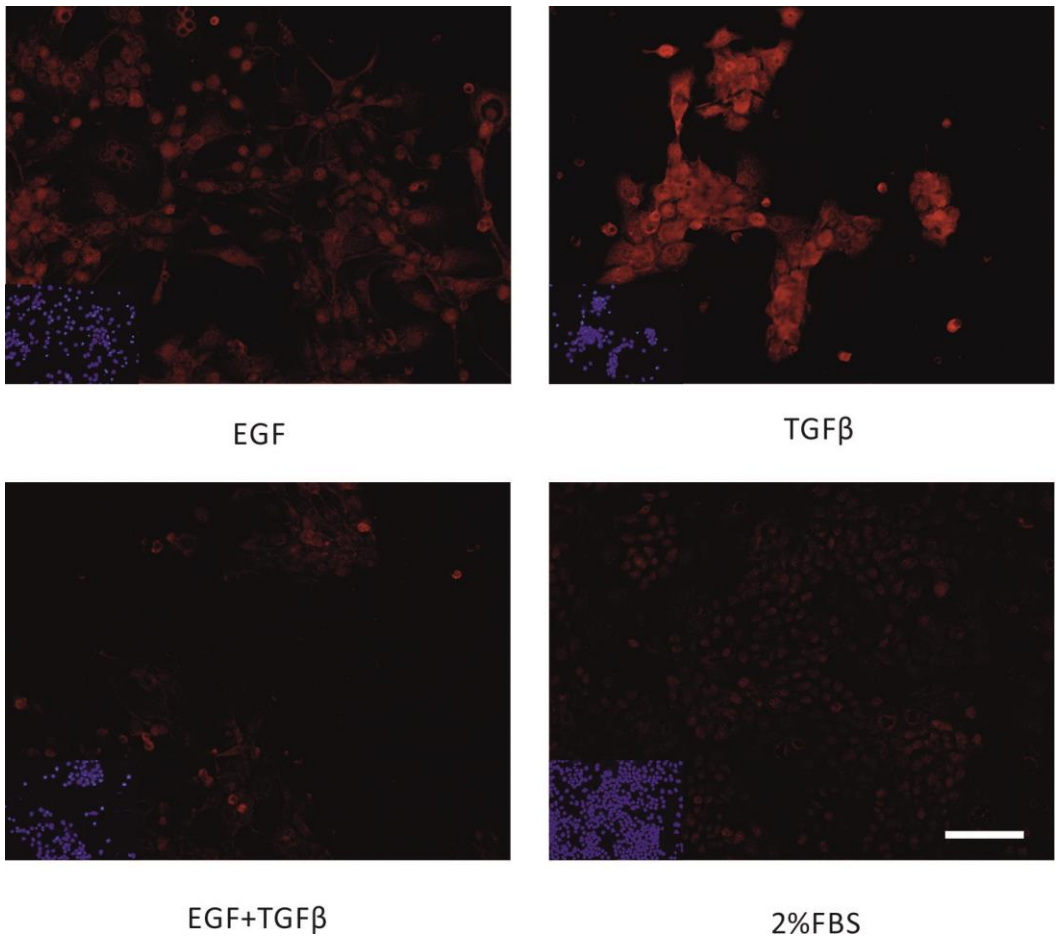

Fig 4.3.16 Expression of PPARγ in UMUC9 cells (low magnification). UMUC9 cells in KSFM were treated as indicated in the figure for 7 days and immunolabelled with PPARγ antibody after Me/Ac fixation. Immunofluorescence images were captured using X20 oil lens to demonstrate the expression of PPARγ by different treatments. Pictures were taken with constant exposure time for comparison. Scale bar represents 100μm. Note, the expression of PPARγ was increased by TGFβ only treatment.

The expression of PPARγ in UMUC9 cells (Figs 4.3.7, 4.3.15 and 4.3.16) is summarised in Table 4.3.3. PPARγ expression of UMUC9 cells cultured in DMEM (10% FBS) is included as positive control. Only EGF-treated UMUC9

cells in KSFM demonstrated nuclear expression (Fig 4.3.15). TGFβ alone induced the up-regulation of PPARγ expression in both nucleus and cytoplasm (Fig 4.3.15).

Expression and localisation of PPARγ	10% FBS (DMEM)	EGF (KSFM)	TGFβ (KSFM)	EGF + TGFβ (KSFM)	2% FBS (KSFM)
Nuclear	√√	√√			
Cytoplasmic		√			
Diffuse			√√√	√	√

Table 4.3.3 Expression of PPARγ in UMUC9 cells. The amount of protein expression was shown as √. Increased fluorescence intensity was demonstrated by √√ or √√√. PPARγ expression in UMUC9 cells growing in DMEM (10% FBS) was included as positive control. Where expression was observed in both nucleus and cytoplasm in the majority of cells, it was classified as diffuse.

To explore the downstream pathways that EGF and/or TGFβ treated UMUC9 cells grown in KSFM used for growth, canonical pathways promoting proliferation in NHU cells were further examined. By EGF and/or TGFβ treatments, active β-catenin was expressed and mostly demonstrated a diffuse cytoplasmic localisation, whereas in positive control cells in 2% FBS, β-catenin was localised to the membrane. The expression of phosphorylated ERK was not prominent. Phosphorylated AKT showed some membrane labelling in TGFβ-treated cells (Fig 4.3.17).

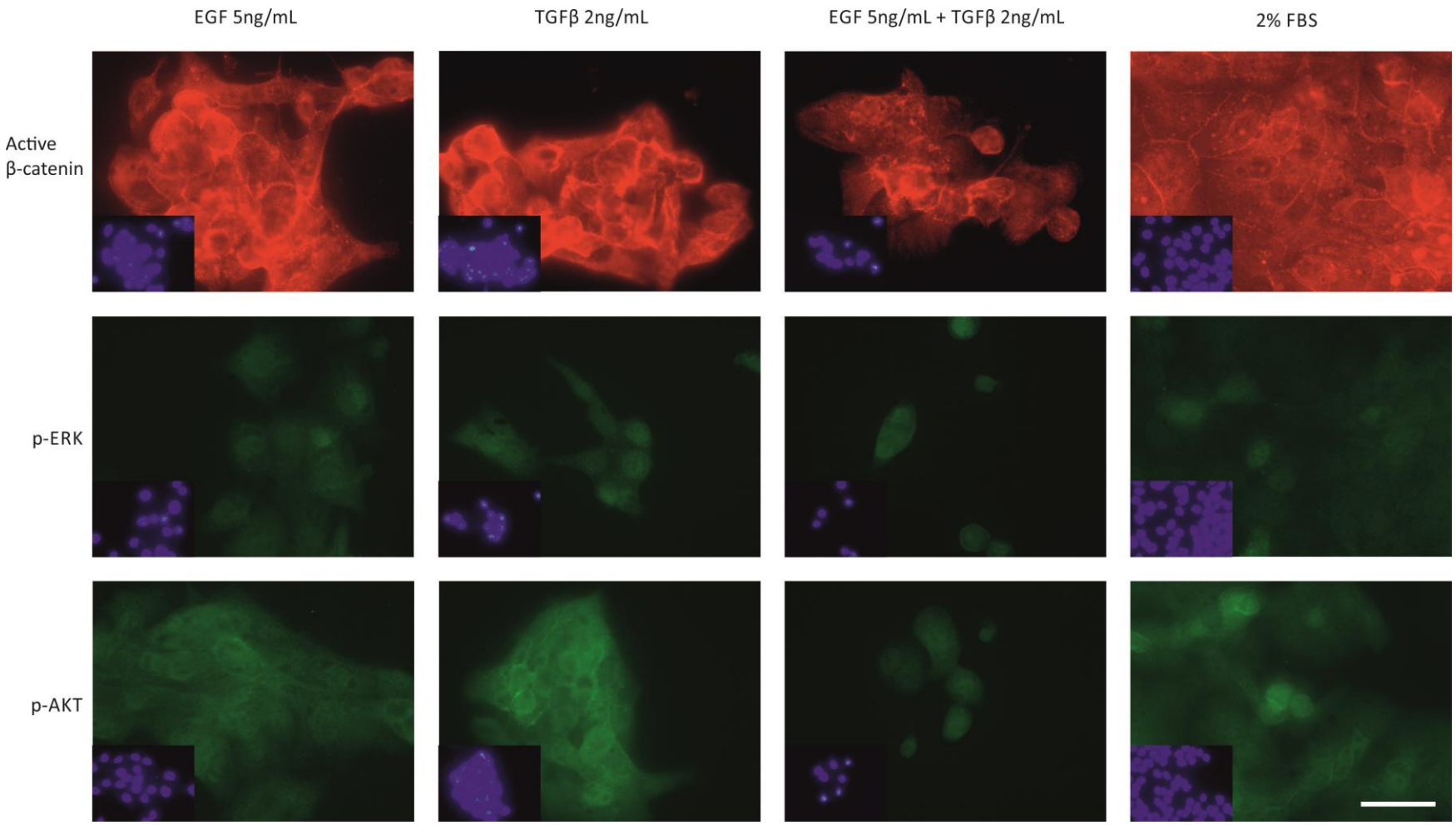

Fig 4.3.17 Signalling pathways of UMUC9 cells. UMUC9 cells were seeded at $1X10^5$ /mL on 12 well slides in KSFM with various treatments for 7 days. Slides were fixed using formalin fixation and permeabilised with 0.5% Triton X-100 before processing for immunofluorescence. Primary antibodies against active β-catenin, phosphorylated ERK and phosphorylated AKT were applied. Scale bar represents 50μm.

Further characterisation on EGF and/or TGFβ treated UMUC9 cells was performed by immunofluorescence. In EGF and/or TGFβ treated UMUC9 cells, the most significant change was the expression of CK14. CK13 did not show a detectable change. RT112 cells were included to show positive expression of CK13. Expression of CK20 was still present in EGF treated cells but not detectable in other treatments with TGFβ. These findings suggested that the phenotype of UMUC9 cells was affected by the EGF and/or TGFβ treatment and altered to a more basal-like phenotype (Fig 4.3.18).

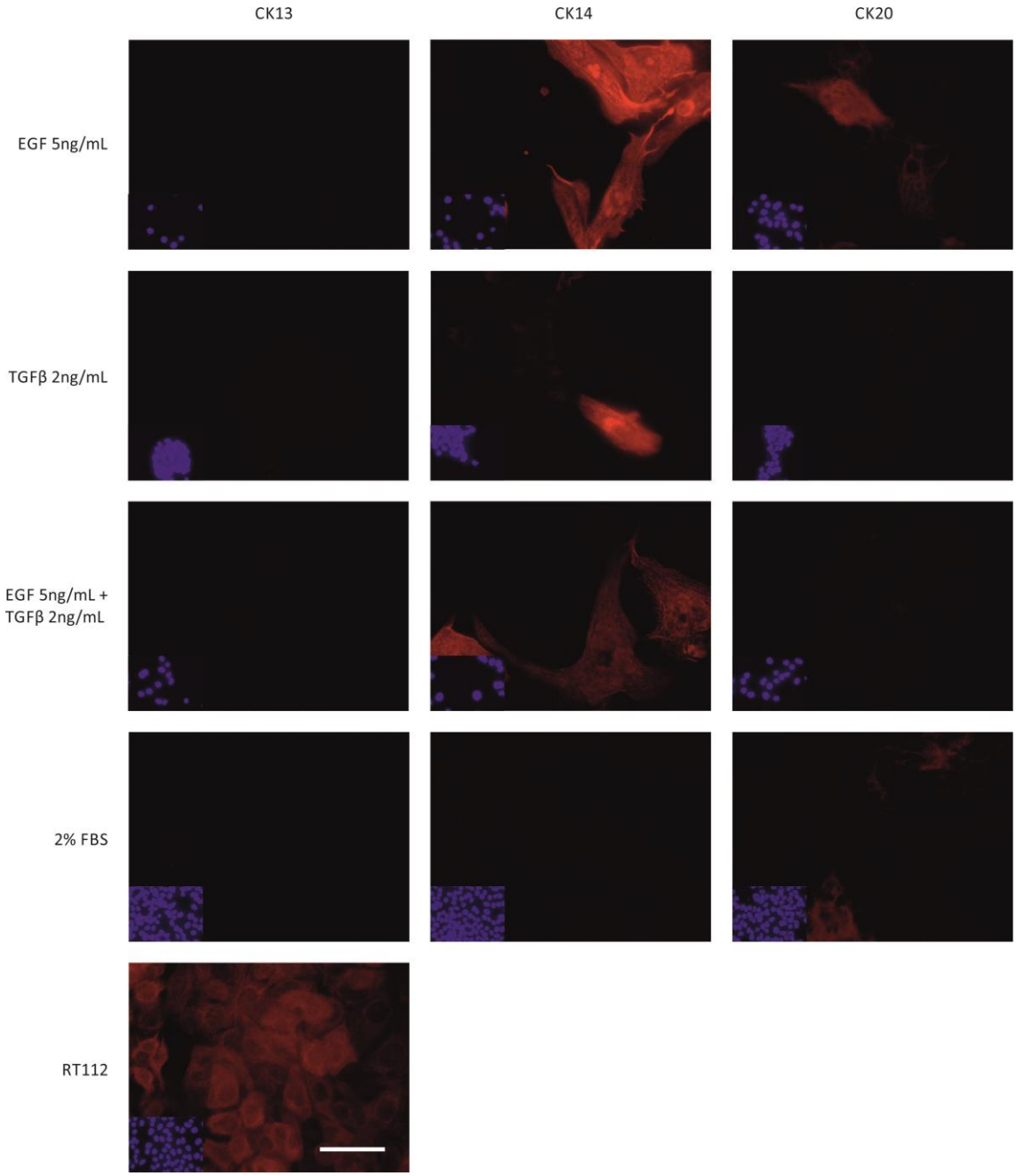

Fig 4.3.18 Phenotype of UMUC9 cells. UMUC9 cells were seeded at $1X10^5$ /mL on 12 well slides in KSFM with treatments for 7 days and fixed with methanol /acetone. UMUC9 cells treated with 2% FBS showing CK13 (-), CK14 (-) and CK20 (+) was used to demonstrate the phenotype of UMUC9 cells in the presence of serum. RT112 was included as positive control for CK13. Scale bar represents 50μm.

The EMT process might be a possible mechanism for the alteration of phenotype in treated UMUC9 cells. Key factors like E-cadherin and vimentin were examined. Proliferating NHU cells demonstrated vimentin protein expression and were included as positive control. The expression of vimentin was expressed *de novo* in EGF and/or TGFβ treated UMUC9 cells, as UMUC9 cells cultured in 2% FBS showed no detectable vimentin expression. However, in EGF and/or TGFβ treated cells, E-cadherin was still present and did not demonstrate any obvious loss following treatments (Fig 4.3.19).

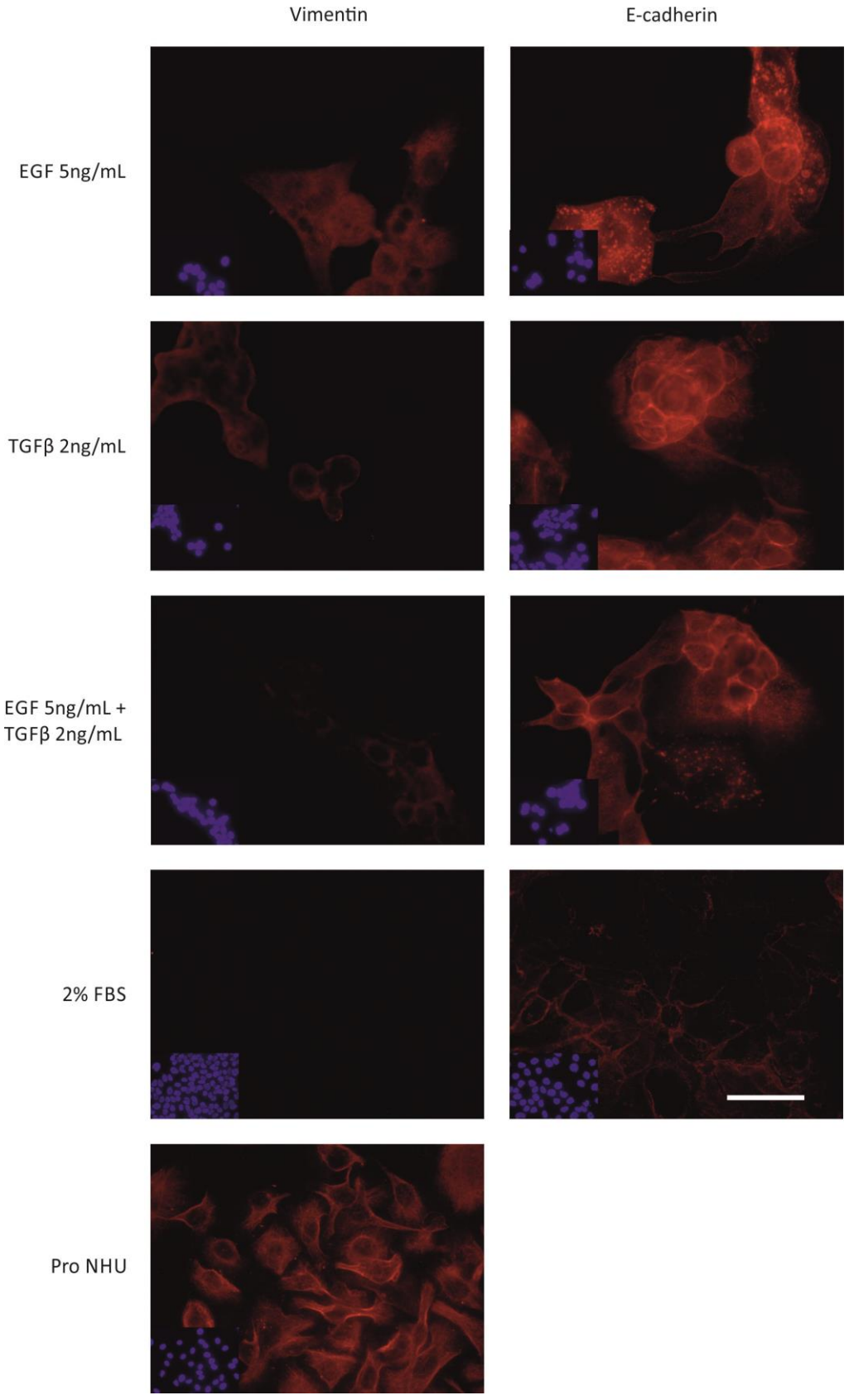

Fig 4.3.19 Phenotype of UMUC9 cells. UMUC9 cells were seeded at $1X10^5$ /mL on 12 well slides in KSFM with treatments for 7 days and fixed with methanol /acetone before processing for immunofluorescence. Proliferating NHU cells (Y1156) showed the expression of vimentin as positive control. Scale bar represents 50 μm.

The phenotypes of UMUC9 cells in different conditions are summarised in Table 4.3.4.

Markers	DMEM (10% FBS)	KSFM EGF	KSFM TGFβ	KSFM EGF+TGFβ	KSFM 2%FBS
CK13	-	-	-	-	-
CK14	-	+	+	+	-
CK20	+	+	-*	-*	+
E-cadherin	+	+	+	+	+
Vimentin	Not tested	+	+	+	-

Table 4.3.4 Phenotype of UMUC9 cells in different conditions. UMUC9 cells in different media were tested. KSFM with 2% FBS was used as positive control medium for UMUC9 cells showing phenotype of cells in the presence of serum. For expression of CK20 in cells maintained in media with TGFβ, no detectable protein was observed on tested slides, which is noted by *.

It appeared from these results that exogenous EGF might have altered the phenotype of UMUC9 cells. To confirm this finding, inhibitors were then added to UMUC9 cells. When treated with EGF, UMUC9 cells demonstrated noticeable proliferation, which was abolished by the ERK inhibitor U0126, suggesting a direct growth promotion by EGF via the MEK/ERK pathway. Other inhibitors like LY294002 and PD153035 inhibited the proliferation of EGF-treated UMUC9 cells significantly but not as noticeably as U0126. TZ was included as PPARγ activator that induced differentiation in NHU cells. In EGF-treated UMUC9 cells grown in KSFM, TZ inhibited the EGF-promoted growth significantly but not dramatically. By contrast, T0070907 did not affect the EGF-promoted growth, suggested that either the proliferation had little relationship with PPARγ pathway or the ligand binding site of PPARγ in UMUC9 cells was mutated (Fig 4.3.20).

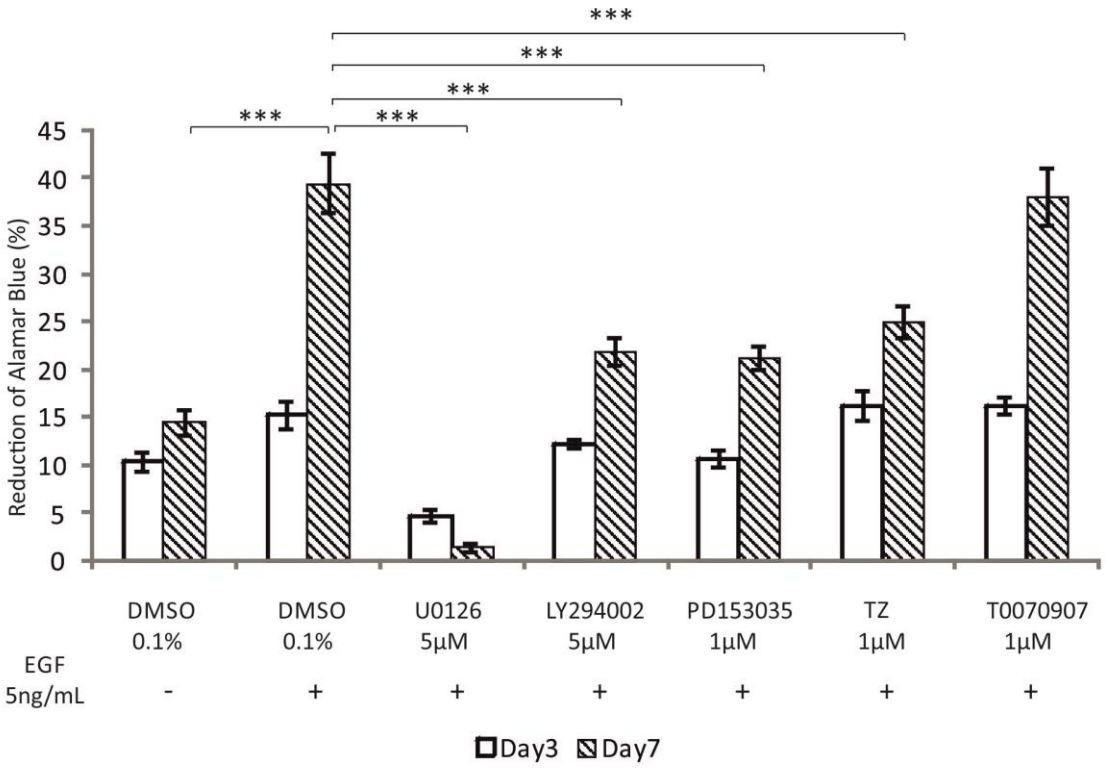

Fig 4.3.20 Growth inhibition by the inhibitors. UMUC9 cells were seeded at $5X10^4$ /mL in KSFM and treated with or without EGF. For cells treated with EGF, various pathway inhibitors were added. DMSO was added in non-treated cells as vehicle control. Growth assay was performed using Alamar Blue reagent. Error bars indicate standard deviation of six experimental replicates. Statistical analysis was calculated by one-way ANOVA with Bonferroni multiple comparisons post-test (*** $P<0.001$).

UMUC9 cells demonstrated almost no proliferation when cultured in KSFM. This growth arrest observed was reversed by EGF treatment partly (Fig 4.3.20), compared to UMUC9 cells grown in medium with serum (Fig 4.3.13). However, this improved growth by EGF was associated with alteration of phenotype and morphology, as the original differentiated phenotype of UMUC9 cells was altered to a more basal-like one, showing CK14 expression by EGF treatment, which was similar to proliferating NHU cells (Table 4.3.5). Other factors may be as well crucial for UMUC9 cells to proliferate, but whether maintaining the differentiated phenotype is required needs further study.

	NHU (proliferating)	UMUC9 (serum)	UMUC9 (EGF and/or TGFβ)
CK14	√	x	√
E-cadherin	√ (with 2mM calcium)	√	√
Vimentin	√	x	√

Table 4.3.5 Phenotype of UMUC9 cells. UMUC9 cells grown in KSFM were compared to NHU cells and UMUC9 cells grown in medium with serum. Whether the proteins were expressed or not are indicated with either √ or x.

4.3.6 Investigating signalling pathways of 5637 cells adapted to KSFM

UMUC9 cells showed a differentiated phenotype in medium with serum but a basal-like phenotype in serum free medium. By contrast, 5637 cells were less differentiated. Fig 4.3.21 demonstrates the expression of PPARγ, ELF3, E-cadherin and active β-catenin of 5637 cells cultured in RPMI (5% FBS). Active β-catenin was not evidently expressed. Expression of ELF3 was minimal in 5637 cells. The expression of total PPARγ was nuclear and prevalent, but PPARγ2 specific antibody suggested that PPARγ2 was not detectable (Fig 4.3.21).

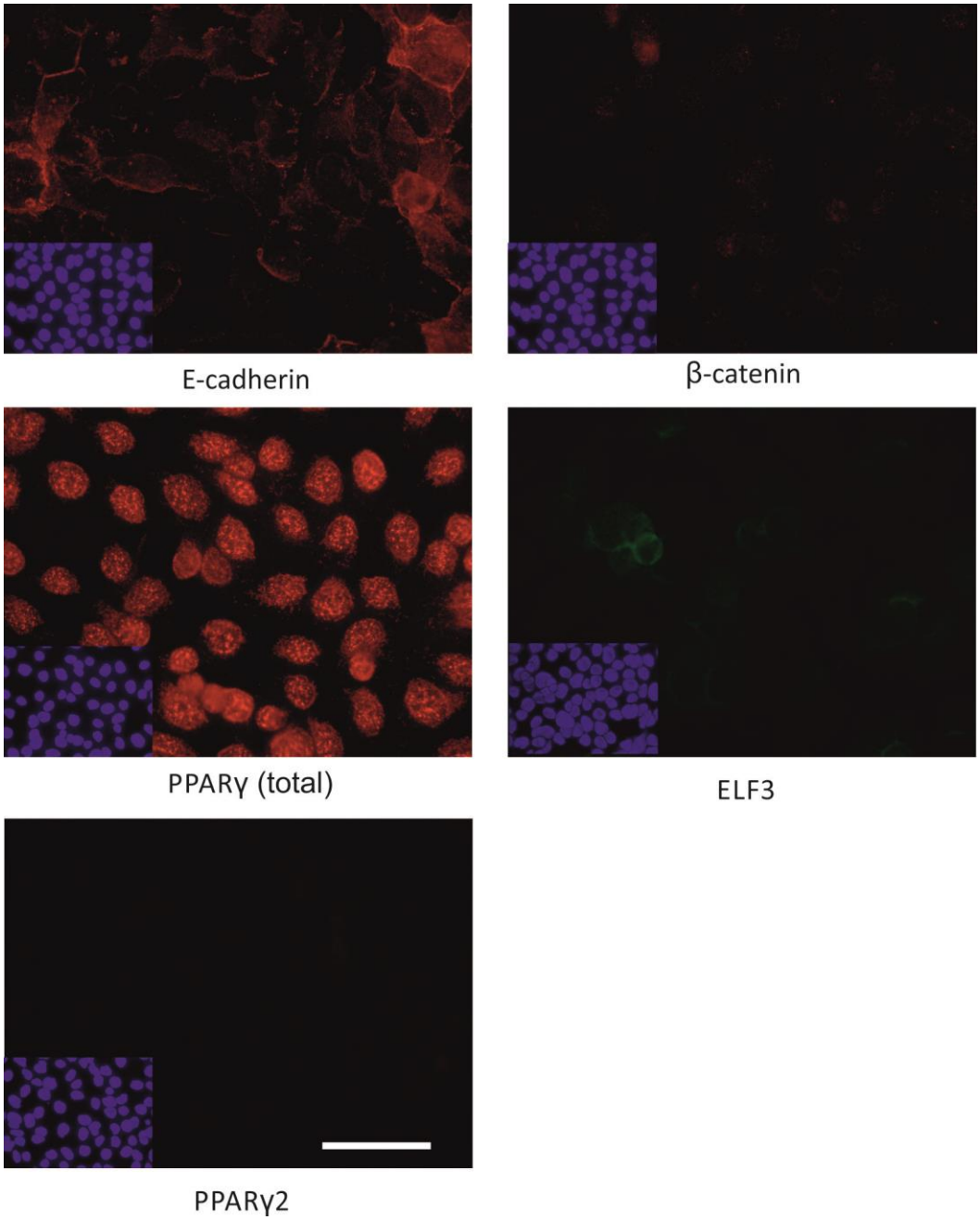

Fig 4.3.21 Expression of E-cadherin, active β-catenin, PPARγ and ELF3 in 5637 cells. Cells were seeded in RPMI (5% FBS) on slides and fixed with Me/Ac at about 80% confluence. Scale bar represents 50 μm.

Adapting 5637 cells to KSFM did not affect the proliferation of cells (unlike UMUC9 cells). Also, 5637 cells were able to grow without exogenous EGF. To explore whether the phenotype of 5637 cells had altered when the cells were adapted to KSFM, cytokeratin proteins were first examined. When adapted from medium with serum to serum-free KSFM, 5637 cells obtained a positive expression of CK14, suggesting a more basal-like phenotype (Fig 4.3.22).

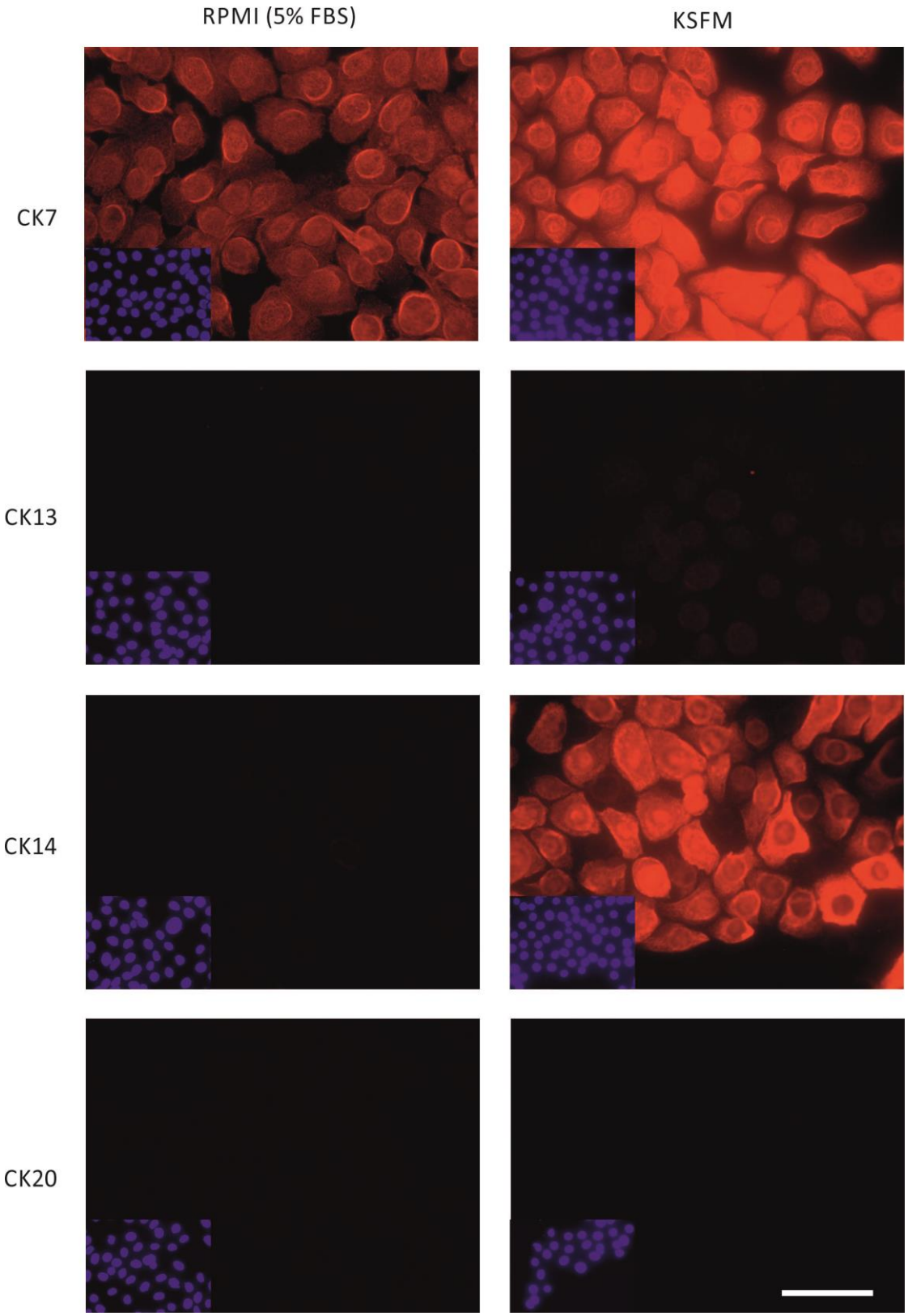

Fig 4.3.22 Phenotype alteration of 5637 cells by adapting to serum-free medium. 5637 cells in different media were seeded separately at $1x10^5$ cells /mL. Slides were fixed using Me/Ac method. CK13, CK14 and CK20 were assessed to demonstrate the phenotype of 5637 cells in different media. CK7 was examined as positive control for the experiment. Note the *de novo* expression of CK14 in serum free KSFM. Scale bar represents 50 μm.

To identify the essential pathways for 5637 cells to proliferate in KSFM, growth assay was performed with addition of growth inhibitors. 5637 cells demonstrated a significant growth inhibition by EGFR inhibitor PD153035 and MEK/ERK inhibitor U0126. Also, the GSK3β inhibitor SB415286 inhibited the proliferation significantly, which was reversed by inhibition of the PI3K/AKT pathway. Combination of SB415286 and the PPARγ inhibitor T0070907 demonstrated limited cell proliferation. Inhibition of TGFβ pathway did not affecte the growth of 5637 cells compared to DMSO control (Fig 4.3.23).

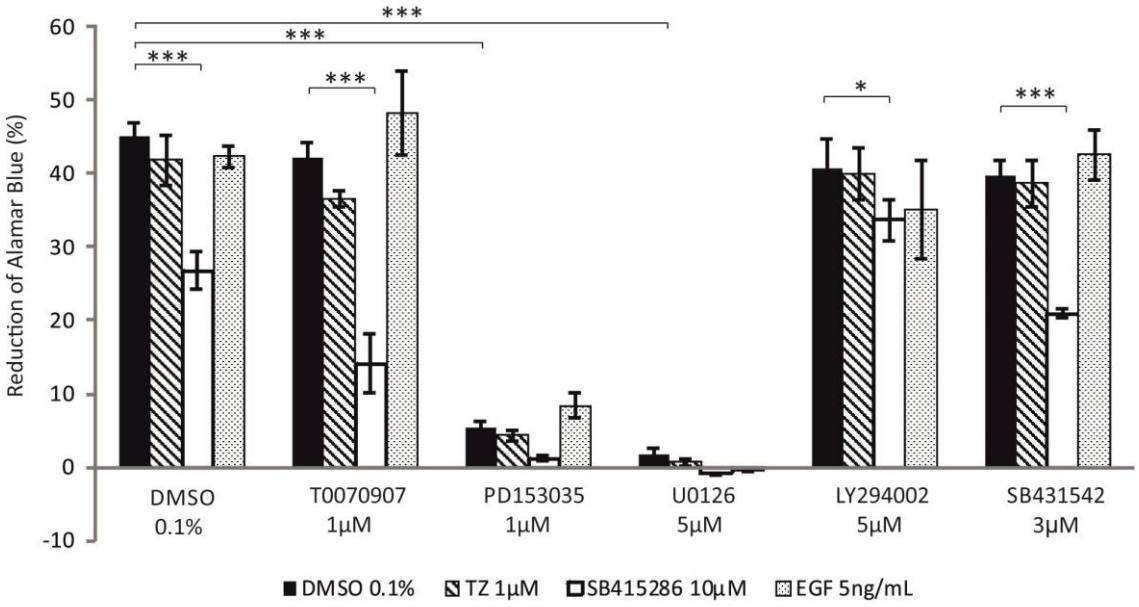

Fig 4.3.23 Growth assay to demonstrate the effect of pathway activators and inhibitors. 5637 cells were cultured in KSFM without supplements and then treated with various inhibitors. After 8 days of treatment, Alamar blue assay was performed. Error bars indicate standard deviation of five experimental replicates. Statistical analysis was calculated by one-way ANOVA with Bonferroni multiple comparisons post-test (*** P<0.001).

To examine the pathways associated with SB415286 induced growth inhibition and the growth rescue by LY294002, expression of total β-catenin (Fig 4.3.24), active β-catenin (Fig 4.3.25) and E-cadherin (Fig 4.3.26) was analysed by immunofluorescence.

Total β-catenin was examined, as SB415286 induced GSK3β inhibition is known for preventing β-catenin degradation and releasing it to either the nucleus or

the membrane. However, SB415286-treated 5637 cells showed less total β-catenin expression, whereas treatment with LY294002 induced high expression of total β-catenin. This increased total β-catenin expression was enhanced by SB415286 and LY294002, and reversed by SB415286 and T0070907. This expression pattern induced by different treatments correlated with the growth rate of 5637 cells treated correspondingly (Fig 4.3.24).

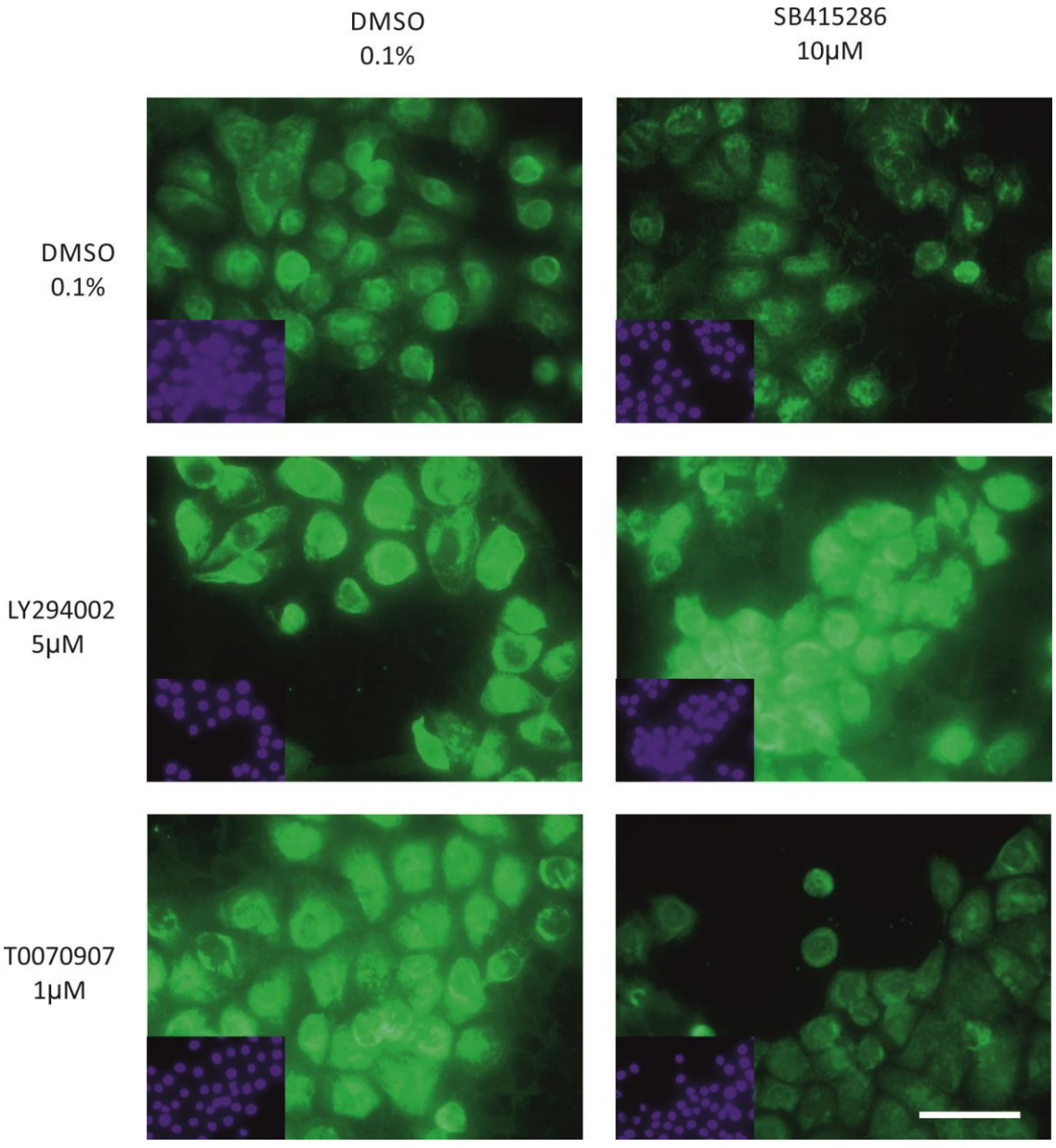

Fig 4.3.24 Expression of total β-catenin in 5637 cells. 5637 cells were seeded in KSFM and treated for 72h. Treatments are displayed as combination of horizontal and vertical headings. Slides were fixed using formalin method. Total β-catenin antibody was applied. Scale bar represents 50μm.

The active form of β-catenin by immunofluorescence showed nuclear localisation with diffuse cytoplasmic expression in DMSO control group. After treatment with SB415286, active β-catenin was localised more to the membrane and less in the cytoplasm. The amount of active β-catenin was enhanced by combined treatment with LY294002. By contrast, LY294002 alone induced the nuclear expression of active β-catenin. T0070907 did not affect the localisation or the expression of active β-catenin (Fig 4.3.25).

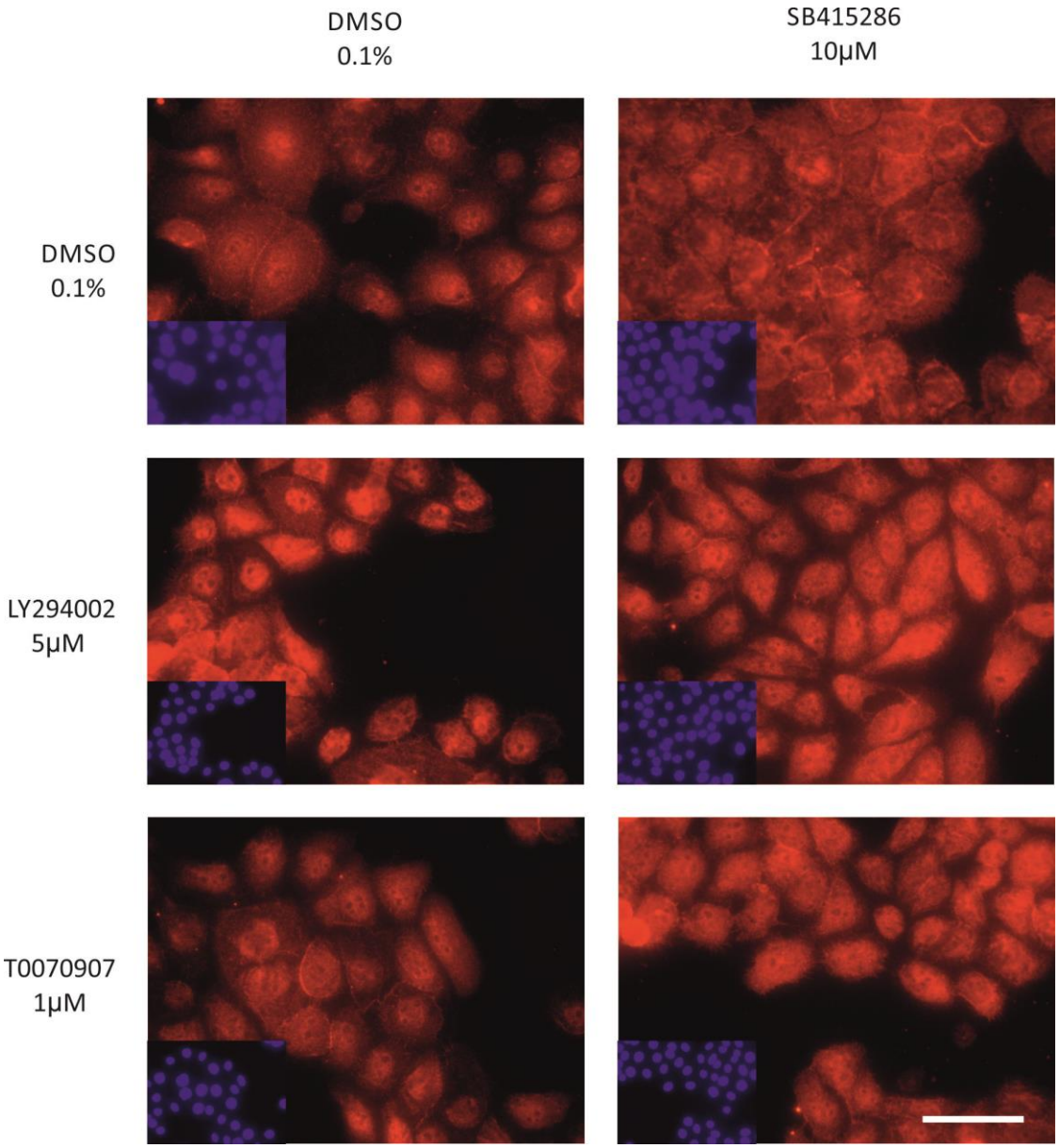

Fig 4.3.25 Expression of active β-catenin in 5637 cells. Cultures were grown in KSFM and fixed using formalin method after 72h treatment. Active β-catenin antibody was applied. Scale bar represents 50μm.

To further investigate whether there was association between β-catenin and E-cadherin after treatment of SB415286, expression and localisation of E-cadherin was further explored. E-cadherin demonstrated membrane expression in 5637 cells treated with DMSO and grown in KSFM. The membrane localisation was more obvious in SB415286-treated cells. LY294002 induced a diffuse E-cadherin localisation, resulted in less membrane localised E-cadherin expression. Though the proliferation was significantly reduced by combined treatment of SB415286 and T0070907, the expression and localisation of E-cadherin did not show any noticeable change (Fig 4.3.26).

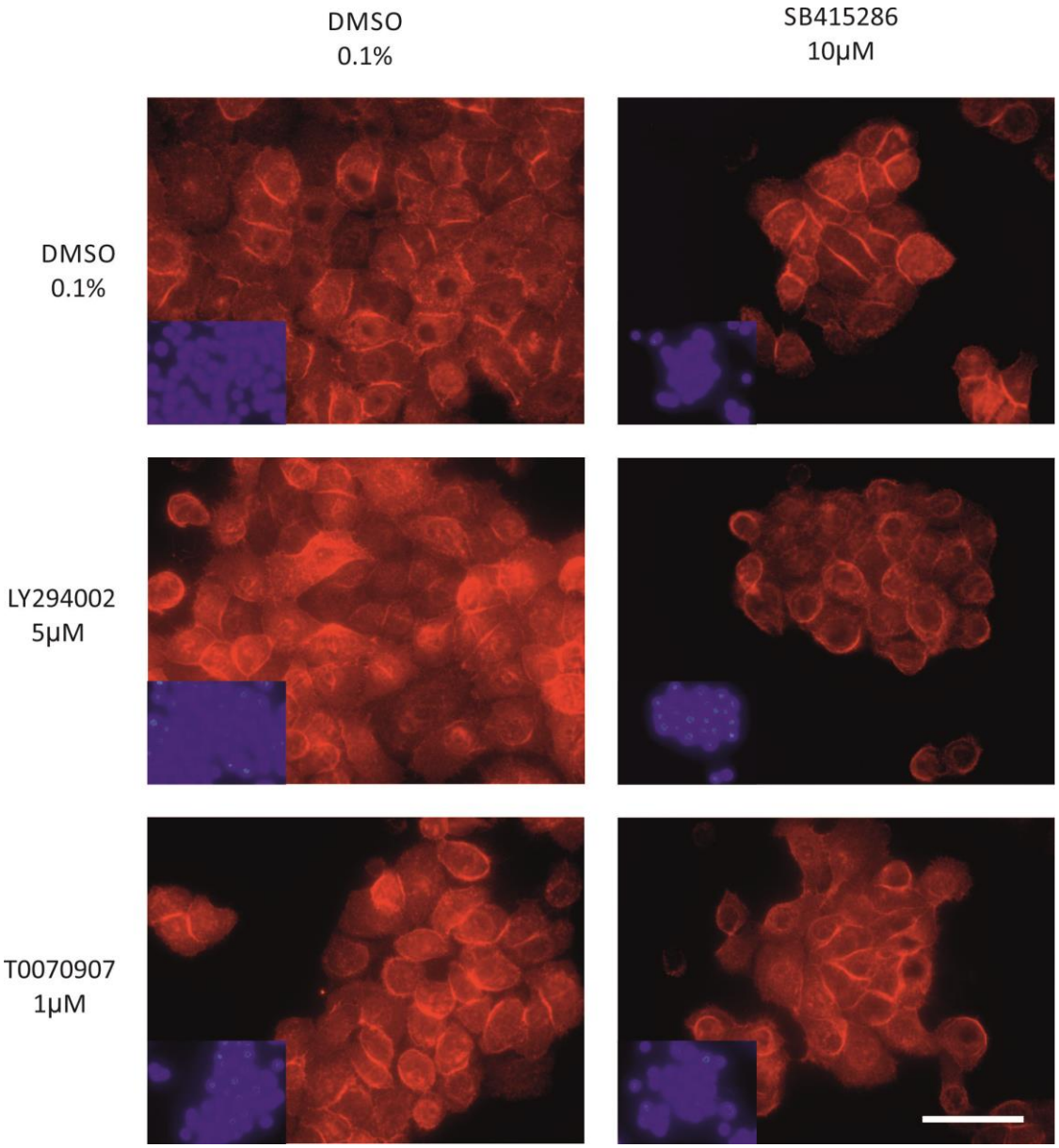

Fig 4.3.26 Expression of E-cadherin in 5637 cells. 5637 cells were seeded in KSFM and treated for 72h before fixed using Me/Ac method. Treatments are displayed as combination of the horizontal and vertical headings. Primary antibody against E-cadherin was applied. Scale bar equals 50μm.

As T0070907 reduced the cell proliferation dramatically with SB415286, the expression of PPARγ was further analysed. PPARγ showed diffuse expression in SB415286-treated cells, and demonstrated increased expression when LY294002 was also added. T0070907 resulted in cytoplasmic expression, which was cytoplasmic exclusively when cells were treated with SB415286 together. LY294002 alone induced a heterogeneous population regarding PPARγ localisation, distributing either to the nucleus or cytoplasm (Fig 4.3.27).

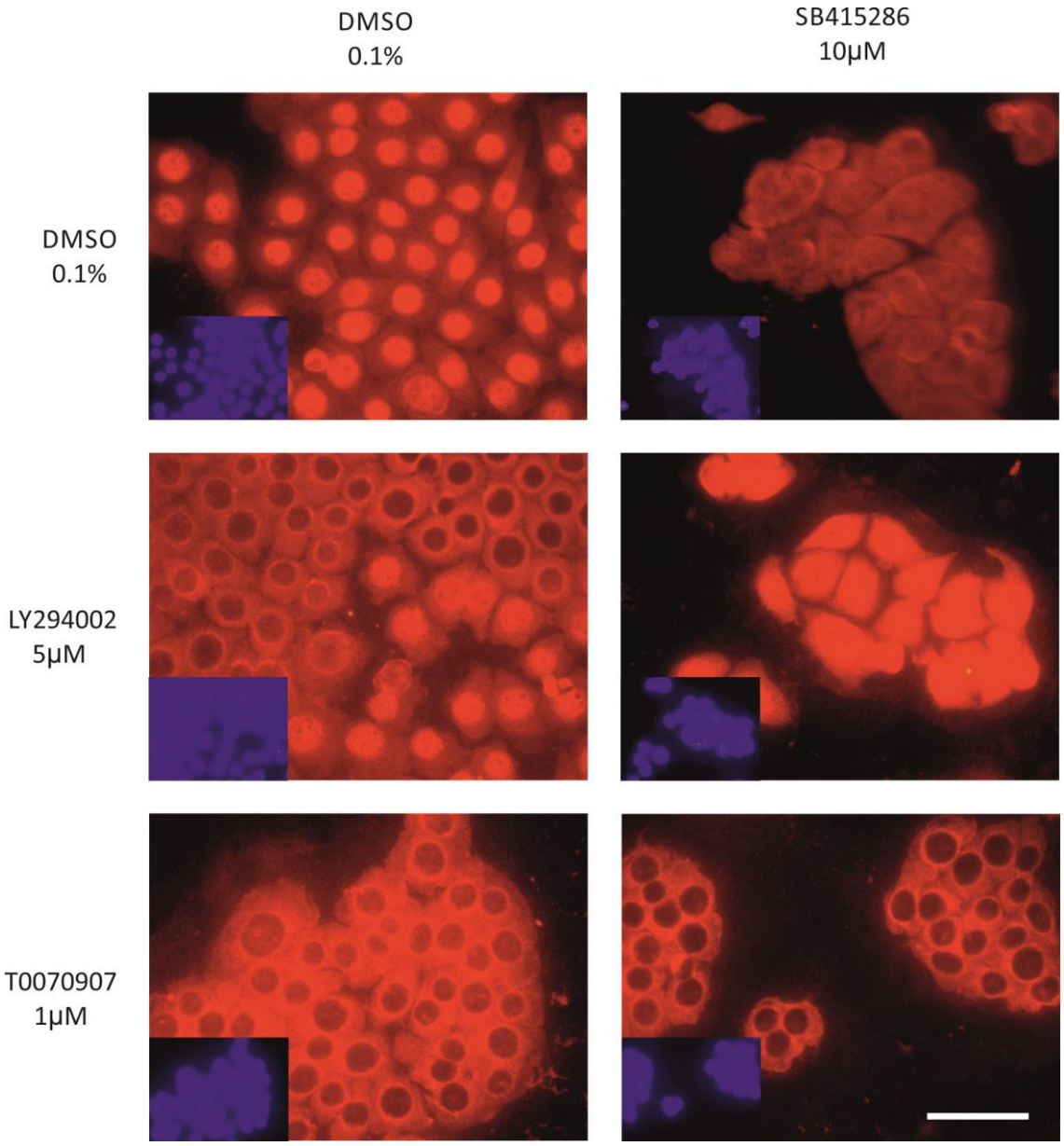

Fig 4.3.27 Expression of PPARγ in 5637 cells. 5637 cells were cultured in KSFM and treated for 72h before fixed with Me/Ac method. PPARγ antibody for both all PPARγ isoforms was applied. Scale bar represents 50μm.

After treatment with SB415286, the nuclear expression of PPARγ and total β-catenin decreased. Nuclear expression intensity was analysed to inform the relationship of the expression of the three proteins. The analysis of nuclear fluorescence intensity confirmed that the expression of PPARγ, active β-catenin and total β-catenin had reduced nuclear expression when treated with SB415286, which also associated with growth inhibition of 5637 cells in KSFM (Fig 4.3.28). The reduced nuclear expression was reversed by addition of

LY294002. Total β-catenin and active β-catenin demonstrated similar expression pattern in the majority of treatments, but when T0070907 was added to the cultures, they showed different nuclear expression, which might be caused by the involvement of PPARγ pathway.

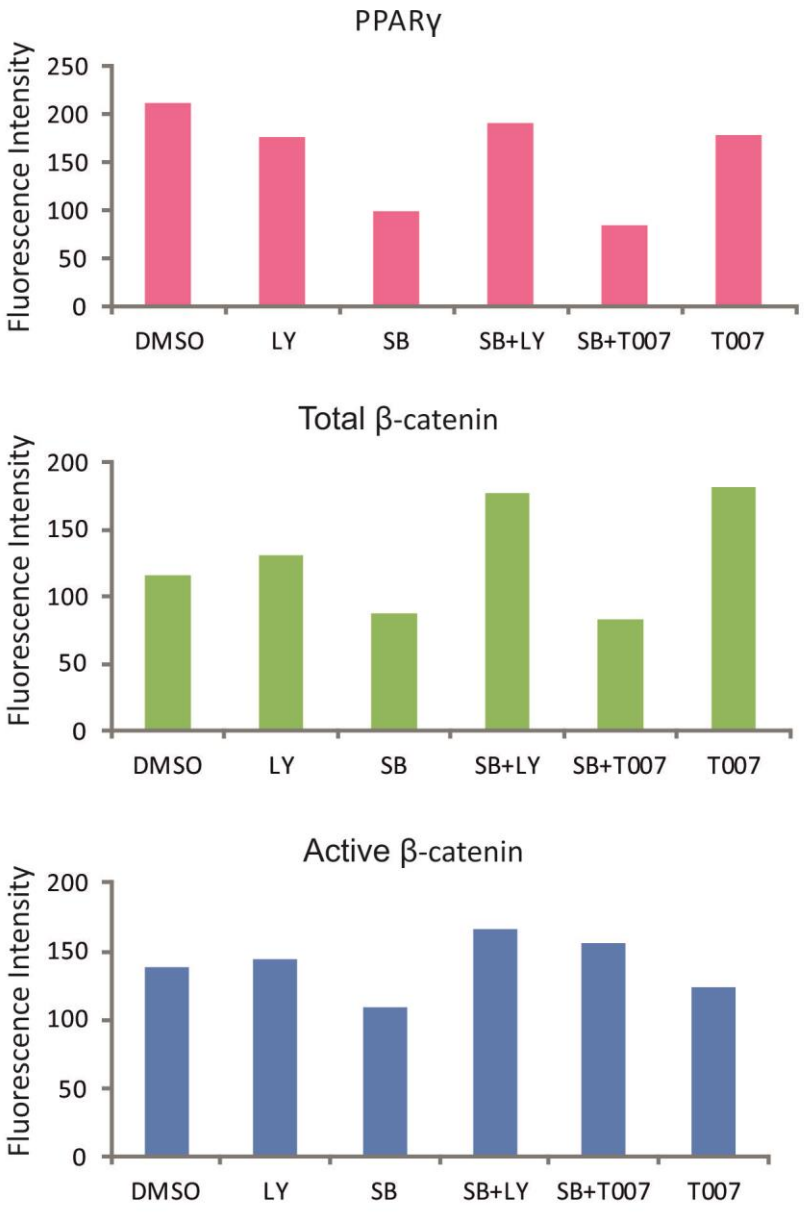

Fig 4.3.28 Nuclear fluorescence intensity of treated 5637 cells. The nuclear fluorescence intensity was measured using Image-Pro Plus software and showed as bar graphs. LY (LY294002, 5μM), SB (SB415286, 10 μM) and T007 (T0070907, 1 μM) was added to cultures. DMSO (0.1%, v/v) was included as vehicle control.

To summarise the alteration of cell proliferation by growth assay and expression of associated pathways by immunofluorescence, Table 4.3.4 is listed

below. Growth inhibition induced by SB415286 was associated with down-regulation of PPARγ and β-catenin (total and active), which could be reversed by combined treatment with LY294002. Such reversed growth inhibition was accompanied by enhanced expression of PPARγ and β-catenin (total and active), all of which distributed in whole cells though. By contrast, combined with T0070907, growth inhibition caused by SB415286 was intensified, which also led to down-regulation of total β-catenin and nuclear PPARγ (trans-located to cytoplasm). For treatments that did not alter proliferation of cells, no clear expression pattern of tested pathways was observed.

	DMSO	SB415286	LY294002	SB415286+LY294002	T0070907	SB415286+T0070907
Growth rate	Control	↓↓***	NS	↓*	NS	↓↓↓***
PPARγ (total)	Control Nuclear	Diffuse ↓	Nuclear +cytoplasmic	Diffuse↑	Cytoplasmic	Exclusively cytoplasmic
Total β-catenin	Diffuse	Diffuse ↓	Diffuse ↑	Diffuse ↑↑	Diffuse ↑	Diffuse ↓↓
Active β-catenin	Diffuse	Membrane Diffuse↓	Nuclear↑	Diffuse↑	Diffuse ↓	Diffuse
E-cadherin	Membrane	Membrane	Membrane Diffuse↑	Peri-nuclear↓	Membrane	Peri-nuclear

Table 4.3.4 Affected cell growth rate and expression or localisation of associated pathways of 5637 cells in KSFM. Treatments that resulted in cell growth inhibition are listed. ↓ shows the inhibited growth or overall down-regulated expression. ↑ shows up-regulated expression. * indicates P value (NS, not significant, * $P<0.05$, ***$P<0.001$). Localisation was determined according to majority of cells, unless heterogeneous distribution was evident. Where the amount of protein expressed demonstrated no obvious change, no label was shown.

4.3.7 Summary of results

UMUC9 cells demonstrated a differentiated phenotype with UPK2 and CK20 expression at transcription and protein level. Both CK13 and CK14 were absent in UMUC9 cells cultured in medium with serum.

UMUC9 cells showed extremely high expression of PPARγ2 transcript and nuclear PPARγ2 localisation. 5637 cells demonstrated expression of different PPARγ protein isoforms in different media by Western blots.

Less differentiated urothelial cancer cell line 5637 was able to be adapted to serum-free medium (KSFM), whereas UMUC9 cells demonstrated no growth in KSFM.

UMUC9 cells showed slower proliferation in KSFM supplemented with EGF (compared to UMUC9 cells grown in medium with serum).

EGF promoted cell growth and induced a phenotype alteration of UMUC9 cells to a vimentin-positive and CK14 positive phenotype. But the role of TGFβ was not obvious, inhibition of TGFβ pathway did not affect UMUC9 cells grown in medium with serum.

Proliferation of 5637 cells in KSFM could be inhibited by EGFR or MEK/ERK pathways inhibitors. Inhibition of GSK3β reduced growth of 5637 cells, which could be reversed by inhibition of the PI3K/AKT pathway.

	UMUC9	5637
Phenotype	Well-differentiated	Less-differentiated
Adapt to KSFM	No	Yes
Difference in medium with or without serum	*De novo* expression of CK14 without serum	Expression of different PPARγ isoforms
Pathways may affect the cell growth	MEK/ERK	MEK/ERK, Wnt/β-catenin

Table 4.3.5 Summary of two UC cell lines.

Chapter 5 Transcript Variants and Protein Isoforms of PPARγ

5.1 Introduction

5.1.1 Identification of PPARγ and its function

PPARγ is a nuclear receptor containing a DNA binding domain (DBD) and a ligand binding domain (LBD). These domains are similar to other nuclear receptor family members (Mangelsdorf et al., 1995). Together with other PPARs (α, β/δ), this family was first found in mouse liver, kidney and heart with abundant expression (Issemann and Green, 1990). PPARγ has been mostly studied of this family. Fajas et al. showed that in human tissues, PPARγ1 was the predominant PPARγ isoform in large intestine, adipose, kidney and liver. PPARγ2 transcripts were most abundantly expressed in adipose tissue and liver (Fajas et al., 1997). PPARγ was shown to play an important role in regulating metabolism of glucose and fatty acids by induction of adipogenesis (reviewed by Kersten et al., 2000). Also, PPARγ is the target for the synthetic insulin sensitizers, thiazolidinediones (TZD), and studies of PPARγ may bring insight to type II diabetes (reviewed by Janani and Ranjitha Kumari, 2015).

5.1.2 Transcript variants of PPARγ

PPARγ is recognised as a key regulator of metabolism. Two main PPARγ isoforms PPARγ1 and PPARγ2 have been identified and extensively studied. In mice, PPARγ1 and PPARγ2 were reported to have different promoters and encode different transcripts (Zhu et al., 1995). There are 8 exons in PPARγ1 and 7 exons in PPARγ2. The last six exons are shared between the two PPARγ isoforms. The first two exons in PPARγ1 (A1 and A2) contribute to the 5′ UTR, whereas the first exon (B) in PPARγ2 encodes the 5′ UTR with 30 (28 in human) amino acids different between PPARγ1 and PPARγ2 (Fajas et al., 1997; Zhu et

al., 1995). Research in human showed that the PPARγ protein isoforms are 99% similar and 95% identical to mouse isoforms (Fajas et al., 1997). The cDNA sequence of hPPARγ1 was 91% identical to mPPARγ1, whereas hPPARγ2 was 81% identical to mPPARγ2 (Elbrecht et al., 1996; Greene et al., 1995). A simple schematic diagram displays the difference between human PPARγ1 and PPARγ2.

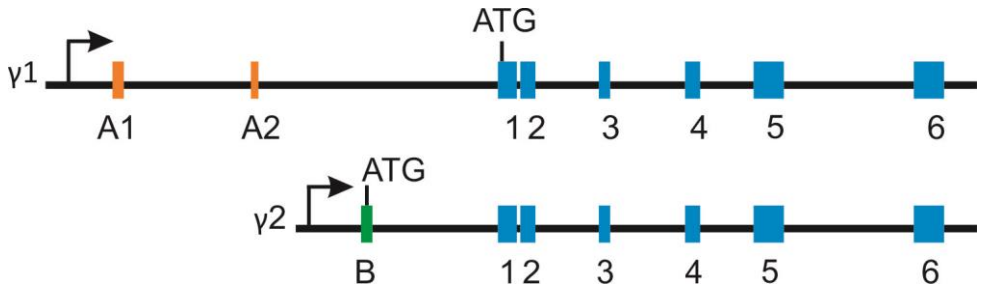

Fig 5.1.1 Schematic diagram to demonstrate exons on human PPARγ transcripts, γ1 and γ2, respectively. The orange exons show γ1 specific exons, whereas the green exon demonstrates γ2 specific exon. Blue exons show the exons shared between γ1 and γ2. Arrows heading right demonstrate the direction of promoters. The ATG site shows the starting site of coding sequence for each transcript. Adapted from (Fajas et al., 1997; Zhou et al., 2002; Zhu et al., 1995).

A novel human PPARγ3 transcript was identified with exons 1-6 in coding sequence and exon A2 in 5′ UTR. This transcript encodes the identical protein as the transcript for PPARγ1, but the protein translated from PPARγ3 was more specific to adipose tissue and large intestine, suggesting that different promoters may regulate the expression of the same protein (Fajas et al., 1998).

More PPARγ transcripts were identified in monkey macrophages and named as PPARγ4, 5, 6 and 7. They shared identical ORF (Open Reading Frame) region encoded by exons 1-6 for protein coding and were only different from the 5′ UTR with novel exons C or D at the N-terminal UTR, which were also found in the human genome. Transcript expression of these novel transcripts were not affected by fat feeding compared to macrophages of monkeys with normal diet, whereas the total PPARγ transcripts showed accumulation in the adipose tissue of fat-fed monkeys assessed by using primer set binding to all the isoforms (Zhou et al., 2002). In human macrophages, PPARγ4, 5 and 7 transcript variants

were also detected (Chen et al., 2006b). Upon binding of troglitazone, transcript expression of PPARγ5 was induced in human THP-1 macrophage cells, whereas expression of both PPARγ1 and PPARγ2 was inhibited, indicating that different PPARγ transcripts had distinct expression pattern after activation by ligand in human THP-1 cells. This regulation of PPARγ transcripts suggested that in human macrophages, different isoforms of PPARγ transcripts may have different roles in regulating functions of macrophages upon binding of ligands (Chen et al., 2006b).

5.1.3 PPARγ2 is the most critical isoform in adipocyte differentiation

Among all the transcript variants, PPARγ2 showed the most obvious difference in terms of expression in differentiated adipocytes. It was considered as the predominant isoform of PPARγ in murine adipose tissue, as 5'-end cDNA sequence showed that all five tested samples contained the PPARγ2 specific sequence (Tontonoz et al., 1994a). Further differentiation experiments suggested PPARγ2 was an early adipocyte specific regulator in both 3T3-F442A and 3T3-L1 cells, as the transcript of PPARγ2 was up-regulated dramatically on day 2 and plateaued on day 9. Two other downstream genes LPL (lipoprotein lipase) and ap2 (adipocyte p2, exclusively expressed in adipose cells) were up-regulated following the time course and showed abundant expression on day 9 (Tontonoz et al., 1994a). By over expression of PPARγ2 in NIH3T3 cells, the entire differentiation programme was activated, as late differentiation genes such as adipsin and ap2 were up-regulated, the effect of which was not achievable by over-expressing either PPARα or RXRα (Tontonoz et al., 1994b). However, no data regarding over-expression of PPARγ1 or total PPARγ was shown, possibly because of previous demonstrated results of specific PPARγ2 transcript expression in murine adipose tissue (Tontonoz et al., 1994a). The differentiation process initiated by over-expression of PPARγ2 was more

dependent on the entirety of the DNA binding domain rather than the N-terminal domain of PPARγ2. Deletion of the N-terminal domain containing but not confined to the first 30 amino acids (the difference between PPARγ1 and PPARγ2), even increased the production of lipid, indicating advanced functional differentiation. By contrast, replacement of two conserved cysteine residues to serine in the DNA binding domain abolished the lipid accumulation, which suggested that interaction with other transcription factors and binding to the DNA sequence of target genes were required and essential for PPARγ2-induced adipogenesis (Tontonoz et al., 1994b).

5.1.4 Isoforms of PPARγ proteins in urothelium and other tissues

The protein isoforms of PPARγ have been studied in different types of tissues. In adipose tissues that predominantly express PPARγ2 (Tontonoz et al., 1994a), a 67kDa PPARγ2 band was observed in induced adipocytes on day2 by using a PPARγ2 antibody binding to the N-terminal of protein obtained from Santa Cruz (Aprile et al., 2014).

In mouse prostate cells (Strand et al., 2012) and benign human prostate epithelial cells (Strand et al., 2013), two PPARγ bands identified as PPARγ1 and PPARγ2 were reported by western blotting using antibody from Santa Cruz. Knock down of PPARγ2 was suggested as a key event for prostate cells to transdifferentiate to urothelial cells. However, details of PPARγ antibody used in this paper were not sufficient (Strand et al., 2013).

In NHU cells, only one band was observed consistently with the molecular weight same as PPARγ1 (Kawakami et al., 2002; Varley et al., 2004a). Information regarding the PPARγ antibody can only be found from Varley et al. paper, which was PPARγ E-8 from Santa Cruz. This PPARγ isoform was also detected in UC cell lines by Western blots using the same Santa Cruz

antibody (sc7273, PPARγ E-8), and the amounts of protein expressed in different UC lines were different (Mansure et al., 2013).

5.1.5 Summary

There are at least seven PPARγ transcript variants with different promoters reported and these transcripts may have different roles in regulating differentiation. PPARγ2 has been demonstrated as the most significant isoform regulating adipogenesis.

Two main PPARγ protein isoforms have been described as present in different tissues. But controversy in recognising different PPARγ isoforms using different antibodies or insufficient information of antibodies used in paper limited the understanding of PPARγ isoforms. The role of individual isoforms may be important, but analysis using consistent PPARγ antibody will be critical.

5.2 Rationale and aims

Results shown in the previous chapter suggested that transcript expression of PPARγ2 was related to the extent of differentiated phenotype in UC cell lines. Due to the complex splicing mechanism, there are multiple PPARγ transcript variants present. To understand the roles of different PPARγ transcript variants, it was essential to know the difference among them. Thus, examining the expression of individual exons may inform us of the splicing variants that exist and their expression in urothelial cells related to different phenotypes (proliferative or differentiated). By using primers designed to bind within different exons, with various combinations, RT-PCR can be performed to determine whether one or more exons were missing in PPARγ transcripts. Expression of PPARγ transcripts in UC lines showing different phenotype may provide additional information about links between UC and expression pattern of different PPARγ variants.

The differential expression of PPARγ protein isoforms in different UC cell lines suggested that the distinct isoforms may regulate different phenotypes. To explore whether there was a difference in localisation of different PPARγ isoforms, proteins were extracted using different concentrations of salt and/or DNAse I to extract proteins from different cellular or nuclear compartments. Higher concentration of salt or digestion with DNAse I has been shown to disaggregate the binding between proteins and nuclear matrix (Ainscough et al., 2007; Stenoien et al., 2000). Therefore, with increased salt concentration or incubation with DNAse I, proteins expressed in different cellular compartments were extracted differentially. After the extraction, different PPARγ isoform proteins were detected by western blotting using protein lysates generated from different cytoplasmic or nuclear compartments, which would suggest the localisation of different PPARγ isoforms in urothelial cells.

The aims for this chapter were to

- Explore the expression pattern of PPARγ transcript variants in NHU cells and UC cell lines.
- Examine the expression and compartmentalisation of different PPARγ protein isoforms in NHU cells.
- Investigate whether this differential expression was related to differentiated phenotypes displayed by NHU cells and UC cell lines.

5.3 Experimental approach

5.3.1 Expression of different PPARγ transcripts

The first coding exon is specific to PPARγ2, the rest of the exons are common to PPARγ1 and PPARγ2. Fig 5.3.1 shows the binding sites of primers for individual exons.

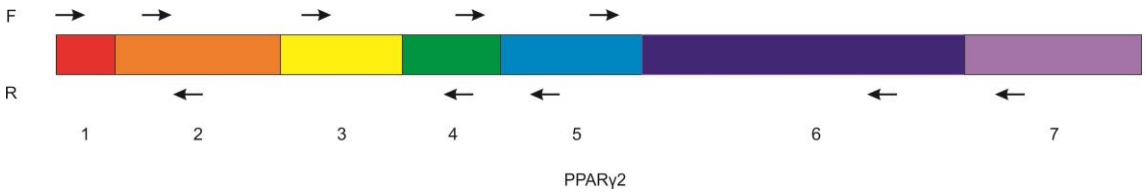

Fig 5.3.1 Schematic diagram showing the 7 coding exons and the positions of primer binding sites. Diagram was drawn to display the exons proportional to the length of individual exons. The 7 exons in PPARγ2 are shown with distinct colours. Primers are indicated as arrows heading to opposite direction. Arrows heading right indicate forward primers (F), whereas arrows heading left imply reverse primers (R).

As the primers were designed against coding sequence, the limitation was the impossibility to identify whether the 1st and 7th exon was absent. There is a start codon in the 2nd exon, acting as the first exon in PPARγ1. Thus, experiments were designed to identify the possibility of missing other exons. The following table showed the primers used to detect combinations of exons missing (Table 5.3.1). To start with, two main PPARγ transcript variants labelled as PPARγ1 and PPARγ2 were also examined.

Combination	Regions amplified/Missing Exons	Primer sets	Size (bp) of missing exons
Normal transcripts	PPARγ1	2F 7R	NA
	PPARγ2	1F 7R	NA
Single exon missing	3rd	2F 4R	170
	4th	3F 5R	139
	5th	4F 6R	200
	6th	5F 7R	451
Double exons missing	3rd and 4th	2F 5R	309
	4th and 5th	3F 6R	339
	5th and 6th	4F 7R	651
Triple exons missing	3rd, 4th and 5th	2F 6R	509
	4th, 5th and 6th	3F 7R	790

Table 5.3.1 Combination and primer sets for determination of the missing exons. Possibilities of missing one or more exons were grouped separately. Primer sets were listed to show the primers utilised to determine the missing exons. F or R indicates the forward or reverse primers, respectively. The size of potential missing exon(s) was calculated and displayed. For double or triple exons missing, only the maximal size was listed, as smaller ones were listed in single or double exon missing rows.

Primers were either obtained from lab or designed to identify whether certain exons were present in PPARγ transcript variants. Sequence of the primers is shown in Table 5.3.2.

Name	Sequence 5′-3′
PPARG2_Ex1F	TCCTTCACTGATACACTGTCTGC
PPARG2_Ex2F	ACTTTGGGATCAGCTCCGTG
PPARG2_Ex3F	GCAATCAAAGTGGAGCCTGC
PPARG2 Ex 4F	CTTGCAGTGGGGATGTCTCAT
PPARG2 Ex 5F	AGGGCGATCTTGACAGGAAAG
PPARG2_EX1-2 R	CAAAGGAGTGGGAGTGGTCT
PPARG2_EX3-4 R(4R)	TTATGAGACATCCCCACTGC
PPARG2 Ex 5R	AGGTCAGCGGACTCTGGATT
PPARG2 Ex 6R	CCCTCGGATATGAGAACCCC
PPARG2_Ex7R	GGGCTTGTAGCAGGTTGTCT

Table 5.3.2 Sequence of primers binding to different exons of PPARγ. Ex represents exon. Exon counting was based on coding sequence of PPARγ2. F or R indicates forward or reverse primer, respectively. Sequence was displayed from 5′ to 3′. All primers were designed with annealing temperature at 60°C.

To understand whether there was any relationship between exons missing and urothelial differentiation, PPARγ transcript variants were examined in both proliferating and 7 days TZ/PD differentiated NHU cells (Y1289). One well-

differentiated UC cell line and one poorly differentiated UC cell line were included to inform the expression of exons in UC cell lines. PCR was performed using same amount of cDNA from different samples. In order to calculate the potentially missing exons, all PCR reactions were performed for 40 cycles to obtain sufficient transcript products and have all potential splice variants amplified.

5.3.2 Expression of different PPARγ protein isoforms assessed by CSK extraction and western blotting

To examine the compartmentalisation of individual PPARγ isoforms in NHU cells, cytoskeletal extraction was performed. 0.5 M salt with 0.1% TX-100 was added to extract the cytoplasmic proteins or nuclear proteins not binding to nuclear matrix. DNase I was utilised to treat the pellet after salt wash, after which both supernatant and pellet were harvested. Mock digestion was included using digestion buffer alone (See section 2.6.2 for detailed method). Lysates from whole cell extracts, supernatants or pellet from every step were collected.

In this experiment, antibody against histone H2A was applied on the blot following western blot to demonstrate whether proteins harvested were binding to the chromatin. The blot was afterwards incubated with PPARγ E8 antibody to elucidate the expression of distinct isoforms in different cellular compartments.

5.4 Results

5.4.1 Transcript variants of PPARγ

To determine the transcript expression of PPARγ isoforms and investigate whether exons were missed when transcripts were spliced before translation, two main PPARγ isoforms were analysed by PCR. Proliferating and differentiated NHU cells were both examined to display whether the expression was different when differentiation was induced. UMUC9 cells were selected as well-differentiated UC cells, whereas T24 cells were poorly differentiated. These two cell lines were examined to show the expression of PPARγ in cancer cell lines.

PPARγ1 was amplified using primer sets 2F&7R, and abundantly expressed in both NHU cell lines and UC cell lines (Fig 5.4.1 left panel, pointed with an arrow). The extent of differentiation did not show any difference in terms of the expression of the full length band in all cell lines (Fig 5.4.1 left panel). There was more PPARγ1 expression in UMUC9 cells. However, multiple bands smaller than the full length PPARγ1 band in all cell lines were detected, some of which were present in NHU cells and cancer cell lines, whereas some other bands were unique to certain cell lines (Fig 5.4.1 left panel, arrow head). However, with such complicated splicing combination among 7 exons, it was not possible to define the bands.

Using primer sets 1F&7R, PPARγ2 was detected and shown in Fig 5.4.1 (right panel, pointed with an arrow). The full length PPARγ2 band was weakly detected in NHU cell lines and T24 cell line, whereas the expression was extremely robust in UMUC9 cells which was consistent with the RT-QPCR result shown in Fig 4.3.2. Smaller bands were still detectable in UMUC9 cells, but not in NHU cell lines, which may be due to the low abundance of PPARγ2 in NHU cell lines.

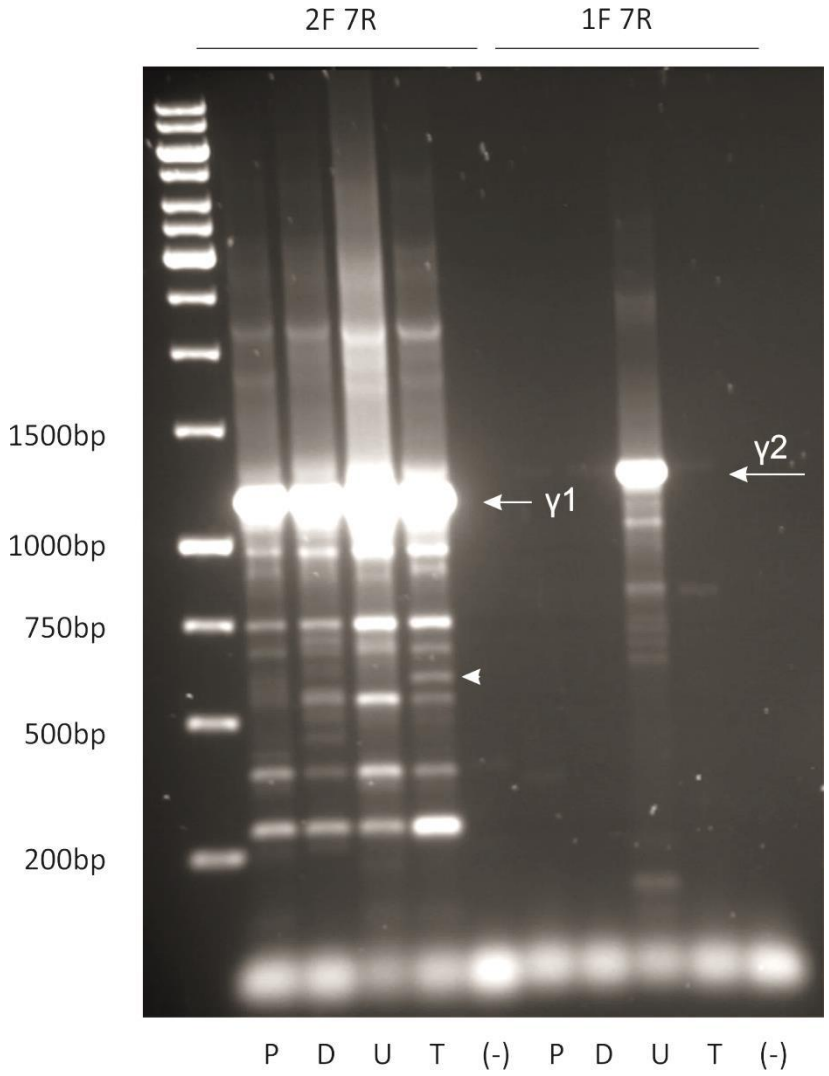

Fig 5.4.1 Transcript expression of PPARγ1 and PPARγ2. PPARγ1 was amplified using primer sets 2F 7R; PPARγ2 was amplified using 1F 7R. Extension step was 2 min. The full length band was 1209bp for PPARγ1 (left arrow) and 1288bp for PPARγ2 (right arrow). The Arrow head indicates a specific band expressed in T24 cell line. P or D indicates proliferating or differentiated NHU cells (Y1289), respectively. UMUC9 or T24 cells were cultured in medium with addition of serum, and labelled as U or T, respectively. The no template water control was shown as (-). Equal amount of cDNA was used as template.

To distinguish among the PPARγ splice variants, further PCR was performed. However, the band was so weak using forward primer binding to PPARγ2 specific exon, which is the 1st exon, that it was hardly detectable at 572bp even in the most abundant PPARγ2 expressing UMUC9 cell line (Fig. 5.4.2 left panel). Thus, further experiments mainly focused on investigating whether exons were missing in PPARγ1 transcript variants.

Whether the 3rd exon was missing was detected using primer set 2F and 4R. In all tested cell lines, a robust band at 493bp was detected. Missing 3rd exon may result in a smaller band at 323bp. The band shown in the image was at about the size or slightly smaller, which could be the product of missing the 3rd exon. Also, the smaller band demonstrated less expression in both differentiated NHU cells and the well-differentiated UMUC9 cancer cell line, whereas the expression was more abundant in proliferating and T24 cells (Fig. 5.4.2 middle panel). The finding was repeated in other two NHU cell lines, but one of which was not the same as shown in Fig 5.4.2 (See appendix, Fig 7.1.3).

Primer set 3F and 7R was utilised to detect the possibility of missing exons of 4th, 5th or 6th. Multiple bands were still present in all cell lines with slight different expression pattern. The expression of full length band with size of 1021bp was the most abundant in UMUC9 cells. The band at the size of 231bp could be missing of triple exons (4th, 5th and 6th). But the other bands were hard to determine as the information shown by the DNA ladder was not enough (Fig 5.4.2 right panel). Thus, to simplify the experiment, the possibility of missing exons was investigated from individual missing exons.

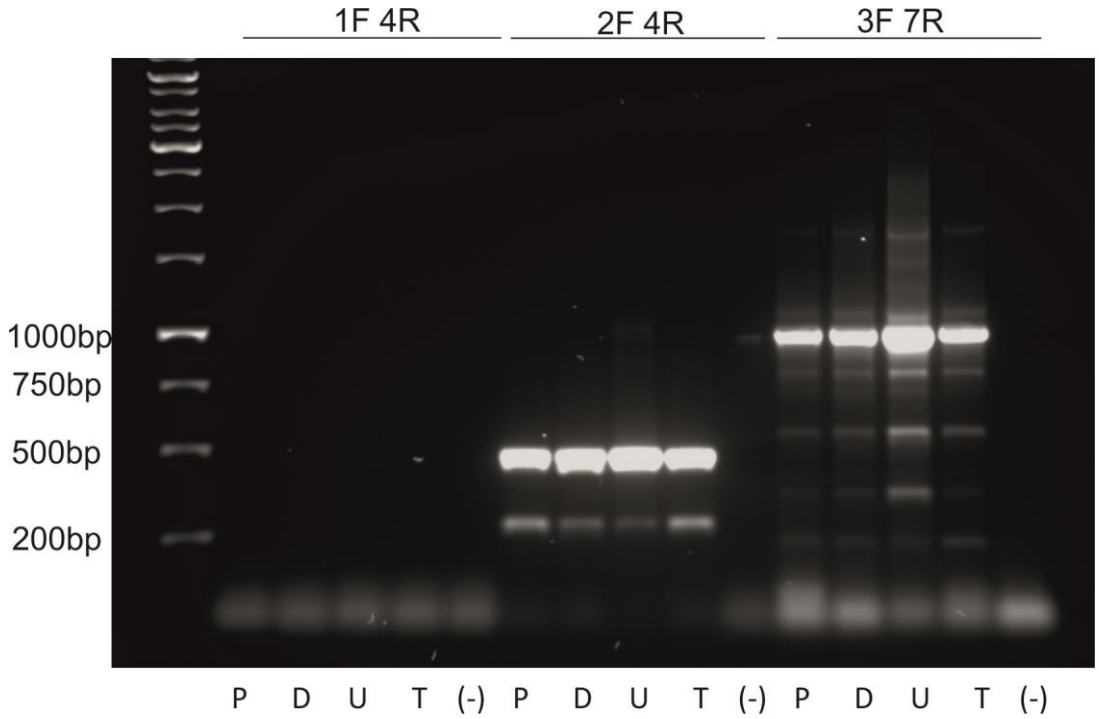

Fig 5.4.2 Missing exons in PPARγ1 and PPARγ2. Primer sets for detecting of missing different exons are shown. 1F and 4R was specific for PPARγ2 with a product of 572bp. The full length band for primer 2F and 4R was 493bp. Primer set 3F and 7R was utilised to amplify a band of 1021bp. P or D indicates proliferating or differentiated NHU cells (Y1289), respectively. UMUC9 or T24 cells were cultured in medium with addition of serum, and labelled as U or T, respectively. The no template water control was shown as (-). Equal amount of cDNA was used as template.

To determine whether a single exon was missing, primer sets across the potential missing exon was used. Only full length band for primers 3F and 5R was amplified with the size of 404bp. No detectable band smaller than the full length one was observed, indicating that exon 4 was mostly present when exons 3 and 5 expressed (Fig 5.4.3 left panel).

Full length band for primers 4F and 6R was visible at 521bp. With 5th exon missing, a band at 321bp was present in NHU cells and UMUC9 cells. The full length band was not as abundant in T24 cells as in the others, whereas the smaller band was even not visible (Fig 5.4.3 middle panel).

For primers 5F and 7R, both the full length band at 550bp and the smaller band at 99bp indicating the absent of exon 6 were present in all the cell lines. No

obvious difference was detected except that the two bands were most abundant in UMUC9 cells (Fig 5.4.3 right panel).

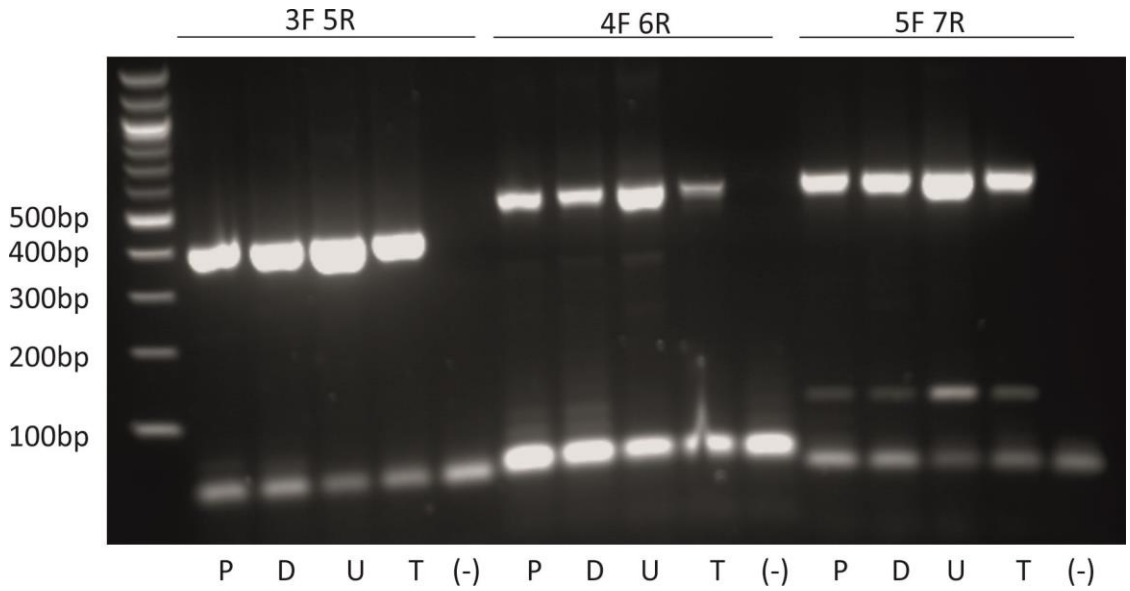

Fig 5.4.3 Detecting the possibility of missing single exon. Size of full length bands for each primer set was 404bp, 521bp and 550bp, respectively. P or D indicates proliferating or differentiated NHU cells (Y1289), respectively. UMUC9 or T24 cells were cultured in medium with serum, and labelled as U or T, respectively. Equal amount of cDNA was used as template. The no template water control was shown as (-).

PCR result for testing of single exon missing showed the possibility of missing the 3rd and the 6th exon. To further determine the potential of double exon missing, primer sets across 4 exons were utilised.

A full length band of 592bp for primers 2F and 5R was present in all cell lines. Even if the 3rd and the 4th exon were double missed, the size (283bp) would still be larger than any detectable bands, which were between 100bp and 200bp (Fig 5.4.4 left panel). This result may suggest the presence of other unknown spliced products.

For primers binding to 3rd and 6th exons, the full length band with the size of 803bp was detected. Missing the 4th or the 5th exon would result in a band with the size of 664bp or 603bp, which was detectable in all four cell lines but without dramatic expression. The double exons missing resulted in a band at 464bp, and was present in the proliferating, differentiated NHU cell lines and

UMUC9 cell line, but not visible in T24 cell line. Smaller bands between 100bp and 300bp were present in NHU cells and UMUC9 cells (Fig 5.4.4 right panel).

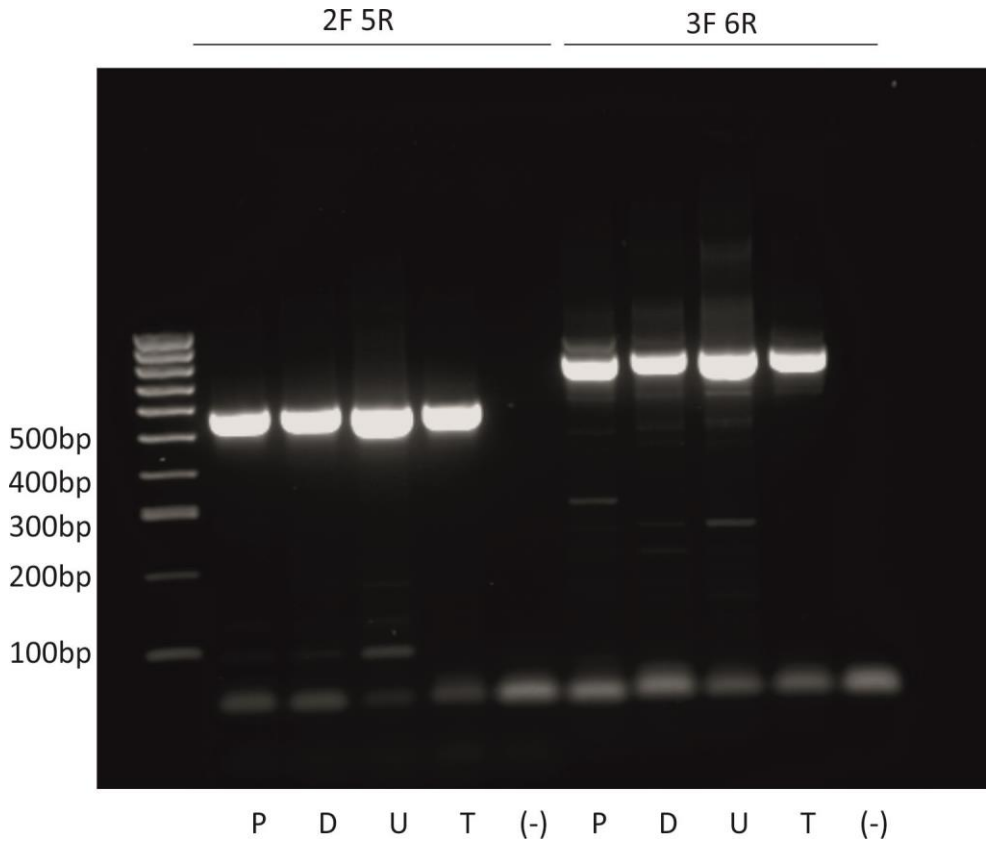

Fig 5.4.4 Examination the possibility of missing double exons. Full length bands for 2F5R and 3F6R were at 592bp and 803bp, respectively. P or D indicates proliferating or differentiated NHU cells (Y1289), respectively. UMUC9 or T24 cells were cultured in medium with serum, and labelled as U or T, respectively. The no template water control was shown as (-). Equal amount of cDNA was used as template.

To find out whether the 5th or the 6th exon was missing, primers binding to 4th and 7th exons were utilised. The full length band was present at 739bp. If the 5th exon was missed, the band would be 539bp, whereas missing of 6th exon would result in a band at 288bp. The missing of double exons would show a band at 88bp. The 288bp band was abundant in all four cell lines with the most abundance in UMUC9 cells. The 88bp band was prominent in UMUC9 cells but still detectable in the others. But the 539bp band was not obvious in all four cell lines (Fig 5.4.5 left panel).

To determine the possibility of missing triple exons, primers 2F and 6R were utilised. The visible band at 482bp could be the product of missing 3rd, 4th and 5th exon in proliferating NHU cells. Bands at about 800bp were detected and could be missing of either the 3rd or the 4th exon (Fig 5.4.5 right panel).

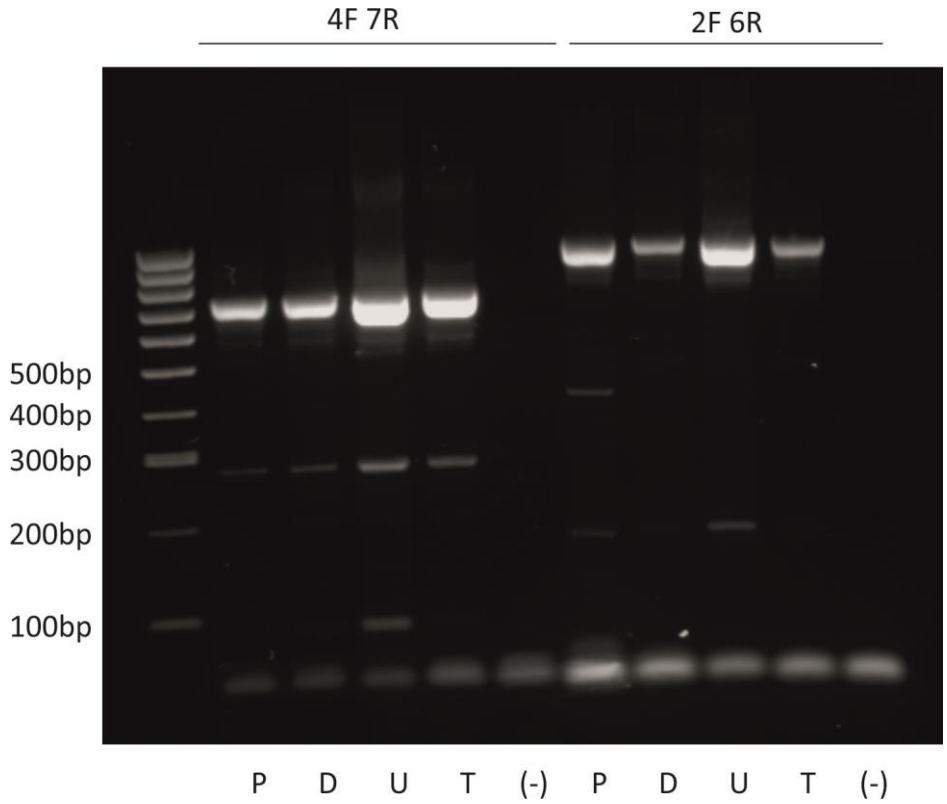

Fig 5.4.5 Detecting the possibility of missing double or triple exons. Size of full length bands was 739bp for primers 4F7R and 991bp for primers 2F6R. P or D indicates proliferating or differentiated NHU cells (Y1289), respectively. UMUC9 or T24 cells were cultured in medium with serum, and labelled as U or T, respectively. The no template water control was shown as (-). Equal amount of cDNA was used as template.

The RT-PCR results suggested that there are different PPARγ splicing variants expressed in NHU cells and UC cell lines. There might be relationship between splicing of exons and differentiated phenotype, but it was not yet understood.

5.4.2 Protein expression of different PPARγ isoforms following cytoskeletal extraction

To explore whether different PPARγ isoforms were expressed in different cellular compartments, differential extraction was performed followed by

western blotting. The blots below showed the expression of PPARγ isoforms in different cellular compartments (Fig 5.4.6). With PPARγ E8 antibody binding to C-terminus of PPARγ protein, both of the two main PPARγ isoforms were detectable on the blot. Histone H2A band indicates whether the proteins extracted were associated with chromatin.

Salt solution at 0.5M was not high enough to disturb the DNA-protein interaction, as histone H2A was not detectable in the supernatant after the salt wash. After digestion with DNase I, the interaction was broken, which released some amount of histone H2A protein. But there were still H2A proteins left, suggesting the salt and DNA enzyme extractions performed were not sufficient to release tightly binding proteins. The buffer-only lysates showed that without interruption of DNA-histone interaction, no chromatin proteins were extracted.

PPARγ isoform A was only detected in the pellet, even after the DNA digestion, implying its close interaction with the nuclear matrix. By contrast, PPARγ isoform B was mostly present in the supernatant after salt wash, suggesting the binding of isoform B to nuclear matrix was not as strong as chromatin proteins, which resulted in extraction of PPARγ isoform B before the binding of chromatin proteins was interrupted. Thus, isoform B was predominantly expressed in the cytoplasm and might be partially present in the nucleus with weak binding to the chromatin. In spite of that, small amount of isoform B was still detectable after enzyme digestion in the pellet. Other PPARγ bands with different molecular weight were detected in whole cell extracts and supernatant after salt wash, though the expression was not abundant.

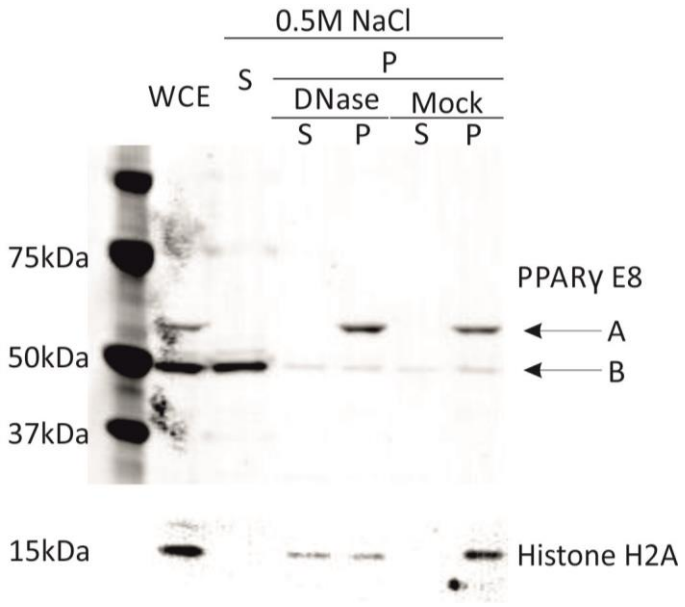

Fig 5.4.6 Blot of proteins extracted using CSK method. Proliferating NHU cells (Y1314) were extracted using cytoskeletal extraction. Whole cell extracts (WCE) showed the total proteins harvested. After washing with 0.5M NaCl solution, supernatant was collected (S). Pellet (P) was either treated with DNase I or the digesting buffer (Mock). Supernatant and pellet were collected from all groups after digestion. Two main PPARγ isoforms were detected using PPARγ E8 antibody, and labelled as A and B. Histone H2A antibody was applied to demonstrate the solubility of chromatin proteins.

The cytoskeletal extraction and western blot afterwards demonstrated that the two main PPARγ isoforms were mainly expressed in different compartments in NHU cells. However, whether it was related to differentiated phenotype needs further investigation.

5.4.3 Summary

- There was strong evidence supporting the missing exons of the 3rd, 5th and the 6th in PPARγ splice variants. In some cases, the possibility of missing more than two exons was considerable.

- The splicing pattern was not clear, but might be involved in urothelial cancer or differentiation of urothelial cells, as the expression pattern was distinct for missing of certain exons in different urothelial cell lines. One speculation is that missing exon 3 might be associated with a more differentiated phenotype.

- Missing of certain exons are detectable. But the size of some exons is not divisible by three. Detailed information regarding the expression of different PPARγ transcripts is listed in Table 5.4.1.

Absence of exons tested	Possibility of missing	Comments
3rd	Yes	Not divisible by 3
4th	Not detectable	
5th	May be yes	Bands were faint
6th	Yes	Not divisible by 3, might be spliced together with 5th exon

Table 5.4.1 Possibility of missing certain exons.

- PPARγ protein isoforms were detectable by western blotting after cytoskeletal extraction. The 50kDa band was mostly expressed in either cytoplasm or weakly present in the nucleus, whereas the 58kDa one was only detectable in proteins binding to the nuclear matrix. However, the antibody used in the experiment showed inconsistency in other blots (see chapter 3 and chapter 4) and needs further evidence.

Chapter 6 Discussion

Major findings of the current study are listed and further discussed in following sections.

- Transcript expression of ELF3 was mainly up-regulated by activated PPARγ pathway, but evidence also suggests the influence by other pathways (section 6.1.1).
- Regulation of some widely studied genes by ELF3 was observed at transcript level (section 6.1.2).
- Transcription factors may affect each other through negative feedback (section 6.1.3).
- UC cell lines demonstrated different expression pattern of differentiation-associated markers compared to NHU cells (section 6.2.1).
- UMUC9 cells showed a differentiated phenotype and were not able to proliferate in serum-free medium (section 6.2.2).
- 5637 cells demonstrated a less differentiated phenotype assessed by reduced expression of differentiation-associated markers. When adapted to serum-free medium, cells were shown to be dependent on GSK3β and PPARγ pathway for growth (section 6.2.3).
- Transcript expression and protein isoforms of PPARγ were different in UC cells from NHU cells (section 6.3).

6.1 The impact of ELF3 in urothelial differentiation

6.1.1 Pathways involved in regulating ELF3 expression

In this study, ELF3 was shown to be up-regulated by TZPD. This regulation was demonstrated to be mediated through the PPARγ signalling pathway, as previous results have shown that the PPARγ antagonist T0070907 reversed the increased expression of ELF3 (Bock et al., 2013).

Other pathways may also be involved. Firstly, the result of this study indicated that expression of ELF3 was elevated slightly in long term (96h) control cultures. But it was suggested that *in vitro* cultured urothelial cells were unable to switch to a differentiated phenotype without specific induction of differentiation, as no terminal differentiation features such as expression of uroplakins was observed only by reaching confluence (Lobban et al., 1998; Southgate et al., 1994).

When cells become confluent, the expression of EGFR and HB-EGF was not affected evidently, whereas the expression of ERBB2 (HER2) was up-regulated upon confluence (Varley et al., 2005). ERBB2 is one of the four EGFR gene family members, and found to be highly involved in human cancer, especially breast cancer. In human epithelial cell lines, it has been demonstrated that with endogenous expression of both ERBB2 and ELF3 proteins, ELF3 promoter exogenously transfected could be activated, suggesting possible regulation of ELF3 promoter activity by ERBB2. The activity of the ELF3 promoter was inhibited by the ERBB2 inhibitor AG1478 in the SKBR3 breast cancer cell line, which expresses a high amount of ERBB2 (Neve et al., 2002). Therefore, this up-regulation of ELF3 observed in the current study could be caused by enhanced ERBB2 expression, which resulted from the NHU cells obtaining confluence.

Also, there might be crosstalk between pathways to regulate ELF3 expression. The ELF3 transcript study demonstrated that treatment with PD153035 alone

increased the expression of ELF3, but not statistically significant. PPARγ has been shown to translocate to the nuclei of NHU cells by PD153035, regardless of addition of TZ (Varley et al., 2004a). In non-invasive MCF10A mammary cells, a more invasive phenotype could be induced by over-expression of ELF3 and presence of EGF signal. But with ERBB2 over-expression, the presence of EGF was no longer indispensable for the cells to be invasive (Coppe et al., 2010). As the enhanced ELF3 transcript expression was more dramatic when the NHU cells were treated with PD153035 than the DMSO control and further increased at late time point, the result could be the combination of PPARγ nuclear translocation and increased ERBB2 expression generated by the confluence of cells at late time point, which would need to be confirmed experimentally.

Furthermore, Alamar blue assay suggested the proliferation of both ELF3 knock down and ELF3 over expressing cells was reduced. The reduced proliferation rate in ELF3 over-expressing cells at late time point may be due to growth regulation through the PI3K/AKT pathway that resembled the growth of NHU cells cultured in physiological concentration of calcium on day 7 (Georgopoulos et al., 2010). The promoter of ELF3 showed the lowest activity when inhibited by PI3K inhibitor LY294002 compared to other inhibitors like PD98089 in breast cancer cell line SKBR3 present with high amount of ERBB2 expression, suggesting an essential role of PI3K pathway in regulating ELF3 transcriptional activity (Neve et al., 2002). There might be a negative feedback to ERBB2 or PI3K pathway by over-expression of ELF3 in NHU cells, which further inhibited the proliferation of ELF3 over-expressing NHU cells. But the low growth rate may also result from the senescence of transduced cells, as they have gone through many passages to be selected by antibiotics.

6.1.2 Possible downstream targets

6.1.2.1 CLDN7 as an ELF3 downstream target gene

The result in this study demonstrated that the knock down of ELF3 compromised the formation of functional barrier. This indicates an essential role of ELF3 in urothelial differentiation in terms of formation of functional barrier either directly or through the regulation of other factors required to form a functional barrier, such as tight junction proteins.

In urothelial cells, expression of CLDN7 was relatively stable (Varley et al., 2006). The up-regulation of CLDN7 observed in this study by induction of PPARγ using TZPD may suggest it a downstream target gene of PPARγ, and knock down of ELF3 also resulted in the reduction of CLDN7 transcripts but not the proteins.

CLDN7 was reported as a downstream gene regulated by ELF3 in synovial sarcoma cells (Kohno et al., 2006). ELF3 knock down in the SW480 cell line (human colon cancer; ELF3 and CLDN7 positive) resulted in decreased CLDN7 gene expression consistent with the reduction of ELF3 expression (Kohno et al., 2006). De novo expression of CLDN7 transcript could be induced by exogenous ELF3 expression in HT1080 (human fibrosarcoma; ELF3 and CLDN7 negative) and SYO-1 (human synovial sarcoma cell line; ELF3 and CLDN7 negative), but CLDN7 protein expression could not be detected following exogenous expression of ELF3 in these two cell lines (Kohno et al., 2006). This may indicate that ELF3 was not the only factor regulating expression of CLDN7, which could explain the inconsistency of CLDN7 transcript and protein expression in ELF3 knock down cells observed in this study.

6.1.2.2 Relationship of ELF3 and TGFβRII

Knockout of ELF3 in mice demonstrated its role in intestinal development (Ng et al., 2002). The formation of functional enterocytes can be rescued by

exogenous expression of TGFβRII in ELF3 knockout mice, suggesting regulation of TGFβRII by ELF3 and importance of TGFβRII in intestinal development (Flentjar et al., 2007).

In urothelial differentiation, ELF3 was identified as a transcription factor involved in urothelial differentiation *in vitro* (Bock et al., 2013). As exogenous addition of TGFβ1 accelerated the wound healing process by activation of p-SMAD3 (Fleming et al., 2012), it was hypothesised that knock down of ELF3 may have affected the TGFβ signalling pathway, which led to an inefficient repair of wounded cultures. In the current study, there appeared to be a reduction in the activation of the TGFβRII pathway downstream factor p-SMAD3. However, transcript expression of TGFβRII was demonstrated to be down-regulated in differentiated NHU cells (Fleming et al., 2012). Therefore, conclusions regarding the effect of ELF3 on TGFβRII should only be made with confirmation of further experiments.

6.1.3 Hierarchy of transcription factors

6.1.3.1 PPARγ and its downstream transcription network

The up-regulation of PPARγ2 transcript found at 6h by TZPD in this study suggested its role as a transcription factor mediating early differentiation in urothelial cells. The low transcript expression in proliferating and late differentiated NHU cells detected in the current study also indicated that PPARγ2 might be degraded after the differentiation programme has been initiated. However, a more complicated mechanism involving the production of transcript variants by alternative splicing may need to be taken into consideration, which will be discussed in section 6.3.

Knock down of ELF3 resulted in reduction of ELF3 transcripts and proteins (by western blotting only). The expression change of ELF3 knock down cell sheets by IHC was not obvious, which could be caused by the non-specific binding of

this antibody (blots with two different ELF3 antibodies were included in Appendix 7.1.4).

This study showed that apart from ELF3, the PPARγ downstream transcription factor FOXA1 was up-regulated significantly by TZ treatment alone, though it was not as dramatic as the treatment of TZPD, which blocked the phosphorylated PPARγ entirely and further activated the PPARγ pathway. Most importantly, this effect can only be observed on FOXA1 transcript but not on other transcription factors tested. Such an effect on FOXA1 was reported previously, and by using PPARγ antagonist T0070907 or GW9662, the increased FOXA1 protein was reduced, suggesting the direct regulation of FOXA1 by PPARγ pathway (Varley et al., 2009).

6.1.3.2 Feedback on other transcription factors by alteration of ELF3 expression

As ELF3 was inducible by TZPD, it is considered downstream of the PPARγ signalling pathway (Bock et al., 2013). However, the preliminary IHC result on ELF3 knock down cells in this study suggested possible knock down of nuclear PPARγ expression. The regulation of ELF3 by PPARγ was supported by demonstrating a reduced ELF3 expression using the PPARγ antagonist T0070907 (Bock et al., 2013). Therefore, the down-regulation of total PPARγ in ELF3 knock down cells may suggest a negative feedback, which would need further experiment to confirm.

The over-expression of ELF3 in this study demonstrated the dramatic up-regulation of ELF3 at transcript level. But the transcripts of other transcription factors such as FOXA1 and GRHL3 did not show any obvious alteration by ELF3 over-expression. One possible reason was that these factors were regulated by PPARγ directly, as the PPRE site was identified upstream of FOXA1 promoter (Varley et al., 2009). Alternatively, the over-expression of

ELF3 was only achieved at transcript level and not sufficient to initiate the differentiation program, so that the expression of other differentiation-associated transcription factors was not induced.

6.1.3.3 Transcription factor involved in early stage of differentiation

RT-qPCR using ELF3 knock down cells in this study showed that knock down of ELF3 reduced the amount of KLF5. But the amount of KLF5 transcripts was the most abundant among transcription factors. It has been previously demonstrated that KLF5 was essential in mouse urothelial development (Bell et al., 2011). Knock out of KLF5 compromised the maturation of mouse bladder and reduced the protein expression of transcription factors such as FOXA1. RT-qPCR also showed the statistically significant knock down of transcription factors including PPARγ, ELF3 and GRHL3 (Bell et al., 2011). Reduced KLF5 transcripts by ELF3 knock down demonstrated in the current study may be caused by feedback of ELF3 knock down. Thus, the hierarchy of these transcription factors may be more complicated and would require further work to be unravelled.

6.1.4 Other transcript variant/protein isoform of ELF3

A 25kDa band was observed by western blotting using the ELF3 antibody in NHU cells. It is potentially the product of a 3′ incomplete CDS, with truncation at the 3′ ending of ELF3 coding sequence. This transcript is displayed both in Ensembl (ENST00000446188) and Havana database (OTTHUMT00000087361) but without further information. Both the knock down and over-expression of ELF3 in the current study showed visible effects on this 25kDa ELF3 protein, however, there is no apparent evidence suggesting the function of this truncated ELF3 isoform.

6.1.5 Summary

ELF3 is up-regulated by PPARγ signalling pathway and there is possibility that ELF3 is regulated by other pathway, such as ERBB2. As one of the transcription factors involved in urothelial differentiation, the regulation by other factors or the feedback after alteration of gene expression was present with preliminary evidence and might indicate the importance of their roles. Other genes including CLDN7 and TGFβRII were reported to be regulated by ELF3, but the regulation on them in NHU cells was not apparent, which might be due to the involvement of other factors or a different mechanism in different species/tissue types.

6.2 Signalling pathways associated with UC cell proliferation

6.2.1 Expression pattern of differentiation markers

6.2.1.1 Comparison of expression pattern of genes/proteins between UC lines to NHU cells

RTqPCR results in this study demonstrated that UC cell lines have different phenotypes in terms of the expression of differentiation-associated genes and transcription factors. Expression pattern of markers in UC cell lines was compared to the pattern of NHU cells and listed in Table 6.1.

Cell line	UMUC9	5637	5637	RT4	RT112	T24	NHU (pro)	NHU (dif)
Medium	DMEM (10%)	KSFM	RPMI (5%)	D:R (5%)	D:R (5%)	D:R (5%)	KSFMc	KSFMc
ELF3 transcripts	++	-	++	++	+	-	-	+++
FOXA1 transcripts	+++	-	+	+++	+	+	-	+++
PPARG2 transcripts	+++	+	+	+	+	-	-	+
PPARγ 52kDa protein band	++	-	+	+	+	+	-	+
PPARγ 58kDa protein band	-	+	+	-	-	-	+	+
UPK2 transcripts	+++	-	-	++	+	-	-	+++
CK20 transcripts	+++	-	-	+	++	-	-	++
CK20 proteins	++	-	-	NT	NT	NT	-	+
CK13 proteins	-	-	-	-	+	-	-	+
CK14 proteins	-	+	-	-	+	-	+	+

Table 6.2.1 Transcript/protein expression of differentiation-associated markers. Transcripts in NHU cells and UC cell lines were compared according to the amount of transcript or protein assessed qualitatively. Transcripts were assessed by RT-qPCR; protein expression was assessed

by western blots or IF. Differentiated transcripts of NHU cultures were induced by TZ/PD; differentiated protein lysates of NHU cells were induced by ABS/Ca^{2+}. NT indicates the protein was not tested. Symbols indicate the amount of transcripts/proteins (- for negative, + for low, ++ for moderate and +++ for high). D:R indicates the medium comprised with 50% DMEM and 50% RPMI.

The acquisition of a squamous phenotype in 5637 cells when cultured in KSFM was similar to the phenotype observed in NHU cells cultured *in vitro* in serum-free low calcium medium (Southgate et al., 1994; Varley et al., 2004b). As 5637 cells were able to be maintained in KSFM without exogenous growth factors, it appeared that the 5637 cells were able to maintain their growth by autocrine activity, possibly via the EGFR pathway similarly as the NHU cells (Georgopoulos et al., 2014; Varley et al., 2005).

UMUC9 cells demonstrated dependence on serum for growth, whereas NHU cells would be induced to differentiate if cultured in medium supplemented with serum (Cross et al., 2005). This suggested that the differentiated phenotype maintained by UMUC9 cells might be related to the proliferation of cells. The acquisition of CK14 protein expression in UMUC9 cells treated with EGF or TGFβ suggested a switch to a more squamous phenotype that resembled the proliferating NHU cells (Harnden and Southgate, 1997), alteration of other features were also observed and will be discussed in following sections.

6.2.1.2 Indication of grade of UC and UMUC9 cell lines

Compared to RT4 cells, which was extensively studied and described as a grade 1 tumour-derived cell line, UMUC9 cells demonstrated more abundant UPK2 transcripts typical of a more differentiated phenotype. Nevertheless, it was suggested that features similar to normal superficial urothelial cells were present in some high grade NMIBC, as in carcinoma in situ (CIS) tissues (19 cases), 83.3% were positive for UPK2 expression and 84.2% were positive for CK20 expression (Jia et al., 2013). Another study also showed that the samples having most abundant expression of differentiation-associated genes were

tumours of high grade (G3) (Biton et al., 2014). Thus, the expression of differentiation-associated genes may not be associated with histopathological grade of UC.

UMUC9 cells was first reported in 1988 and found to be able to produce tumour in nude mice (Grossman et al., 1988). Tumours of 1-1.5 cm diameter were produced less than three weeks (17 days) in athymic nude mice after injection of trypsinised UMUC9 cells (Sabichi et al., 2006). UMUC9 was characterised as a grade III high stage carcinoma (Liebert et al., 1994; Liebert et al., 1989; Zou et al., 2001). A recent study about high grade MIBC demonstrated the expression of differentiation-associated transcripts in luminal subtype (Choi et al., 2014). After treatment with PPARγ selective agonist rosiglitazone, UMUC9 cell line demonstrated PPARγ downstream signalling pathway gene expression, which was analysed using Ingenuity Pathway Analysis (IPA, Ingenuity Systems) (Choi et al., 2014). UMUC9 was also characterised to be resistant to chemotherapy and was grouped as a p53-like MIBC, as incubation with cisplatin for 48h did not demonstrate as high apoptosis rate as the other UC cell lines (Choi et al., 2014). Sequencing data suggested exon 7 of TP53 was mutated in the UMUC9 cell line, and this mutation resulted in overexpression of P53 protein displayed as strong nuclear P53 staining by immunohistochemistry (Sabichi et al., 2006). Whether this mutation was related to cell survival is not clear, but may help further investigation.

6.2.1.3 The expression pattern of PPARγ transcripts and proteins

A dramatic expression of PPARγ2 transcripts was detected in UMUC9 cells in the current study. Another study also showed that knock down of PPARγ in some of the bladder cancer cell lines (for example, UMUC9, SD48 and RT112) significantly reduced the viability of cells. Formation of colonies was significantly affected in UMUC9 and SD48 cell lines as well (Biton et al., 2014). They also demonstrated a correlation between decreased PPARγ transcripts

and inhibition of proliferation by PPARγ siRNA, which indicated that in cell lines like UMUC9 that expressed the most PPARγ transcripts, proliferation was affected most effectively by knock down of PPARγ, suggesting dependency on PPARγ or the differentiated phenotype for survival (Biton et al., 2014).

PPARγ protein was also investigated in various cell lines in this study. Loss of the 52kDa band was observed in 5637 cells cultured in serum-free, whereas in medium with serum, this 52kDa band was present and was the same situation in differentiated NHU cells. Medium with serum combined with physiological concentration of calcium was used to differentiate NHU cells (Cross et al., 2005), so the band at 52kDa could be related to a more differentiated phenotype of 5637 cells in medium with serum and calcium. These bands were observed in other reports in human adipocytes but without detailed interpretation (Visweswaran et al., 2015), whereas another group claimed the 52kDa band as PPARγ2 (Liu et al., 2014). To identify the difference between PPARγ bands in UC lines with lysates generated from other tissues or species, a comparison was performed with UC cells, buccal epithelial cells and 3T3-L1 cells (See appendix, Fig 7.1.2). It appeared that 3T3-L1 cells showed distinct pattern of PPARγ protein isoforms. One band was present in both the UC lines and 3T3-L1 cells using PPARγ E8 antibody for detection of total PPARγ.

Given that UMUC9 cells showed the most abundant expression of PPARγ2 transcripts, compared to RT4 and RT112 cell lines, the similar height of the PPARγ bands in UMUC9 cells might be due to the post-transcriptional modification of PPARγ, such as sumoylation (Diezko and Suske, 2013), protein degradation mediated via activated MAPK pathway (Hedvat et al., 2004) or ligand induced ubiquitination followed by protein degradation (Hauser et al., 2000). Different isoforms of PPARγ and reports related to possible degradation mechanism will be discussed in section 6.3.

6.2.2 EMT process and possible growth pathways of UMUC9 cells

6.2.2.1 Possibly involved EMT process

The elongated morphology of UMUC9 cells treated with EGF and TGFβ in KSFM suggested that the cells might have undergone an EMT process. Although expression of vimentin was detectable after EGF/TGFβ treatment in the current study, the expression of E-cadherin was still visible, which was not consistent with reports demonstrating loss of E-cadherin in cells undergone EMT process (Chen et al., 2012). But another study showed that loss of E-cadherin was not necessary for EMT (specified by positive expression of Caveolin-1 as EMT marker) in breast cancer cells, as 50% samples (34 in total) had E-cadherin expression (Hollestelle et al., 2013). Therefore, whether it was an EMT or alteration to a more basal-like phenotype of the UMUC9 cells cultured in KSFM with EGF or TGFβ requires further investigation to assess.

6.2.2.2 Signalling pathways related to EMT and speculated mechanisms

It was reviewed that exogenous TGFβ was the most important growth factor in induction of the EMT process (reviewed by Xu et al., 2009), but EGF pathway was also suggested to be essential. In normal murine mammary gland epithelial cells, the EMT process was demonstrated to occur only with activated ERK pathway, without which the cuboidal shape of cells was still observable with expression of differentiation-associated protein like ZO1 (Lu et al., 2004). Similarly, the addition of EGF in current study altered the morphology of UMUC9 cells in KSFM and promoted proliferation at the same time.

Another study in intestinal cells demonstrated the essential role of PPARγ in promoting EMT by activating the Rho family, as block of MEK pathway inhibited ligand-activated PPARγ-induced EMT (Chen et al., 2006a). Although in the current study the growth of UMUC9 cells with TGFβ alone was similar to control cells, the increase of PPARγ expression was obvious. Treatment with

TGFβ has been shown to increase protein expression of β-catenin and its nuclear accumulation in human fibroblasts (Akhmetshina et al., 2012). Therefore, the up-regulation of PPARγ protein could be due to the increased β-catenin expression, as the up-regulation of PPARγ was reported as the result of over-expression of β-catenin in colon cancer cells (Jansson et al., 2005). However, the negative regulation of PPARγ by exogenous TGFβ was reported in hepatic stellate cells via up-regulation of β-catenin, which was contrary to the speculation (Qian et al., 2012). Importantly, in NHU cells, TGFβ pathway-associated transcripts such as TGFβRII were down-regulated in TZ/PD or ABS/Calcium induced differentiated cultures compared to control cultures (Fleming et al., 2012). Exogenous TGFβ1 inhibited the differentiation of NHU cells as transcript expression of UPK2 decreased significantly, suggesting a negative effect of TGFβ on differentiated NHU cultures (Fleming et al., 2012). But an accelerated wound repair in differentiated cultures and decelerated cell migration in non-differentiated cultures were observed (Fleming et al., 2012). Therefore, it is currently difficult to interpret whether TGFβ pathway was involved in the morphology alteration of UMUC9 cells cultured in KSFM.

Coincidentally, one report demonstrated an interrelationship between vimentin expression and PPARγ degradation and suggested that vimentin might be essential in preventing ubiquitination and degradation of PPARγ upon ligand-induced adipocyte differentiation. They showed that knock down of vimentin accelerated the degradation of PPARγ protein when 3T3-L1 cells were induced to differentiate by BRH49653 (Tsai et al., 2013). Therefore, the de novo expression of vimentin in UMUC9 cells grown in KSFM with EGF supplement in the current study may decelerate the degradation of PPARγ, which might further indicate that expression of PPARγ was essential for proliferation of UMUC9 cells. But further experiments are needed to verify this speculation.

6.2.3 Involvement of GSK3β in regulating cell proliferation

6.2.3.1 Role of activated β-catenin in cell growth

The growth inhibition of 5637 cancer cells in KSFM resulting from inactivation of the GSK3β pathway by SB415286 observed in the current study was reversible by inhibition of PI3K/AKT pathway with LY294002. Other reports also demonstrated that inhibition of the AKT pathway with down-regulation of phosphorylated AKT led to reduced p-GSK3β (Gan et al., 2010; Wu et al., 2012). In GSK3β-inactivated prostate cancer cells, increased expression of β-catenin eventually resulted in the up-regulation of the EGFR pathway. CHIP assay and promoter analysis suggested that after being activated (dephosphorylated), β-catenin was able to bind to the promoter of the EGFR gene and increased its expression. Downstream target pathways such as ERK1/2 were also activated following the binding of β-catenin to EGFR promoter (Guturi et al., 2012). In NHU cells, down-regulated phosphorylated-ERK expression in β-catenin-knock down NHU cells was observed, suggesting β-catenin might be able to regulate the expression of EGFR pathway (Georgopoulos et al., 2014).

However, in the current study with bladder cancer line 5637 cells cultured in KSFM, the inactivation of GSK3β led to reduced cell proliferation, which was in disagreement with the reports mentioned above. In NHU cell cultured in physiological concentration of calcium (2mM), β-catenin was located to membrane and interacted with E-cadherin (Georgopoulos et al., 2010), which was also observed in 5637 cells maintained in KSFM. This might be part of the reason of reduced growth in 5637 cells cultured in KSFM after inactivation of GSK3β.

6.2.3.2 Growth inhibition by inactivated GSK3β signalling pathway

There is controversy between different studies demonstrating roles of GSK3β pathways on proliferation. One report suggested that decreased cell

proliferation was observed in neuroblastoma B65 cells after treatment of either lithium or SB415286, both are GSK3β inhibitors, and this growth inhibition was associated with G2/M cell cycle arrest. This might have resulted from increased phosphorylated GSK3β on Ser9, which further enhanced phosphorylation of CDC2 (CDK1) on Tyr15 (inactive form) (Pizarro et al., 2009). Nevertheless, another report in human myeloid leukemia cells suggested that pharmacological inhibition or knock down of GSK3α/β decreased apoptosis (Rahmani et al., 2013).

In the current study, the growth rate of 5637 cells cultured in KSFM appeared to be associated with localisation of PPARγ protein, and may further affected the expression of active β-catenin (Table 4.3.4).

6.2.3.3 Influence on GSK3β-mediated growth inhibition by PPARγ signalling pathway

The decreased proliferation by GSK3β inhibition was further enhanced after inhibition of PPARγ signalling pathway using T0070907. In agreement with this result, GSK3β-mediated growth inhibition has been reported to be related to PPARγ. One report in mouse adipocytes suggested that protein expression and function of PPARγ was regulated indirectly by GSK3β and directly by Snail (Lee et al., 2013). The transcript and protein expression of PPARγ was negatively correlated with Snail. E-box-707 and E-box-154 on the promoter of mouse PPARγ2 were the binding sites of Snail, as the promoter activity investigated by luciferase assay suggested that PPARγ2 promoter activity was down-regulated after transfection of Snail in 3T3-L1 cells, whereas mutation on either E-box on PPARγ2 promoter abolished the Snail-induced down-regulation (Lee et al., 2013). By contrast, induced adipogenesis inhibited the protein expression of Snail. Furthermore, expression of Snail was up-regulated by treatment of Wnt10b or LiCl, which resulted in inactivation of GSK3β, decreased protein expression of adipocyte differentiation-associated proteins

and reduction of oil red staining (Lee et al., 2013). Whether the Snail pathway was involved in inhibited growth of 5637 cells in KSFM was not clear in the current study and would need further investigation.

Other reports demonstrated a PPARγ regulated growth control, which may help interpret the reversed GSK3β-mediated growth inhibition by LY294002 and enhanced inhibition by T0070907. Firstly, one report showed that PPARγ antagonist GW9662 could inhibit the expression of p-AKT and p-GSK3. In neurons, decreased expression of p-AKT and p-GSK3 could lead to apoptosis. They demonstrated that nutrient deprivation-induced apoptosis can be inhibited by addition of Telmisartan, which is an angiotensin II receptor antagonist and also activates PPARγ (Pang et al., 2014). In NIH3T3 cells, however, Telmisartan as a PPARγ ligand was able to inhibit p-AKT (Yamamoto et al., 2009). This PPARγ ligand-mediated p-AKT down-regulation was also observed in myofibroblast differentiation (Kulkarni et al., 2011). Therefore, inhibition of PPARγ by T0070907 may reverse the inhibition of p-AKT, which resulted in the enhanced growth inhibition in the current study on 5637 cells treated with SB415286 and T0070907. This growth inhibition might be due to increased p-AKT and p-GSK3β expression via both GSK3β and PPARγ pathways, which would need further experiments to investigate. The proposed signalling pathways affecting proliferation in NHU cells and 5637 cells were summarised in Fig 6.1.

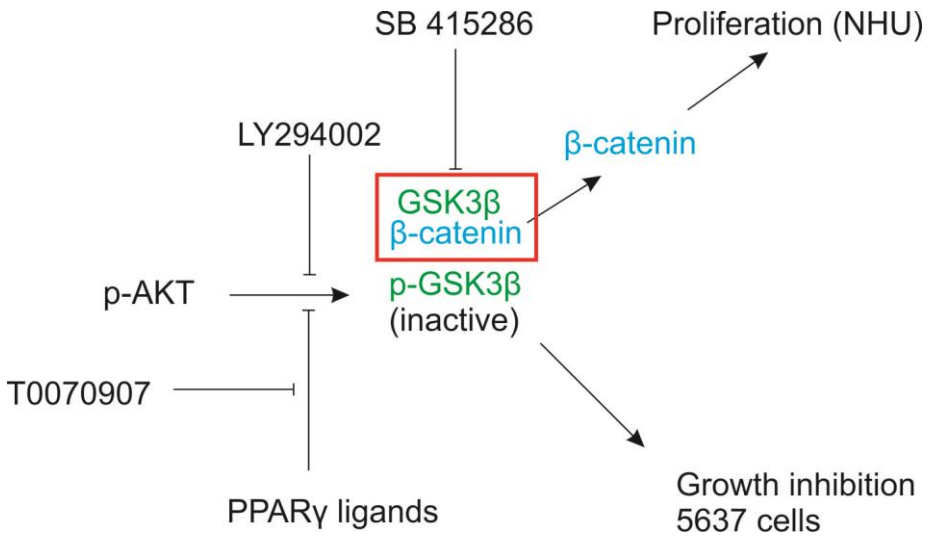

Fig 6.2.1 Diagram to show the proposed relationship of signalling pathways involved in proliferation. Red rectangular indicates the destruction complex which can be destroyed by SB415286. Then, GSK3β was phosphorylated and β-catenin was released.

6.2.3.4 Relationship of PPARγ and β-catenin

Contrary findings of the relationship between PPARγ and β-catenin were reported in different cell lines. The up-regulation of β-catenin was suggested to induce PPARγ protein expression, which has been reported in colon cancer cells (Jansson et al., 2005).

Nevertheless, relationship between PPARγ and β-catenin seems to be more complicated, as another report showed that PPARγ functioned as a suppressor of β-catenin by targeting phosphorylated β-catenin to the proteasome, whereas oncogenic expression of β-catenin demonstrated resistance to PPARγ-mediated degradation, which required the TCF/LEF binding domain of β-catenin (Liu et al., 2006). During adipogenesis from mouse fibroblasts, β-catenin protein was negatively correlated with differentiation-associated proteins. Addition of troglitazone activated PPARγ and decreased the amount of β-catenin protein (Liu and Farmer, 2004). In mouse adipocytes, where the only activated and functional PPARγ form is PPARγ2 (Ren et al., 2002), this negative regulation of β-catenin protein expression was suggested to be controlled by PPARγ2 (Rahman et al., 2012).

6.3 Regulating the expression of PPARγ

The differential PPARγ transcript expression pattern between NHU cells and cancer cell lines and different PPARγ protein isoforms observed may suggest that the different PPARγ transcripts and proteins have specific roles in regulating downstream genes.

6.3.1 Splicing variants

RT-PCR analysis suggested that missing certain exons (e.g., exon3) might be associated with a more differentiated phenotype. However, length of the coding nucleotides of exon3 is 170bp, which is not divisible by three, suggesting that theoretically it could not be the only missing part. Thus, there might be a more complicated splicing event that has been reported by several groups in different tissues/cell lines (see below). These truncated PPARγ variants may be involved in regulating expression and function of the principal PPARγ isoforms in differentiated tissues and/or carcinomas.

One case was associated with the 4th intron. A novel PPARγ isoform which contained part of the 4th intron was identified in an human ovary fibrothecoma and an adenocarcinoma using human genome sequencing data and was named γORF4 (Sabatino et al., 2005). The majority of the LBD domain present in the other PPARγ isoforms was truncated, leaving 22 amino acids followed by 21 amino acids of the 4th intron. Reporter assay suggested that this isoform functioned as a dominant-negative protein of PPARγ in regulating PPRE reporter activity in COS7 cells (Sabatino et al., 2005). This truncated variant was found in PPARγ1, 2 and 3, showing similar functions as dominant negative proteins. Adipocyte differentiation using human MSC (mesenchymal stem cells) demonstrated that both transcripts and proteins of γ2ORF4 were up-regulated after differentiation for 2 days and decreased gradually, the pattern of which matched the expression of PPARγ2. Such matched expressing pattern,

however, was neither detectable for PPARγ1, which showed a consistently high amount of transcript in undifferentiated and differentiated MSC cells, nor γ1ORF4, which demonstrated no obvious expression pattern (Aprile et al., 2014). This result confirmed a differentiation-associated role of PPARγ2, and may also suggest a role in regulation of PPARγ2 expression by γ2ORF4. However, another research report claimed that the γ1ORF4 comprised less than 10% of PPARγ transcripts and existed in general (Bouancheau et al., 2007). Thus, whether a read-through of introns and truncation of following exons are cases present in NHU cells needs further investigation.

Another similar case suggested a truncated PPARγ1 isoform was expressed in human lung cancer tissues, whereas full length PPARγ1 was expressed in the normal tissue surrounding the cancer area (Kim et al., 2007). The truncated variant was the N-terminal sequence of wild type human PPARγ1 lacking part of the hinge domain and the entire Ligand Binding Domain, which resulted from an extra 143bp in the hinge domain as a novel exon (exon 3'). The additional 143bp resulted in a frameshift in the ORF, creating 8 alternative amino acids and a premature stop codon. The splice variant showed sequence that conformed to the GT-donor/ AG-acceptor rule for exon splicing (Kim et al., 2006). As the majority of exons are not divisible by three, containing of intron and frameshift might be involved in the splicing events of PPARγ variants found in NHU cells.

The truncated variant did not show activity in a transactivated PPRE luciferase reporter, and acted as a dominant negative protein that decreased the activity of full length PPARγ1. It also significantly increased CHO cell viability to oxidative stress or cisplatin. Reduction of tumour suppressor proteins was associated with over-expression of PPARγ truncated proteins, suggesting that expression of truncated PPARγ was related to resistance to tumour therapy and might be involved in regulating pathways associated with PPARγ in tumour

tissues (Kim et al., 2007). Some evidence also suggested that an isoform switch of PPARγ was found in human lung squamous cell carcinoma among the nine tested cancer types. The switch of isoforms affected pathways regarding gene expression, development and metabolism. By comparing normal and tumour samples from the same patient, the amino acid sequence of PPARγ was found to be different (Sebestyen et al., 2015). Further experiments regarding the function of PPARγ transcript variants are needed to find out whether there is a link between expression of different variants and phenotype of NHU cells (proliferating or differentiated) and role in UC.

6.3.2 Post-translational modification and protein degradation

6.3.2.1 SUMOylation

One report using *in vitro* transcription/translation system suggested that PPARγ2 was able to be SUMOylated after addition of SUMOylation pathway proteins, as extra bands at about 75kDa were observed and considered as single SUMOylated PPARγ. Some other higher bands were considered as double SUMOylated PPARγ. Lysine 107 on PPARγ2 could be a potential site of SUMOylation; mutation on this amino acid resulted in reduced SUMOylation of PPARγ (Floyd and Stephens, 2004).

Another report also demonstrated that exogenous SUMOylation of PPARγ in HEK293 cells was impaired when cells were treated with PPARγ ligands like GW1929 or rosiglitazone. The SUMOylation site affected by binding of ligands was lysine 33 but not lysine 77 on PPARγ1 protein (lysine 107 on PPARγ2) (Diezko and Suske, 2013).

6.3.2.2 Ubiquitination

The stable expression of PPARγ was also reported to be regulated by HAUSP (herpes virus-associated ubiquitin-specific protease). This regulation deubiquitinated PPARγ proteins and was detectable for both endogenous and

exogenous expression of PPARγ. Deubiquitination of PPARγ resulted in the expression of more stable PPARγ proteins at protein level, whereas the transcripts of PPARγ were stable and not affected by HAUSP expression (Lee et al., 2013). Most importantly, deubiquitination of PPARγ by HAUSP increased the transcriptional activity of PPARγ independent of the presence of PPARγ ligand (e.g., rosiglitazone). This enhanced transcription of PPARγ was reversed by siRNA knockdown of HAUSP or mutation on C223 of HAUSP, which confirmed the role of deubiquitination of PPARγ by HAUSP in maintaining the PPARγ transcriptional activity. *In vivo* experiments in mouse liver also verified the regulation on PPARγ by HAUSP, as oil red stain increased along with enhanced protein expression of PPARγ. Downstream adipogenesis-associated transcripts were up-regulated significantly (Lee et al., 2013).

6.4 Ideas for future work

- To test whether ELF3 was regulated by ERBB2 in NHU cells, ERBB2 inhibitor could be used on nearly confluent cultures.
- Whether PI3K/AKT pathway affected growth of ELF3 over-expressed NHU cells might be examined by checking the p-AKT and E-cadherin in the cells.
- The growth inhibition induced by SB415286 in 5637 cells may be controlled by p-AKT (Fig 6.1.1), and could be examined by IF or western blotting.
- If the alteration of PPARγ localisation in 5637 cells is reproducible by IF, cytoskeletal extraction can be performed to check the result and understand whether the protein has interaction with the nuclear matrix.
- PPARγ protein might be modified and not detectable. Sumoylated or ubiquitinated isoforms might be alternative forms and appear at different height on the blot.

Appendices

Appendix A Transcript and protein expression of differentiation-associated markers

Appendix A1 Transcript of KRT20 in UC cell line (log scale)

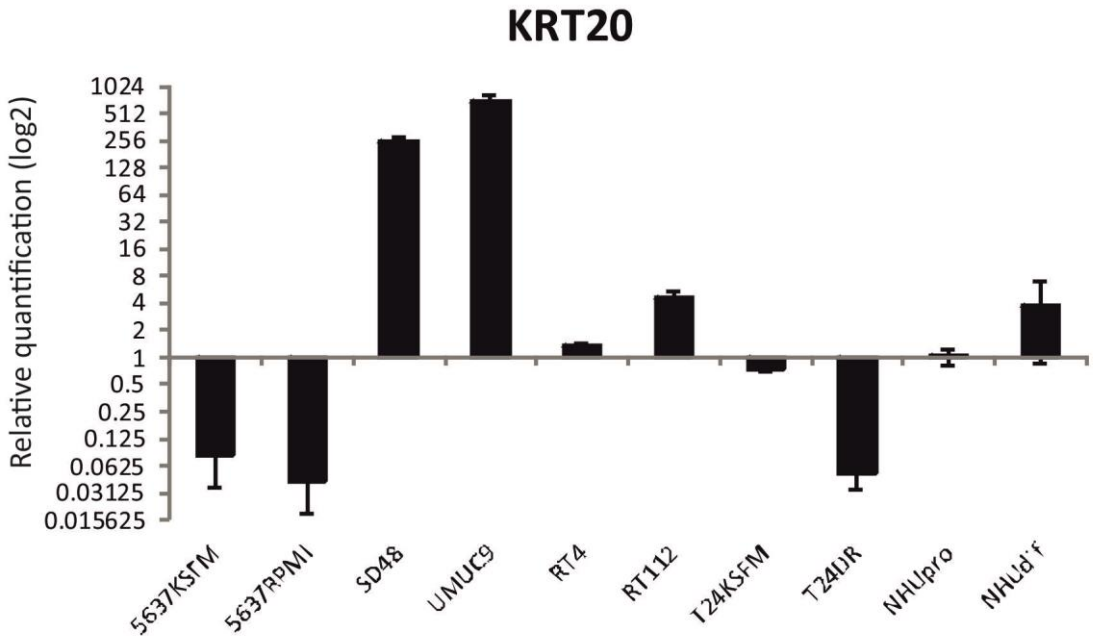

Fig Appendix A1 Transcript expression of CK20 (KRT20) in UC cells using log scale. RNA samples were obtained from cancer cells cultured in medium with serum or adapted to KSFM (5637 cells and T24 cells). 5637RPMI indicated RNA sample of 5637 cells cultured in RPMI with serum; T24DR indicated RNA sample of T24 cells cultured in DMEM& RPMI with serum. Proliferating (NHU pro) and 7 days TZ/PD differentiated (NHU dif) NHU cells (Y1289) were included as control. RT-QPCR was performed. Gene expression of KRT20 was normalized to GAPDH. Fold change of each sample was obtained by comparing to the proliferating NHU cell sample. Log scale was used to demonstrate the difference between cell lines showing low KRT20 transcript. Error bars indicate standard deviation of three technical replicates.

Appendix A2 Comparisons of PPARγ protein isoforms between UC cells and 3T3-L1 cells

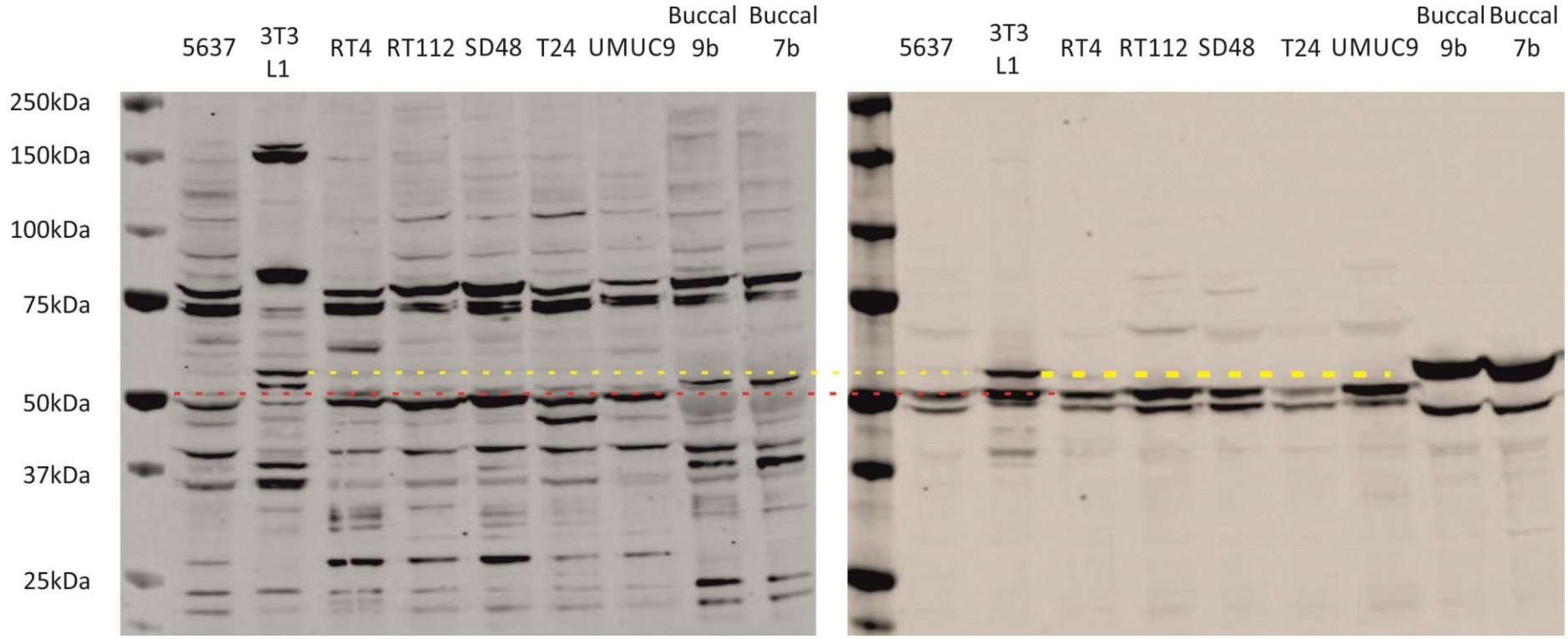

Fig Appendix A2 Blots showing the different PPARγ isoforms in various UC lines, two buccal epithelial cell lines and 3T3-L1 cells. All UC cell lines were cultured in growth media supplemented with serum. 3T3-L1 lysate was obtained using nuclear protein preparation by Jonathan Fleming. Buccal cell lysates were proliferative cultures generated by Arianna Hustler. The left blot was immunolabelled with PPARγ2 antibody (Abcam), whereas the right one was labelled with PPARγ E8 antibody (Santa Cruz) for total PPARγ protein isoforms. Dotted red line showed the upper band present in the majority of UC cell lines at 52kDa using total PPARγ antibody and not detectable in 3T3-L1 cells using γ2 antibody. The distinguished band present in 3T3-L1 cells noted with yellow dotted line was not obvious in UC cells but was at about the height of the bands detected in buccal cell lines and NHU cells (Fig 4.3.3). The work was done together with Dr. Carl Fishwick and Han Yang.

Appendix A3 Repeat of interested RT-PCR showing expression of PPARγ transcripts

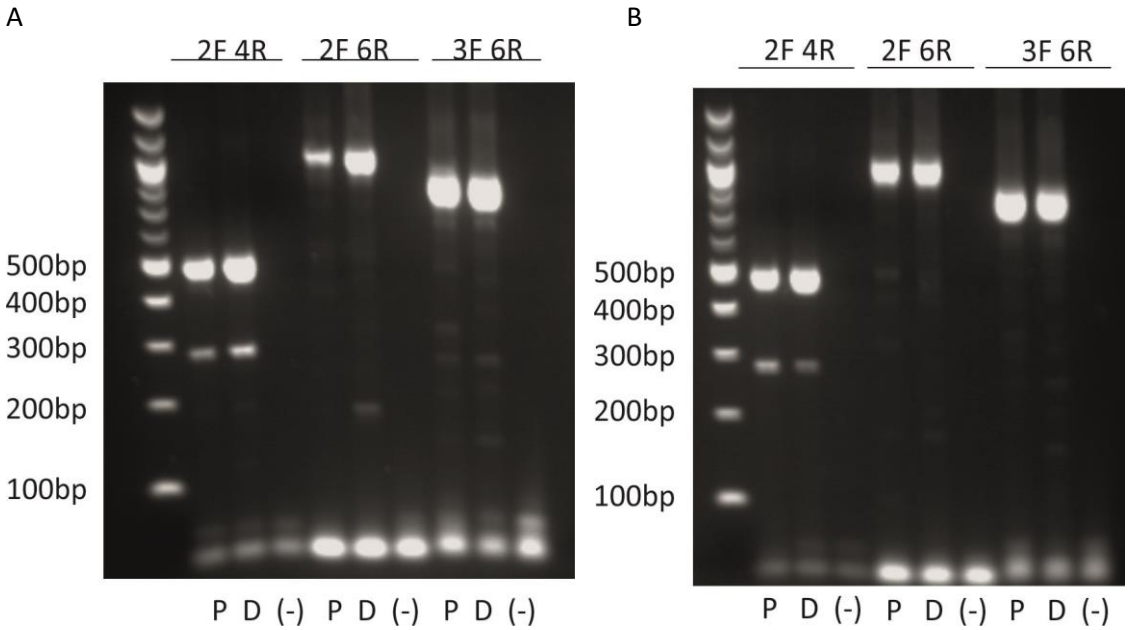

Fig Appendix A3 Expressing pattern of PPARγ transcripts. Primers targeting different exons were used. Primer sets demonstrating difference between proliferating and differentiated NHU cells in chapter 5 were used in other two different NHU cell lines (A, Y1194; B, Y1529) to verify the previous identified expressing trend. The enhanced expression of band smaller than 300bp detected using primer sets 2F4R was speculated to be relevant with a more proliferative phenotype observed in Fig 5.4.2 and panel B. However, the difference of PPARγ transcript amount showed no consistency compared to previous data, which might be dependent on different cell lines.

Appendix A4 Comparison of ELF3 antibodies by western blots

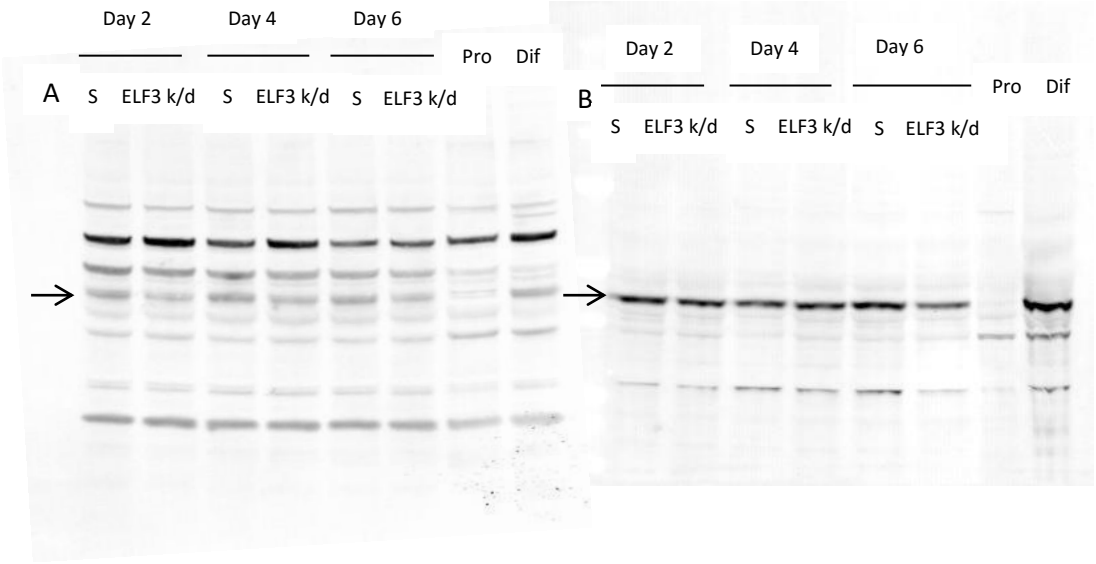

Fig Appendix A4 Comparison of two ELF3 rabbit antibodies. A, ab97310; B, ab133621. Arrows indicate the ELF3 full length protein band that is absent in the proliferating (Pro) control. Detailed information regarding these two antibodies is listed in Table 2.6.1. Ab97310 was the antibody used for IHC showing positive staining in urothelial tissue, whereas ab133621 does not work by IHC.

Appendix B Primer efficiency test

Newly designed primer sets for RT-qPCR were optimised before use in experiments. Results of optimised primers are shown.

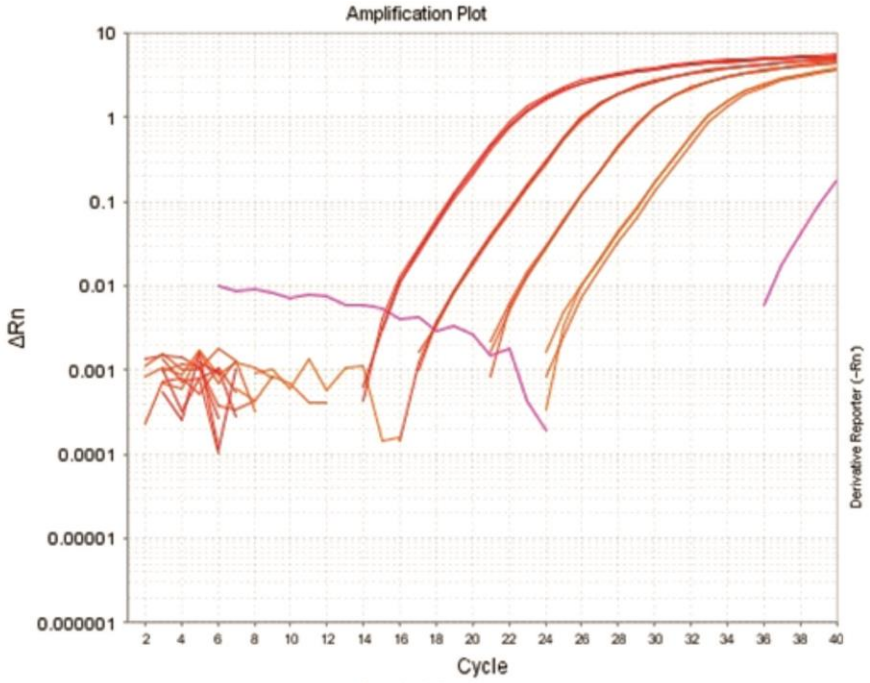

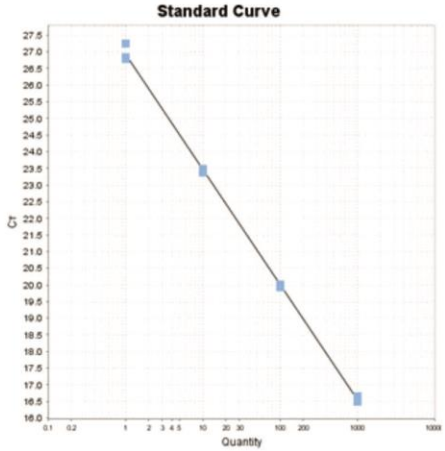

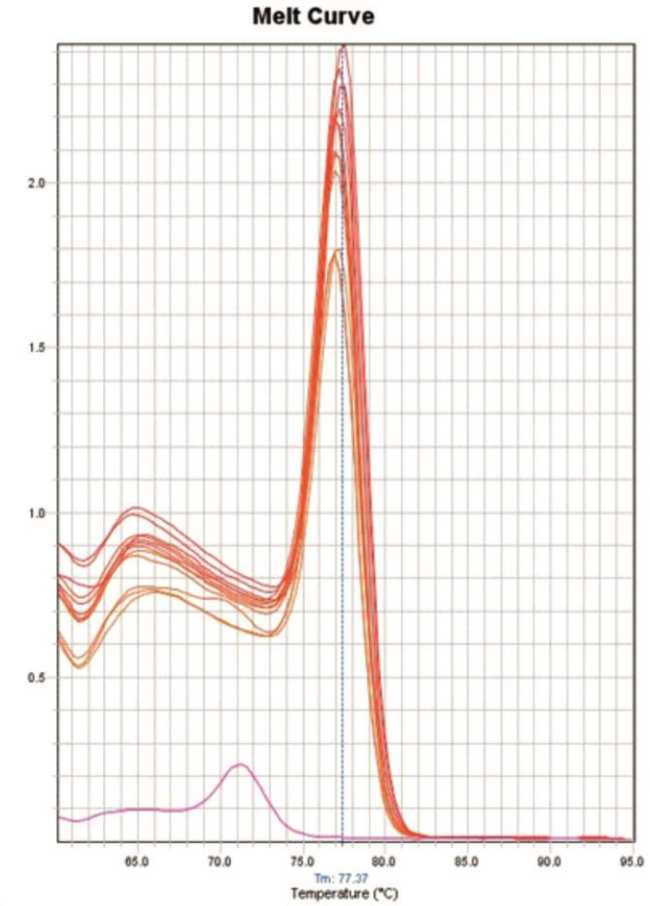

Target: KLF5 **Slope**: -3.458 **Y-Inter**: 26.923 R^2: 0.999 **Eff%**: 94.604

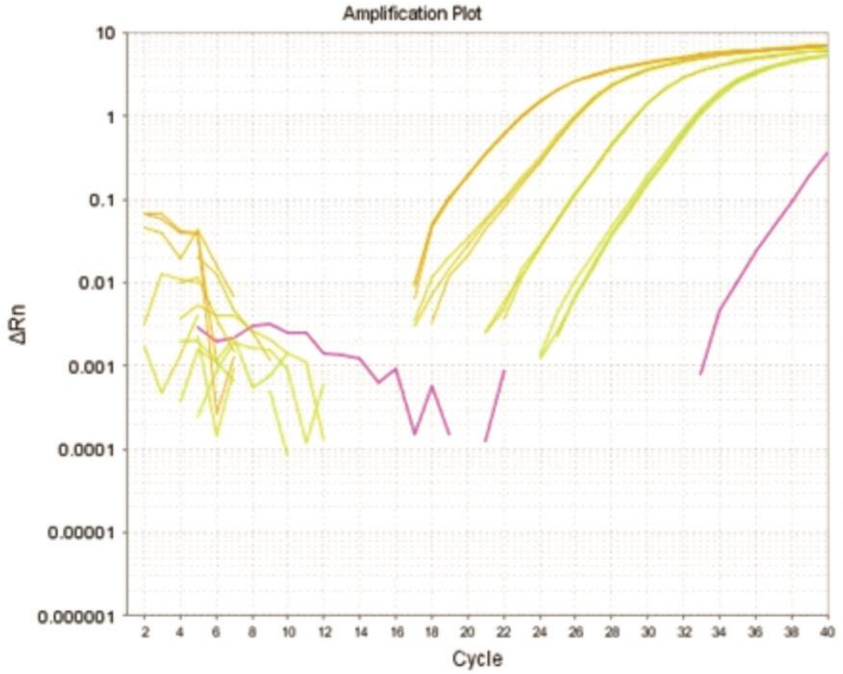

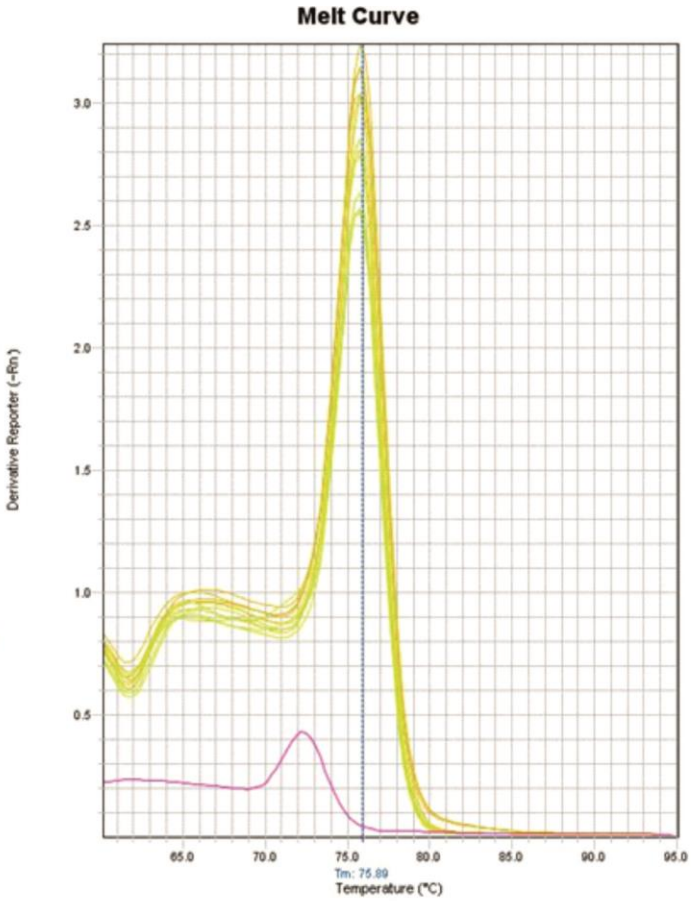

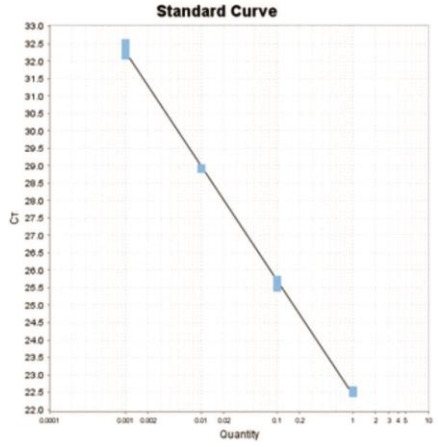

Target: GRHL3 Slope: -3.277 Y-Inter: 22.434 R^2: 0.999 Eff%: 101.905

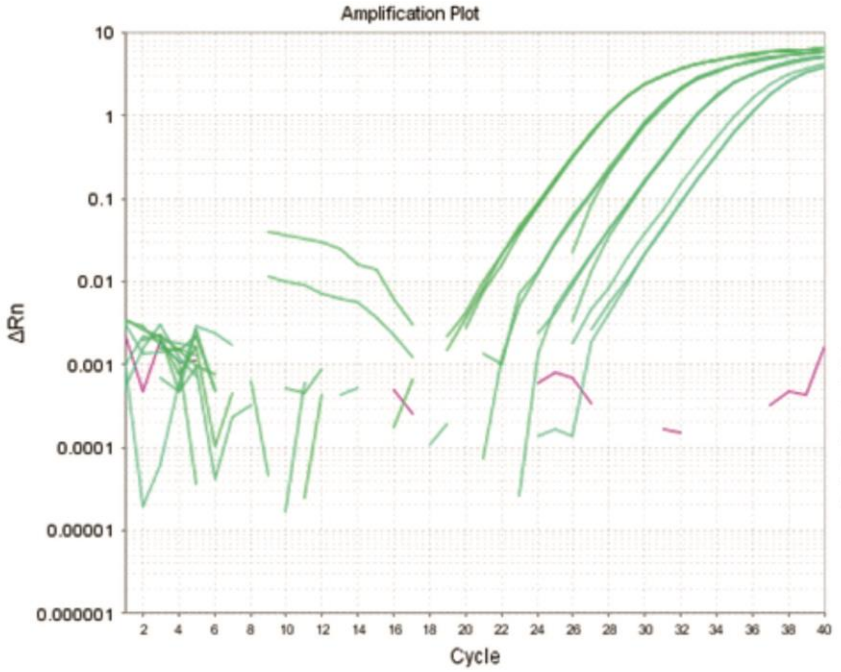

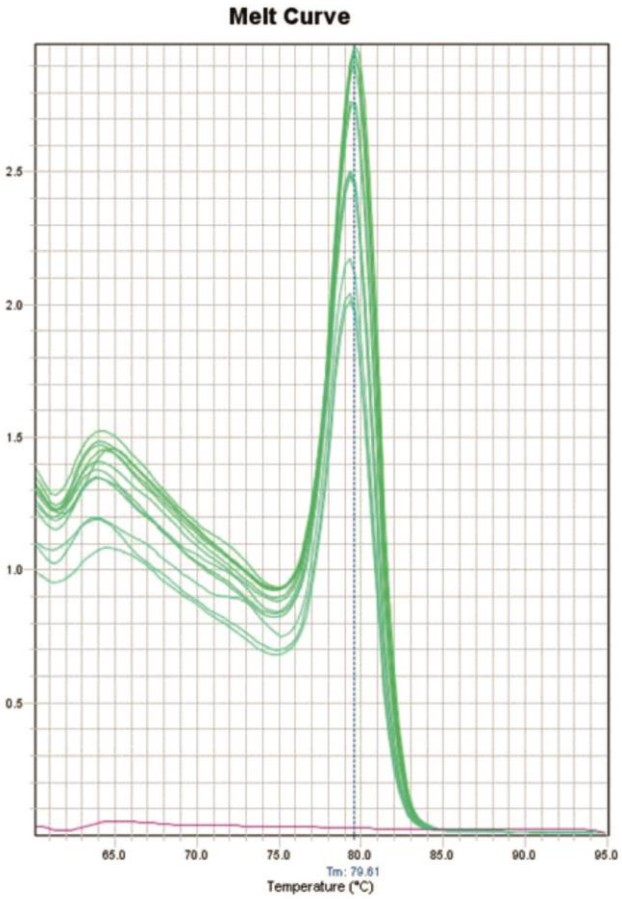

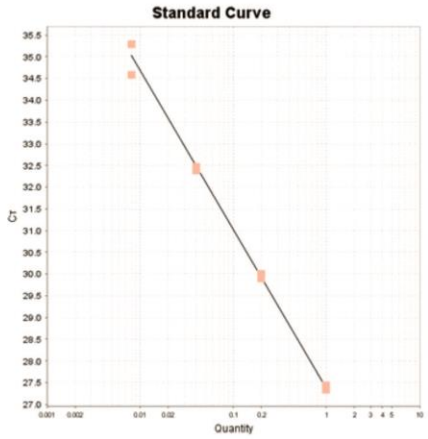

Target: IRF1 Slope: -3.647 Y-Inter: 27.372 R^2: 0.996 Eff%: 88.008

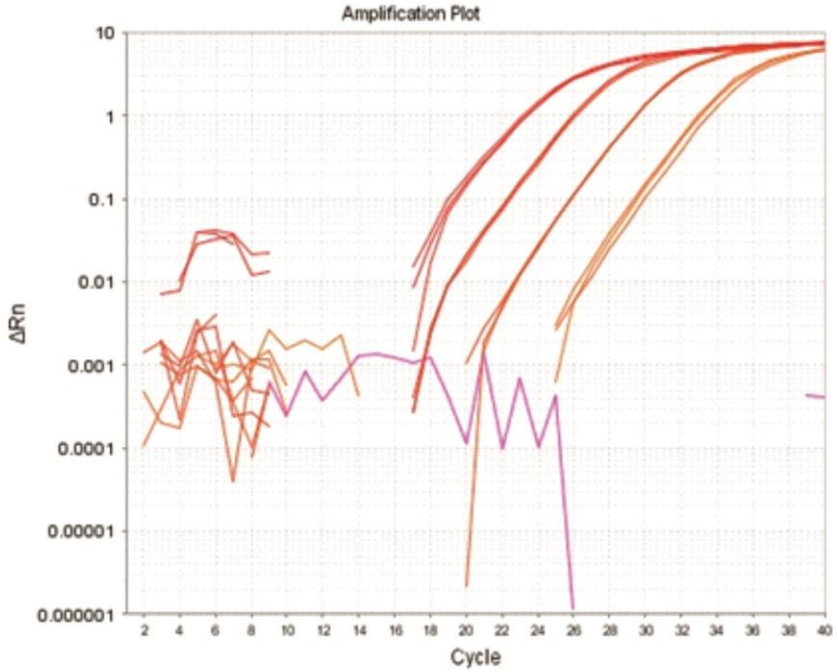

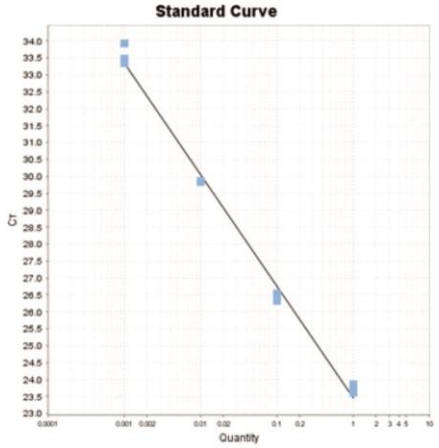

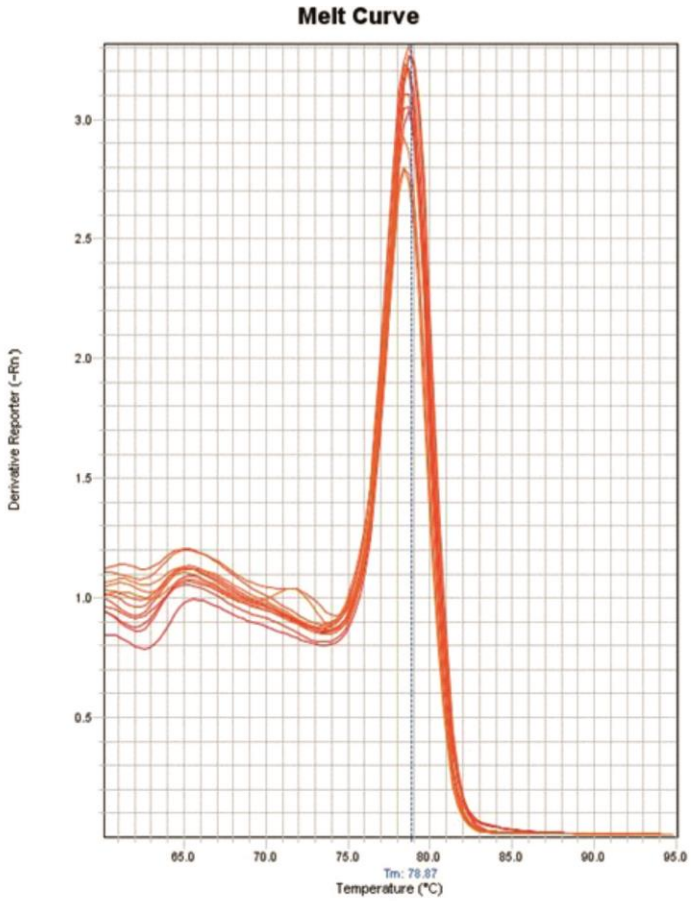

Target: CLDN7 Slope: -3.291 Y-Inter: 23.465 R^2: 0.993 Eff%: 101.307

Fig Appendix B Primer efficiency test for KLF5, GRHL3, IRF1 and CLDN7. Primer sets for RT-qPCR were tested using relative standard curve program. Samples known for expression of target primers were diluted gradually (1, 1/10, 1/100, 1/1000). Standard process was performed including melt curve cycle. Acceptable optimised primers are supposed to demonstrate a unique peak with slope of -3.333 (±10% deviation) and R square of 0.999 (±10% deviation).

Appendix C Example of analysing IHC slides using HistoQuest Software

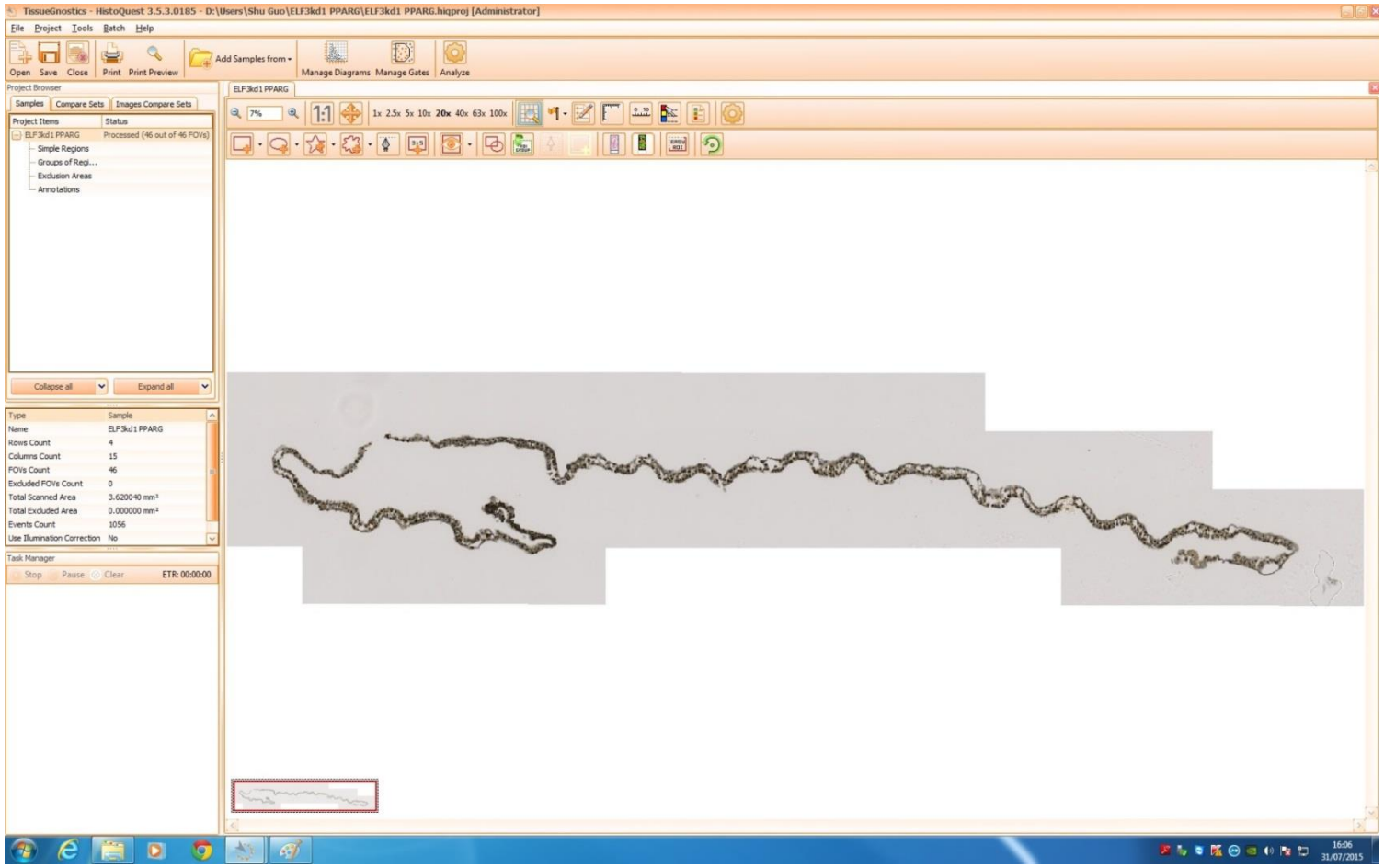

Fig Appendix C1 Analysis of IHC slides using HistoQuest. ELF3 knock down cell sheet was used as an example to show the workflow of the analysing process.

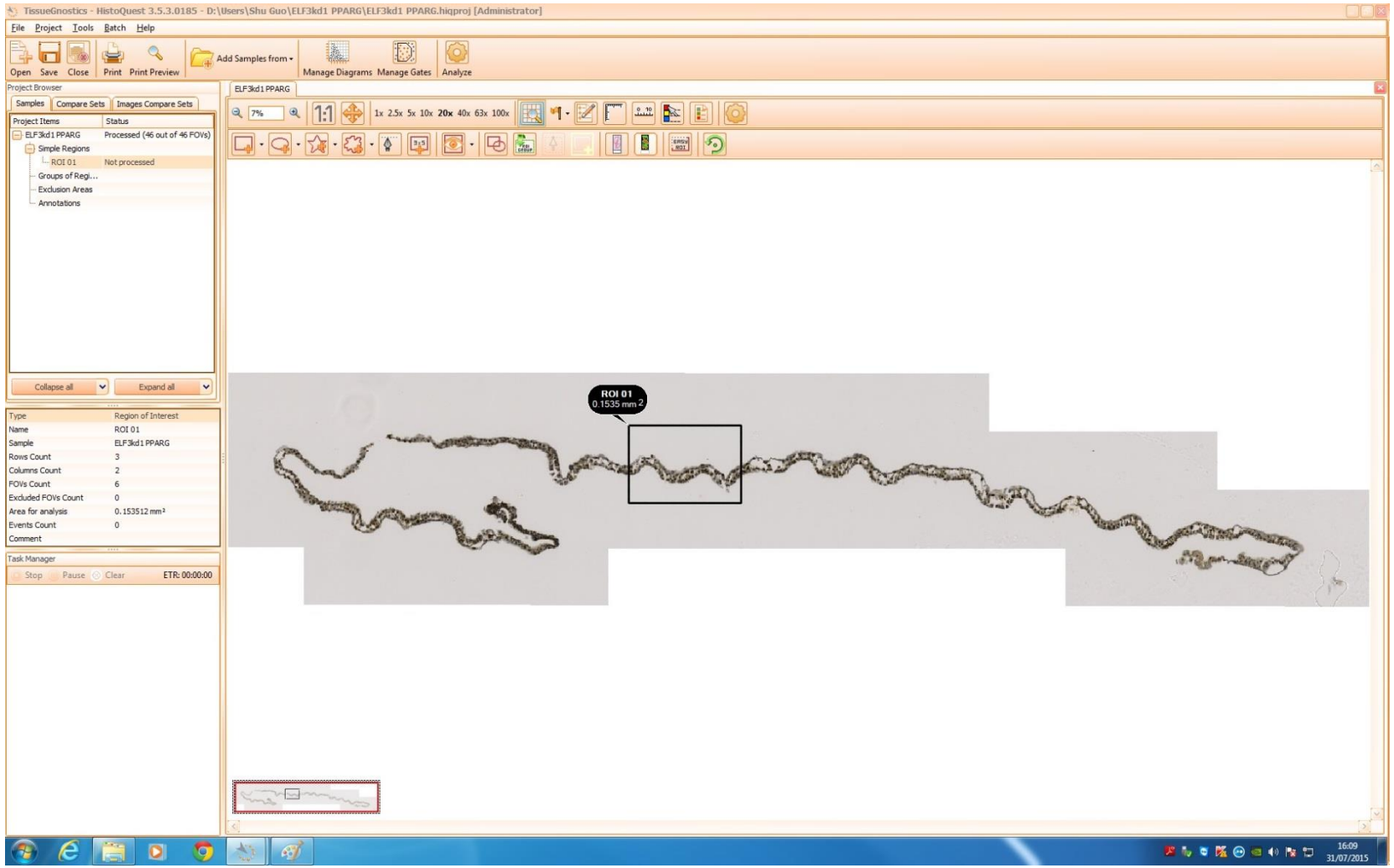

Fig Appendix C2 Creation of ROI (region of interest). ROI was created to set up parameters of analysis.

Fig Appendix C3 Magnification of ROI. ROI was magnified and indicated by a rectangular.

Fig Appendix C4 Autodetection of nuclei. Haematoxylin and DAB staining were used as markers of nuclear labelling. After defining size of nuclei, staining background and setting of the threshold, nuclei were picked up by the software (surrounded by green circles).

Fig Appendix C5 Manual correction. Manual corrections were applied if the nuclei were not selected correctly.

Fig Appendix C6 Corrected nuclei. Nuclei were labelled with green circles.

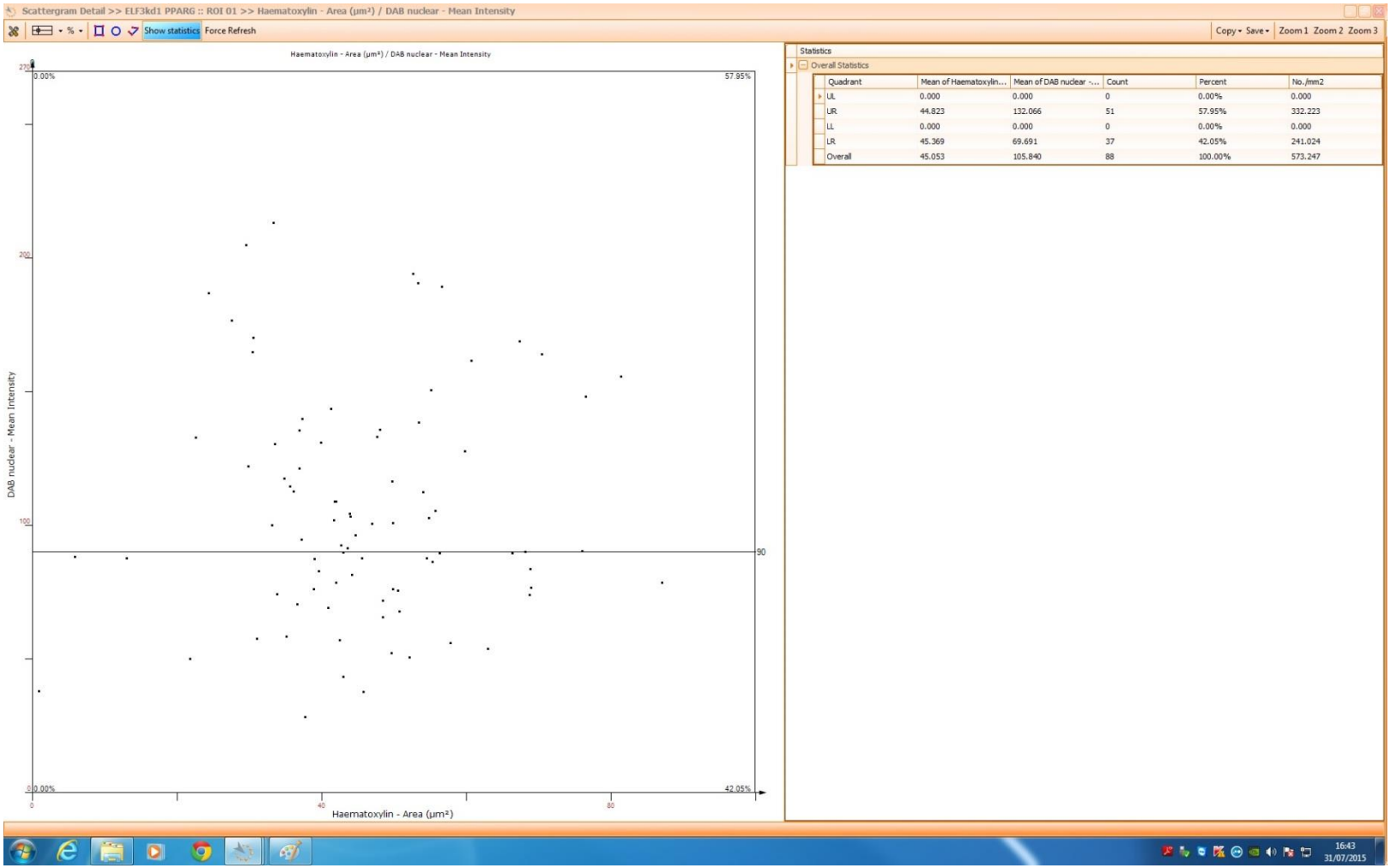

Fig Appendix C7 Backward gating and set up of cut-off value. Cut-off value was set based on the DAB staining of positive/negative cell population. Individual cells were linked with corresponding data points and can be visualized by backward gating.

Fig Appendix C8 Percentage of positive staining cells. By viewing of backward data in upper quadrant, positive PPARγ staining cells were indicated by red circles. Percentage of positive cells was shown (bottom right corner, red oval).

A

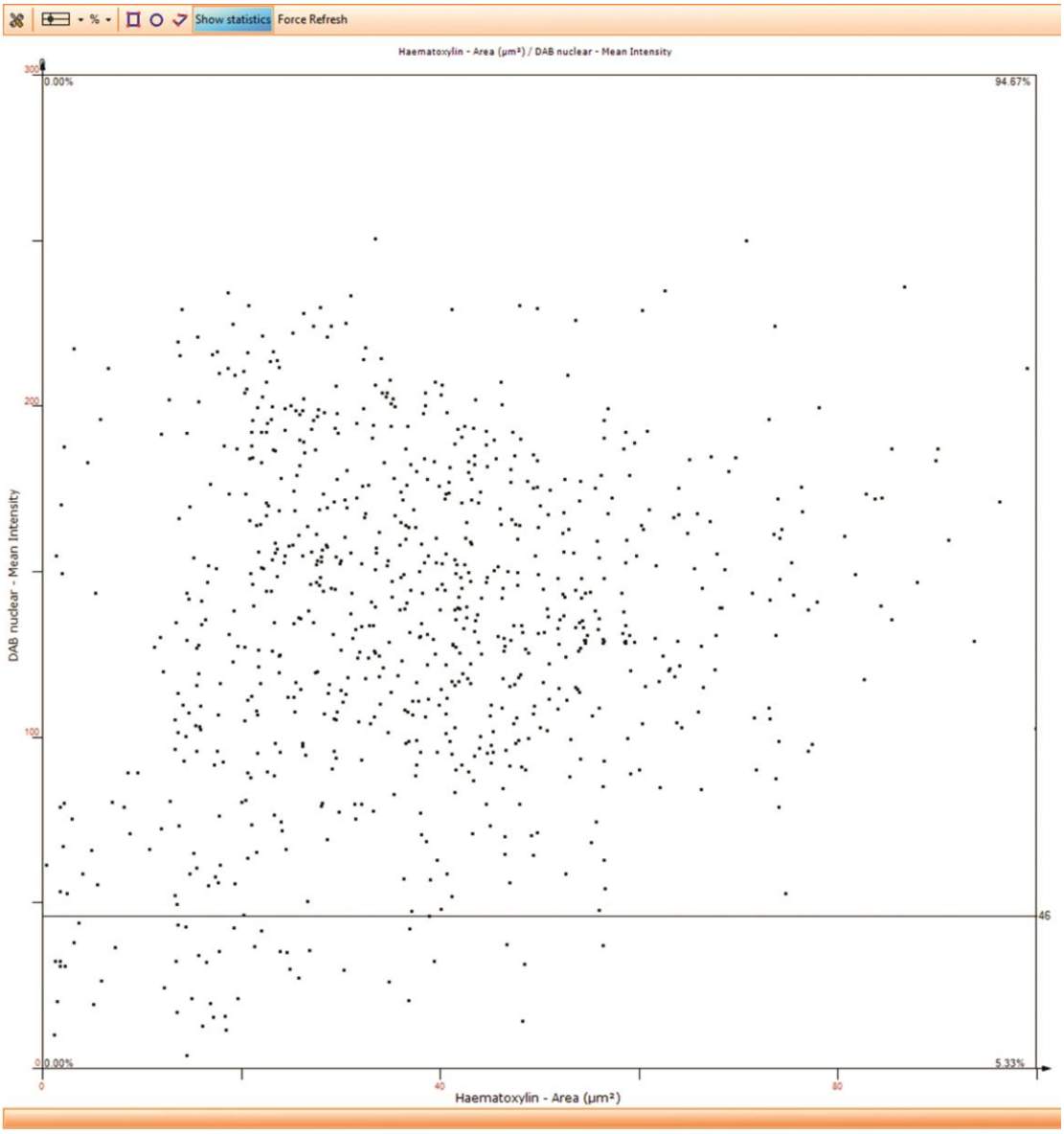

Copy Save Zoom 1 Zoom 2 Zoom 3

Statistics

Overall Statistics

Quadrant	Mean of Haematoxylin...	Mean of DAB nuclear -...	Count	Percent	No./mm2
UL	0.000	0.000	0	0.00%	0.000
UR	39.533	141.433	781	94.67%	80.876
LL	0.000	0.000	0	0.00%	0.000
LR	19.450	28.583	44	5.33%	4.556
Overall	38.462	135.415	825	100.00%	85.432

B

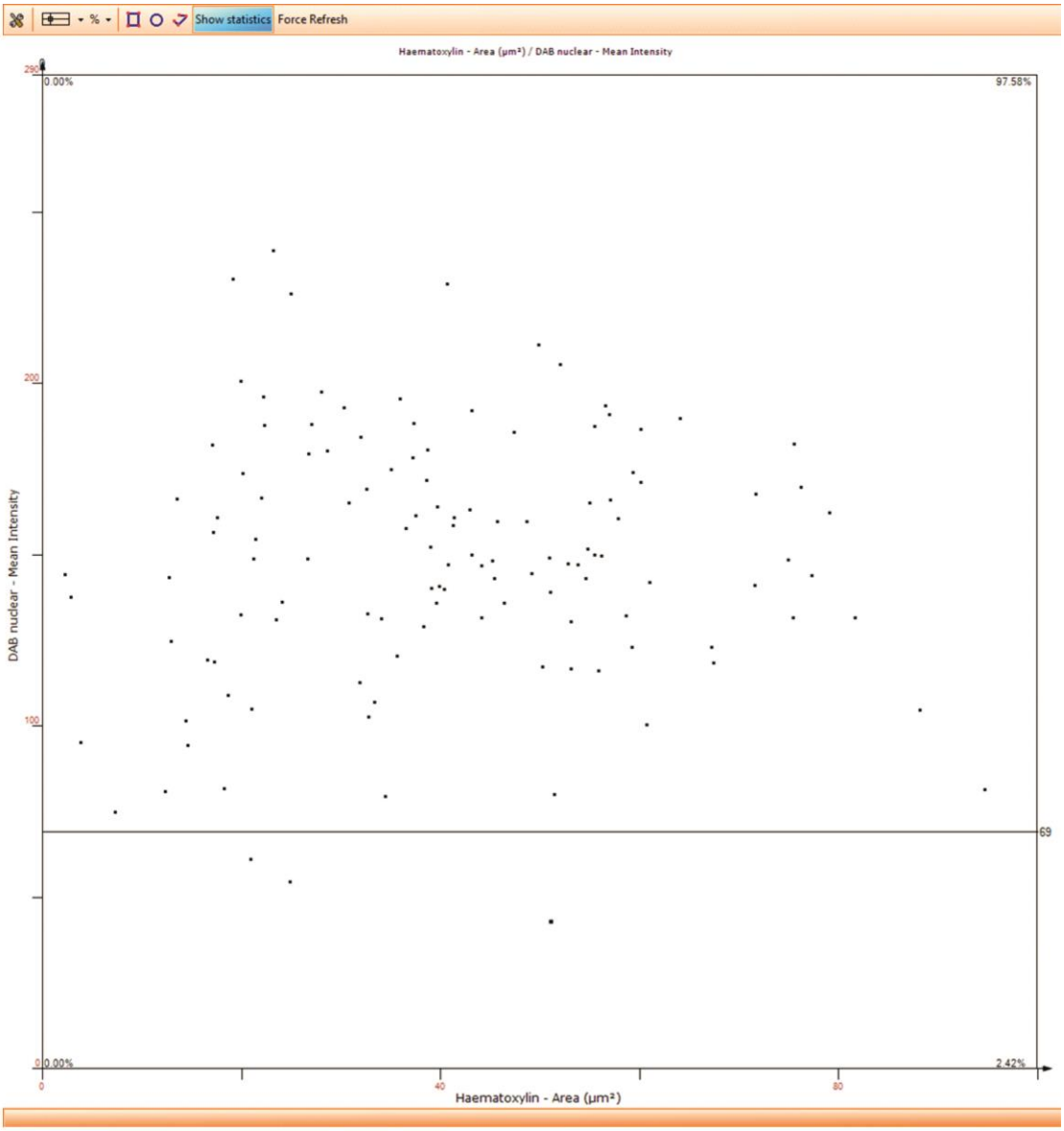

Copy Save Zoom 1 Zoom 2 Zoom 3

Statistics

Overall Statistics

Quadrant	Mean of Haematoxylin...	Mean of DAB nuclear -...	Count	Percent	No./mm2
UL	0.000	0.000	0	0.00%	0.000
UR	41.628	150.555	121	97.58%	85.386
LL	0.000	0.000	0	0.00%	0.000
LR	32.329	52.716	3	2.42%	2.117
Overall	41.403	148.188	124	100.00%	87.503

C

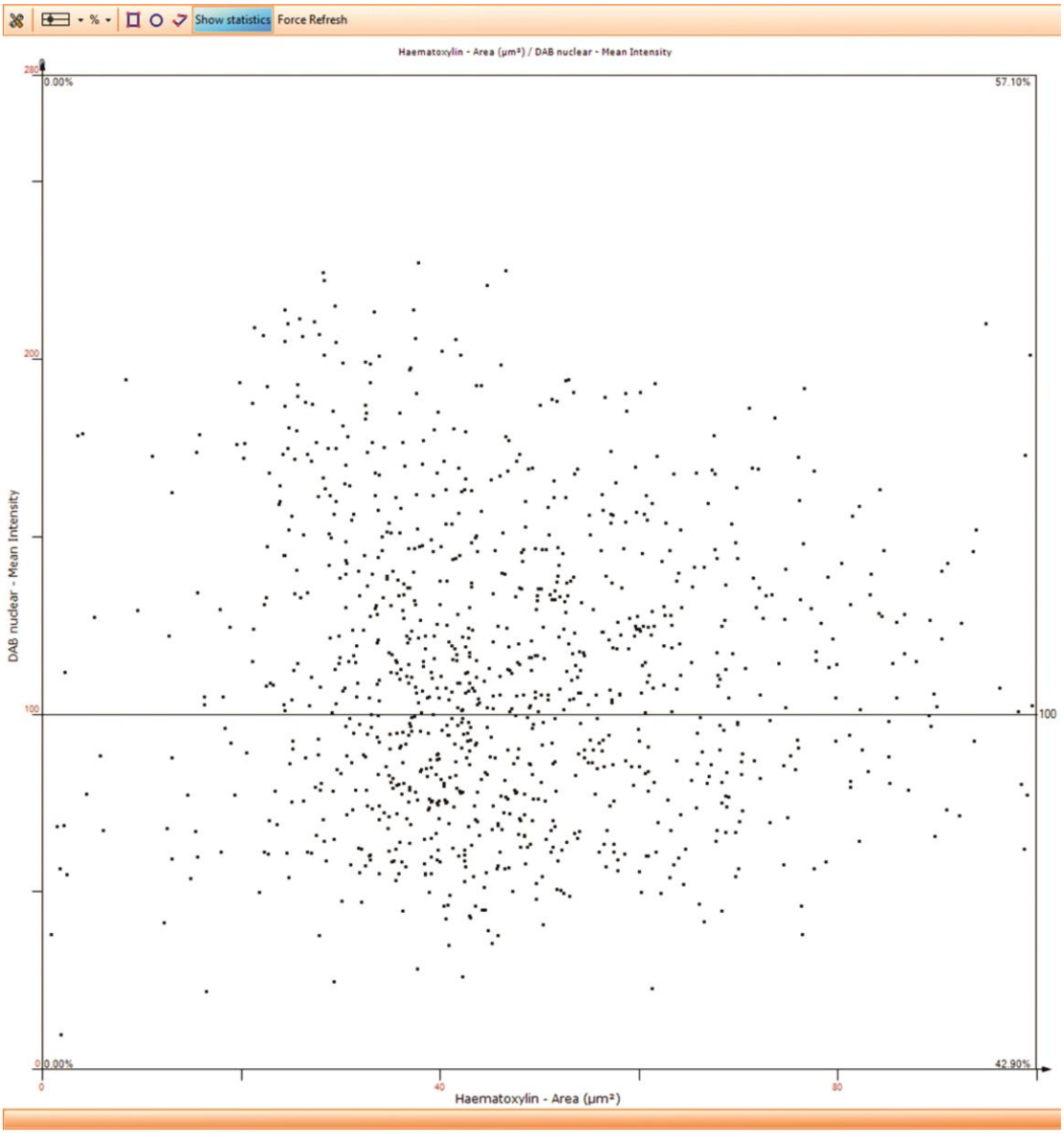

Copy Save Zoom 1 Zoom 2 Zoom 3

Statistics

Overall Statistics

Quadrant	Mean of Haematoxylin...	Mean of DAB nuclear -...	Count	Percent	No./mm2
UL	0.000	0.000	0	0.00%	0.000
UR	47.709	140.302	603	57.10%	166.573
LL	0.000	0.000	0	0.00%	0.000
LR	48.108	73.836	453	42.90%	125.137
Overall	47.880	111.789	1056	100.00%	291.709

D

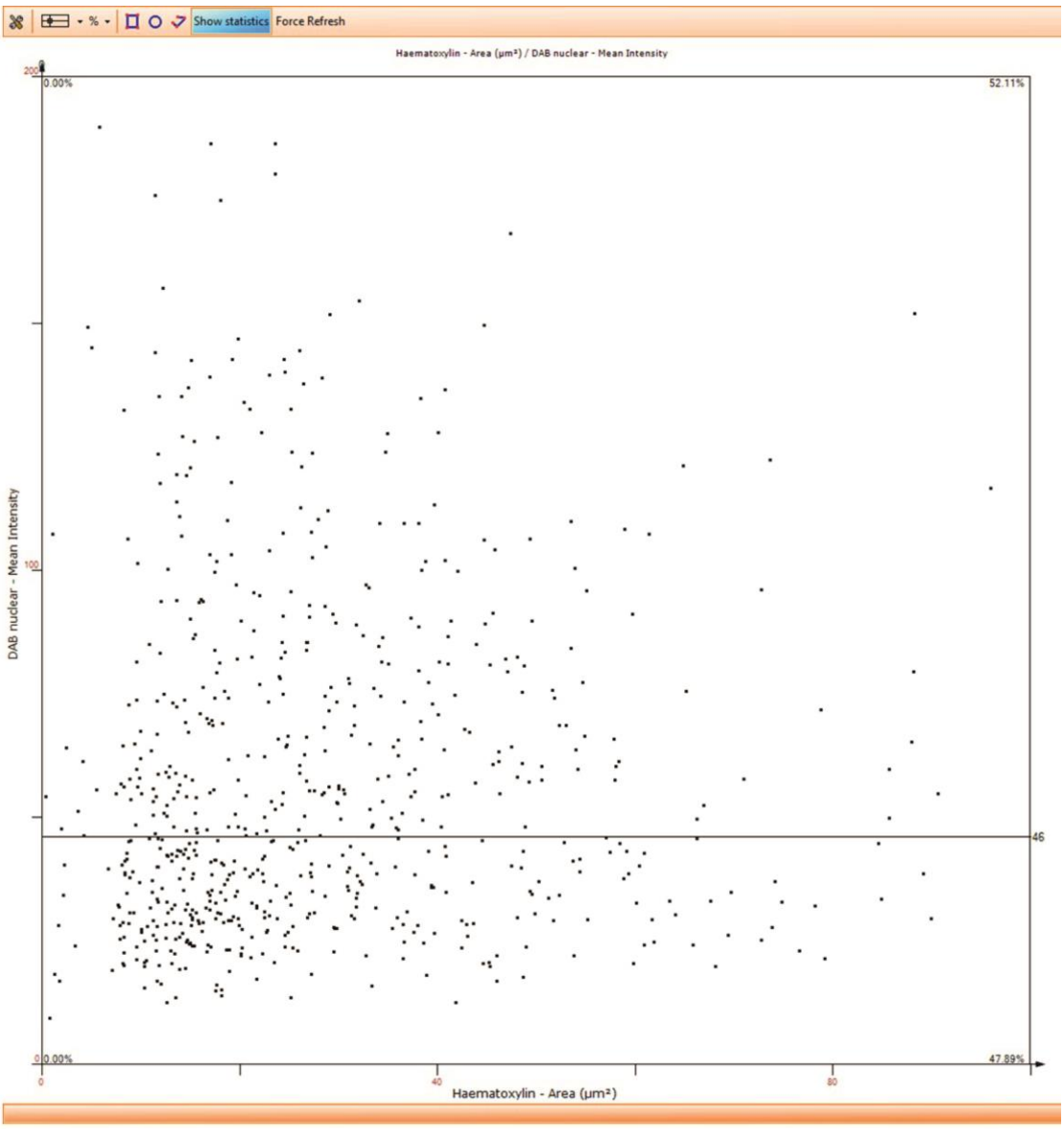

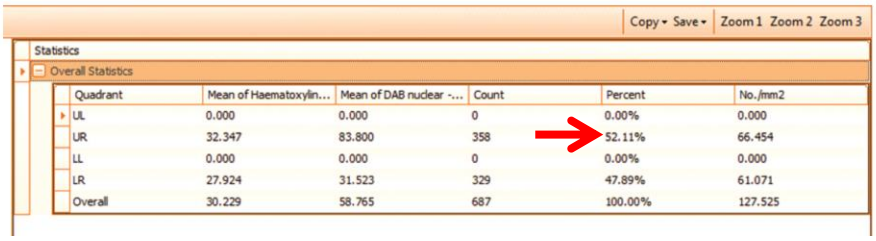

Quadrant	Mean of Haematoxylin...	Mean of DAB nuclear -...	Count	Percent	No./mm2
UL	0.000	0.000	0	0.00%	0.000
UR	32.347	83.800	358	52.11%	66.454
LL	0.000	0.000	0	0.00%	0.000
LR	27.924	31.523	329	47.89%	61.071
Overall	30.229	58.765	687	100.00%	127.525

Fig Appendix C9 Positive staining of nuclear PPARγ in control and ELF3 knock down cell sheets. Percentage of positive staining cells was demonstrated by upper quadrant cell population and noted by red arrow.A and B, scramble control; C and D, ELF3 knock down.

Appendix D Buffer recipe

- 0.1% EDTA

1 g EDTA disodium salt in 1000 mL of PBS (made from 10x DPBS (Gibco) in Elga distilled water).

- Trypsin Inhibitor (TI):

Trypsin Inhibitor- Sigma T6522 100 mg stored at 4 °C (1 mg TI inhibits 1.94 mg trypsin)

Dissolve 100 mg vial in 5 mL D-PBS, aspirate into a syringe and filter sterilise with 0.2 μm filter.

Aliquot 100 μL into Universal tubes, store at -20 °C.

One aliquot inhibits 1 mL of TV

- Trypsin in Versene (TV):

Trypsin - Sigma T4549 100 mL (10 x solution)

On arrival thaw and aliquot into 20 mL -store at -20 °C

20 mL Trypsin

4 mL 1% EDTA

176 mL HBSS (without Ca^{2+} and Mg^{2+})

Aliquot into 5 mL and store at -20 °C

- 10% (v/v) Formalin in PBSc

100 mL 37% Formalin

900 mL PBSc

PBSc 0.5 mM $MgCl_2$, 0.9 mM $CaCl_2$

998.6 mL PBS

900 L 1M $CaCl_2$

500 L 1M $MgCl_2$

- 10xTris Borate EDTA (TBE)

108 g of Tris

55 g boric acid

9.1 g EDTA

- 2x SDS Sample Buffer:

10 mL Glycerol (20% v/v)

1 g SDS (2% w/v)

6.25 mL Tris-HCl (pH 6.8)

0.42 g Sodium fluoride (NaF)

18.4 mg Sodium orthovanadate (Na3PO4)

0.446 g tetra-Sodium pyrophosphate

dH_2O up to 50 mL

Store at –20 °C in 5 mL aliquots

- Transfer Buffer (1x):

Tris 1.45 g (12 mM)

Glycine 7.2 g (96 mM)

Methanol 200 mL (20%)

dH_2O to 1 L

- Ponceau red (10X):

5 g Ponceau

10 mL glacial acetic acid

dH_2O up to 100 mL

- TBS for western blotting

Tris 1.21 g (10 mM)

NaCl 8.18 g (140 mM)

dH_2O to 1L

pH 7.4

- TBS-Tween 20 for western blotting

Tris 1.21 g 10 mM

NaCl 8.18 g 140 mM

Tween 20 0.1%

dH_2O to 1L

pH 7.4

- TBS for IF:

50 mM Tris-HCl (pH 7.6) & 150 mM NaCl

25 mL 2M Tris (pH 7.6)

50 mL 3M NaCl

10 mL 10% (w/v) NaN_3 solution

10 mL 10% (w/v) BSA in TBS

Make to 1L with dH_2O and store at 4 °C.

- Antifade mountant

0.1% (w/v) p-Phenylendiamino Dihydrochloride (Sigma) in 90% Glycerol.

Dissolve 100 mg of p-Phenylendiamino Dihydrochloride in 10 mL PBS.

Adjust to pH 8.0 with carbonate-bicarbonate buffer pH 9.6 (0.42 g $NaHCO_3$ in 10 mL H_2O, adjust pH to 9.6 with NaOH).

Add 90 mL Glycerol, mix well, store in the dark bottle at -20 °C.

- TBS for IHC

0.05 M Tris-HCl + 0.15 M NaCl pH 7.6

Stock solutions:

3 M NaCl 175.32 g/L

2 M Tris pH 7.6 242.28 g/L

To make 1 L of TBS buffer

25 mL of 2 M Tris pH 7.6

50 mL of 3 M NaCl

Make up to 1 L with dH_2O

- Citric Acid Buffer pH6.0

0.8 g Citric Acid per 350 mL of water+ several pellets of NaOH, adjust pH to 6.0

- 0.1% Calcium Chloride ($CaCl_2$) pH 7.8

Dissolve 1 g of $CaCl_2$ in 900 mL of dH_2O, pH to 7.8 with NaOH, make up to a final volume of 1 L.

- CSK buffer:
  - For 1 litre;

    Make 200 mL 50 mM PIPES (final 10 mM after dilution) and pH to 6.8 with KOH before adding any other reagents

Dilute to ~ 700 mL and add; 1 mM EGTA, 300 mM sucrose, 1 mM $MgCl_2$ (sufficient for 1 L).

Make aliquots with:

(500 mL) 0.1 M NaCl and No TX-100

(400 mL) 0.5 M NaCl and 0.1% TX-100

(100 mL) 1 M NaCl and 0.2 % TX-100

On day of experiment add ATP to 0.1 mM, 1/1000 protease inhibitors, DTT to 1 mM and PMSF to 1mM

Add PMSF immediately before harvesting /incubations as it has a lifetime in aqueous solution of < 5 min

- 1X DNaseI buffer:

10 mM Tris pH 7.5, 10 mM $MgCl_2$, 5 mM $CaCl_2$.

Appendix E List of suppliers

Abcam	332 Cambridge Science Park Milton Road Cambridge CB14 0WN
Ambion	Supplied by fisher Scientific
Applied Biosystems	Supplied by Life technology
Becton-Dickinson	The Danby BuildingEdmund Halley Road Oxford Science Park Oxford OX4 4DQ
Bioline	Bioline Reagents Limited, Unit 16 The Edge Business Centre Humber Road London NW2 6EW
BioRad	Maxted Road Hemel Hempstead Hertfordshire HP2 7DX
Calbiochem	Supplied by Millipore

Cell Signaling	New England Biolabs (UK) Ltd. 75-77 Knowl Piece Wilbury Way Hitchin, Hertfordshire SG4 0TY
Clontech	2 Avenue du President Kennedy 78100 Saint-Germain-en-Laye France
Corning	Elwy House Lakeside Business Village St. David's Park Flintshire CH5 3XD
Cymbus	Unit J Eagle Close Southampton Hampshire
Dako	Cambridge House St Thomas Place, Ely Cambridgeshire CB7 4EX
Dynex	Yeoman Gate, Yeoman Way Worthing West Sussex BN13 3QZ

Eurofins	Eurofins Genomics Anzinger Str. 7a 85560 Ebersberg Germany
Fisher Scientific	Bishop Meadow Road Loughborough LE11 5RG
GraphPad	7825 Fay Avenue, Suite 230 La Jolla, CA 92037 USA
Greiner Bio-One	Brunel Way Stroudwater Business Park Stonehouse
GSK	Harmire Road Barnard Castle, County Durham DL12 8DT
Harlan Sera-Lab	1 Westminster Way Oxford OX2 0PZ
Invitrogen	Supplied by Life technology
Li-CoR	St. John's Innovation Centre Cowley Road Cambridge

	CB4 0WS
Life Technologies	3 Fountain Drive Inchinnan Business Park Paisley PA4 9RF
Media Cybernetics	Beech House 27 Little Marlow Road Marlow Buckinghamshire SL7 1HA
Millipore	Croxley Green Business Park Watford Hertfordshire WD18 8YH
Molecular Probes	Supplied by Life technology
Novocastra	Larch House, Woodlands Business Park, Breckland, Linford Wood Milton Keynes MK14 6FG
Pierce	Supplied by Life technology
Promega	Delta House Southampton Science Park

	Southampton SO16 7NS
Qiagen	Skelton House Lloyd Street North Manchester M15 6SH
RA Lamb	Supplied by fisher Scientific
Roche	Charles Avenue Burgess Hill West Sussex RH15 9RY
Santa Cruz	10410 Finnell Street Dallas, Texas 75220 U.S.A.
Scientific Laboratory Supplies	Orchard House, The Square, Hessle East Riding of Yorkshire HU13 0AE
Serotec	Endeavour House Langford Lane Kidlington OX5 1GE

Sigma Aldrich	The Old Brickyard New Road Gillingham Dorset SP8 4XT
Source Bioscience	1 Orchard Place Nottingham Business Park Nottingham NG8 6PX
Starlab	5 Tanners Drive Blakelands Milton Keynes MK14 5BU
Syngene	Beacon House Nuffield Road Cambridge CB4 1TF
Thermo Scientific	Unit 5/Ringway Centre Edison Road Basingstoke RG21 6YH
TissueGnostics	TissueGnostics GmbH Taborstraße 10/2/8

	1020 Vienna Austria
Veolia Water Technologies	Windsor Court Kingsmead Business Park High Wycombe HP11 1JU
VWR	Hunter Boulevard Magna Park Lutterworth, Leicestershire LE17 4XN
Zeiss	509 Coldhams Lane Cambridge CB1 3JS
Zymed	Supplied by Life technology

Glossary

AUM asymmetric unit membrane

CSK Cytoskeleton

CK Cytokeratin

EGFR Epidermal growth factor receptor

EMT Epithelial–mesenchymal transition

GSK3β Glycogen synthase kinase-3β

KSFM Keratinocyte serum-free medium

MIBC muscle invasive bladder cancer

NHU Normal human urothelium

PD PD153035, EGFR inhibor

TER transepithelial electrical resistance

TJ Tight junction

TZ troglitazone, PPARγ activator

UC Urothelial cancer

UPEC Uropathogenic Escherichia coli

UPK Uroplakin

List of references

Aboushwareb, T., Zhou, G., Deng, F.M., Turner, C., Andersson, K.E., Tar, M., Zhao, W., Melman, A., D'Agostino, R., Jr., Sun, T.T., *et al.* (2009). Alterations in bladder function associated with urothelial defects in uroplakin II and IIIa knockout mice. Neurourol Urodyn *28*, 1028-1033.

Ahmad, I., Patel, R., Liu, Y., Singh, L.B., Taketo, M.M., Wu, X.R., Leung, H.Y., and Sansom, O.J. (2011). Ras mutation cooperates with beta-catenin activation to drive bladder tumourigenesis. Cell Death Dis *2*, e124.

Ainscough, J.F., Rahman, F.A., Sercombe, H., Sedo, A., Gerlach, B., and Coverley, D. (2007). C-terminal domains deliver the DNA replication factor Ciz1 to the nuclear matrix. J Cell Sci *120*, 115-124.

Akhmetshina, A., Palumbo, K., Dees, C., Bergmann, C., Venalis, P., Zerr, P., Horn, A., Kireva, T., Beyer, C., Zwerina, J., *et al.* (2012). Activation of canonical Wnt signalling is required for TGF-beta-mediated fibrosis. Nature Communications *3*, *735*-.

Andreoli, J.M., Jang, S.I., Chung, E., Coticchia, C.M., Steinert, P.M., and Markova, N.G. (1997). The expression of a novel, epithelium-specific ets transcription factor is restricted to the most differentiated layers in the epidermis. Nucleic Acids Res *25*, 4287-4295.

Aprile, M., Ambrosio, M.R., D'Esposito, V., Beguinot, F., Formisano, P., Costa, V., and Ciccodicola, A. (2014). PPARG in Human Adipogenesis: Differential Contribution of Canonical Transcripts and Dominant Negative Isoforms. PPAR research *2014*, 537865.

Bell, S.M., Zhang, L., Mendell, A., Xu, Y., Haitchi, H.M., Lessard, J.L., and Whitsett, J.A. (2011). Kruppel-like factor 5 is required for formation and differentiation of the bladder urothelium. Dev Biol *358*, 79-90.

Bianchi, M.E., and Agresti, A. (2005). HMG proteins: dynamic players in gene regulation and differentiation. Current opinion in genetics & development *15*, 496-506.

Billerey, C., Chopin, D., Aubriot-Lorton, M.H., Ricol, D., Gil Diez de Medina, S., Van Rhijn, B., Bralet, M.P., Lefrere-Belda, M.A., Lahaye, J.B., Abbou, C.C., *et al.* (2001). Frequent FGFR3 mutations in papillary non-invasive bladder (pTa) tumors. Am J Pathol *158*, 1955-1959.

Bindels, E.M., van der Kwast, T.H., Izadifar, V., Chopin, D.K., and de Boer, W.I. (2002). Functions of epidermal growth factor-like growth factors during human urothelial reepithelialization in vitro and the role of erbB2. Urol Res *30*, 240-247.

Biton, A., Bernard-Pierrot, I., Lou, Y., Krucker, C., Chapeaublanc, E., Rubio-Pérez, C., López-Bigas, N., Kamoun, A., Neuzillet, Y., Gestraud, P., *et al.* (2014). Independent Component Analysis Uncovers the Landscape of the Bladder Tumor Transcriptome and Reveals Insights into Luminal and Basal Subtypes. Cell Reports 9, 1235-1245.

Bock, M., Hinley, J., Schmitt, C., Wahlicht, T., Kramer, S., and Southgate, J. (2013). Identification of ELF3 as an early transcriptional regulator of human urothelium. Dev Biol. 386, 321-330.

Bolt, H.M. (2014). Causation of human urothelial cancer: there are challenging new data! Archives of toxicology *88*, 1769-1770.

Brembeck, F.H., Opitz, O.G., Libermann, T.A., and Rustgi, A.K. (2000). Dual function of the epithelial specific ets transcription factor, ELF3, in modulating differentiation. Oncogene *19*, 1941-1949.

Cabral, A., Fischer, D.F., Vermeij, W.P., and Backendorf, C. (2003). Distinct functional interactions of human Skn-1 isoforms with Ese-1 during keratinocyte terminal differentiation. J Biol Chem *278*, 17792-17799.

Camp, H.S., and Tafuri, S.R. (1997). Regulation of peroxisome proliferator-activated receptor gamma activity by mitogen-activated protein kinase. J Biol Chem *272*, 10811-10816.

Cancer Genome Atlas Research, N. (2014). Comprehensive molecular characterization of urothelial bladder carcinoma. Nature *507*, 315-322.

Chamorro, C.I., Zeiai, S., Reinfeldt Engberg, G., Brodin, D., Nordenskjold, A., and Fossum, M. (2015). A study on proliferation and gene expression in normal human urothelial cells in culture. Tissue engineering Part A *21*, 510-517.

Chang, J., Lee, C., Hahm, K.B., Yi, Y., Choi, S.G., and Kim, S.J. (2000). Over-expression of ERT(ESX/ESE-1/ELF3), an ets-related transcription factor, induces endogenous TGF-beta type II receptor expression and restores the TGF-beta signaling pathway in Hs578t human breast cancer cells. Oncogene *19*, 151-154.

Chang, L., Shi, R., Yang, T., Li, F., Li, G., Guo, Y., Lang, B., Yang, W., Zhuang, Q., and Xu, H. (2013). Restoration of LRIG1 suppresses bladder cancer cell growth by directly targeting EGFR activity. J Exp Clin Cancer Res *32*, 101.

Chen, L., Necela, B.M., Su, W., Yanagisawa, M., Anastasiadis, P.Z., Fields, A.P., and Thompson, E.A. (2006a). Peroxisome proliferator-activated receptor gamma promotes epithelial to mesenchymal transformation by Rho GTPase-dependent activation of ERK1/2. J Biol Chem *281*, 24575-24587.

Chen, Y., Jimenez, A.R., and Medh, J.D. (2006b). Identification and regulation of novel PPAR-gamma splice variants in human THP-1 macrophages. Biochim Biophys Acta *1759*, 32-43.

Chen, Y., Luo, Q., Xiong, Z., Liang, W., Chen, L., and Xiong, Z. (2012). Telmisartan counteracts TGF-beta1 induced epithelial-to-mesenchymal transition via PPAR-gamma in human proximal tubule epithelial cells. International journal of clinical and experimental pathology *5*, 522-529.

Cheng, J., Huang, H., Zhang, Z.T., Shapiro, E., Pellicer, A., Sun, T.T., and Wu, X.R. (2002). Overexpression of epidermal growth factor receptor in urothelium elicits urothelial hyperplasia and promotes bladder tumor growth. Cancer Res *62*, 4157-4163.

Choi, W., Porten, S., Kim, S., Willis, D., Plimack, E.R., Hoffman-Censits, J., Roth, B., Cheng, T., Tran, M., Lee, I.L., *et al.* (2014). Identification of distinct basal and luminal subtypes of muscle-invasive bladder cancer with different sensitivities to frontline chemotherapy. Cancer Cell *25*, 152-165.

Chopra, B., Georgopoulos, N.T., Nicholl, A., Hinley, J., Oleksiewicz, M.B., and Southgate, J. (2009). Structurally diverse peroxisome proliferator-activated receptor agonists induce apoptosis in human uro-epithelial cells by a receptor-independent mechanism involving store-operated calcium channels. Cell Prolif *42*, 688-700.

Clevers, H., and Nusse, R. (2012). Wnt/beta-catenin signaling and disease. Cell *149*, 1192-1205.

Coghlan, M.P., Culbert, A.A., Cross, D.A., Corcoran, S.L., Yates, J.W., Pearce, N.J., Rausch, O.L., Murphy, G.J., Carter, P.S., Roxbee Cox, L., *et al.* (2000). Selective small molecule inhibitors of glycogen synthase kinase-3 modulate glycogen metabolism and gene transcription. Chem Biol *7*, 793-803.

Colopy, S.A., Bjorling, D.E., Mulligan, W.A., and Bushman, W. (2014). A population of progenitor cells in the basal and intermediate layers of the murine bladder urothelium contributes to urothelial development and regeneration. Dev Dyn *243*, 988-998.

Conconi, D., Panzeri, E., Redaelli, S., Bovo, G., Volante, M., Vigano, P., Strada, G., Dalpra, L., and Bentivegna, A. (2012). DNA copy number alterations and PPARG amplification in a patient with multifocal bladder urothelial carcinoma. BMC research notes *5*, 607.

Coppe, J.-P., Amend, C., Semeiks, J., Baehner, F.L., Bayani, N., Campisi, J., Benz, C.C., Gray, J.W., and Neve, R.M. (2010). ERBB receptor regulation of ESX/ELF3 promotes invasion in breast epithelial cells. Open Cancer Journal *3*, 89-100.

Cross, W.R., Eardley, I., Leese, H.J., and Southgate, J. (2005). A biomimetic tissue from cultured normal human urothelial cells: analysis of physiological function. Am J Physiol Renal Physiol *289*, F459-468.

Daher, A., de Boer, W.I., El-Marjou, A., van der Kwast, T., Abbou, C.C., Thiery, J.P., Radvanyi, F., and Chopin, D.K. (2003). Epidermal growth factor receptor regulates normal urothelial regeneration. Lab Invest *83*, 1333-1341.

Damrauer, J.S., Hoadley, K.A., Chism, D.D., Fan, C., Tiganelli, C.J., Wobker, S.E., Yeh, J.J., Milowsky, M.I., Iyer, G., Parker, J.S., *et al.* (2014). Intrinsic subtypes of high-grade bladder cancer reflect the hallmarks of breast cancer biology. Proc Natl Acad Sci U S A *111*, 3110-3115.

de Boer, W.I., Schuller, A.G., Vermey, M., and van der Kwast, T.H. (1994). Expression of growth factors and receptors during specific phases in regenerating urothelium after acute injury in vivo. Am J Pathol *145*, 1199-1207.

DeGraff, D.J., Clark, P.E., Cates, J.M., Yamashita, H., Robinson, V.L., Yu, X., Smolkin, M.E., Chang, S.S., Cookson, M.S., Herrick, M.K., *et al.* (2012). Loss of the urothelial differentiation marker FOXA1 is associated with high grade, late stage bladder cancer and increased tumor proliferation. PLoS One *7*, e36669.

Diezko, R., and Suske, G. (2013). Ligand binding reduces SUMOylation of the peroxisome proliferator-activated receptor gamma (PPARgamma) activation function 1 (AF1) domain. PLoS One *8*, e66947.

Elbrecht, A., Chen, Y., Cullinan, C.A., Hayes, N., Leibowitz, M., Moller, D.E., and Berger, J. (1996). Molecular cloning, expression and characterization of human peroxisome proliferator activated receptors gamma 1 and gamma 2. Biochem Biophys Res Commun *224*, 431-437.

Erman, A., Veranic, P., Psenicnik, M., and Jezernik, K. (2006). Superficial cell differentiation during embryonic and postnatal development of mouse urothelium. Tissue Cell *38*, 293-301.

Fajas, L., Auboeuf, D., Raspe, E., Schoonjans, K., Lefebvre, A.M., Saladin, R., Najib, J., Laville, M., Fruchart, J.C., Deeb, S., *et al.* (1997). The organization, promoter analysis, and expression of the human PPARgamma gene. J Biol Chem *272*, 18779-18789.

Fajas, L., Fruchart, J.C., and Auwerx, J. (1998). PPARgamma3 mRNA: a distinct PPARgamma mRNA subtype transcribed from an independent promoter. FEBS Lett *438*, 55-60.

Fan, Y., Song, X., Du, H., Luo, C., Wang, X., Yang, X., Wang, Y., and Wu, X. (2014). Down-regulation of miR-29c in human bladder cancer and the inhibition of proliferation in T24 cell via PI3K-AKT pathway. Medical oncology *31*, 65.

Ferlay, J., Soerjomataram, I., Dikshit, R., Eser, S., Mathers, C., Rebelo, M., Parkin, D.M., Forman, D., and Bray, F. (2015). Cancer incidence and mortality worldwide: Sources, methods and major patterns in GLOBOCAN 2012. International Journal of Cancer *136*, E359-E386.

Ferreccio, C., Yuan, Y., Calle, J., Benitez, H., Parra, R.L., Acevedo, J., Smith, A.H., Liaw, J., and Steinmaus, C. (2013). Arsenic, tobacco smoke, and occupation: associations of multiple agents with lung and bladder cancer. Epidemiology *24*, 898-905.

Fleming, J.M., Shabir, S., Varley, C.L., Kirkwood, L.A., White, A., Holder, J., Trejdosiewicz, L.K., and Southgate, J. (2012). Differentiation-associated reprogramming of the transforming growth factor beta receptor pathway establishes the circuitry for epithelial autocrine/paracrine repair. PLoS One *7*, e51404.

Flentjar, N., Chu, P.Y., Ng, A.Y., Johnstone, C.N., Heath, J.K., Ernst, M., Hertzog, P.J., and Pritchard, M.A. (2007). TGF-betaRII rescues development of small intestinal epithelial cells in Elf3-deficient mice. Gastroenterology *132*, 1410-1419.

Fogh, J., Fogh, J.M., and Orfeo, T. (1977). One hundred and twenty-seven cultured human tumor cell lines producing tumors in nude mice. J Natl Cancer Inst *59*, 221-226.

Foulds, C.E., Nelson, M.L., Blaszczak, A.G., and Graves, B.J. (2004). Ras/mitogen-activated protein kinase signaling activates Ets-1 and Ets-2 by CBP/p300 recruitment. Mol Cell Biol *24*, 10954-10964.

Fujita, H., Hamazaki, Y., Noda, Y., Oshima, M., and Minato, N. (2012). Claudin-4 Deficiency Results in Urothelial Hyperplasia and Lethal Hydronephrosis. Plos One *7*, *e52272*.

Gan, Y., Shi, C., Inge, L., Hibner, M., Balducci, J., and Huang, Y. (2010). Differential roles of ERK and Akt pathways in regulation of EGFR-mediated signaling and motility in prostate cancer cells. Oncogene *29*, 4947-4958.

Georgopoulos, N.T., Kirkwood, L.A., and Southgate, J. (2014). A novel bidirectional positive-feedback loop between Wnt-beta-catenin and EGFR-ERK plays a role in context-specific modulation of epithelial tissue regeneration. J Cell Sci *127*, 2967-2982.

Georgopoulos, N.T., Kirkwood, L.A., Walker, D.C., and Southgate, J. (2010). Differential regulation of growth-promoting signalling pathways by E-cadherin. PLoS One *5*, e13621.

Goebell, P.J., and Knowles, M.A. (2010). Bladder cancer or bladder cancers? Genetically distinct malignant conditions of the urothelium. Urol Oncol *28*, 409-428.

Greene, M.E., Blumberg, B., McBride, O.W., Yi, H.F., Kronquist, K., Kwan, K., Hsieh, L., Greene, G., and Nimer, S.D. (1995). Isolation of the human peroxisome proliferator activated receptor gamma cDNA: expression in hematopoietic cells and chromosomal mapping. Gene expression *4*, 281-299.

Grossman, H.B., Wedemeyer, G., and Stein, J. (1988). Autologous Antibodies to Human Bladder-Cancer. Cancer Immunol Immun *26*, 269-272.

Gui, Y.T., Guo, G.W., Huang, Y., Hu, X.D., Tang, A.F., Gao, S.J., Wu, R.H., Chen, C., Li, X.X., Zhou, L., *et al.* (2011). Frequent mutations of chromatin remodeling genes in transitional cell carcinoma of the bladder. Nature Genetics *43*, 875-U884.

Guturi, K.K., Mandal, T., Chatterjee, A., Sarkar, M., Bhattacharya, S., Chatterjee, U., and Ghosh, M.K. (2012). Mechanism of beta-catenin-mediated transcriptional regulation of epidermal growth factor receptor expression in glycogen synthase kinase 3 beta-inactivated prostate cancer cells. J Biol Chem *287*, 18287-18296.

Harnden, P., Allam, A., Joyce, A.D., Patel, A., Selby, P., and Southgate, J. (1995). Cytokeratin 20 expression by non-invasive transitional cell carcinomas: potential for distinguishing recurrent from non-recurrent disease. Histopathology *27*, 169-174.

Harnden, P., and Southgate, J. (1997). Cytokeratin 14 as a marker of squamous differentiation in transitional cell carcinomas. Journal of Clinical Pathology *50*, 1032-1033.

Hauser, S., Adelmant, G., Sarraf, P., Wright, H.M., Mueller, E., and Spiegelman, B.M. (2000). Degradation of the peroxisome proliferator-activated receptor gamma is linked to ligand-dependent activation. Journal of Biological Chemistry *275*, 18527-18533.

Hedvat, M., Jain, A., Carson, D.A., Leoni, L.M., Huang, G., Holden, S., Lu, D., Corr, M., Fox, W., and Agus, D.B. (2004). Inhibition of HER-kinase activation prevents ERK-mediated degradation of PPARgamma. Cancer Cell *5*, 565-574.

Hicks, R.M. (1965). The fine structure of the transitional epithelium of rat ureter. J Cell Biol *26*, 25-48.

Hollestelle, A., Peeters, J.K., Smid, M., Timmermans, M., Verhoog, L.C., Westenend, P.J., Heine, A.A., Chan, A., Sieuwerts, A.M., and Wiemer, E.A. (2013). Loss of E-cadherin is not a necessity for epithelial to mesenchymal transition in human breast cancer. Breast cancer research and treatment *138*, 47-57.

Hou, J., Gomes, A.S., Paul, D.L., and Goodenough, D.A. (2006). Study of claudin function by RNA interference. J Biol Chem *281*, 36117-36123.

Hou, J., Wilder, P.J., Bernadt, C.T., Boer, B., Neve, R.M., and Rizzino, A. (2004). Transcriptional regulation of the murine Elf3 gene in embryonal carcinoma cells and their differentiated counterparts: requirement for a novel upstream regulatory region. Gene *340*, 123-131.

Hu, P., Deng, F.M., Liang, F.X., Hu, C.M., Auerbach, A.B., Shapiro, E., Wu, X.R., Kachar, B., and Sun, T.T. (2000). Ablation of uroplakin III gene results in small urothelial plaques, urothelial leakage, and vesicoureteral reflux. J Cell Biol *151*, 961-972.

Hu, P., Meyers, S., Liang, F.X., Deng, F.M., Kachar, B., Zeidel, M.L., and Sun, T.T. (2002). Role of membrane proteins in permeability barrier function: uroplakin ablation elevates urothelial permeability. Am J Physiol Renal Physiol *283*, F1200-1207.

Ichikawa-Tomikawa, N., Sugimoto, K., Satohisa, S., Nishiura, K., and Chiba, H. (2011). Possible involvement of tight junctions, extracellular matrix and nuclear receptors in epithelial differentiation. J Biomed Biotechnol *2011*, 253048.

Issemann, I., and Green, S. (1990). Activation of a member of the steroid hormone receptor superfamily by peroxisome proliferators. Nature *347*, 645-650.

Janani, C., and Ranjitha Kumari, B.D. (2015). PPAR gamma gene - A review. Diabetes & metabolic syndrome *9*, 46-50.

Jansson, E.A., Are, A., Greicius, G., Kuo, I.C., Kelly, D., Arulampalam, V., and Pettersson, S. (2005). The Wnt/beta-catenin signaling pathway targets

PPAR gamma activity in colon cancer cells. P Natl Acad Sci USA *102*, 1460-1465.

Jenkins, D., and Woolf, A.S. (2007). Uroplakins: new molecular players in the biology of urinary tract malformations. Kidney Int *71*, 195-200.

Jia, A.Y., Castillo-Martin, M., Domingo-Domenech, J., Bonal, D.M., Sanchez-Carbayo, M., Silva, J.M., and Cordon-Cardo, C. (2013). A common MicroRNA signature consisting of miR-133a, miR-139-3p, and miR-142-3p clusters bladder carcinoma in situ with normal umbrella cells. Am J Pathol *182*, 1171-1179.

Jost, S.P. (1986). Renewal of normal urothelium in adult mice. Virchows Arch B Cell Pathol Incl Mol Pathol *51*, 65-70.

Jost, S.P. (1989). Cell cycle of normal bladder urothelium in developing and adult mice. Virchows Arch B Cell Pathol Incl Mol Pathol *57*, 27-36.

Jost, S.P., Gosling, J.A., and Dixon, J.S. (1989). The morphology of normal human bladder urothelium. J Anat *167*, 103-115.

Jost, S.P., and Potten, C.S. (1986). Urothelial proliferation in growing mice. Cell and tissue kinetics *19*, 155-160.

Kawakami, S., Arai, G., Hayashi, T., Fujii, Y., Xia, G.B., Kageyama, Y., and Kihara, K. (2002). PPAR gamma ligands suppress proliferation of human urothelial basal cells in vitro. Journal of Cellular Physiology *191*, 310-319.

Kersten, S., Desvergne, B., and Wahli, W. (2000). Roles of PPARs in health and disease. Nature *405*, 421-424.

Knowles, M.A., and Hurst, C.D. (2015). Molecular biology of bladder cancer: new insights into pathogenesis and clinical diversity. Nature Reviews Cancer *15*, 25-41.

Kohno, Y., Okamoto, T., Ishibe, T., Nagayama, S., Shima, Y., Nishijo, K., Shibata, K.R., Fukiage, K., Otsuka, S., Uejima, D., *et al.* (2006). Expression of claudin7 is tightly associated with epithelial structures in synovial sarcomas and regulated by an Ets family transcription factor, ELF3. J Biol Chem *281*, 38941-38950.

Kong, X.T., Deng, F.M., Hu, P., Liang, F.X., Zhou, G., Auerbach, A.B., Genieser, N., Nelson, P.K., Robbins, E.S., Shapiro, E., *et al.* (2004). Roles of uroplakins in plaque formation, umbrella cell enlargement, and urinary tract diseases. J Cell Biol *167*, 1195-1204.

Kopp, J.L., Wilder, P.J., Desler, M., Kim, J.H., Hou, J., Nowling, T., and Rizzino, A. (2004). Unique and selective effects of five Ets family members, Elf3, Ets1, Ets2, PEA3, and PU.1, on the promoter of the type II transforming growth factor-beta receptor gene. J Biol Chem *279*, 19407-19420.

Kopp, J.L., Wilder, P.J., Desler, M., Kinarsky, L., and Rizzino, A. (2007). Different domains of the transcription factor ELF3 are required in a promoter-specific manner and multiple domains control its binding to DNA. J Biol Chem *282*, 3027-3041.

Kulkarni, A.A., Thatcher, T.H., Olsen, K.C., Maggirwar, S.B., Phipps, R.P., and Sime, P.J. (2011). PPAR-gamma ligands repress TGFbeta-induced myofibroblast differentiation by targeting the PI3K/Akt pathway: implications for therapy of fibrosis. PLoS One *6*, e15909.

Kwon, M.C., Koo, B.K., Kim, Y.Y., Lee, S.H., Kim, N.S., Kim, J.H., and Kong, Y.Y. (2009). Essential role of CR6-interacting factor 1 (Crif1) in E74-like factor 3 (ELF3)-mediated intestinal development. J Biol Chem *284*, 33634-33641.

Lee, Y.H., Kim, S.H., Lee, Y.J., Kang, E.S., Lee, B.W., Cha, B.S., Kim, J.W., Song, D.H., and Lee, H.C. (2013). Transcription factor Snail is a novel regulator

of adipocyte differentiation via inhibiting the expression of peroxisome proliferator-activated receptor gamma. Cellular and Molecular Life Sciences *70*, 3959-3971.

Lewis, S.A. (2000). Everything you wanted to know about the bladder epithelium but were afraid to ask. Am J Physiol Renal Physiol *278*, F867-874.

Li, X., Yang, X., Xu, Y., Jiang, X., Li, X., Nan, F., and Tang, H. (2009). Troglitazone inhibits cell proliferation by attenuation of epidermal growth factor receptor signaling independent of peroxisome proliferator-activated receptor gamma. Cell research *19*, 720-732.

Liebert, M., Washington, R., Wedemeyer, G., Carey, T.E., and Grossman, H.B. (1994). Loss of co-localization of alpha 6 beta 4 integrin and collagen VII in bladder cancer. Am J Pathol *144*, 787-795.

Liebert, M., Wedemeyer, G.A., Stein, J.A., Washington, R.W., Jr., Flint, A., Ren, L.Q., and Grossman, H.B. (1989). Identification by monoclonal antibodies of an antigen shed by human bladder cancer cells. Cancer Res *49*, 6720-6726.

Lin, J.H., Zhao, H.P., and Sun, T.T. (1995). A Tissue-Specific Promoter That Can Drive a Foreign Gene to Express in the Suprabasal Urothelial Cells of Transgenic Mice. P Natl Acad Sci USA *92*, 679-683.

Liu, J., Wang, H., Zuo, Y., and Farmer, S.R. (2006). Functional interaction between peroxisome proliferator-activated receptor gamma and beta-catenin. Mol Cell Biol *26*, 5827-5837.

Liu, J.J., and Farmer, S.R. (2004). Regulating the balance between peroxisome proliferator-activated receptor gamma and beta-catenin signaling during adipogenesis - A glycogen synthase kinase 3 beta phosphorylation-

defective mutant of beta-catenin inhibits expression of a subset of adipogenic genes. Journal of Biological Chemistry *279*, 45020-45027.

Liu, Y., Weng, J., Huang, S., Shen, Y., Sheng, X., Han, Y., Xu, M., and Weng, Q. (2014). Immunoreactivities of PPARgamma2, leptin and leptin receptor in oviduct of Chinese brown frog during breeding period and pre-hibernation. European journal of histochemistry : EJH *58*, 2422.

Lobban, E.D., Smith, B.A., Hall, G.D., Harnden, P., Roberts, P., Selby, P.J., Trejdosiewicz, L.K., and Southgate, J. (1998). Uroplakin gene expression by normal and neoplastic human urothelium. Am J Pathol *153*, 1957-1967.

Lu, X., Law, B.K., Chytil, A.M., Brown, K.A., Aakre, M.E., and Moses, H.L. (2004). Activation of the Erk pathway is required for TGF-beta 1-induced EMT in vitro. Neoplasia *6*, 603-610.

MacAulay, K., Hajduch, E., Blair, A.S., Coghlan, M.P., Smith, S.A., and Hundal, H.S. (2003). Use of lithium and SB-415286 to explore the role of glycogen synthase kinase-3 in the regulation of glucose transport and glycogen synthase. Eur J Biochem *270*, 3829-3838.

MacLaine, N.J., Wood, M.D., Holder, J.C., Rees, R.W., and Southgate, J. (2008). Sensitivity of normal, paramalignant, and malignant human urothelial cells to inhibitors of the epidermal growth factor receptor signaling pathway. Molecular cancer research : MCR *6*, 53-63.

Manetsch, M., Che, W., Seidel, P., Chen, Y., and Ammit, A.J. (2012). MKP-1: a negative feedback effector that represses MAPK-mediated pro-inflammatory signaling pathways and cytokine secretion in human airway smooth muscle cells. Cell Signal *24*, 907-913.

Mangelsdorf, D.J., Thummel, C., Beato, M., Herrlich, P., Schutz, G., Umesono, K., Blumberg, B., Kastner, P., Mark, M., Chambon, P., *et al.* (1995). The nuclear receptor superfamily: the second decade. Cell *83*, 835-839.

Mansure, J.J., Nassim, R., Chevalier, S., Szymanski, K., Rocha, J., Aldousari, S., and Kassouf, W. (2013). A Novel Mechanism of PPAR Gamma Induction via EGFR Signalling Constitutes Rational for Combination Therapy in Bladder Cancer. PLoS One *8*, e55997.

Marshall, C.J., Franks, L.M., and Carbonell, A.W. (1977). Markers of neoplastic transformation in epithelial cell lines derived from human carcinomas. J Natl Cancer Inst *58*, 1743-1751.

Mesquita, B., Lopes, P., Rodrigues, A., Pereira, D., Afonso, M., Leal, C., Henrique, R., Lind, G.E., Jeronimo, C., Lothe, R.A., *et al.* (2013). Frequent copy number gains at 1q21 and 1q32 are associated with overexpression of the ETS transcription factors ETV3 and ELF3 in breast cancer irrespective of molecular subtypes. Breast Cancer Res Treat *138*, 37-45.

Mysorekar, I.U., Mulvey, M.A., Hultgren, S.J., and Gordon, J.I. (2002). Molecular regulation of urothelial renewal and host defenses during infection with uropathogenic Escherichia coli. J Biol Chem *277*, 7412-7419.

Negrete, H.O., Lavelle, J.P., Berg, J., Lewis, S.A., and Zeidel, M.L. (1996). Permeability properties of the intact mammalian bladder epithelium. Am J Physiol *271*, F886-894.

Nelson, W.J., and Nusse, R. (2004). Convergence of Wnt, beta-catenin, and cadherin pathways. Science *303*, 1483-1487.

Neve, R.M., Ylstra, B., Chang, C.H., Albertson, D.G., and Benz, C.C. (2002). ErbB2 activation of ESX gene expression. Oncogene *21*, 3934-3938.

Ng, A.Y., Waring, P., Ristevski, S., Wang, C., Wilson, T., Pritchard, M., Hertzog, P., and Kola, I. (2002). Inactivation of the transcription factor Elf3 in mice results in dysmorphogenesis and altered differentiation of intestinal epithelium. Gastroenterology *122*, 1455-1466.

Oettgen, P., Alani, R.M., Barcinski, M.A., Brown, L., Akbarali, Y., Boltax, J., Kunsch, C., Munger, K., and Libermann, T.A. (1997). Isolation and characterization of a novel epithelium-specific transcription factor, ESE-1, a member of the ets family. Mol Cell Biol *17*, 4419-4433.

Oettgen, P., Barcinski, M., Boltax, J., Stolt, P., Akbarali, Y., and Libermann, T.A. (1999). Genomic organization of the human ELF3 (ESE-1/ESX) gene, a member of the Ets transcription factor family, and identification of a functional promoter. Genomics *55*, 358-362.

Ojesina, A.I., Lichtenstein, L., Freeman, S.S., Pedamallu, C.S., Imaz-Rosshandler, I., Pugh, T.J., Cherniack, A.D., Ambrogio, L., Cibulskis, K., Bertelsen, B., *et al.* (2014). Landscape of genomic alterations in cervical carcinomas. Nature *506*, 371-375.

Oliver, J.R., Kushwah, R., Wu, J., Pan, J., Cutz, E., Yeger, H., Waddell, T.K., and Hu, J. (2011). Elf3 plays a role in regulating bronchiolar epithelial repair kinetics following Clara cell-specific injury. Lab Invest *91*, 1514-1529.

Olsburgh, J., Harnden, P., Weeks, R., Smith, B., Joyce, A., Hall, G., Poulsom, R., Selby, P., and Southgate, J. (2003). Uroplakin gene expression in normal human tissues and locally advanced bladder cancer. J Pathol *199*, 41-49.

Oottamasathien, S., Wang, Y., Williams, K., Franco, O.E., Wills, M.L., Thomas, J.C., Saba, K., Sharif-Afshar, A.R., Makari, J.H., Bhowmick, N.A., *et al.* (2007). Directed differentiation of embryonic stem cells into bladder tissue. Dev Biol *304*, 556-566.

Otero, M., Plumb, D.A., Tsuchimochi, K., Dragomir, C.L., Hashimoto, K., Peng, H., Olivotto, E., Bevilacqua, M., Tan, L., Yang, Z., *et al.* (2012). E74-like factor 3 (ELF3) impacts on matrix metalloproteinase 13 (MMP13) transcriptional control in articular chondrocytes under proinflammatory stress. J Biol Chem *287*, 3559-3572.

Pang, T., Sun, L.X., Wang, T., Jiang, Z.Z., Liao, H., and Zhang, L.Y. (2014). Telmisartan protects central neurons against nutrient deprivation-induced apoptosis in vitro through activation of PPARy and the Akt/GSK-beta pathway. Acta Pharmacol Sin *35*, 727-737.

Park, S.H., Kim, Y.S., Park, B.K., Hougaard, S., and Kim, S.J. (2001). Sequence-specific enhancer binding protein is responsible for the differential expression of ERT/ESX/ELF-3/ESE-1/jen gene in human gastric cancer cell lines: Implication for the loss of TCF-beta type II receptor expression. Oncogene *20*, 1235-1245.

Pizarro, J.G., Folch, J., Esparza, J.L., Jordan, J., Pallas, M., and Camins, A. (2009). A molecular study of pathways involved in the inhibition of cell proliferation in neuroblastoma B65 cells by the GSK-3 inhibitors lithium and SB-415286. J Cell Mol Med *13*, 3906-3917.

Prescott, J.D., Koto, K.S., Singh, M., and Gutierrez-Hartmann, A. (2004). The ETS transcription factor ESE-1 transforms MCF-12A human mammary epithelial cells via a novel cytoplasmic mechanism. Mol Cell Biol *24*, 5548-5564.

Qian, J.J., Niu, M.H., Zhai, X.G., Zhou, Q., and Zhou, Y.J. (2012). beta-Catenin pathway is required for TGF-beta 1 inhibition of PPAR gamma expression in cultured hepatic stellate cells. Pharmacological Research *66*, 219-225.

Quentmeier, H., Zaborski, M., and Drexler, H.G. (1997). The human bladder carcinoma cell line 5637 constitutively secretes functional cytokines. Leuk Res *21*, 343-350.

Rahman, S., Czernik, P.J., Lu, Y.L., and Lecka-Czernik, B. (2012). beta-Catenin Directly Sequesters Adipocytic and Insulin Sensitizing Activities but Not Osteoblastic Activity of PPAR gamma 2 in Marrow Mesenchymal Stem Cells. Plos One *7, e51746*.

Rahmani, M., Aust, M.M., Attkisson, E., Williams, D.C., Ferreira-Gonzalez, A., and Grant, S. (2013). Dual Inhibition of Bcl-2 and Bcl-xL Strikingly Enhances PI3K Inhibition-Induced Apoptosis in Human Myeloid Leukemia Cells through a GSK3- and Bim-Dependent Mechanism. Cancer Research *73*, 1340-1351.

Rebouissou, S., Bernard-Pierrot, I., de Reynies, A., Lepage, M.L., Krucker, C., Chapeaublanc, E., Herault, A., Kamoun, A., Caillault, A., Letouze, E., *et al.* (2014). EGFR as a potential therapeutic target for a subset of muscle-invasive bladder cancers presenting a basal-like phenotype. Sci Transl Med *6 pp. 244ra91*.

Ren, D.L., Collingwood, T.N., Rebar, E.J., Wolffe, A.P., and Camp, H.S. (2002). PPAR gamma knockdown by engineered transcription factors: exogenous PPAR gamma 2 but not PPAR gamma 1 reactivates adipogenesis. Gene Dev *16*, 27-32.

Rigby, C.C., and Franks, L.M. (1970). A human tissue culture cell line from a transitional cell tumour of the urinary bladder: growth, chromosone pattern and ultrastructure. Br J Cancer *24*, 746-754.

Rosen, E.D., Sarraf, P., Troy, A.E., Bradwin, G., Moore, K., Milstone, D.S., Spiegelman, B.M., and Mortensen, R.M. (1999). PPAR gamma is required

for the differentiation of adipose tissue in vivo and in vitro. Mol Cell *4*, 611-617.

Rushton, L., Hutchings, S.J., Fortunato, L., Young, C., Evans, G.S., Brown, T., Bevan, R., Slack, R., Holmes, P., Bagga, S., *et al.* (2012). Occupational cancer burden in Great Britain. Br J Cancer *107 Suppl 1*, S3-7.

Sabichi, A., Keyhani, A., Tanaka, N., Delacerda, J., Lee, I.L., Zou, C., Zhou, J.H., Benedict, W.F., and Grossman, H.B. (2006). Characterization of a panel of cell lines derived from urothelial neoplasms: genetic alterations, growth in vivo and the relationship of adenoviral mediated gene transfer to coxsackie adenovirus receptor expression. J Urol *175*, 1133-1137.

Sarraf, P., Mueller, E., Jones, D., King, F.J., DeAngelo, D.J., Partridge, J.B., Holden, S.A., Chen, L.B., Singer, S., Fletcher, C., *et al.* (1998). Differentiation and reversal of malignant changes in colon cancer through PPAR gamma. Nature Medicine *4*, 1046-1052.

Schmittgen, T.D., and Livak, K.J. (2008). Analyzing real-time PCR data by the comparative C(T) method. Nature protocols *3*, 1101-1108.

Seidel, J.J., and Graves, B.J. (2002). An ERK2 docking site in the Pointed domain distinguishes a subset of ETS transcription factors. Genes Dev *16*, 127-137.

Shatnawi, A., Norris, J.D., Chaveroux, C., Jasper, J.S., Sherk, A.B., McDonnell, D.P., and Giguere, V. (2014). ELF3 is a repressor of androgen receptor action in prostate cancer cells. Oncogene *33*, 862-871.

Shi, S.R., Cote, R.J., and Taylor, C.R. (1997). Antigen retrieval immunohistochemistry: Past, present, and future. Journal of Histochemistry & Cytochemistry *45*, 327-343.

Smith, N.J., Hinley, J.S., Varley, C.L., Eardley, I., Trejdosiewicz, L.K., and Southgate, J. (2015). The human urothelial tight junction: claudin 3 and the ZO-1α+ switch. Bladder *2*, e9.

Southgate, J., Harnden, P., and Trejdosiewicz, L.K. (1999). Cytokeratin expression patterns in normal and malignant urothelium: a review of the biological and diagnostic implications. Histol Histopathol *14*, 657-664.

Southgate, J., Hutton, K.A.R., Thomas, D.F.M., and Trejdosiewicz, L.K. (1994). Methods in Laboratory Investigation - Normal Human Urothelial Cells in-Vitro - Proliferation and Induction of Stratification. Lab Invest *71*, 583-594.

Southgate, J., Masters, J.R.W., and Trejdosiewicz, L.K. (2002). Culture of Human Urothelium. In Culture of Epithelial Cells (John Wiley & Sons, Inc.), pp. 381-399.

Spencer, K.S.R., Graus-Porta, D., Leng, J., Hynes, N.E., and Klemke, R.L. (2000). ErbB2 is necessary for induction of carcinoma cell invasion by ErbB family receptor tyrosine kinases. Journal of Cell Biology *148*, 385-397.

Stenoien, D.L., Mancini, M.G., Patel, K., Allegretto, E.A., Smith, C.L., and Mancini, M.A. (2000). Subnuclear trafficking of estrogen receptor-alpha and steroid receptor coactivator-1. Mol Endocrinol *14*, 518-534.

Strand, D.W., DeGraff, D.J., Jiang, M., Sameni, M., Franco, O.E., Love, H.D., Hayward, W.J., Lin-Tsai, O., Wang, A.Y., Cates, J.M.*, et al.* (2013). Deficiency in metabolic regulators PPARgamma and PTEN cooperates to drive keratinizing squamous metaplasia in novel models of human tissue regeneration. Am J Pathol *182*, 449-459.

Strand, D.W., Jiang, M., Murphy, T.A., Yi, Y., Konvinse, K.C., Franco, O.E., Wang, Y., Young, J.D., and Hayward, S.W. (2012). PPAR gamma isoforms

differentially regulate metabolic networks to mediate mouse prostatic epithelial differentiation. Cell Death & Disease *3, e361*.

Tatum, R., Zhang, Y.G., Salleng, K., Lu, Z., Lin, J.J., Lu, Q., Jeansonne, B.G., Ding, L., and Chen, Y.H. (2010). Renal salt wasting and chronic dehydration in claudin-7-deficient mice. Am J Physiol-Renal *298*, F24-F34.

Thrasivoulou, C., Millar, M., and Ahmed, A. (2013). Activation of Intracellular Calcium by Multiple Wnt Ligands and Translocation of beta-Catenin into the Nucleus A CONVERGENT MODEL OF Wnt Ca2+ AND Wnt/beta-CATENIN PATHWAYS. Journal of Biological Chemistry *288*, 35651-35659.

Tontonoz, P., Hu, E., Graves, R.A., Budavari, A.I., and Spiegelman, B.M. (1994a). mPPAR gamma 2: tissue-specific regulator of an adipocyte enhancer. Genes Dev *8*, 1224-1234.

Tontonoz, P., Hu, E., and Spiegelman, B.M. (1994b). Stimulation of adipogenesis in fibroblasts by PPAR gamma 2, a lipid-activated transcription factor. Cell *79*, 1147-1156.

Tsai, Y.C., Tsai, S.H., Chang, E.Y., Hee, S.W., Chen, W.H., Lee, S.C., and Chuang, L.M. (2013). Cytoskeletal protein vimentin interacts with and regulates peroxisome proliferator-activated receptor gamma via a proteasomal degradation process. J Cell Biochem *114*, 1559-1567.

Tymms, M.J., Ng, A.Y., Thomas, R.S., Schutte, B.C., Zhou, J., Eyre, H.J., Sutherland, G.R., Seth, A., Rosenberg, M., Papas, T., *et al.* (1997). A novel epithelial-expressed ETS gene, ELF3: human and murine cDNA sequences, murine genomic organization, human mapping to 1q32.2 and expression in tissues and cancer. Oncogene *15*, 2449-2462.

Urist, M.J., Di Como, C.J., Lu, M.L., Charytonowicz, E., Verbel, D., Crum, C.P., Ince, T.A., McKeon, F.D., and Cordon-Cardo, C. (2002). Loss of p63

expression is associated with tumor progression in bladder cancer. American Journal of Pathology *161*, 1199-1206.

Varley, C., Hill, G., Pellegrin, S., Shaw, N.J., Selby, P.J., Trejdosiewicz, L.K., and Southgate, J. (2005). Autocrine regulation of human urothelial cell proliferation and migration during regenerative responses in vitro. Exp Cell Res *306*, 216-229.

Varley, C.L., Bacon, E.J., Holder, J.C., and Southgate, J. (2009). FOXA1 and IRF-1 intermediary transcriptional regulators of PPARgamma-induced urothelial cytodifferentiation. Cell Death Differ *16*, 103-114.

Varley, C.L., Garthwaite, M.A., Cross, W., Hinley, J., Trejdosiewicz, L.K., and Southgate, J. (2006). PPARgamma-regulated tight junction development during human urothelial cytodifferentiation. J Cell Physiol *208*, 407-417.

Varley, C.L., and Southgate, J. (2008). Effects of PPAR agonists on proliferation and differentiation in human urothelium. Exp Toxicol Pathol *60*, 435-441.

Varley, C.L., Stahlschmidt, J., Lee, W.C., Holder, J., Diggle, C., Selby, P.J., Trejdosiewicz, L.K., and Southgate, J. (2004a). Role of PPARgamma and EGFR signalling in the urothelial terminal differentiation programme. J Cell Sci *117*, 2029-2036.

Varley, C.L., Stahlschmidt, J., Smith, B., Stower, M., and Southgate, J. (2004b). Activation of peroxisome proliferator-activated receptor-gamma reverses squamous metaplasia and induces transitional differentiation in normal human urothelial cells. Am J Pathol *164*, 1789-1798.

Visweswaran, M., Schiefer, L., Arfuso, F., Dilley, R.J., Newsholme, P., and Dharmarajan, A. (2015). Wnt antagonist secreted frizzled-related protein 4 upregulates adipogenic differentiation in human adipose tissue-derived mesenchymal stem cells. PLoS One *10*, e0118005.

Wasylyk, B., Hahn, S.L., and Giovane, A. (1993). The Ets family of transcription factors. Eur J Biochem *211*, 7-18.

Wijnhoven, B.P.L., Dinjens, W.N.M., and Pignatelli, M. (2000). E-cadherin-catenin cell-cell adhesion complex and human cancer. Brit J Surg *87*, 992-1005.

Wu, K.J., Fan, J.H., Zhang, L.L., Ning, Z.Y., Zeng, J., Zhou, J.C., Li, L., Chen, Y.L., Zhang, T.T., Wang, X.Y., *et al.* (2012). PI3K/Akt to GSK beta/beta-catenin signaling cascade coordinates cell colonization for bladder cancer bone metastasis through regulating ZEB1 transcription. Cellular Signalling *24*, 2273-2282.

Wu, X.R., Kong, X.P., Pellicer, A., Kreibich, G., and Sun, T.T. (2009). Uroplakins in urothelial biology, function, and disease. Kidney Int *75*, 1153-1165.

Xu, J., Lamouille, S., and Derynck, R. (2009). TGF-beta-induced epithelial to mesenchymal transition. Cell research *19*, 156-172.

Yamamoto, K., Ohishi, M., Ho, C., Kurtz, T.W., and Rakugi, H. (2009). Telmisartan-induced inhibition of vascular cell proliferation beyond angiotensin receptor blockade and peroxisome proliferator-activated receptor-gamma activation. Hypertension *54*, 1353-1359.

Yang, D.R., Lin, S.J., Ding, X.F., Miyamoto, H., Messing, E., Li, L.Q., Wang, N., and Chang, C. (2013). Higher Expression of Peroxisome Proliferator-activated Receptor gamma or Its Activation by Agonist Thiazolidinedione-rosiglitazone Promotes Bladder Cancer Cell Migration and Invasion. Urology *81*, 1109 e1101-1106.

Yoshida, N., Yoshida, S., Araie, M., Handa, H., and Nabeshima, Y.-i. (2000). Ets family transcription factor ESE-1 is expressed in corneal epithelial cells

and is involved in their differentiation. Mechanisms of Development *97*, 27-34.

Yu, Z., Mannik, J., Soto, A., Lin, K.K., and Andersen, B. (2009). The epidermal differentiation-associated Grainyhead gene Get1/Grhl3 also regulates urothelial differentiation. EMBO J *28*, 1890-1903.

Zhou, J., Wilson, K.M., and Medh, J.D. (2002). Genetic analysis of four novel peroxisome proliferator activated receptor-gamma splice variants in monkey macrophages. Biochem Biophys Res Commun *293*, 274-283.

Zhou, Q., Yan, B., Hu, X., Li, X.B., Zhang, J., and Fang, J. (2009). Luteolin inhibits invasion of prostate cancer PC3 cells through E-cadherin. Mol Cancer Ther *8*, 1684-1691.

Zhu, Y., Qi, C., Korenberg, J.R., Chen, X.N., Noya, D., Rao, M.S., and Reddy, J.K. (1995). Structural organization of mouse peroxisome proliferator-activated receptor gamma (mPPAR gamma) gene: alternative promoter use and different splicing yield two mPPAR gamma isoforms. Proc Natl Acad Sci U S A *92*, 7921-7925.

Zou, C., Liebert, M., Zou, C., Grossman, H.B., and Lotan, R. (2001). Identification of effective retinoids for inhibiting growth and inducing apoptosis in bladder cancer cells. J Urol *165*, 986-992.